Functional Characterisation of the Myofibrillar Myopathy-Associated KY Protein

Ahmed Nouh

PhD

University of York

Biomedical Science

July 2025

Abstract

The kyphoscoliosis peptidase (KY) protein is a Z-disc–associated factor implicated in skeletal muscle maintenance, yet its molecular function has remained poorly defined. This thesis set out to characterise KY's role in muscle integrity, proteostasis, and stress adaptation by integrating cellular imaging, *in vivo* expression by electroporation, biochemical assays, structural modelling, and proteomic profiling.

Initial investigations into KY's subcellular behaviour under stress revealed a striking species-specific distinction: while human KY accumulated in cytoplasmic and nuclear puncta following heat shock, mouse KY did not exhibit this redistribution. Under normal conditions, KY displayed a diffuse sarcoplasmic distribution with clear Z-disc localisation, consistent with its role as a structural component of the sarcomere. These changes were further modulated by proteasomal and autophagic inhibition, pointing to KY's dynamic response to proteotoxic stress.

To test KY's functional role in muscle maintenance, *in vivo* rescue experiments were performed in *ky/ky* mice. Re-expression of full-length KY successfully restored muscle fibre cross-sectional area, whereas deletion of the TGN/PROT domain abolished rescue capacity. Interestingly, point mutations disrupting the catalytic triad did not impair function, suggesting that the domain serves a structural or scaffolding role rather than enzymatic activity. AlphaFold-based modelling predicted structural conservation of the catalytic fold, but the predicted active site geometry suggested catalytic inactivity, consistent with experimental evidence showing no enzymatic function.

Further analysis demonstrated that Z-disc localisation was preserved even when the TGN/PROT domain was removed, implicating other regions of the protein in sarcomeric anchoring. Proteomic screening using immunoprecipitation–mass spectrometry (IP–MS) identified several stress-related KY interactors, including PPM1B and HSP70 family members, linking KY to autophagy and chaperone-mediated proteostasis. Functional assays using GFP–LC3–RFP–LC3ΔG reporters confirmed impaired autophagic flux in KY-deficient cells, evidenced by disrupted LC3 processing and cargo accumulation.

ZAKβ, a stress-activated kinase that promotes muscle hypertrophy through MAPK signalling**,** was also examined in relation to KY. Expression of constitutively active ZAKβ induced hypertrophy in both wild-type and KY-deficient muscle, establishing that KY is unnecessary for ZAKβ-driven growth. Altogether, this work positions KY as a non-enzymatic scaffold that integrates proteostatic, structural, and stress-response pathways essential for maintaining skeletal muscle homeostasis.

Table of Contents

List of Figures and Tables

Acknowledgements

All praise is due to God.

First and foremost, I would like to express my sincere gratitude to my supervisor, Dr Gonzalo Blanco, for his outstanding mentorship, scientific insight, and continuous support throughout this PhD journey. His guidance has been instrumental in shaping both the direction and quality of this work, and his mentorship has been invaluable in developing my scientific thinking and professional growth.

I also extend my appreciation to my second supervisor, Professor Marek Brzozowski, for his valuable advice and constructive feedback during key stages of this project. I am equally grateful to my thesis advisory panel member, Professor William Brackenbury, for his helpful guidance and ongoing input throughout my research.

Special thanks go to all members of the Blanco Lab, past and present, particularly Oscar Harrad and Elliot Jokl, for their support and collaboration. I am especially grateful to Amy Stonage for her assistance and encouragement. My thanks also extend to Dr William Grey and his laboratory team; your scientific discussions and camaraderie made the lab an engaging and supportive environment.

I would like to thank my sponsor, the Government of Saudi Arabia, represented by the Saudi Arabian Cultural Bureau, for their generous support throughout my studies.

I am sincerely grateful to Dr Chris Taylor, Dr Adam Dowle, and Chloë Baldreki from the Metabolomics & Proteomics Laboratory, as well as all members of the Technology Facility at the University of York, for their technical expertise and support. I also thank the Biology Infrastructure and Stores teams for providing essential training and assistance, and the Animal Facility team for an experience that meaningfully contributed to my professional development.

On a personal level, I wish to express my heartfelt appreciation to my family. To my beloved wife and children—Juliana, Aws, and Qays—thank you for your endless love, patience, and for being a constant source of inspiration and joy.

To my late father, who always encouraged and motivated me to complete my postgraduate studies, your belief in me continues to guide me. To my dear mother, who prays every day for my success and constantly asks when I will return, your unwavering love and support mean the world to me. Special appreciation also goes to my big brother Khalid, and to all my brothers and sisters thank you for the values, prayers, and support that laid the foundation for my academic journey and for always being there when I needed it.

I carry this achievement not alone, but with all of you in my heart.

Declaration

I declare that this thesis is a presentation of original work conducted by me. It has not been previously presented for a degree at this or any other institution. All sources of information have been acknowledged and appropriately referenced.

This work was carried out at the Department of Biology, University of York, under the supervision of Dr Gonzalo Blanco.

Any collaborative work, contributions from colleagues, or previously published material included in this thesis are clearly indicated and referenced in the relevant sections.

I confirm that this thesis is the result of my own investigations, except where otherwise stated, and that it has not been submitted either in the same or different form for any other degree.

CHAPTER ONE:

Introduction

CHAPTER 1. Introduction

1.1 KY Underlies Myofibrillar Myopathy in Mice and Humans

Myofibrillar myopathy (MFM) comprises a heterogeneous group of rare inherited neuromuscular disorders characterised by the progressive disintegration of myofibrils—the fundamental contractile elements of skeletal and cardiac muscle—and the abnormal accumulation of protein degradation products within muscle fibres. Histopathologically, this condition is marked by the presence of ectopic protein aggregates, often involving Z-disc–associated proteins such as small heat shock proteins (sHSPs), desmin and αB-crystallin, reflecting early and central involvement of the sarcomeric cytoskeleton (Fichna et al., 2018; Selcen, 2011).

Clinically, MFM typically presents with slowly progressive muscle weakness that often begins in the distal limbs and may extend to proximal muscles and, in advanced cases, the respiratory musculature. Patients may experience gait difficulties, frequent falls, or difficulties performing fine motor tasks. Extramuscular manifestations such as peripheral neuropathy are relatively frequent. Cardiac involvement, including arrhythmias, conduction defects, and dilated or restrictive cardiomyopathy is common and represents a major source of morbidity and mortality, often necessitating ongoing cardiological surveillance (Liewluck, 2021; Selcen, 2011).

Diagnosis of MFM remains complex due to considerable phenotypic variability and overlapping clinical features with other myopathies. Although muscle biopsy findings such as Z-disc disorganisation, myofibrillar disintegration, and protein aggregates are essential diagnostic clues, electromyography and muscle imaging (MRI) can further support diagnosis, while genetic testing using next-generation sequencing (NGS) has become indispensable for confirming the diagnosis and identifying causative mutations (Arndt et al., 2010; Selcen, 2011).

To date, pathogenic mutations in more than 17 genes have been associated with MFM or MFM-like phenotypes. These include DES (desmin), CRYAB (αB-crystallin), MYOT (myotilin), LDB3 (also known as ZASP, LIM domain-binding 3), FLNC (filamin C), BAG3 (BCL2-associated athanogene 3), FHL1 (four and a half LIM domains protein 1), TTN (titin), DNAJB6 (DnaJ homolog subfamily B member 6), PLEC (plectin), LMNA (lamin A/C), ACTA1 (skeletal muscle α-actin), HSPB8 (heat shock protein beta-8), KY (kyphoscoliosis peptidase), and PYROXD1 (pyridine nucleotide-disulphide oxidoreductase domain 1). In rare cases, compound mutations—such as those affecting SQSTM1 (sequestosome 1) and TIA1 (T-cell intracellular antigen-1)—have also been reported. Many of these genes are implicated in other neuromuscular disorders as well, highlighting the shared molecular pathology and emphasising the concept of a disease continuum among myopathies. Although MFM is most often inherited in an autosomal dominant manner, autosomal recessive forms have also been documented (Fichna et al., 2018; Liewluck, 2021; Palmio & Udd, 2016; Selcen, 2011).

The implementation of high-throughput next-generation sequencing (NGS), including whole genome and exome sequencing, has significantly advanced the discovery of novel mutations and provided insights into the genetic complexity of MFM. Notably, many individuals carry multiple rare variants in genes related to muscle function**.** This has led to the emerging concept of “variant load,” where cumulative rare variants rather than a single mutation shape disease severity and onset. This could help explain why individuals with the same primary mutation often show very different symptoms or rates of progression (Fichna et al., 2018).

Despite these advances, a curative treatment for MFM remains elusive. Current management strategies are supportive and multidisciplinary, focusing on physical therapy to maintain mobility, respiratory monitoring, and routine cardiac evaluations such as echocardiography and Holter monitoring to address cardiomyopathic progression and arrhythmias. The overarching goal of treatment is to alleviate symptoms and preserve the patient’s quality of life (Olivé, Kley and Goldfarb, 2013; Selcen et al., 2011).

MFM exemplifies the intersection of structural muscle pathology and complex genetic underpinnings. Its clinical variability, genetic diversity, and molecular overlap with other myopathies make it a compelling model for studying the interplay between sarcomeric integrity and cellular proteostasis. Continued research is essential to unravel the mechanisms of disease progression and to identify targets for therapeutic intervention.

Table 1-1 Genes Associated with Myofibrillar Myopathy and Related Phenotypes

Gene	Encoded Protein	Function / Pathway	Inheritance	References
DES	**Desmin**	**Intermediate filament, sarcomere integrity**	**AD / AR**	**Selcen (2011)**
CRYAB	**αB-crystallin**	**sHSP, chaperone for desmin filaments**	**AD**	**Fichna et al. (2018)**
MYOT	**Myotilin**	**Actin crosslinking at Z-disc**	**AD**	**Palmio & Udd (2016)**
LDB3 (ZASP)	**LIM-domain-binding 3**	**Z-disc adaptor, mechanosensing**	**AD**	**Fichna et al. (2018)**
FLNC	**Filamin C**	**Actin-binding, CASA pathway**	**AD**	**Arndt et al. (2010)**
BAG3	**BAG family molecular chaperone 3**	**CASA-mediated autophagy**	**AD**	**Selcen (2011)**
FHL1	**Four and a half LIM domains 1**	**Sarcomeric signalling**	**XL**	**Liewluck (2021)**
TTN	**Titin**	**Sarcomere elasticity**	**AD / AR**	**Fichna et al. (2018)**

DNAJB6	**DnaJ homolog subfamily B 6**	**HSP-co-chaperone**	**AD**	**Palmio & Udd (2016)**
PLEC	**Plectin**	**Cytoskeletal crosslinker**	**AR**	**Fichna et al. (2018)**
LMNA	**Lamin A/C**	**Nuclear envelope**	**AD / AR**	**Liewluck (2021)**
ACTA1	**α-Actin 1**	**Thin filament protein**	**AD**	**Fichna et al. (2018)**
HSPB8	**Heat shock protein β-8**	**CASA complex**	**AD**	**Fichna et al. (2018)**
KY	**Kyphoscoliosis peptidase**	**Muscle proteostasis regulator**	**AR**	**Blanco et al. (2001)**
PYROXD1	**Pyridine nucleotide-disulphide oxidoreductase 1**	**Redox homeostasis**	**AR**	**Fichna et al. (2018)**
SQSTM1 / TIA1	**Sequestosome 1 / T-cell intracellular antigen-1**	**Stress granule / autophagy**	**AD**	**Palmio & Udd (2016)**

1.2 Skeletal muscle

Skeletal muscle is among the most functionally adaptable tissues in the human body, accounting for approximately 40% of total body weight and containing 50–75% of the body's total protein content. Its composition includes roughly 75% water, 20% proteins, and 5% other constituents such as lipids, carbohydrates, and minerals. Muscle mass is regulated by several factors, including hormonal balance, physical activity, nutritional status, and disease—all of which primarily influence protein synthesis and degradation pathways (Peters, 1989; Zamorani & Valle, 2007).

Skeletal muscle comprises heterogeneous fibre types, and the size and number of these fibres are major determinants of overall muscle mass. Pathological conditions, such as fatty infiltration, can disrupt this relationship, leading to muscle fibre atrophy and impaired function (Frontera and Ochala, 2015).

1.2.1 Structural Organisation of Skeletal Muscle

Skeletal muscle exhibits a hierarchical structure. Muscle fibres, the basic cellular units, are grouped into fascicles, which collectively form individual muscles (Purslow, 2002; Zamorani & Valle, 2007). Each muscle fibre contains numerous myofibrils, which are embedded within the sarcoplasm and enclosed by the sarcolemma (BARER, 1948). Myofibrils display characteristic cross-striations composed of repeating sarcomeres, the fundamental contractile units. Within sarcomeres, interdigitating myosin (thick) and actin (thin) filaments interact and slide past one another to generate contraction (Squire, 1975).

The muscle is supported by connective tissue layers: the endomysium surrounds individual fibres, the perimysium encases fascicles, and the epimysium envelops the entire muscle. This structural organization is represented in (Figure 1.1) (adapted from UKPosters, n.d.), which illustrates the compartmentalisation of fibres, fascicles, and connective tissue.

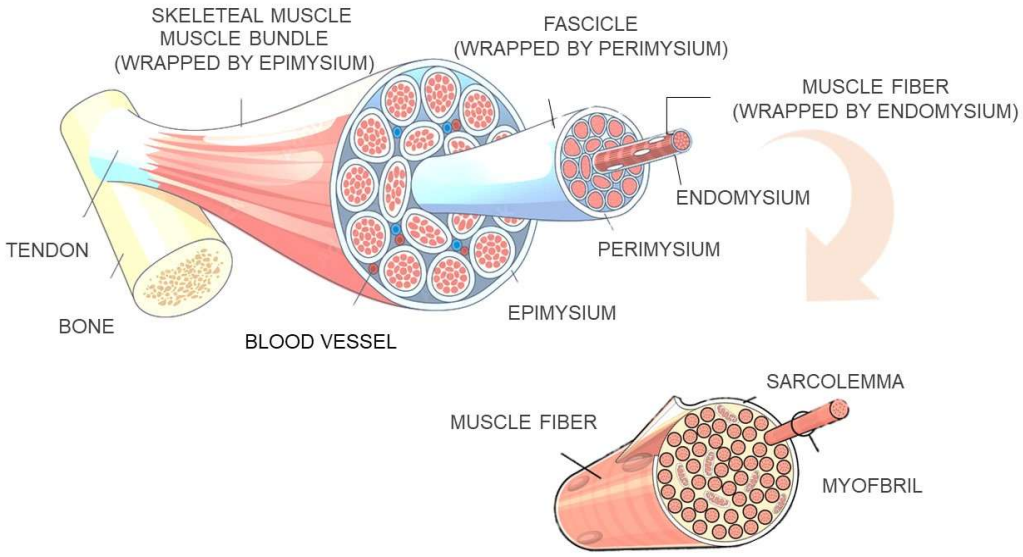

Figure 1.1 A hierarchical diagram illustrating the structural organization of skeletal muscle from whole muscle to individual myofibrils.

Key connective tissue layers—epimysium, perimysium, and endomysium—are highlighted, along with major anatomical features including fascicles, muscle fibers, sarcolemma, and myofibrils. (Adapted from UKPosters, n.d.)

At a higher magnification, the organisation of sarcomeres and myofibrillar elements is detailed in (Figure 1.2), showing the arrangement of Z-discs, A and I bands, and thick and thin filaments within the sarcomere.

Skeletal muscle fibres are classified into distinct types based on their metabolic properties, contractile speed and fatigue resistance. Type I (slow-oxidative) fibres rely predominantly on mitochondrial oxidative phosphorylation, possess high capillary density and are resistant to fatigue, supporting sustained, low-force activities. Type IIa (fast oxidative-glycolytic) fibres represent an intermediate phenotype capable of both aerobic and anaerobic metabolism, enabling rapid contractions with moderate fatigue resistance. Type IIx/IIb (fast glycolytic) fibres generate high force and contract rapidly but fatigue quickly due to their reliance on glycolysis and lower mitochondrial content (Bloemberg & Quadrilatero, 2012; Schiaffino & Reggiani, 2011; Squire, 1975).

The distribution of these fibre types varies across muscles according to functional demand and can shift in response to physiological stimuli or pathological stress.

In the context of this thesis, fibre type composition is particularly relevant because KY-related pathology predominantly affects postural muscles enriched in oxidative fibres, suggesting that KY may play a critical role in maintaining proteostasis and autophagic homeostasis in fibres that are metabolically active and continuously subjected to mechanical load.

In laboratory settings, muscle fibre types are distinguished by the expression of distinct myosin heavy chain (MyHC) isoforms, which define contractile and metabolic characteristics**.** Type I fibres express MyHC-I (encoded by *MYH7*), Type IIa fibres express MyHC-IIa (*MYH2*), and Type IIx/IIb fibres express MyHC-IIx/IIb (*MYH1* and *MYH4*). These isoforms can be identified using immunohistochemistry with isoform-specific antibodies or by SDS–PAGE electrophoresis of isolated myosin. Alternatively, ATPase histochemistry following pre-incubation at different pH values provides a classic method for differentiating fibre types based on enzymatic activity. Such techniques are routinely used in both research and diagnostic muscle pathology to assess fibre-type composition, transitions, and selective vulnerability in disease (Bloemberg & Quadrilatero, 2012; Schiaffino & Reggiani, 2011).

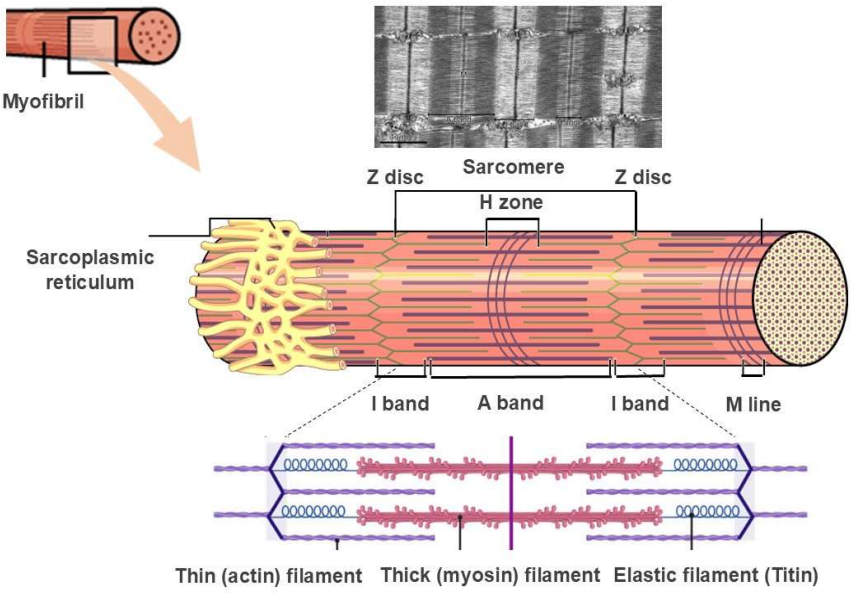

Figure 1.2 schematic representation of the ultrastructure of a myofibril, illustrating the sarcomere—the fundamental contractile unit of skeletal muscle.

Major structural features are highlighted, including Z discs, I and A bands, H zone, M line, and the sarcoplasmic reticulum. The lower inset details the organization of actin (thin), myosin (thick), and titin (elastic) filaments that enable muscle contraction via the sliding filament mechanism. (Adapted and modified from Physio-Pedia https://www.physio-pedia.com/Myofibril and UNISCIEL Physiology Resources https://ressources.unisciel.fr/physiologie/co/2b_1.html.

The costamere is a structural complex located beneath the sarcolemma that connects the contractile apparatus of muscle fibres to the extracellular matrix via the sarcolemma. It plays a critical role in lateral force transmission and in maintaining the structural integrity of muscle fibres during contraction and stretch (Peters, 1989).

One key protein involved in linking the Z-disc to the costamere is plectin, a large cytoskeleton linker protein that organises and anchors intermediate filaments to cytoskeletal and membrane-associated structures. Plectin is essential for myofibre integrity by targeting desmin intermediate filaments to both Z-discs and costameres (Konieczny et al., 2008). Different isoforms of plectin have specialised roles: plectin 1d and 1f link desmin to Z-discs and costameres, whereas plectin 1b connects desmin to mitochondria, indicating its multifunctional cytoskeletal roles.

Mutations in Z-disc-associated proteins, including plectin, can lead to a spectrum of muscle disorders collectively referred to as Z-discopathies (Knöll et al., 2011). These disorders underscore the importance of proper Z-disc–costamere–cytoskeleton linkage in maintaining muscle structure and function.

1.3 Key cellular and molecular mechanisms in skeletal muscle fibres

Muscle fibres are multinucleated, with multiple nuclei positioned peripherally beneath the sarcolemma. These nuclei regulate the synthesis of proteins in spatially distinct regions called nuclear domains, which are precisely structured in size (S. Hikida, 2012). The mitochondria, densely packed between myofibrils, provide ATP for energy-demanding processes like protein synthesis and contraction (Bareja et al., 2014; Wilkins et al., 2001). The proteins such as actin and myosin in adjacent segments of a single muscle fibre is highly coordinated, ensuring uniformity across the fibre's length.

Satellite cells, the adult stem cells of skeletal muscle, reside between the basal lamina and sarcolemma. These cells are activated by myogenic factors to proliferate and differentiate, aiding in muscle repair, growth, and regeneration (Bareja et al., 2014; S. Hikida, 2012). The contractile machinery comprises protein complexes, including myosin (thick filaments) and actin (thin filaments), alongside associated proteins like titin and tropomyosin. Disruptions such as mutations or absence of these proteins are linked to muscle diseases (Ottenheijm & Granzier, 2010; Thomas, 2013), including those associated with mutations in structural regulators such as the kyphoscoliosis (KY) protein. The cellular components of a skeletal muscle fibre are shown in (Figure 1.3).

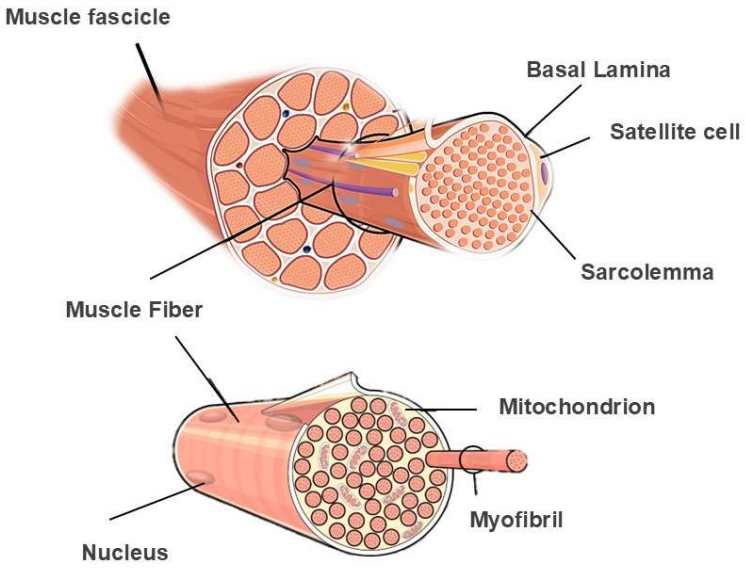

Figure 1.3 shows the structural and cellular components of a skeletal muscle fibre, highlighting elements involved in contractile function, metabolic support, and regeneration.

The diagram shows the arrangement of myofibrils, mitochondria, and peripheral nuclei, as well as satellite cells located between the sarcolemma and basal lamina—key players in muscle repair and plasticity. (Adapted and modified from UNISCIEL Physiology Resources: https://ressources.unisciel.fr/physiologie/co/2b_1.html.

During muscle repair, satellite cells are activated in response to injury or physiological stress, exiting quiescence and re-entering the cell cycle under the influence of key transcription factors such as Pax7, MyoD, and Myf5. Activated satellite cells proliferate as myoblasts, migrate to sites of damage, and subsequently differentiate into myocytes that fuse either with existing fibres or with each other to form new myofibres, restoring muscle structure and function (H. Yin et al., 2013; Zammit, 2017). *In vitro*, C2C12 myoblasts are commonly used as a model to study this process. When cultured in low-serum differentiation medium, these cells withdraw from the cell cycle and express myogenic markers such as myogenin and myosin heavy chain, fusing to form multinucleated myotubes that resemble developing muscle fibres (Burattini et al.,

2004; Hindi et al., 2013). This system recapitulates key aspects of *in vivo* myogenesis and provides an experimentally tractable model for investigating muscle differentiation, regeneration, and disease mechanisms.

1.4 Structural and Functional Role of the Z-disc in muscle contraction and integrity.

The Z-disc, a protein-rich structure in sarcomeres, plays a crucial role in muscle contraction and integrity (Noureddine & Gehmlich, 2023). It anchors actin filaments, maintains mechanical stability, and serves as a signalling hub (Frank et al., 2007). The Z-disc's structure consists of interdigitated actin filaments crosslinked by α-actinin layers, with a width varying between fast and slow muscle fibres (Luther, 2009). Cryo-electron tomography has revealed a 3D lattice spring within the Z-disc, formed by actin-actinin complexes that exhibit contraction-dependent motions (Oda & Yanagisawa, 2020) . Various proteins, including α-actinin, filamin C, titin, and desmin, contribute to the Z-disc's structural and functional properties. Mutations in Z-disc proteins have been linked to cardiomyopathies, highlighting its importance in muscle health (Frank et al., 2007; Noureddine & Gehmlich, 2023). Considering the Z-disc's role as both a structural and signalling hub, proteins like KY that localise to this domain are likely to play a critical role in maintaining sarcomeric integrity and overall muscle function.

1.4.1 The importance of the Z-disc.

The Z-disc is a fundamental structural and functional component of muscle cells, acting as both a mechanical anchor and a dynamic signalling hub (Knöll et al., 2011; Wang & Su, 2010). It connects adjacent sarcomeres, integrates myofibrils with the cell membrane, and facilitates communication with the nucleus, making it essential for force transmission and mechanotransduction. Recent studies have identified the Z-disc as a phosphorylation hotspot, highlighting its central role in intracellular signalling and its potential involvement in muscle pathologies (Reimann et al., 2017).

1.5 Mechanisms Regulating Muscle Fibre Size

1.5.1 Muscle Hypertrophy

Muscle hypertrophy refers to an increase in muscle size, typically assessed by muscle mass, fibre thickness, or fibre cross-sectional area (CSA). This physiological response arises from mechanical overload or anabolic stimuli and involves complex adaptations at the cellular and molecular levels. (Haun et al., 2019; Schiaffino et al., 2021).

At the molecular level, hypertrophy is driven predominantly by activation of the PI3K/Akt/mTOR pathway, which promotes protein synthesis and inhibits autophagy. Mechanical loading or growth factor signalling, such as insulin-like growth factor-1 and IGF-1 activates Akt, which in turn phosphorylates and activates mTORC1, a central

regulator of ribosomal biogenesis and translation initiation (Laplante & Sabatini, 2012). mTORC1 also inhibits ULK1, reducing autophagy and favouring net protein accumulation.

Additionally, satellite cells play an important role by fusing with existing myofibers, donating nuclei to support increased transcriptional capacity (Davids et al., 2023). This process is mediated by myogenic regulatory factors (MRFs) such as MyoD and myogenin, which are upregulated during hypertrophic growth (Schiaffino et al., 2021).

While muscle hypertrophy is often assumed to reflect proportional increases in myofibrillar content, recent studies suggest that hypertrophy may also involve sarcoplasmic expansion, leading to a dilution of myofibrillar protein concentration under some conditions (Haun et al., 2019). Moreover, differences between macroscopic and molecular markers underscore the importance of integrating structural and biochemical readouts when evaluating muscle growth (Davids et al., 2023).

Animal models remain essential for dissecting the temporal and spatial aspects of hypertrophic adaptation, especially where long-term studies are impractical in humans (Alway et al., 2005).

1.5.2 Atrophy

Skeletal muscle atrophy is characterised by a reduction in muscle mass and CSA, often resulting from disuse, ageing, cachexia, or chronic illness. Atrophy occurs when protein degradation surpasses synthesis and is accompanied by reduced muscle strength and metabolic capacity (Bonaldo & Sandri, 2013; L. Yin et al., 2021) .

The primary molecular drivers of atrophy are the ubiquitin–proteasome system (UPS) and the autophagy–lysosome pathway. These are regulated by the FoxO family of transcription factors (especially FoxO3) which upregulate E3 ubiquitin ligases such as MuRF1 (Trim63) and Atrogin-1 (Fbxo32). These ligases tag sarcomeric proteins for degradation via the proteasome (Sandri, 2008).

In parallel, autophagy-related genes such as (Bnip3, LC3) are activated to promote lysosomal degradation of cellular components, especially under conditions of nutrient deprivation or mitochondrial stress. Chronic activation of these pathways leads to muscle wasting (L. Yin et al., 2021).

Regulatory inputs from myostatin, a negative regulator of muscle mass, and pro-inflammatory cytokines (TNF-α, IL-6) further exacerbate catabolic processes by activating NF-κB and JAK/STAT signalling. Conversely, IGF-1/Akt signalling can counteract atrophy by inhibiting FoxO and promoting protein synthesis.

Therapeutic strategies to mitigate atrophy include resistance exercise, nutritional supplementation, and modulation of catabolic pathways, though clinical efficacy

remains limited in certain disease contexts (Bonaldo & Sandri, 2013; Fanzani et al., 2012).

1.5.3 Protein Turnover in Skeletal Muscle

Protein turnover is a dynamic process that maintains skeletal muscle mass and quality through the continuous synthesis and degradation of proteins. This balance is regulated by key signalling pathways, with Akt/mTOR promoting anabolic processes and FoxO3-dependent pathways stimulating proteolysis through activation of the ubiquitin–proteasome system (UPS) and autophagy (Bonaldo & Sandri, 2013; Ferreira & Duarte, 2022).

Muscle adapts to physiological and environmental cues such as exercise, nutrient availability, and ageing by modulating these networks. The Akt/mTOR axis enhances protein synthesis in response to resistance exercise and nutrient intake, particularly amino acids. Conversely, during catabolic conditions such as disuse or fasting, FoxO transcription factors become activated, leading to increased expression of genes involved in protein degradation (Bonaldo & Sandri, 2013; McKendry et al., 2021).

Different protein classes exhibit distinct turnover rates. For example, mitochondrial proteins undergo accelerated degradation under catabolic stress, whereas myofibrillar proteins such as myosin and actin are preferentially synthesised during hypertrophy (Ferreira & Duarte, 2022). Understanding the signalling mechanisms governing this balance is crucial for developing therapeutic strategies to counteract muscle atrophy associated with ageing and disease.

1.5.4 The Ubiquitin-Proteasome System (UPS)

The UPS represents the primary pathway for selective protein degradation in skeletal muscle, particularly during atrophy. It functions by conjugating ubiquitin molecules to damaged or misfolded proteins through a cascade of E1 (activating), E2 (conjugating),

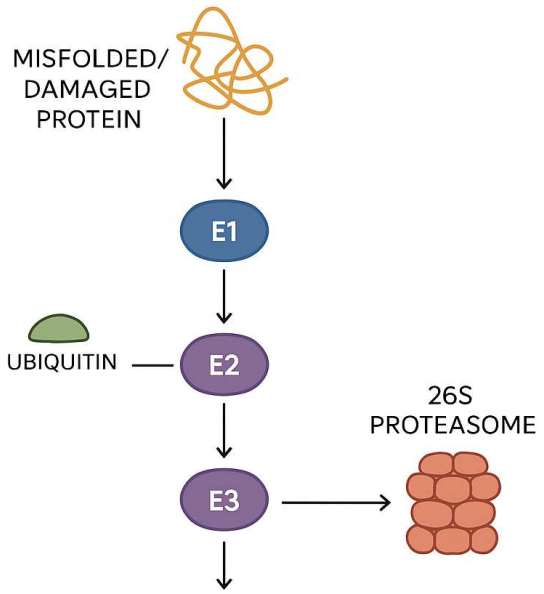

Figure 1.4 The ubiquitin–proteasome system (UPS) mediates selective protein degradation in skeletal muscle.

Damaged or misfolded proteins are tagged with ubiquitin via a cascade involving E1, E2, and E3 enzymes. Polyubiquitinated substrates are recognised and degraded by the 26S proteasome, releasing peptides and recycling ubiquitin. The pathway is upregulated during muscle atrophy and suppressed by anabolic signals.

and E3 (ligase) enzymes, targeting them for degradation by the 26S proteasome (Figure 1.4) (Kitajima et al., 2020). Among the muscle-specific E3 ligases, *Muscle RING-Finger 1 (MuRF1)* and *Muscle Atrophy F-box (MAFbx/Atrogin-1)* play central roles in mediating the breakdown of contractile and regulatory proteins during catabolic stress (Attaix et al., 2003; Taillandier et al., 2004). Conversely, sustained contractile activity can enhance proteasomal function, supporting continuous removal of damaged proteins and contributing to overall muscle quality control (Ordway et al., 2000).

The UPS therefore serves a dual role, maintaining protein homeostasis under physiological conditions while contributing to muscle wasting when overactivated.

1.5.5 Autophagy in Muscle Homeostasis and Disease

Autophagy is a lysosomal degradation pathway essential for removing damaged proteins and organelles, thereby preserving cellular homeostasis in skeletal muscle. It is particularly crucial under stress conditions such as nutrient deprivation, exercise, and ageing (Franco-Romero & Sandri, 2021; Neel et al., 2013).

The initiation of autophagy is regulated by the AMPK–ULK1 pathway during energy stress and by FoxO3 under catabolic conditions. Autophagosomes engulf cytoplasmic content and fuse with lysosomes for degradation (Bonaldo & Sandri, 2013; Park et al., 2019). Proper autophagic flux ensures the removal of dysfunctional mitochondria (mitophagy), aggregates, and damaged sarcomeric components, which is essential for muscle integrity and adaptation (figure1.5).

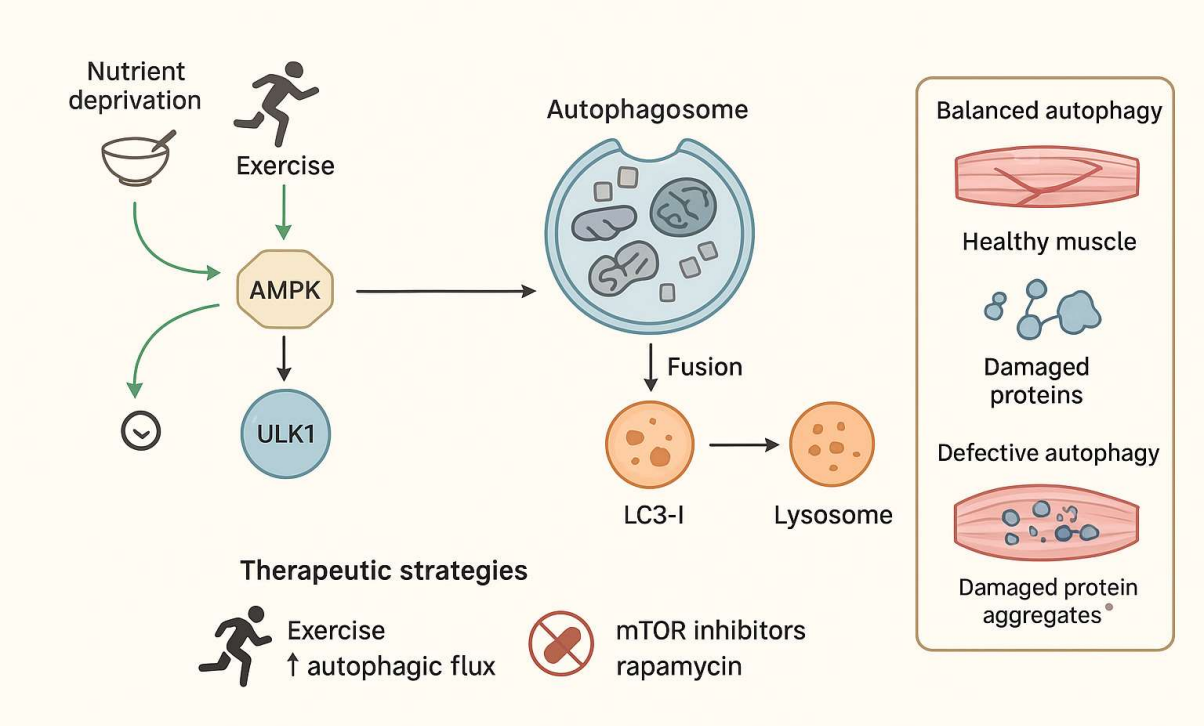

Figure 1.5 Schematic overview of autophagy regulation and its functional significance in skeletal muscle.

AMPK activation by energy stress (e.g., exercise) promotes ULK1-mediated autophagosome formation, whereas mTORC1 inhibits initiation under nutrient-rich conditions. LC3 lipidation drives autophagosome maturation, which subsequently fuses with lysosomes for degradation of damaged proteins and organelles. Balanced autophagy preserves muscle homeostasis, whereas impaired flux contributes to myofibrillar myopathies and sarcopenia. Pharmacological and physiological modulators such as exercise and rapamycin can restore autophagic balance.

Dysregulated autophagy contributes to both acute and chronic muscle pathologies. Excessive activation may cause unnecessary degradation of muscle proteins, while insufficient flux leads to toxic accumulation of aggregates, as observed in myofibrillar myopathies (Jiao & Demontis, 2017; Mizushima & Levine, 2020). Impaired autophagy has been implicated in sarcopenia, where autophagic capacity declines with age, exacerbating muscle loss and reducing regenerative potential. Therapeutic strategies targeting autophagy include Exercise: A physiological inducer that enhances autophagic flux and supports muscle regeneration via satellite cell activation. Pharmacological agents: mTOR inhibitors such as rapamycin have shown promise in

restoring autophagic balance in preclinical models of myopathies (Xia et al., 2021). As a whole, autophagy plays a critical role in muscle maintenance, adaptation, and disease, with growing interest in its modulation for therapeutic purposes.

1.5.6 Chaperone-Assisted Selective Autophagy (CASA)

(CASA) is a conserved quality-control pathway that safeguards protein homeostasis in tissues exposed to mechanical or proteotoxic stress, such as skeletal muscle and neurons (Arndt et al., 2010). It functions by recognising and removing damaged or misfolded proteins that arise during repetitive contraction, heat stress, or oxidative imbalance. Although initially described in muscle, CASA also plays important roles in neurons, where it helps preserve synaptic function and prevent the accumulation of protein aggregates under metabolic or oxidative stress (Gamerdinger et al., 2011). This wider distribution emphasises CASA's fundamental role in maintaining cellular integrity in mechanically and metabolically active tissues.

In muscle, CASA contributes directly to the maintenance of sarcomeric structure, particularly the Z-disc, where mechanical strain is greatest. The pathway is activated by acute loading and adapts to repeated mechanical stimulation. It is initiated by the mechanical unfolding of filamin C, a key cytoskeletal protein. These unfolding exposes binding sites that recruit molecular chaperones, triggering a coordinated degradation cascade (Tedesco et al., 2023).

CASA proceeds through four main steps. First, unfolded filamin C is recognised by a chaperone complex composed of HSP70, HSP40, and the co-chaperone BAG3. Second, the E3 ubiquitin ligase CHIP (STUB1) catalyses K63-linked polyubiquitination of the damaged substrate. Third, the ubiquitinated cargo is bound by autophagy receptors such as p62/SQSTM1 and NBR1, which link it to LC3 on developing autophagosomes. Finally, the mature autophagosome fuses with a lysosome, leading to complete degradation of the damaged protein (Figure 1.6).

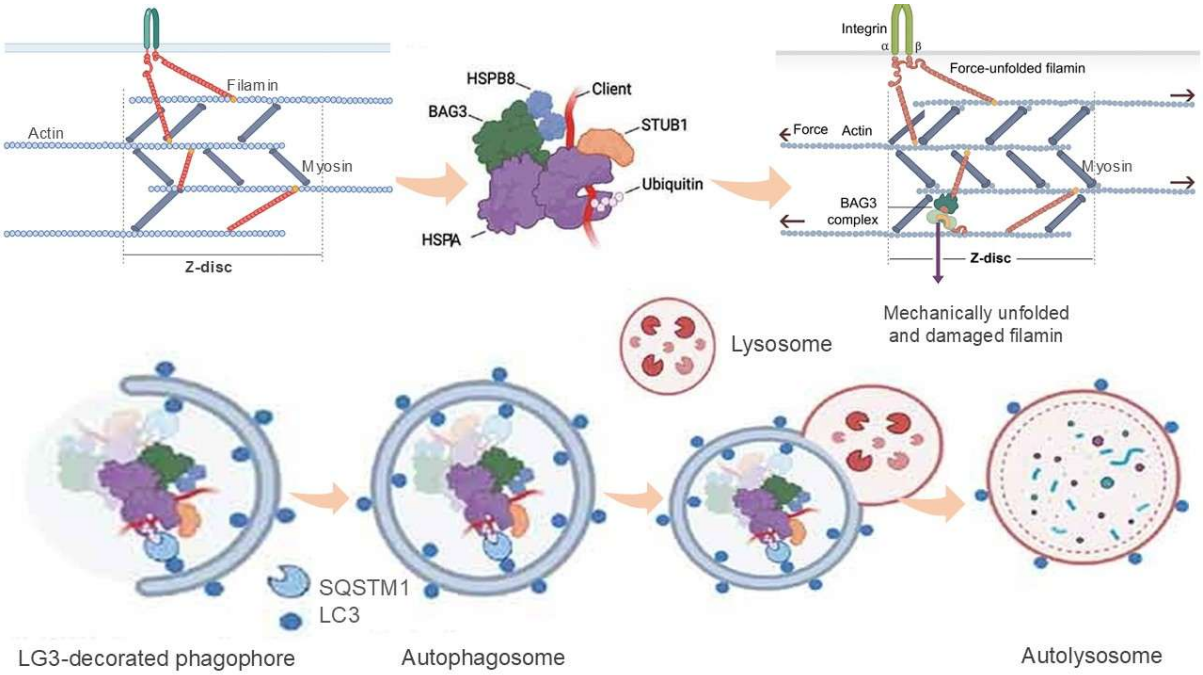

Figure 1.6 CASA pathway in muscle cells.

Mechanical strain induces unfolding of filamin, which is recognized by the BAG3-HSPA-HSPB8 chaperone complex. The damaged protein is then ubiquitinated by STUB1 and targeted to autophagosomes via SQSTM1-LC3 interaction. Subsequent fusion with lysosomes leads to degradation within the autolysosome, ensuring clearance of misfolded proteins and maintenance of proteostasis during mechanical stress. (Adapted and modified from Tedesco et al., 2023).

Unlike (UPS), which primarily handles soluble and short-lived proteins, CASA is specialised in clearing large, chaperone-bound aggregates that the proteasome cannot efficiently process. It becomes particularly important under proteotoxic stress, when misfolded and insoluble proteins accumulate within load-bearing structures like the Z-disc (Arndt et al., 2010).

BAG3 plays a central regulatory role within CASA, coordinating both cargo delivery and stress adaptation. Through its interaction with synaptopodin-2, BAG3 promotes autophagosome formation, and via YAP/TAZ signalling, it enhances filamin C transcription to reinforce Z-disc stability during prolonged tension (Ulbricht et al., 2013). In neuronal systems, BAG3 fulfils similar protective functions, facilitating the removal of misfolded proteins from axons and synapses, and thereby extending the scope of CASA beyond muscle to the nervous system (Gamerdinger et al., 2011) By maintaining the turnover of key cytoskeletal proteins such as α-actinin and titin, CASA ensures the stability of contractile structures and prevents the onset of myofibrillar damage (Ulbricht et al., 2013; Arndt et al., 2010). Defects in CASA, or mutations in its core components, lead to myofibrillar myopathies associated with BAG3 dysfunction and are also implicated in neurodegenerative diseases such as Alzheimer's disease and amyotrophic lateral sclerosis (ALS) (Meister-Broekema et al., 2018).

CASA therefore represents a universal protective mechanism that preserves the structural and functional integrity of both muscle and nerve cells. Importantly, CASA's

role at the Z-disc may overlap with that of the KY protein, which also localises to this region and appears to participate in stress-related protein quality control. Disrupted coordination between KY and CASA pathways could contribute to the pathogenesis of KY-associated myopathies, highlighting CASA as a potential target for therapeutic intervention in diseases linked to impaired proteostasis.

1.6 Kyphoscoliosis peptidase *KY*

KY is encoded by the KY gene and was originally discovered through positional cloning of the *ky/ky* mouse, which presents with progressive degenerative myopathy and thoraco-lumbar kyphoscoliosis (Blanco et al., 2001). Although historically described as a muscle-specific protein, KY is predominantly expressed in skeletal and cardiac muscle and localises to the Z-disc, a central node for mechanotransduction and sarcomere stability. Its Z-disc enrichment, together with interactions with proteins such as FLNC and IGFN1, has led to the view that KY contributes to sarcomeric organisation and structural maintenance (Baker et al., 2010; Beatham et al., 2004; Mason & Palfrey, 1984)

Sequence comparisons originally classified KY within the transglutaminase-like (TGN/PROT) superfamily of cysteine proteases. A schematic of its predicted domain architecture (Figure 1.7) illustrates an N-terminal region, a central TGN/PROT-like domain containing the putative catalytic triad (Cys225, His267, Asp282), and a C-terminal ubiquitin-like (UBL) domain implicated in protein–protein interactions. Early biochemical studies reported weak activity of KY fragments against generic protease substrates such as casein; however, these findings were not reproduced using physiological substrates or cell-based assays, and potential bacterial protease contamination was raised as a confounding factor (Baker et al., 2010).

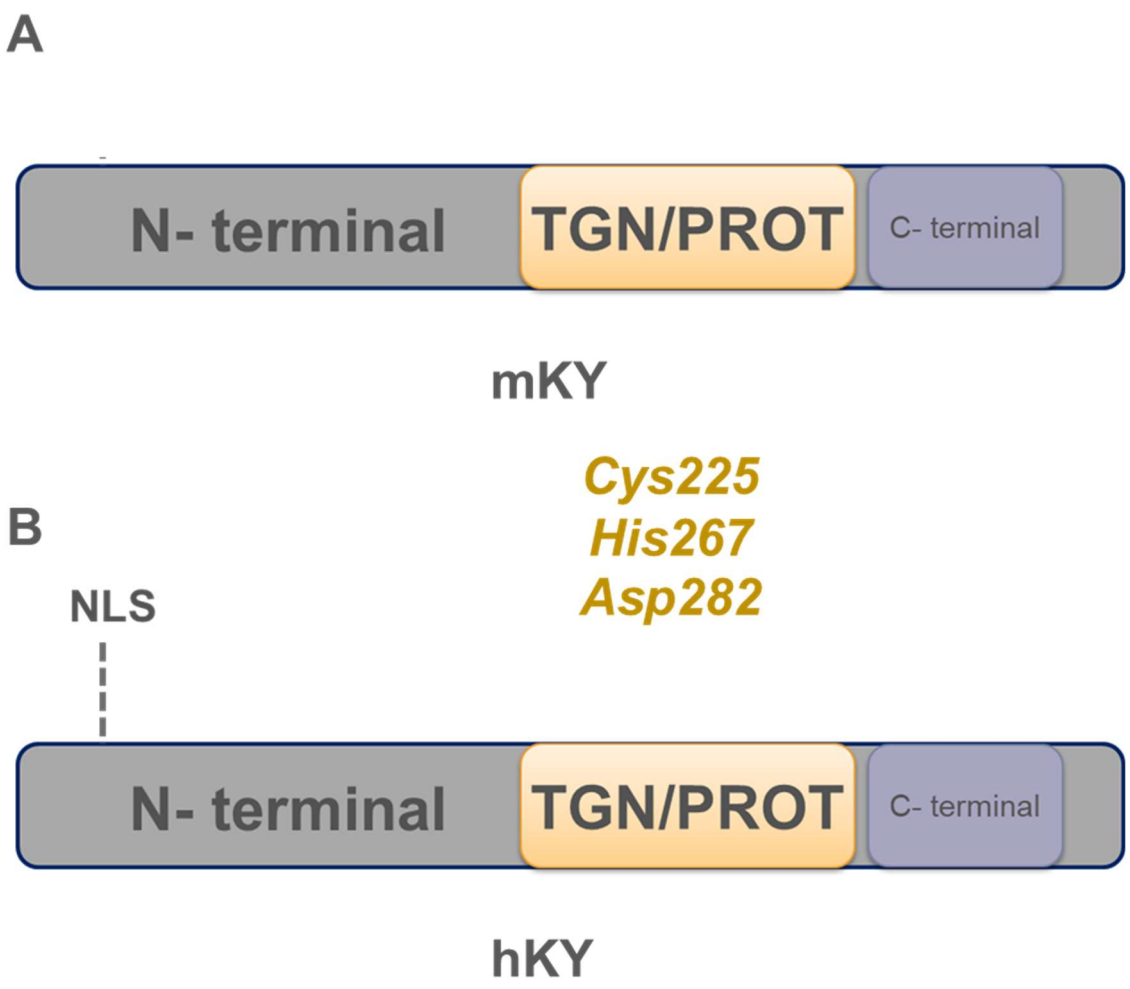

Figure 1.7 Domain structure of KY proteins.

Schematic representation of mouse and human KY proteins illustrating their conserved three-domain organisation. Both proteins comprise an N-terminal region, a central transglutaminase-like/protease (TGN/PROT) domain containing the predicted catalytic triad (Cys225, His267, Asp282), and a C-terminal ubiquitin-like (UBL) domain implicated in protein–protein interactions. The mouse KY protein lacks a nuclear localisation signal (NLS), whereas the human KY protein contains a predicted N-terminal NLS in addition to the conserved TGN/PROT and UBL domains. Together, these domains are hypothesised to mediate KY's structural and regulatory functions at the Z-disc.

These observations argue strongly against intrinsic protease activity *in vivo* and instead support a model in which KY functions as a structural or signalling scaffold. This interpretation is reinforced by its interactions with FLNC and titin at the Z-disc, which position KY within key cytoskeletal and proteostasis pathways.

1.6.1 The *ky /ky* mouse

The *ky/ky* mouse is a spontaneous mutant identified in the BDL strain (Dickinson & Meikle, 1973) and remains the principal model for studying KY deficiency (Blanco et al., 2001). The causative lesion is a two-nucleotide GC deletion that introduces a frameshift and premature stop codon upstream of the TGN/PROT domain. This

mutation triggers nonsense-mediated decay (NMD), resulting in an absence of full-length KY protein and thus representing a true loss-of-function allele.

Phenotypically*, ky/ky* mice develop a progressive myopathy characterised by thoraco-lumbar kyphoscoliosis, impaired muscle maintenance, and loss of postural muscle mass (Mason & Palfrey, 1984). Histological analyses reveal hallmark features of myofibrillar degeneration, including fibre atrophy, central nucleation, fibre-type grouping, regeneration, and necrosis in skeletal muscles such as the back, gracilis, and paraspinal regions (Bridges et al., 1992). Abnormalities in spinal architecture accompany the muscle phenotype, with intervertebral disc degeneration, disc protrusion, and evidence of spinal cord impingement reported at the cervico-thoracic junction (Venn & Mason, 1986).

At the molecular level, *ky/ky* mice show aberrant redistribution of FLNC and Z-disc disorganisation (Beatham et al., 2004), linking KY deficiency directly to defects in cytoskeletal regulation and proteostasis. Because these mice recapitulate the structural, biochemical, and degenerative features observed in human KY-related disease, they form a valuable *in vivo* system for dissecting KY function and evaluating rescue strategies. Within this context, “rescue” refers specifically to restoration of muscle fibre size and structural organisation following reintroduction of KY.

1.6.2 KY deficiency in Human

Pathogenic variants in human *KY* have been associated with a range of neuromuscular disorders, particularly myofibrillar myopathy type 7 (MFM-7) and hereditary spastic paraplegia (HSP) (Arif et al., 2020; Ehsani et al., 2022). The first reported case (Hedberg-Oldfors et al., 2016) involved a homozygous loss-of-function mutation presenting with early-onset muscle weakness and joint contractures. Muscle biopsy demonstrated thickened Z-discs, targetoid inclusions, and small nemaline rods, although the kyphoscoliosis that was prominent in the murine model was absent.

Subsequent reports have broadened the phenotypic spectrum (Yogev et al., 2017) described individuals with biallelic *KY* mutations exhibiting progressive spastic paraplegia and distal muscle weakness, with some displaying spinal deformity. Additional cases have reported congenital myopathy, hypotonia, and contractures (Sarnat, 2020; Straussberg et al., 2016). Despite phenotypic variability, shared pathological features include myofibre atrophy, core-like lesions characterised by disrupted mitochondrial and myofibrillar organisation, and abnormalities in Z-disc structure.

Human and mouse KY share a high degree of sequence conservation (identity ~90.5%; similarity ~94.7%) (Altschul et al., 1997; Blanco et al., 2001), implying conserved functional roles across species. Notably, both species frequently carry

truncating mutations in early exons (e.g., c.72delCG, c.51_52ins28; Figure 1.8), which lie upstream of the TGN/PROT domain and result in NMD and absence of KY protein.

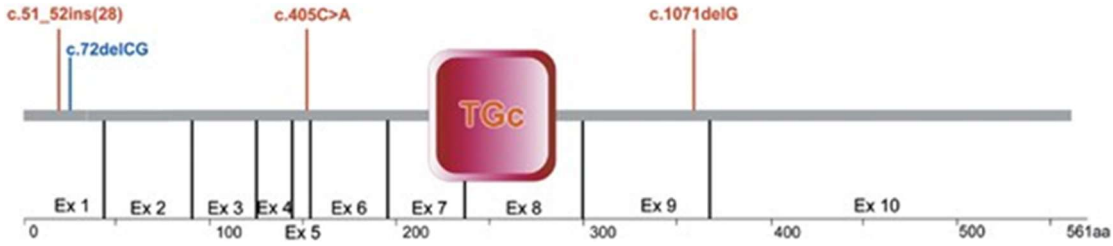

Figure 1.8 Schematic representation of reported KY gene mutations associated with neuromuscular disorders.

The diagram shows the exon structure of the KY) gene, consisting of 10 exons (Ex1–Ex10), aligned to a protein length scale of 561 amino acids (aa). The locations of several known pathogenic variants are highlighted, including c.51_52ins(28), c.72delCG, c.405C>A, and c.1071delG. These mutations are distributed across various exons, with their positions indicated above the respective exon. The transglutaminase-like catalytic domain (TGc) is shown spanning exons 6–8. This domain is critical for the putative enzymatic function of KY and is a common hotspot for disease-associated variants. Scale is approximate in amino acid positions.

Collectively, experimental and clinical evidence points to a conserved pathogenic mechanism in which loss of KY disrupts Z-disc integrity and proteostasis, leading to progressive myofibrillar degeneration. While species-specific modifiers may influence the severity and presentation of disease, the underlying molecular defect appears shared. These observations highlight the need to further characterise KY's structural domains, interacting partners, and involvement in stress-responsive and proteostasis pathways.

1.7 ZAKβ: A Candidate Interactor in the KY Pathway

The decision to investigate ZAKβ originated from converging evidence suggesting a functional connection between KY and Z-disc–associated mechanotransduction pathways. Proteomic data identified IGFN1 as a shared interactor of both KY and ZAKβ, indicating that these proteins may participate in a common signalling complex at the Z-disc (Baker et al., 2010; A. Stonadge et al., 2023). ZAKβ is a stress-activated kinase that localises to the Z-disc and is activated by mechanical stretch, where it phosphorylates downstream MAPK effectors such as p38 and JNK to mediate adaptive responses to load (Chang et al., 2016; Liu et al., 2000a). Given that KY deficiency results in impaired proteostasis and reduced capacity for force adaptation, ZAKβ emerged as a strong mechanistic candidate linking mechanical sensing to protein quality control.

Importantly, both KY and ZAKβ deficiencies lead to the accumulation of Z-disc proteins such as filamin C and BAG3, hallmark features of myofibrillar myopathy (Huang et al., 2009; A. Stonadge et al., 2023). Furthermore, ZAKβ has been implicated in regulating muscle size through kinase-dependent modulation of stress pathways, including negative regulation of hypertrophy (Huang et al., 2009), which mirrors the fibre size defects observed in KY models. These shared structural localisations, interacting

partners, and pathological phenotypes strongly support the hypothesis that KY and ZAKβ operate within the same proteostatic network.

Therefore, studying ZAKβ in the context of KY deficiency is not only justified but essential to determine whether KY functions upstream, downstream, or in parallel with ZAKβ in regulating mechanosensitive signalling and autophagy at the Z-disc. This forms a key mechanistic aim of the thesis.

1.8 C2C12 Cell Line as a Model for Skeletal Muscle Research

To investigate these molecular processes in a controlled environment, *in vitro* models such as the C2C12 myoblast cell line are widely used in skeletal muscle research due to their ability to differentiate into myocytes under specific culture conditions (Isayeva et al., 2023). The C2C12 cell line is a valuable model for studying skeletal muscle diseases and metabolism. It offers an efficient alternative to animal models for investigating cellular and molecular events in muscular dystrophies (Liang et al., 2016). C2C12 cells can differentiate into myocytes under specific culture conditions, allowing researchers to study various stages of myogenesis and their regulatory mechanisms. The differentiation process of C2C12 cells involves the formation of myotubes and the expression of muscle-specific proteins such as myogenin, α-actin, and myosin (Isayeva et al., 2023). Optimised protocols for C2C12 culture, transfection, and differentiation have been developed to enhance research efficiency (LESMANA et al., 2019; Liang et al., 2016). These advancements make C2C12 cells an indispensable tool for studying skeletal muscle diseases and developing potential treatments.

While C2C12 cells remain a standard murine model for *in vitro* myogenesis, several alternative systems offer enhanced physiological relevance to human muscle biology. Primary human satellite cells, which can now be commercially sourced or isolated from biopsy samples, provide a direct human counterpart to C2C12 cells. These cells retain their native capacity for proliferation and differentiation, forming multinucleated myotubes that closely mimic *in vivo* muscle fibre organisation (Bentzinger et al., 2012). However, their limited lifespan and donor variability pose challenges for reproducibility and long-term experiments.

Another powerful alternative involves induced pluripotent stem cells (iPSCs), which can be reprogrammed from adult somatic cells, such as fibroblasts using defined transcription factors (Takahashi & Yamanaka, 2006). Through directed differentiation protocols, iPSCs can be guided into the myogenic lineage by transient expression of master regulators like *MyoD* or *PAX7*, generating expandable populations of human myoblasts (Chal & Pourquié, 2017; Hicks et al., 2018). These iPSC-derived myoblasts not only model early myogenesis but can also capture patient-specific genetic backgrounds, making them highly suitable for disease modelling, drug screening, and regenerative medicine research. These complementary systems C2C12, primary

satellite cells, and iPSC-derived myoblasts, provide a spectrum of models that enable comprehensive investigation of muscle differentiation, pathology, and repair mechanisms.

1.9 Research Gap and Significance

Despite advances in muscle biology, the functional role of the KY protein in muscle maintenance, proteostasis, and cellular stress responses remains poorly defined. Although KY has been identified as a Z-disc-associated protein critical for muscle integrity (Baker et al., 2010). Its precise mechanistic involvement in pathways such as autophagy, protein degradation, and cellular stress adaptation is still unresolved.

Studies in zebrafish have implicated KY in proteostasis regulation, with KY deficiency resulting in the upregulation of CASA components such as BAG3 and FLNC. (Jokl et al., 2018). This finding suggests a broader role in protein quality control beyond structural anchoring. However, the physiological relevance of this function in mammalian muscle, particularly under stress conditions or in disease contexts, has not been clearly demonstrated.

One significant knowledge gap lies in defining KY's contribution to the autophagy–lysosome pathway. Evidence from proteostasis-related studies indicates that KY deficiency may influence the activation of chaperone-assisted autophagy and stress response mechanisms (Jokl et al., 2018; Arndt et al., 2010; Ulbricht et al., 2013). However, it remains unclear whether KY directly participates in autophagosome formation, cargo recruitment, or the regulation of autophagic flux. To date, no studies have systematically examined KY's potential interaction with core autophagy regulators such as LC3 or explored how pharmacological modulation of autophagy and proteasomal pathways affects its localisation or function. Clarifying these relationships is critical for understanding whether KY acts as an upstream regulator of proteostasis or as a downstream effector responding to cellular stress.

Importantly, while KY-deficient models consistently display increased protein accumulation and structural degeneration, the mechanisms driving this phenotype remain elusive. Whether KY actively modulates proteostasis or instead functions downstream of degradation pathways is not known. Clarifying this distinction is essential for understanding its contribution to muscle pathology (Beatham et al., 2004; Jokl et al., 2018; Blanco et al., 2001).

In addition, KY's role in muscle remodelling and maintenance, particularly in the context of muscle fibre size, has not been rigorously examined. This study addresses this gap by investigating whether wild-type KY or catalytically inactive constructs (generated through alanine substitution of conserved histidine, cysteine, and aspartate residues) or deletion of the (TGN/PROT) domain can rescue reduced fibre size in KY-deficient muscle. While fibre CSA is used as a quantitative measure, it is interpreted

here as a marker of maintenance or recovery, rather than as an indicator of active hypertrophy.

Another underexplored area is KY's localisation and behaviour under proteotoxic stress, such as heat shock, which may cause protein unfolding and redistribution within the cell. Early findings suggest the formation of KY-positive accumulations, bright cytoplasmic or nuclear speckles under stress, particularly when proteasomal or autophagic degradation is inhibited. However, these accumulations remain uncharacterised and cannot yet be defined as canonical aggregates. Their formation may reflect impaired protein clearance or a potential role for KY in sensing or responding to proteostasis collapse.

To better understand KY's role in autophagy, GFP–LC3–RFP–LC3ΔG reporters were employed in both *in vitro* and *in vivo* models to assess autophagic flux. Western blotting was used to validate the accumulation of autophagy markers, offering an independent readout of flux efficiency in KY-deficient cells and tissues. These experiments aim to establish whether KY modulates autophagy under nutrient deprivation or basal conditions, or if its absence results in stalled or inefficient flux.

To complement the *in vivo* studies, in silico structural modelling was used to evaluate the predicted consequences of deleting the TGN domain or mutating the conserved catalytic triad. This modelling allows for predictions about domain stability, loss of structural interfaces, or disrupted binding with putative partners—findings that may explain the *in vivo* rescue phenotypes.

Finally, this work explores a potential regulatory crosstalk between KY and the signalling kinase ZAKβ, based on shared interactors such as IGFN1 and their Z-disc localisation. Motivated by the finding that ZAKβ can induce muscle fibre hypertrophy even in wild-type muscle, investigating whether KY is required for or modulates this response may provide new insights into stress-induced muscle remodelling. Collectively, these studies aim to define KY's role in signalling, proteostasis, and the maintenance of muscle structure–function relationships.

In summary, this thesis addresses several critical and previously uncharacterised aspects of KY biology by:

- Evaluating KY protein localisation dynamics in cells under thermal stress to understand its role in stress adaptation and presumed protein aggregation.
- Defining KY's contribution to autophagy regulation and proteostasis maintenance, particularly under basal and pharmacologically inhibited conditions.
- Characterising the functional relevance of the TGN/PROT domain through point mutations and domain deletions *in vivo*.
- Investigating KY's necessity for the maintenance of normal muscle fibre size and its potential role in regulating fibre growth.
- Identifying KY protein–protein interactions, especially with autophagy-related proteins and the kinase ZAKβ, to uncover signalling crosstalk.

- Integrating *in silico* structural modelling with *in vivo* and *in vitro* functional analyses to interpret the consequences of domain loss or mutation.

This multi-level approach provides novel insight into the molecular and functional significance of KY in skeletal muscle maintenance and disease, potentially uncovering therapeutic targets for myofibrillar myopathies and related neuromuscular conditions.

1.10 Hypotheses and Objectives

The key hypotheses derived from the research gaps above were addressed systematically across distinct experimental chapters. The table below maps each question to the corresponding methodology and results chapter, highlighting how the project's objectives were operationalised.

Table 1-2 Overview of Research Questions, Experimental Approaches, and Corresponding Results Chapters

Research Question / Hypothesis	Experimental Approach	Results Chapter
Does KY respond to cellular stress and change localisation under heat shock?	Cellular heat-shock assays, fluorescence microscopy of KY constructs	**Chapter 3**
Does KY interact with autophagy or proteasome pathways?	Bafilomycin A1 and MG132 treatments, imaging analysis	**Chapter 3**
Is the TGN/PROT domain essential for maintaining muscle fibre size?	*In vivo* electroporation of ΔTGN, and catalytic-mutant KY constructs into *ky/ky* mice	**Chapter 4**
Is the TGN/PROT domain necessary for Z-disc localisation?	Colocalisation with α-actinin and titin	**Chapter 5**
What are the structural consequences of domain mutation or deletion?	In silico prediction (AlphaFold, ChimeraX)	**Chapter 6**
What proteins interact with KY in skeletal muscle?	Immunoprecipitation–mass spectrometry, Western validation	**Chapter 7**
Does KY regulate autophagic flux under basal and stress conditions?	GFP-LC3–RFP-LC3ΔG reporters, Western blot analysis of LC3 isoforms	**Chapter 8**
Does KY modulate ZAKβ-driven hypertrophic signalling?	ZAKβ^CA electroporation in wild-type and *ky/ky* mice	**Chapter 9**

This mapping clarifies the experimental logic connecting the overarching hypotheses to specific data chapters, ensuring transparency and continuity throughout the thesis.

CHAPTER TWO:

Methods

CHAPTER 2. Materials and Methods

2.1 Buffer and Reagents

Table 2-1 Shows Buffers and Reagents Used in Experiments

Type	Composition	Source
Cell Culture Medium (DMEM)	DMEM containing 4.5 g/L glucose, L-glutamine, and sodium pyruvate	Gibco, Life Technologies (Cat# S41966-029)
Growth Medium (GM)	DMEM supplemented with 10% fetal bovine serum (FBS) and 100 U/mL penicillin/streptomycin	Prepared in-house
Differentiation Medium (DM)	DMEM with 2% FBS and 100 U/mL penicillin/streptomycin	Prepared in-house
Cell Freezing Medium	Complete growth medium containing 5% (v/v) dimethyl sulfoxide (DMSO)	Prepared in-house
10X Western Running Buffer	25 mM Tris, 192 mM glycine, 0.1% (w/v) SDS in distilled water	Prepared in-house
10X Western Transfer Buffer	25 mM Tris, 192 mM glycine in distilled water (diluted 1:2:7 with methanol and water)	Prepared in-house
Western Wash Buffer (PBST)	1X PBS containing 0.1% (v/v) TWEEN-20	Prepared in-house
Mowiol-DAPI Mounting Medium	24 g glycerol (Sigma #G6279), 9.6 g Mowiol 4-88 (Fluka #81381), 24 mL distilled water, 48 mL 0.2 M Tris (pH 8.5), DAPI 1:1000 (Thermo #62248)	Prepared in-house
MG132	10 µM dissolved in dimethylsulfoxide	Calbiochem (San Diego, CA, USA)
BafA1	100 nM final concentration dissolved in dimetylsufoxide	Calbiochem (San Diego, CA, USA)
TransIT-X2® Dynamic Delivery System	he delivery of plasmid DNA, siRNA/miRNA and CRISPR/Cas9 components	MIR 6004
Dynabeads™ Protein G Immunoprecipitation Kit	2 mL Dynabeads Protein G 16 mL Antibody (Ab) Washing and Binding buffer 28 mL Washing Buffer 1 mL Elution Buffer	10007D
DNA, RNA, and protein purification		M04013A
RIPA Buffer		R0278

Western blocking buffer	5% (w/w) dried skimmed milk dissolved in PBS, supplemented with 0.1% (v/v) TWEEN 20.	Prepared in-house
Western washing buffer (PBST)	PBS containing 0.2% (v/v) TWEEN 20.	Prepared in-house
Immunofluorescence blocking buffer	3% (w/w) Bovine Serum Albumin in PBST, with 0.05% (v/v) Triton X-100 added.	Prepared in-house
Western blocking buffer	5% (w/w) dried skimmed milk dissolved in PBS or TBS, supplemented with 0.1% (v/v) TWEEN 20.	Prepared in-house
Trypsin	0.5% Trypsin-EDTA (10x)	Gibco 15400-054

2.2 Antibodies

Details of all primary and secondary antibodies used are provided in (Table 2.2, Table 2.3). Antibodies were selected for compatibility with Western blotting and immunofluorescence.

2.2.1 Primary

Table 2-2 Primary Antibodies Used for detection in Experiments

Antibody Target/Type	Supplier	Product Code	WB Concentration	IF Concentration
Anti-GFP	Roche	11 8144 460 001	1:1000	1:1000
Anti-GFP serum	Invitrogen	A6455	Not specified	1:1000
Anti-RFP	Abcam	Ab28664	Not specified	1:1000
Anti-RFP	Rockland Immunochemical	600-401-379-RTU	5:1000	1:1000
Anti PPM1B	proteintech	67647	1:1000	1:200
Anti-GAPDH	Sigma	G9295	1:50,000	N/A
Anti-α-actinin	Abcam	EA-53	1:400	1:300
Anti β-Actin	Santa Cruz Biotechnology	E2422	1:10000	
Anti Titin	Biocompare	9D10	Not specified	1:200

2.2.2 Secondary Antibodies Used for Detection

Table 2-3 Shows Secondary Antibodies Used for Detection.

Target	Catalog Number	Company	WB Dilution	Immunofluorescence Dilution
Anti-Mouse IgG (HRP)	sc-2134	Santa Cruz Biotechnology	1:10,000	Not applicable
Anti-Mouse IgA (HRP)	sc-3791	Santa Cruz Biotechnology	1:10,000	Not applicable
Anti-Rabbit IgG (HRP)	sc-2030	Santa Cruz Biotechnology	1:10,000	Not applicable
Anti-Rabbit IgG (FITC)	ab6717	Abcam	Not applicable	1:100
anti mouse IgG (HRP)	40323-2	Santa Cruz Biotechnology	1:10,000	Not applicable
Anti-Rabbit IgG (TRITC)	ab6718	Abcam	Not applicable	1:100
Anti-Mouse IgG (FITC)	ab6785	Abcam	Not applicable	1:100
Anti-Mouse IgG (TRITC)	ab6786	Abcam	Not applicable	1:100
Anti-Mouse IgA (FITC)	ab97234	Abcam	Not applicable	1:100
AlexaFluor 488 anti-rabbit	R37116	Invitrogen	Not applicable	1 drop per ml
AlexaFluor 488 anti-mouse IgG-FITC	R37120	Invitrogen	Not applicable	1 drop per ml
Goat anti-mouse IgM+TRITC	F9006	Sigma	Not applicable	1:150
Goat anti-mouse IgA-FITC	A857234	Abcam	Not applicable	1:150

2.3 Plasmid Constructs and Expression Vectors

To investigate the functional role of KY in skeletal muscle structure, proteostasis, and hypertrophic growth, a series of mammalian expression vectors was employed. These vectors were designed to enable transient overexpression of full-length human KY fused to fluorescent reporters, allowing live and fixed-cell localisation analyses as well as *in vivo* rescue experiments in the KY-deficient mouse model. Empty vector controls expressing either GFP or tdTomato fluorophores alone were used to distinguish KY-specific effects from non-specific influences of fluorophore expression.

2.3.1 pcDNA-DEST47_GFP (Empty Vector Control)

The pcDNA-DEST47_GFP plasmid (6204 bp; Invitrogen) is a Gateway®-compatible mammalian expression vector designed for high-level expression of C-terminally eGFP-tagged proteins. It contains a cytomegalovirus (CMV) immediate-early promoter, an SV40 origin of replication for episomal maintenance in mammalian cells, and an ampicillin resistance cassette for bacterial selection. The vector also includes attR1 and attR2 recombination sites, enabling insertion of coding sequences via LR Clonase–mediated recombination (Figure 2.1).

In this study, the empty GFP vector was used as a negative control in C2C12 transfection assays and *in vivo* tibialis anterior electroporation experiments. Its inclusion allowed discrimination between effects arising from KY construct expression and those attributable solely to CMV-driven overexpression or GFP fluorescence. This ensured accurate interpretation of downstream phenotypes, including muscle fibre morphology, proteostasis, and Z-disc organisation (Beatham et al., 2004; Baker et al., 2010).

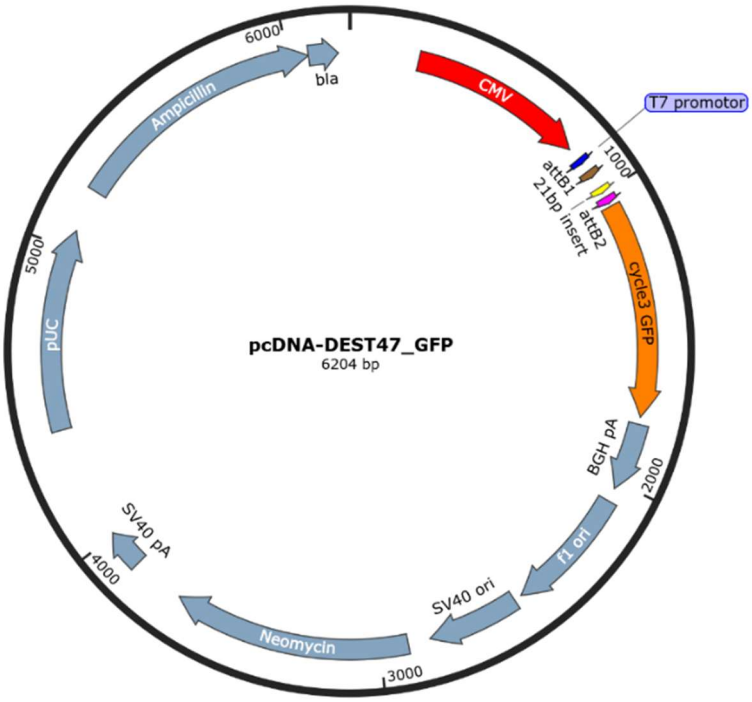

Figure 2.1 Map of the pcDNA-DEST47_GFP plasmid (6204 bp).

Schematic representation of the pcDNA-DEST47_GFP mammalian expression vector. The plasmid features a CMV promoter for strong expression of C-terminally GFP-tagged proteins, an attR1-attR2 cassette for Gateway® LR recombination, an SV40 origin, and an ampicillin resistance gene for bacterial selection. In this study, the empty GFP vector served as a negative control for both in vitro and in vivo experiments, allowing assessment of baseline effects of GFP expression independent of KY constructs (Beatham et al., 2004; Baker et al., 2010)

2.3.2 pcDNA-DEST47_tdTomato (Empty Vector Control)

The pcDNA-DEST47_tdTomato_empty plasmid (7018 bp) is structurally equivalent to pcDNA-DEST47_GFP but encodes a C-terminal tdTomato fluorescent protein instead of eGFP. The construct retains the CMV immediate-early promoter for high-level mammalian expression, an SV40 origin for episomal replication, an ampicillin resistance cassette for bacterial selection, and attR1/attR2 recombination sites enabling Gateway® LR-mediated cloning (Figure 2.2).

In this study, the tdTomato empty vector served as a fluorescent control for red reporter expression in both C2C12 myoblasts and *in vivo* tibialis anterior electroporation assays. Its use, alongside the GFP empty vector, allowed fluorophore-independent validation of KY behaviour. This ensured that any observed Z-disc localisation, proteostasis-related changes, or fibre-size rescue effects were attributable to KY and not to tdTomato expression alone (Baker et al., 2010; A. Stonadge et al., 2023).

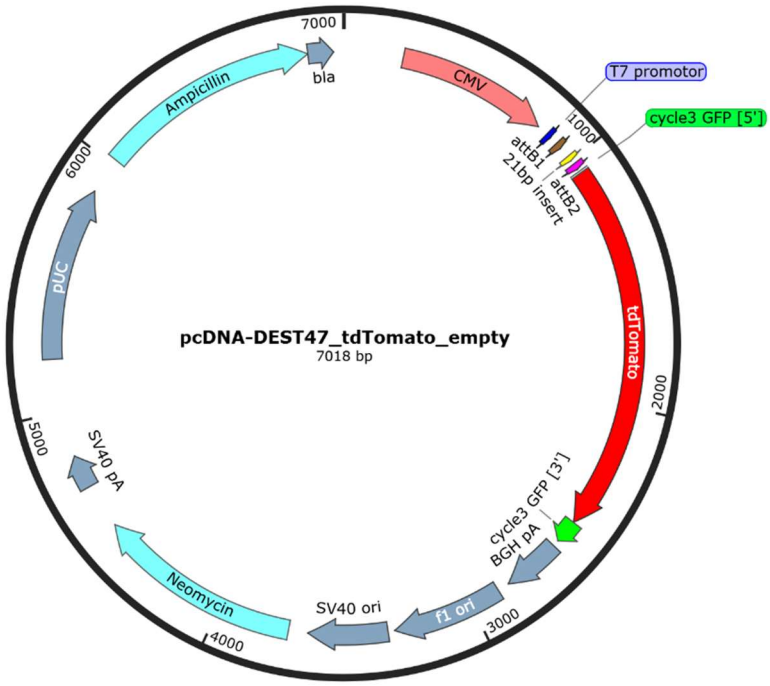

Figure 2.2 Map of the pcDNA-DEST47_tdTomato_empty plasmid (7018 bp).

This plasmid expresses C-terminal tdTomato under the control of the CMV promoter. It contains the SV40 origin of replication for mammalian episomal maintenance, a β-lactamase (ampicillin) resistance gene for bacterial selection, and attR recombination sites that permit Gateway® cloning of inserts. In this thesis, the empty tdTomato vector was used as a red-fluorescent control to distinguish fluorophore-dependent effects from KY-dependent localisation or hypertrophic responses during in vitro transfection and in vivo electroporation experiments (Baker et al., 2010).

2.3.3 pCT31_HumanKY_GFP (Full-Length KY-eGFP Fusion Vector)

The pCT31_HumanKY_GFP plasmid encodes full-length human KY (2055 bp) fused in-frame to a C-terminal enhanced GFP (eGFP) reporter. The construct preserves all major KY structural features, including the conserved TGN/PROT-like domain, thereby enabling assessment of domain-dependent localisation and function in mammalian cells. Expression is driven by a (CMV) promoter, and the plasmid carries an ampicillin resistance cassette for bacterial selection (Figure 2.3). This construct was used to evaluate three key questions:

(i) whether human KY localises correctly to the Z-disc in mammalian muscle.

(ii) whether re-expression of full-length KY can rescue muscle fibre atrophy in ky/ky mice; and

(iii) whether KY influences proteostasis pathways in muscle cells.

Expression and localisation of KY–GFP were validated through direct fluorescence, Western blotting, and co-localisation analyses with Z-disc markers α-actinin and titin in both C2C12 myotubes and *in vivo* electroporated tibialis anterior muscle. The construct therefore served as the primary full-length rescue vector for testing KY function at the structural and proteostasis levels (Harrad, 2021).

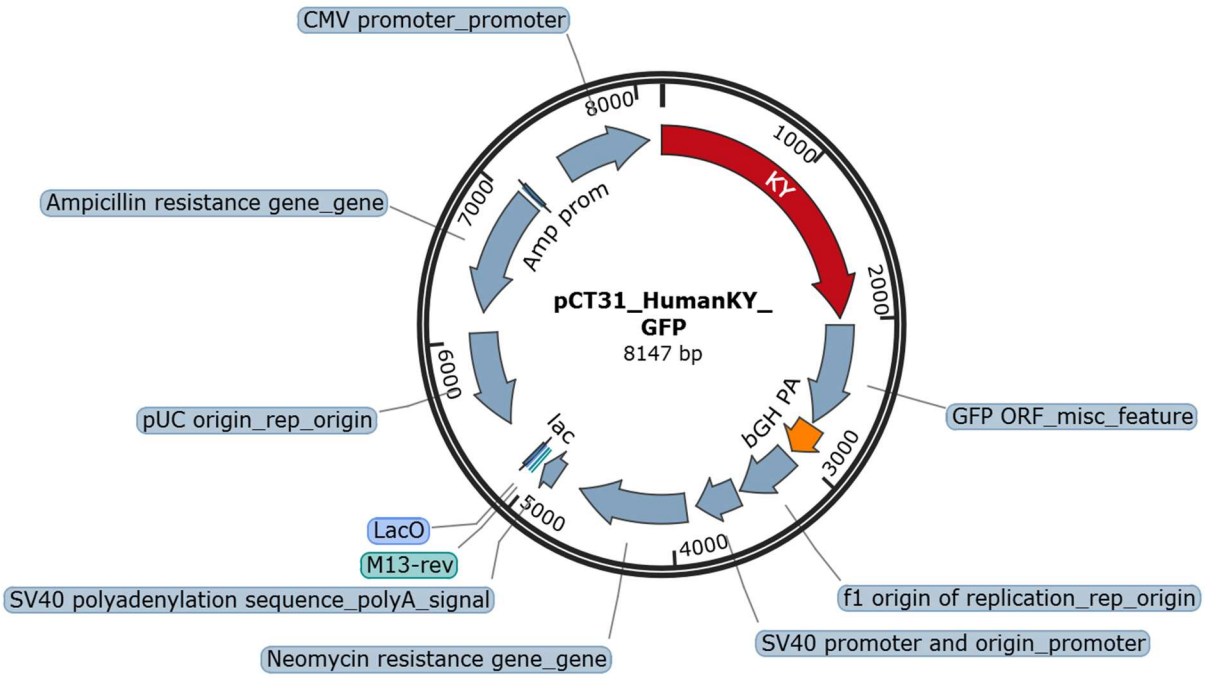

Figure 2.3 Map of the pCT31_HumanKY_GFP plasmid.

The pCT31_HumanKY_GFP construct contains full-length human KY (2055 bp), cloned in-frame with a C-Schematic map of the pCT31_HumanKY_GFP expression vector (8147 bp). The plasmid contains the CMV promoter for robust mammalian expression, the full-length human KY coding sequence fused to a C-terminal GFP tag, an F1 origin of replication, and an ampicillin resistance gene. The construct preserves the entire KY open reading frame, including the conserved TGN/PROT domain, enabling assessment of full-length KY function in vitro and in vivo. This vector was used to examine KY localisation, fibre-size rescue in ky/ky skeletal muscle, and potential involvement of KY in proteostasis through interactions with Z-disc–associated proteins such as FLNC, BAG3, and IGFN1 (Beatham et al., 2004; Harrad,202; Baker et al., 2010).

2.3.4 pDEST47-tdTomato_KY (Full-Length KY-tdTomato Fusion Vector)

The pDEST47-tdTomato_KY plasmid was generated using Gateway® LR recombination to insert full-length human KY downstream of the CMV immediate-early promoter and in-frame with a C-terminal tdTomato reporter. This construct mirrors the design of the KY-GFP vector but incorporates tdTomato as an alternative fluorophore, allowing assessment of KY localisation and behaviour independently of GFP tagging. Expression of the tdTomato-tagged KY fusion enables live-cell visualisation and

facilitates comparative imaging in both *in vitro* C2C12 assays and *in vivo* electroporated tibialis anterior muscle (Figure 2.4).

This construct was used to evaluate whether full-length KY localises to the Z-disc, to assess its capacity to rescue reduced fibre size in KY-deficient (*ky/ky*) muscle, and to visualise KY distribution during cellular stress. Validation of KY–tdTomato expression was confirmed by fluorescence microscopy and Western blotting, and co-localisation studies were performed using α-actinin and titin to examine Z-disc targeting.

The inclusion of the full-length KY coding sequence preserves all major structural features, including the conserved TGN/PROT-like domain, enabling comparison of tdTomato- and GFP-tagged KY constructs. Together with the other plasmids used in this study, pDEST47-tdTomato_KY contributed to examining whether re-expression of intact KY can restore aspects of normal muscle fibre morphology and subcellular organisation in KY-deficient models (Blanco et al., 2001; Baker et al., 2010).

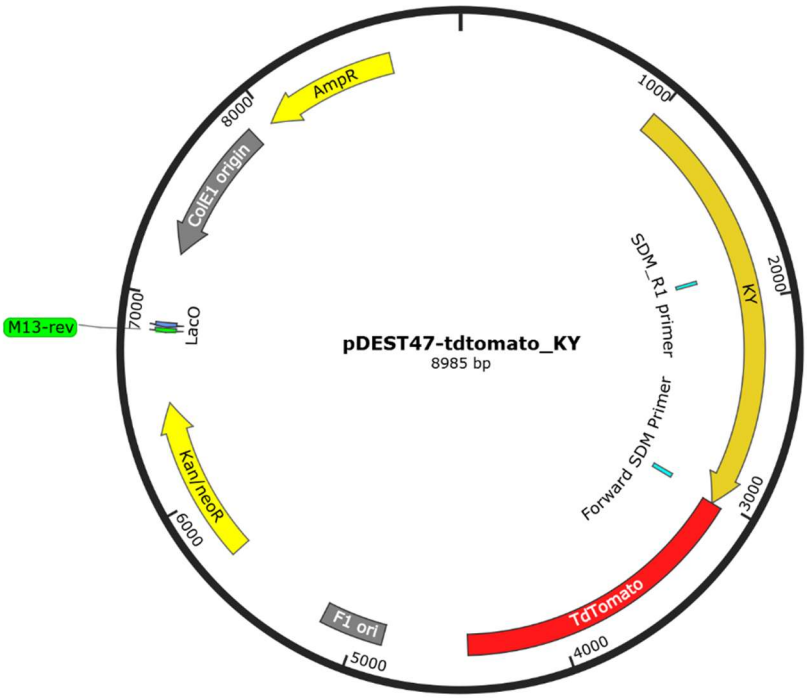

Figure 2.4 Map of the pDEST47-tdTomato_KY plasmid.

This plasmid contains full-length human KY fused at the C-terminus with tdTomato, permitting live-cell imaging of KY dynamics under mechanical stress. The CMV promoter drives robust expression in mammalian cells and in mouse muscle following in vivo electroporation. This construct was used to evaluate KY-mediated rescue of Z-disc structural integrity, localisation in relation to α-actinin and titin, and the capacity of full-length KY to promote muscle hypertrophy in KY-deficient mouse muscle fibres. This plasmid was also used in parallel with GFP-tagged constructs to validate that KY localisation is independent of fluorophore type. The experimental rationale is based on the established role of KY as a Z-disc scaffold protein required for turnover of FLNC and maintenance of sarcomeric stability (Blanco et al., 2001)

All constructs were selected based on previous research demonstrating that mutations in KY cause myofibrillar myopathy and impair muscle hypertrophic responses (Blanco et al., 2001). As KY is a non-enzymatic Z-disc protein, its function is hypothesised to be mediated through scaffolding interactions with regulatory proteins such as FLNC and BAG3, which are central to the autophagic turnover of damaged sarcomeric proteins (Otey et al., 2009; Baker et al., 2010). The vectors used in this study enabled mechanistic assessment of whether reintroduction of full-length KY can restore Z-disc integrity, rescue hypertrophic capacity, and normalise proteostasis in KY-deficient muscle.

2.3.5 Zak plasmid

To investigate the localisation, signalling activity, and functional role of ZAKβ in muscle cells, the ZAKβ-pDEST47_tdTomato_VERIFIED construct was used. This Gateway®-compatible pDEST47-based plasmid drives high-level expression of full-length ZAKβ fused in-frame with a C-terminal tdTomato fluorescent reporter under control of the (CMV) immediate early promoter. The tdTomato tag enables real-time visualisation of ZAKβ distribution, facilitating analysis of its localisation and behaviour in both C2C12 myoblasts and electroporated mouse skeletal muscle.

The vector contains the ampicillin resistance cassette for bacterial selection, the ColE1 origin for plasmid propagation in E. coli, and the SV40 polyadenylation signal to promote efficient mRNA termination and stability in mammalian cells. The ZAKβ coding sequence is flanked by Gateway® attR recombination sites, allowing efficient and directional LR clonase–mediated insertion during construct generation (Figure 2.5) (A. Stonadge et al., 2023).

This plasmid was used to assess ZAKβ-dependent signalling *in vitro* and to evaluate its capacity to influence muscle fibre size, stress-responsive pathways, and subcellular localisation patterns *in vivo*.

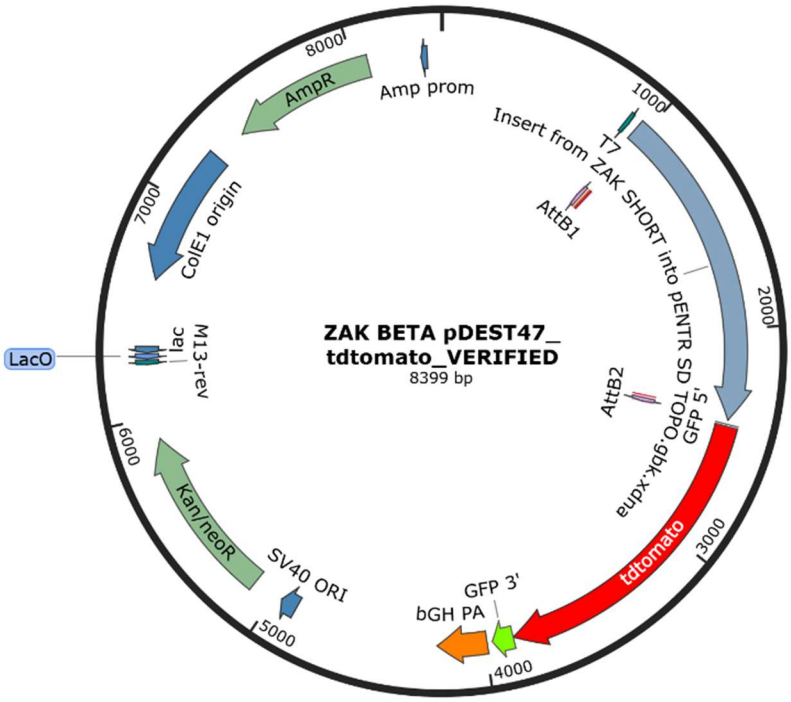

Figure 2.5 This figure shows the circular pDEST47-based construct encoding full-length ZAKβ fused to a C-terminal tdTomato reporter.

The CMV promoter drives robust expression of the ZAKβ-tdTomato fusion protein in mammalian cells. The plasmid contains attR1 and attR2 Gateway® recombination sites used for LR clonase–mediated insertion of the ZAKβ open reading frame. Additional backbone elements include the ampicillin resistance gene for selection in bacteria, the ColE1 origin of replication for plasmid propagation, and the SV40 polyadenylation signal to ensure efficient transcript termination. This construct enables fluorescent visualisation of ZAKβ and supports functional studies in both cultured cells and electroporated skeletal muscle (A. Stonadge et al., 2023).

2.3.6 Autophagy reporter plasmid.

The GFP-LC3 / RFP-LC3ΔG dual-reporter plasmid was used to monitor autophagic flux *in vitro* and *in vivo* (Kaizuka et al., 2016). The GFP-LC3 module encodes a full-length LC3 fusion protein that retains its C-terminal glycine, allowing lipidation (LC3-II formation) and recruitment to autophagosomal membranes. In contrast, the RFP-LC3ΔG module lacks this terminal glycine, cannot undergo lipidation, and therefore remains diffuse within the cytoplasm, serving as a non-lipidatable internal reference.

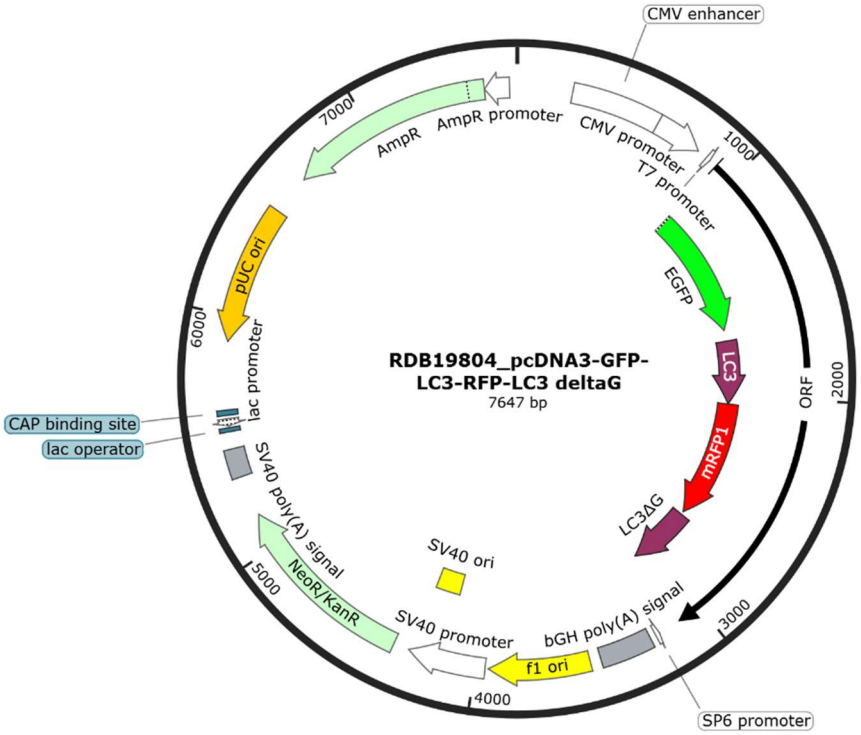

Figure 2.6 Schematic map of the GFP-LC3 / RFP-LC3ΔG autophagy flux reporter plasmid

This figure illustrates the dual-cassette plasmid encoding both GFP-LC3 and the non-lipidatable mutant RFP-LC3ΔG (deletion of the terminal glycine required for LC3 conjugation). Each reporter is driven by its own CMV promoter and terminated by a bovine growth hormone (bGH) polyadenylation signal (CMV→Kozak→GFP-LC3→bGH-polyA; CMV→Kozak→RFP-LC3ΔG→bGH-polyA). The plasmid backbone includes a ColE1 origin and an ampicillin resistance gene for bacterial propagation. This construct enables measurement of autophagic flux by comparing GFP-LC3 puncta formation to the constitutively diffuse RFP-LC3ΔG signal in myoblasts and electroporated mouse skeletal muscle (Kaizuka et al., 2016).

The vector contains two independent CMV-driven expression cassettes (CMV→Kozak→GFP-LC3→bGH polyA; CMV→Kozak→RFP-LC3ΔG→bGH polyA), allowing equimolar and independent expression of both reporters within the same cell. For bacterial propagation, the plasmid includes an ampicillin resistance gene and a ColE1 origin of replication. All constructs were sequence-verified prior to use to confirm the integrity of the LC3 and LC3ΔG open reading frames (Figure 2.6) (Kaizuka et al., 2016).

This reporter system allows quantitative analysis of autophagic activity by comparing autophagosome-associated GFP-LC3 puncta to the stable cytosolic RFP-LC3ΔG signal. It was used to assess autophagic flux in C2C12 myoblasts and in electroporated tibialis anterior muscle fibres.

2.4 PCR Primers

In this study, gene-specific primers were designed based on (Mus musculus NP_077253.3), NCBI GenBank) to target specific gene regions kyphoscoliosis peptidase. The primers were designed by Primer-BLAST NCBI to ensure high purity. The details of primer sequences are provided in (Table 2.4).

Table 2-4 Shows the list of primers used for genotyping

Primer	Sequence	Objective
Mouse Ky Forward 330bp	5'GGGGCCATTTGCAGCCTA	Genotyping the Ky colony
Mouse Ky Reverse 330bp	5'CGGAGAGGTTCGGATTAGCC	Genotyping the Ky colony
Mouse Ky Forward 206bp	5'TCATCGTGCACTCCGAGAAG	Genotyping the Ky colony
Mouse Ky Reverse 206bp	5'GGATTAGCCTCGTTGGGGAG	Genotyping the Ky colony
Mouse Ky Forward 99bp	5'CATCGTGCACTCCGAGAAGC	Genotyping the Ky colony
Mouse Ky Reverse 99bp	5'CGGGTGTTACCTCCTCGGTT	Genotyping the Ky colony
Mouse Ky Forward mutant	5'TCCGAGAAGCGGCGCGCAA	Genotyping the Ky colony

2.5 Reagents and Inhibitor Preparation

MG132 and Bafilomycin A1 (BafA1) were obtained from Calbiochem (San Diego, CA, USA) and dissolved in dimethyl sulfoxide (DMSO; 78.13 g/mol). Stock solutions were freshly diluted in DMEM supplemented with 10% FBS before use. Final concentrations were 10 μM for MG132 and 100 nM for BafA1. DMSO (0.2%) served as a vehicle control. No cytotoxic effects were observed at these concentrations during the 2–3-hour exposure period.

2.6 Cell culture and Treatment

C2C12 myoblasts were cultured in DMEM supplemented with 10% FBS (Gibco, Cat #41966-029) at 37°C in a humidified atmosphere containing 4–5% CO_2. Cells were passaged or processed for experiments upon reaching ~80% confluency.

Cells were detached using 0.05% Trypsin-EDTA (2 mL per 75 cm² flask) for 3–5 minutes at 37°C, neutralised with complete medium, and centrifuged at 200 × g for 5 minutes. The pellet was resuspended and split at a 1:4 ratio into fresh flasks.

C2C12 cells were seeded on coverslips in 24-well plates and grown to ~80% confluency. Transfections were performed using TransIT-X2® Dynamic Delivery System (Cat #MIR 6004) following manufacturer instructions. After 24–48 hours, cells were fixed in 4% formaldehyde for 20 minutes at room temperature. Slides were

mounted using ProLong Glass Antifade Mountant (Invitrogen, Cat #P36983) or Mowiol (Fluka, Cat #81381) with DAPI (1:1000 dilution, Sigma, Cat #D9542).

Cells were subjected to heat stress (42°C for 2–3 hours), MG132 treatment (10 µM, 2 hours), or BafA1 treatment (100 nM, 3 hours). DMSO-treated cells served as controls. Treatments were conducted prior to fixation or lysis. An overview of the treatment timeline is provided in (Figure 2.7).

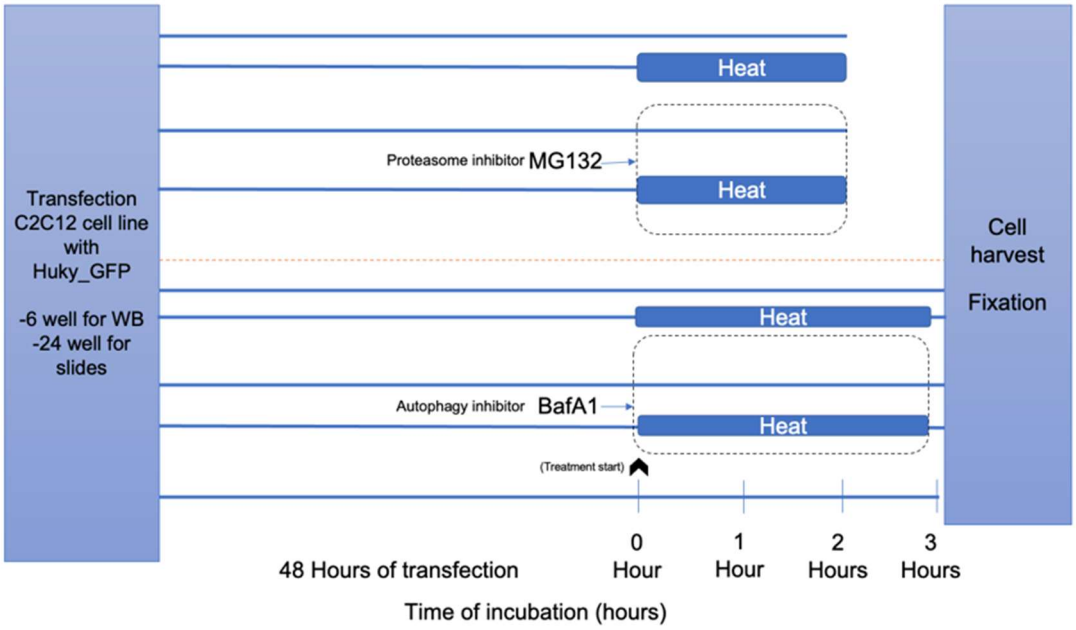

Figure 2.7 Illustrates heat treatment (HT) experimental design.

Transfected C2C12 with hKY were placed into four groups after 48 hours: 37°C, 42°C, 37°C plus MG132 and 42°C plus MG132. Cells were maintained for 2hours under those conditions, then fixed and mounted for microscopy analysis or harvested in RIPA buffer for western blots. A similar set-up was used with the autophagy inhibitor BafA1, but treatment was extended to three hours. The unobstructed lines represent the time spent at 37°C, from the start of the experiment. The grey rectangular boxes represent the time spent at 42°C with MG132 and BafA1or without. The dotted box demonstrates the duration of MG132 and BafA1 treatments.

2.7 Bacterial transformation

Transformation was performed using Zymo 10B chemically competent cells (Zymo Research, Lot No. 164-0123). Cells were incubated on ice with plasmid DNA for 30–45 minutes, heat-shocked at 42°C for 1 minute and recovered in antibiotic-free medium at 37°C for 1 hour with shaking. Transformed cells were plated on LB agar with appropriate antibiotics.

2.8 Genotyping and Heteroduplex Analysis

The *ky* mutation is inherited in an autosomal recessive manner. To maintain the colony and generate experimental *ky/ky* mice, heterozygous carriers (*+/ky*) were bred together, as homozygous pairs (*ky/ky* male × *ky/ky* female*) are infertile and therefore unable to produce offspring. This breeding strategy produced offspring in the expected Mendelian ratios: approximately 25% wild type (+/+), 50% heterozygous (*+/ky*), and 25% homozygous mutant (*ky/ky*).

Phenotypically, *ky/ky* mice can often be distinguished from their wild-type littermates by physical examination, displaying reduced body size, weaker hind-limb reflexes, and a more slender muscle profile compared with +/+ animals. These differences become apparent after weaning, although definitive genotype confirmation was still required to ensure experimental accuracy.

Genotyping was performed using PCR amplification of genomic DNA from ear biopsies collected at weaning (3 weeks of age), followed by heteroduplex analysis on a 15% polyacrylamide gel. PCR reactions were prepared using 12.5 µL GoTaq G2 Green Master Mix, 6.5 µL nuclease-free water, 2.5 µL each of forward and reverse *mKY* primers, and 1–2 µL genomic DNA (total volume = 25 µL). Thermal cycling conditions were: 95 °C for 4 min (initial denaturation), followed by 40 cycles of 95 °C for 30 s, 57 °C for 30 s, and 72 °C for 30 s, with a final extension at 72 °C for 5 min.

Polyacrylamide gels were prepared using 6 mL dH_2O, 1.5 mL 10× TBE, 7.5 mL 30% acrylamide solution, 150 µL 10% APS, and 15 µL TEMED. Gels were polymerised, run overnight at 40–45 V, stained with SYBR Safe, and imaged using a Bio-Rad GelDoc EZ system.

Homozygous and heterozygous alleles were distinguished based on the migration patterns of heteroduplex and homoduplex products, allowing clear identification of *ky/ky*, *+/ky*, and +/+ genotypes. Homozygous *ky/ky* mice showed only the mutant band, wild-type (+/+) mice displayed only the wild-type band, and heterozygotes (*+/ky*) exhibited both. The workflow of the heteroduplex analysis is illustrated in (Figure 2.8)

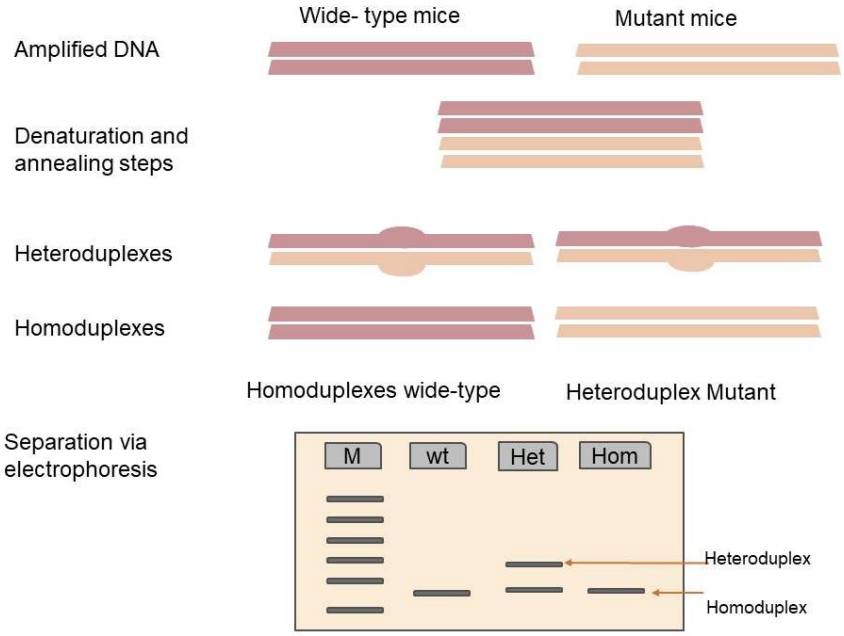

Figure 2.8 illustrates a schematic representation of the principle of the heteroduplex assay.

The amplified DNA now undergoes denaturation, followed by slow reannealing of the denatured alleles, resulting in homoduplex and heteroduplex. The latter migrate more slowly during gel electrophoresis due to their sequence mismatches, so heterozygous (Het) and homozygous (Hom) cases can be easily distinguished from wild type (Wt) based on their electrophoretic pattern. M: Size marker.

Only confirmed heterozygous mice were retained as breeders to sustain the colony and ensure a consistent supply of *ky/ky* experimental animals. This approach enabled efficient colony management and reliable generation of genotype-verified mice while maintaining genetic integrity in accordance with Home Office guidelines.

2.9 DNA Preparation for Electroporation

Plasmids included hKY-GFP, tdTomato, mKY-td-TM (triple mutant), and mKY-td-Del (deletion). DNA was prepared using the NucleoSnap Plasmid Midi Kit (Macherey-Nagel, Cat #740494.50), diluted to 1000–1500 ng/µL. These constructs were previously generated in the Blanco lab.

2.10 Image analysis

Fluorescent images were captured using Nikon Microphot-FXA or LSM880 confocal microscopes. Aggregates were manually counted under blinded conditions. For longitudinal sections, ImageJ software was used for quantification.

2.11 Protein Extraction and Western Blotting

Protein extraction was performed using 1× RIPA buffer (Sigma, Cat #89900) with protease inhibitors (Sigma, Cat #58k4024). Samples were denatured in 4× LDS buffer (NOVEX, Cat #1187053) with DTT (Invitrogen, Cat #471600) at 95°C for 5 minutes. Proteins (10–20 µg) were separated on 8% SDS-PAGE gels and transferred to nitrocellulose membranes (Bio-Rad, Cat #1620115).

Membranes were blocked in 5% milk in PBS-T for 1 hour, probed with primary antibodies overnight at 4°C, then incubated with HRP-conjugated secondary antibodies (1:5000, 2 hours). Chemiluminescence was detected using MILLIPORE substrate (Cat #WBKLS0050) and imaged with an Invitrogen iBright FL1000 system. Band intensities were normalised to GAPDH or β-actin.

2.12 Immunoprecipitation

Immunoprecipitation was conducted using Dynabeads™ Protein G (Invitrogen, Cat #10007D) according to the manufacturer's protocol. Beads were washed and incubated with 1–10 µg of primary antibody for 30 minutes at room temperature with rotation. After washing, beads were incubated with 200–1000 µg of pre-cleared lysate (in RIPA buffer with protease/phosphatase inhibitors) for 2 hours at 4°C. After washing, bound proteins were eluted in Laemmli buffer and analysed by Western blot. Negative controls (IgG-only) and pre-clearing were used to reduce non-specific binding. .

2.13 *In Vivo* Electroporation

All animal procedures were conducted in accordance with the UK Animals (Scientific Procedures) Act 1986 and were approved by the University of York Animal Welfare and Ethical Review Body.

Experiments were performed under a UK Home Office Project Licence (PPL: PP6267867) and carried out by personal licence holders (PIL: I10295242), appropriately trained and authorised to conduct the procedures described. Mice were euthanised using a Schedule 1 method — cervical dislocation — in accordance with Home Office guidelines to ensure rapid and humane termination.

Electroporation was performed in wild-type and *ky/ky* mice maintained on the C3H or C57BL/6J background. All procedures were approved under UK Home Office regulations.

Mice were injected intramuscularly with 2 µL/g hyaluronidase (Sigma, Cat #SLBX4632). Anaesthesia was induced using Bupavet (50 µg/mL, 2 µL/g body weight). After 30 minutes, DNA was electroporated into the TA muscle.

Eight days later, mice were euthanised. TA muscles were dissected, snap-frozen in isopentane pre-cooled in liquid nitrogen, then compound in OCT for cryo-sectioning.

2.13.1 Cryo-sectioning and CSA Quantification

TA muscles were sectioned transversely (9–11 µm), mounted on positively charged slides, fixed in 4% PFA, and blocked in 5% BSA. For membrane labelling, sections expressing mKY-td-TM and mKY-td-Del were stained with Alexa Fluor 488-conjugated WGA (1:200), while sections expressing hKY-GFP were stained with Alexa Fluor 594-conjugated WGA. Slides were counterstained with DAPI.

Fluorescent images were captured using confocal microscopy. Muscle fibre (CSA) was quantified using ImageJ.

2.13.2 Co-localisation Quantification

Longitudinal sections (10–12 µm) were blocked in 4% BSA and incubated overnight at 4°C with primary antibodies. After PBS washes, fluorescently conjugated secondary antibodies were applied for 2 hours. Slides were mounted in DAPI-containing antifade medium.

Images were acquired using confocal microscopy. Manders' overlap coefficients were calculated using Coloc2 in ImageJ. Multiple fields were analysed per sample

2.14 Statistics

Data are presented as mean ± SEM from a minimum of four independent biological replicates. Statistical analyses were conducted using IBM SPSS Statistics (version 28) and GraphPad Prism (version 10). Data normality was evaluated using the Shapiro–Wilk test, and parametric tests were applied only when distributions approximated normality. Unpaired two-tailed t-tests were employed for pairwise comparisons, one-way ANOVA with Tukey's post hoc test for fibre-size rescue experiments, and two-way ANOVA to assess the treatment interactions in heat-stress, proteasome, and autophagy assays. Statistical significance was set at $p < 0.05$.

CHAPTER THREE: RESULTS

Effect of Heat Shock on KY Expression and Subcellular Localisation in C2C12 Cells

CHAPTER 3. Effect of Heat Shock on KY Expression and Subcellular Localisation in C2C12 Cells

3.1 Introduction

Skeletal muscle proteins are fundamental to muscle contraction, metabolism, and structural integrity, playing critical roles in physiological function, proteostasis, and stem cell regulation. The endoplasmic reticulum stress response and unfolded protein response are particularly crucial for muscle stem cell homeostasis, differentiation, and regeneration (Bohnert et al., 2018). Structural, contractile, and regulatory proteins of skeletal muscle, such as actin, myosin, titin, desmin, and associated chaperones, are continuously subjected to environmental stress, including oxidative stress, thermal fluctuation, mechanical loading, and pH fluctuation, which can disrupt their stability, activity, and interactions. These stresses have the potential to cause sarcomeric damage, regulate signalling cascades, and activate adaptive responses like autophagy, proteolysis, and chaperone activation (Solaro & De Tombe, 2008).

Environmental stress experiments provide crucial insights into the functional stability, localisation, and sarcomeric interactions of skeletal muscle proteins. Muscle tissue is constantly exposed to stressors such as exercise, ageing, and pathological conditions like muscular dystrophies (Schiaffino et al., 2013). By simulating such stress conditions, cellular adaptive responses are triggered, including the upregulation of heat shock proteins and activation of proteostasis mechanisms (Locke et al., 1995). Protein misfolding, oxidative stress, and impaired proteostasis do not directly cause myopathies or sarcopenia but contribute substantially to their pathogenesis by disrupting sarcomeric integrity, impairing protein turnover, and eliciting chronic stress responses. These pathological processes are commonly observed in degenerative muscle diseases and are thought to exacerbate muscle wasting and functional decline (Marzetti et al., 2013).

Sustained expression of misfolded proteins in skeletal muscle can trigger maladaptive activation of the heat shock response (HSR), initially aimed at restoring proteostasis. However, chronic HSR activation, as seen in some myofibrillar myopathies, may become counterproductive, impairing normal protein folding and turnover. For example, mutations in the small heat shock protein αB-crystallin, expressed in cardiac and skeletal muscle, are associated with protein aggregation cardiomyopathy and desmin-related myopathy. These mutations can induce reductive stress and disrupt redox homeostasis, contributing to disease progression (Roth et al., 2014).

The Z-disc in striated muscle serves as a crucial structural and signalling hub, anchoring thin filaments and coordinating mechanotransduction (Pyle & Solaro, 2004; Wang & Su, 2010). It contains numerous proteins, including α-actinin, filamin C, and telethonin, which are essential for maintaining sarcomere architecture and facilitating force transduction (Wadmore et al., 2021). These Z-disc proteins are extremely

sensitive to mechanical and biochemical stressors, making them key players in cellular adaptation and proteostasis. Environmental perturbations, such as mechanical strain or oxidative stress, can destabilise Z-disc components, affecting muscle resilience and recovery (Arndt et al., 2010). To maintain Z-disc integrity, a conserved chaperone machinery facilitates the degradation of damaged components through CASA, which is essential for muscle maintenance. Impaired CASA can lead to Z-disc disintegration and progressive muscle weakness, highlighting the importance of proteostasis in muscle health (Arndt et al., 2010).

Recent research has revealed that Z-disk proteins, including the KY protein, are not merely structural scaffolds but also act as dynamic regulators of muscle cell function, participating in mechanotransduction, stress sensing, and gene regulation. For example, in both mouse and human cardiac muscle, the Z-disk protein myopodin has been shown to shuttle between the cytoplasm and the nucleus in response to differentiation and cellular stress (Takeda et al., 2000; Weins et al., 2001). Under stress conditions, such as mechanical strain or oxidative insult, myopodin forms importin-mediated complexes that translocate to the nucleus, where they modulate gene expression programs related to cytoskeletal remodelling, survival, and differentiation. This stress-sensitive relocalisation suggests that Z-disk proteins function as molecular sensors, linking mechanical or biochemical stress to nuclear signalling (Wang & Su, 2010). The ability of Z-disk proteins to couple structural integrity with transcriptional regulation highlights their essential roles in muscle development, regeneration, and adaptation to stress, and underscores their relevance in disorders such as cardiomyopathies and myopathies, where mechanical and signaling dysfunction often intersect.

Within this context, the KY protein has emerged as a potentially important player in protein quality control, particularly under conditions of thermal stress and autophagy activation. Evidence from recent studies indicates that KY's stability and subcellular localisation are responsive to cellular stressors such as heat shock, suggesting a role in the muscle cell's adaptation to proteotoxic stress (Jokl et al., 2018; Baker et al., 2010). Such stress-dependent redistribution may influence downstream processes including autophagy induction, stress granule formation, or aggregate clearance. This supports a model in which Z-disc–associated proteins like KY function as stress-responsive integrators, linking mechanical and biochemical cues to proteostasis, repair, and gene-regulatory pathways (Arndt et al., 2010; Ulbricht et al., 2013). Loss of KY function, as reported in myopathic models, may therefore compromise both sarcomeric integrity and the ability of muscle cells to mount effective adaptive stress responses—a dual defect that likely contributes to the pathogenesis of myofibrillar myopathy and related muscular disorders.

The KY protein is predominantly expressed in striated muscle, including skeletal and cardiac tissue, where it localises to the Z-disc—a key site for force transmission, mechanosensing, and sarcomeric organisation (Blanco et al., 2001; Baker et al.,

2010). Initially identified through its mutation in kyphoscoliotic (*ky/ky*) mice, KY was thought to serve primarily a structural role at the sarcomere. However, emerging evidence indicates that KY has broader roles in maintaining protein homeostasis, particularly under conditions of mechanical and environmental stress (Jokl et al., 2018).

It has been demonstrated that KY deficiency impairs the CASA pathway, a critical quality control mechanism in muscle cells (Jokl et al., 2018). The CASA pathway coordinates the selective autophagic removal of damaged cytoskeletal proteins and relies on the coordinated action of BAG3, HSP70, and small heat shock proteins to preserve sarcomeric proteostasis (Ulbricht et al., 2015; Yogev et al., 2017) Notably, KY-deficient models exhibit accumulation and misregulation of filamin C (FLNC), a well-characterised CASA client protein, suggesting that KY may play a facilitative or regulatory role in FLNC turnover (Jokl et al., 2018). These findings indicate that KY contributes to the targeted degradation of damaged or misfolded proteins under stress conditions, implicating it in proteostasis maintenance beyond its established structural role.

Assuming that stress-responsive protein turnover is a hallmark of muscle adaptation and pathology, a deeper understanding of KY's behaviour under proteotoxic stress is warranted. In particular, heat shock is a well-established method for experimentally inducing protein misfolding, triggering both autophagic and proteasomal clearance pathways. Because mechanical stress, though physiologically relevant, is difficult to replicate *in vitro* with consistency, thermal stress provides a controlled platform for eliciting protein turnover and stress pathway activation.

Furthermore, it has been observed that human KY (hKY) exhibits dual localisation in both the cytoplasm and nucleus, in contrast to mouse KY (mKY), which remains strictly cytoplasmic (Harrad, 2021). This divergence in subcellular localisation suggests evolutionary specialisation and raises the question of whether hKY plays additional roles in nuclear signalling or transcriptional regulation, particularly under stress conditions. However, the functional consequences of this localisation pattern and how it changes under environmental stress remain unclear.

Based on these findings, it is hypothesised that KY contributes to protein quality control in muscle cells by responding to environmental stress through subcellular relocalisation and modulation of autophagy or proteasome pathways. Specifically, heat-induced proteotoxic stress is expected to alter the stability, localisation, and aggregation dynamics of KY, reflecting its potential role in stress-responsive protein turnover, possibly involving CASA pathway components such as FLNC.

To test this hypothesis, this study evaluates the effect of thermal stress on the subcellular localisation of hKY, with particular focus on its nuclear–cytoplasmic partitioning before and after heat shock exposure. The behaviour of hKY and mKY is compared under identical thermal stress conditions to determine whether dual

localisation contributes to differential stress responses. The formation and clearance of KY-containing aggregates are assessed under heat shock and recovery conditions using immunofluorescence and biochemical analysis. In addition, the expression and localisation of CASA pathway components are monitored under heat stress to establish whether KY participates in their regulation.

3.2 Experimental design

To evaluate the conformational stability, aggregation propensity, and stress-responsive behaviour of hKY, an *in vitro* C2C12 myoblast model was employed. The hKY–GFP expression plasmid, originally generated and validated in the Blanco laboratory as part of a master's thesis (Harrad, 2021), was transfected into C2C12 cells to enable real-time visualisation of KY distribution via GFP fluorescence.

Following transfection, cells were exposed to controlled heat stress to investigate alterations in KY subcellular localisation, the formation of intracellular accumulations, and potential aggregation under environmental perturbations. These experiments aimed to assess whether hKY responds dynamically to proteotoxic conditions and to determine whether stress affects its localisation or promotes misfolding and sequestration.

Fluorescence and confocal microscopy were used to examine hKY–GFP localisation and aggregation patterns in both untreated and heat-stressed cells. Comparative analysis allowed us to distinguish between physiological relocalisation events and aberrant protein accumulations suggestive of proteostasis impairment. These cellular responses were interpreted in the context of KY's potential role in stress adaptation and muscle proteostasis regulation (Figure 3.1).

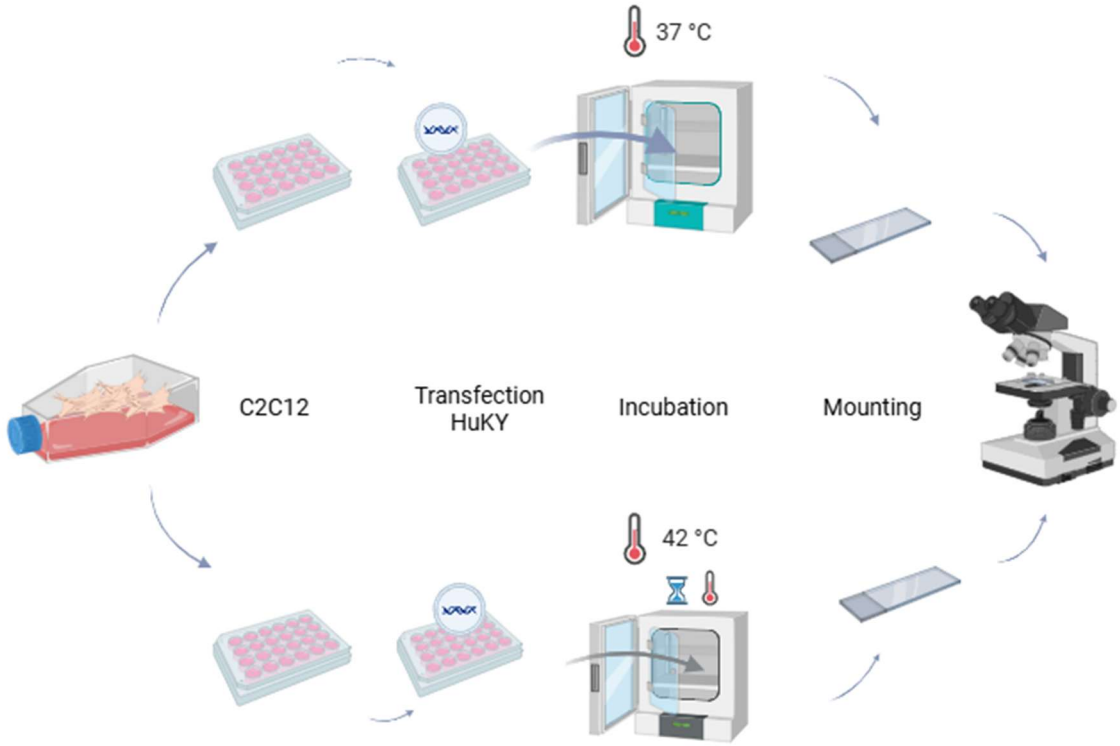

Figure 3.1 Thermal stress assay in C2C12 cells transfected with hKY.

Show an experimental workflow comparing the effects of two different temperatures (37°C and 42°C) on C2C12 cells transfected with hKY. Temperature Conditions: 37°C: Represents a control/normal physiological temperature.42°C: Represents a heat stress condition (hyperthermia). C2C12 Cells: A murine myoblast cell line, commonly used to study muscle biology. Transfection hKY: Introduction of human KY protein into C2C12 cells to analyse its behaviour. Incubation: Cells are exposed to either 37°C or 42°C for a specified duration one hour. Mounting: Post-incubation, cells are probably prepared for imaging (fixation, mounting, and a microscopy) and analysis.

This experimental framework was designed to determine whether hKY localisation is environmentally regulated and whether its stability is compromised by thermal stress, providing insights into its possible functions during muscle stress responses.

3.3 hKY-gfp and mKY-td Verifications

3.3.1 hKY-gfp with NLS

To identify the human orthologs of mKY, a protein BLAST (BLASTp) search was performed against the *Homo sapiens* proteome. All identified hKY isoforms exhibited >80% amino acid identity with mKY and contained the conserved N-terminal MELKKD motif. Notably, one isoform, hKY_X5, displayed an extended N-terminal region comprising 59 additional amino acids upstream of the MELKKD sequence. Bioinformatic prediction using NLS Mapper and NLStradamus indicated that this extension contains a putative nuclear localisation signal (RRPGRK) with high confidence (prediction score >0.9) (Nguyen Ba et al., 2009). This suggests that hKY-

X5 may undergo nuclear translocation, potentially representing a regulatory function not shared by other isoforms (Harrad, 2021).

The hKY_X5-eGFP construct was commercially synthesised (GenScript) and obtained in-frame with eGFP for mammalian expression, using the pcDNA3.1(+) vector backbone. The construct was validated and documented by Oscar Harrad, including sequence confirmation and structural comparison with mouse KY. A schematic comparison of mKY and hKY-X5, highlighting the predicted NLS, is provided in Figure 3.2 based on Oscar's annotated report. For comparative purposes, the mKY-td construct was provided by the Blanco laboratory, and further validation was conducted before use.

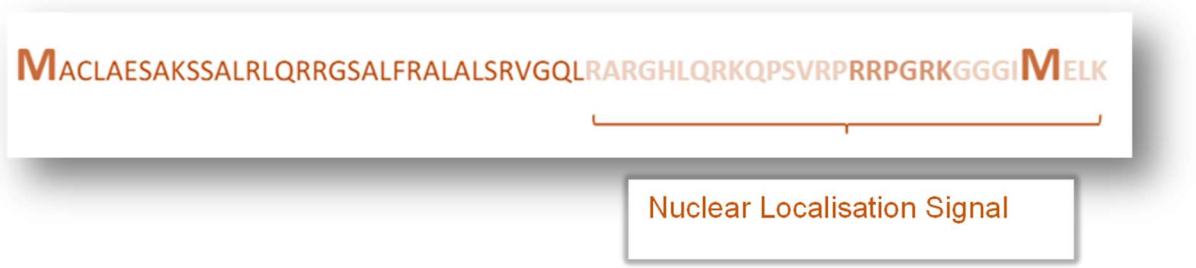

Figure 3.2 The isoform (hKY-X5) displayed an extended N-terminal region containing an additional 59 amino acids upstream of the MELKKD sequence.

Analysis revealed this extension begins with an in-frame methionine residue and contains a putative NLS.

3.3.2 The structure of the constructs

The construct encodes full-length hKY, flanked by an N-terminal NLS to facilitate nuclear targeting and a C-terminal GFP tag for live-cell visualisation. Importantly, the hKY sequence contains a predicted transglutaminase-like domain, which may confer enzymatic activity associated with post-translational protein crosslinking. Transglutaminases catalyse the formation of covalent bonds between lysine and glutamine residues on target proteins, leading to the stabilisation of protein complexes or the formation of insoluble aggregates. (Figure 3.3 -A).

3.3.3 Confirmation of hKY-GFP Construct Expression in C2C12 Cells

To validate the expression and localisation of the hKY-GFP and mKY-tdTomato fusion constructs, transient transfections were performed in C2C12 myoblasts, followed by fluorescence microscopy analysis. Robust GFP and tdTomato signals confirmed successful transfection and expression of the respective constructs (Figure 3.3 -B). As expected, hKY-GFP displayed both cytoplasmic and nuclear localisation, consistent with the presence of N-terminal NLS and its predicted dual subcellular distribution. In

contrast, mKY-td is predominantly localised to the cytoplasm, in agreement with prior reports describing mouse KY as cytoplasm-restricted.

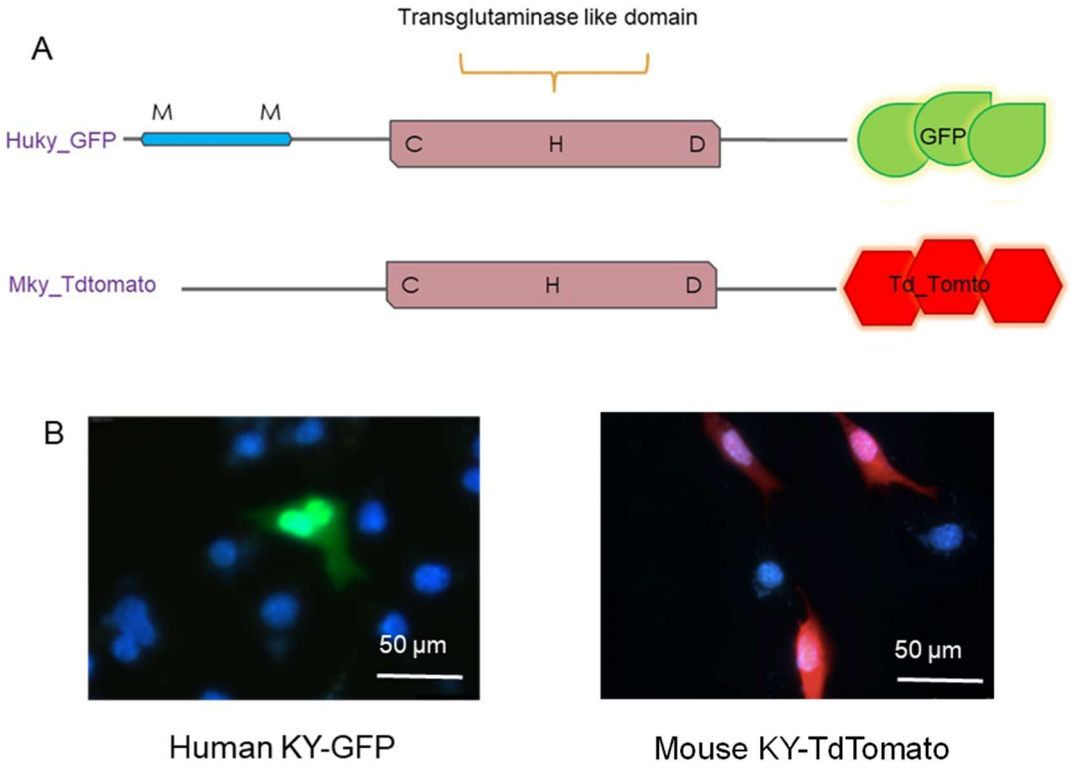

Figure 3.3 A diagram of hKY.gfp construct.

A) hKY.gfp encodes the wild-type KY protein that includes the transglutaminase domain (orange box) with Cysteine(C), Histidine (H) and Aspartate (D) catalytic residues, with the green florescent tag (GFP). (M-M) marked in blue refer to the extra sequences found between two Methionine containing NLS. B) Confirmation of hKY.gfp and mKY.td Constructs Expression in C2C12 Cells, Fluorescence microscopy image of C2C12 cells transiently transfected with the hKY-gfp fusion construct. The GFP signal (green) demonstrates localisation of the hKY-gfp protein, showing the expected subcellular localisation pattern. The construct's NLS directs hKY-gfp accumulation in the nucleus, while cytoplasmic distribution is also evident, consistent with hKY's dual localisation properties. Cell nuclei were counterstained with DAPI (blue) for reference. Brightfield overlay confirms cellular morphology and viability post-transfection. Scale bar: 20 µm.

While some images appeared to show tdTomato signal within the nucleus, this likely reflects signal bleed-through, high background, as the overall pattern across multiple cells and replicates confirmed the expected cytoplasmic localisation of mKY. These results validated both constructs for subsequent experiments investigating their localisation dynamics and aggregation behaviour under thermal stress conditions.

Interpretation of the differential localisation between hKY-GFP and mKY-td must be approached with caution due to two key experimental considerations. First, two different fluorescent tags were used: GFP for the human construct and tdTomato for the mouse construct. These fluorophores differ in molecular weight, folding kinetics and diffusion properties, which may influence protein trafficking and subcellular localisation. GFP (~27 kDa) is small enough to passively diffuse into the nucleus, whereas tdTomato (~54 kDa, dimeric) is less likely to do so, potentially contributing to differences in nuclear versus cytoplasmic distribution that are not solely due to intrinsic properties of the KY protein.

Second, the human KY construct contains an N-terminal region encoding NLS, whereas genomic analysis of the mouse *Ky* locus revealed no equivalent exon with NLS-coding potential. This raises the possibility that localisation differences could reflect either a genuine species-specific regulatory divergence or the presence of uncharacterised mouse splice isoforms that are not currently annotated. Although no alternative NLS-containing mouse isoform has been reported to date, this possibility cannot be entirely excluded and should be acknowledged.

3.4 Expression analysis of *hKY* in C2C12 myoblasts

3.4.1 Heat Shock Induces hKY Relocalisation and Formation of Stress-Responsive Foci

To investigate the impact of thermal stress on hKY stability and localisation, the expression of hKY-GFP in C2C12 myoblasts was analysed before and after heat shock. Under standard culture conditions (37 °C), hKY-GFP exhibited a diffuse distribution across both the cytoplasm and nucleus, occasionally presenting as small puncta. These puncta may reflect sites of subcellular concentration, such as uncharacterised nuclear bodies or cytoplasmic foci, but are not definitively classified as protein aggregates (Figure 3.4).

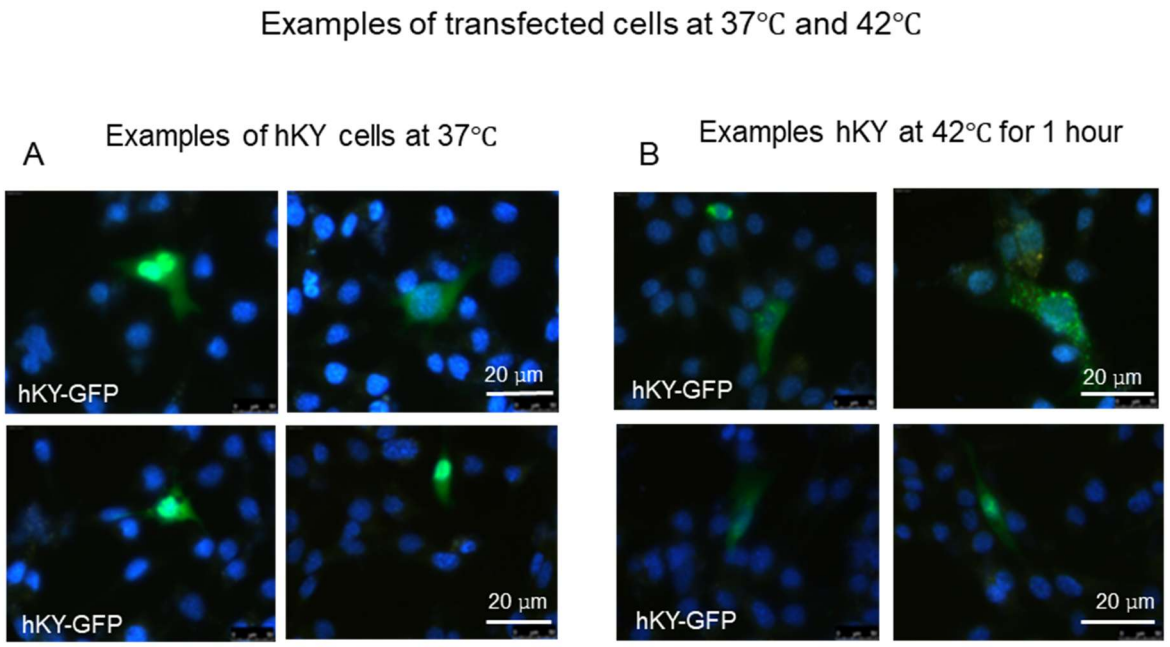

Figure 3.4 Expressed hKY-gfp protein response to heat shock in C2C12 myoblast.

Examples of transfected cells maintained at 37°C or exposed at 42°C for 1hour as indicated in the figure. Images show an overlay of the green and DAPI channels. A) Examples of expressed hKY at 37℃ that show strong GFP signals. B) Examples hKY at 42℃ for 1 hour, indicating the decrease of intensity of GFP signals. Scale bar in bottom right corner in each group of images. All images were snapshotted at magnification of 40x magnification using identical exposure settings. Scale bars are shown in the bottom right of each image group. A GFP-only control (shown in next expermints) retained stable fluorescence under both temperature conditions.

Following a 1-hour exposure to 42 °C, a notable reduction in GFP fluorescence intensity was observed in a subset of cells, accompanied by the appearance of larger, brighter GFP-positive puncta. These structures may indicate stress-induced accumulations of the hKY protein. In contrast, cells transfected with a GFP-only vector retained consistent signal intensity under identical conditions, confirming that the reduction in hKY-GFP fluorescence was not due to GFP quenching by heat but instead reflects altered behaviour of the fusion protein. All imaging was conducted using identical acquisition settings to ensure comparability.

Quantitative fluorescence intensity analysis was not performed across the entire cell population; however, representative fields (Figure 3.4) consistently showed a visible reduction in overall signal and increased puncta formation in heat-stressed cells compared with controls. Nuclear morphology appeared more condensed in some hKY-GFP–expressing cells following heat shock; however, this observation is based solely on the redistribution pattern of the fusion protein rather than on direct assessment of nuclear structure using DNA stains or specific nuclear markers.

Importantly, a GFP-only control was included under identical heat shock conditions, and no comparable signal loss was observed, confirming that the reduction in hKY-GFP intensity is not due to thermal quenching of the GFP fluorophore itself. All

fluorescence imaging was performed under identical exposure and acquisition settings to ensure valid comparison between control and heat-stressed samples.

Microscopy analysis revealed that hKY-GFP localises to both the nucleus and cytoplasm at 37 °C, displaying a mostly diffuse distribution. Upon exposure to 42 °C for one hour, a subset of cells exhibited a distinct speckled GFP pattern, suggestive of stress-induced structures or protein aggregates. In parallel, although fluorescence intensity was not quantitatively measured, the hKY-GFP signal appeared visibly reduced in images obtained under identical acquisition settings, consistent with potential heat-induced destabilisation or redistribution of the protein.

The localisation of hKY-GFP to apparent aggregates raises the possibility that KY may play an active role in recognising or facilitating the clearance of misfolded proteins formed during heat stress. Such clearance could be mediated via autophagic or proteasomal degradation pathways. To test this hypothesis, heat-shocked cells were treated with specific pathway inhibitors, and quantitative analysis of hKY-positive aggregates was performed to determine whether inhibition of these pathways altered KY stability or aggregation dynamics under stress.

3.5 Testing The Role of Proteasome and Autophgy In The Formation of KY Aggregates

This experiment was designed to characterise hKY–GFP protein by both Western blotting and fluorescence imaging, and to investigate its stability under proteotoxic and autophagic stress, as well as its subcellular behaviour following heat shock. C2C12 myoblasts were transfected with the hKY-GFP construct for 48 hours to ensure robust expression prior to treatment. For Western blot analysis, cells were cultured in 6-well plates, while imaging was performed on cells seeded in 24-well plates.

To investigate the effects of proteasome-mediated degradation, cells were pre-treated with MG132 and exposed to 42 °C for 2 hours. In parallel, the role of autophagic degradation was assessed using BafA1, with cells incubated at 42 °C for 3 hours. These treatments aimed to determine whether inhibition of these pathways would stabilise hKY-GFP levels or alter its localisation in response to heat stress. Cells for imaging were fixed with 4% PFA to preserve GFP localisation, while protein lysates

were collected for Western blotting to evaluate expression levels and stress-induced degradation of hKY-GFP (figure 3.5).

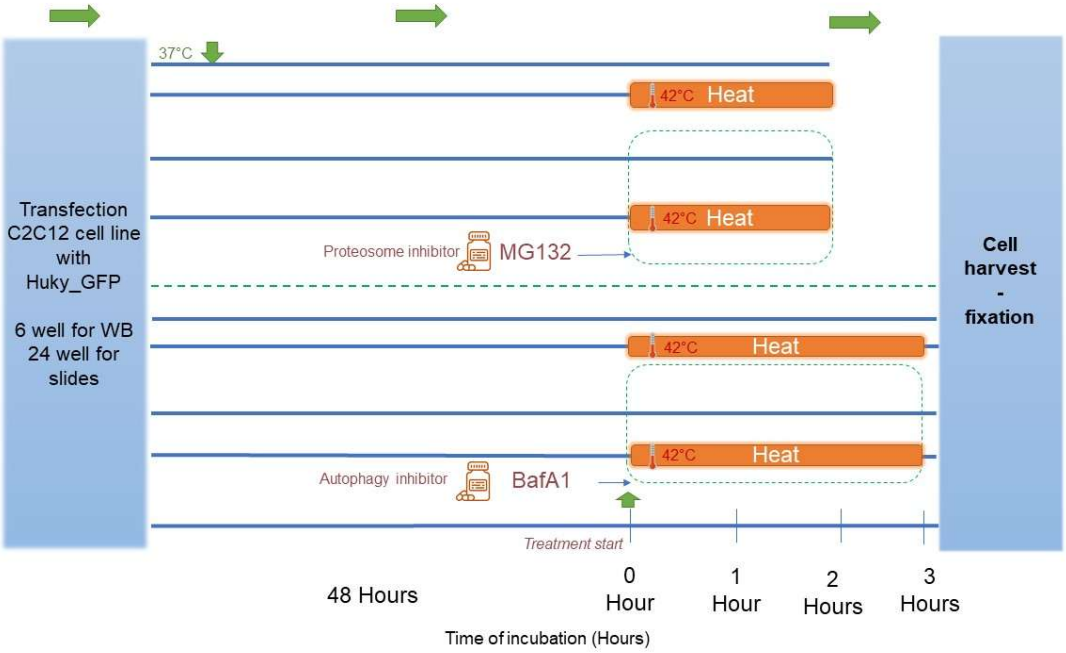

Figure 3.5 The Experimental Workflow for hKY.gfp Transfection and Heat Stress Treatments in C2C12 Cells.

Transfected C2C12 with hKY.gfp were placed into four groups after 48 hours: 37°C, 42°C, 37°C plus MG132 and 42°C plus MG132. Cells were maintained for 2 hours under those conditions, then fixed and mounted for microscopy analysis or harvested in RIPA buffer for western blots. A similar set-up was used with the autophagy inhibitor BafA1, but treatment was extended to three hours. The unobstructed lines represent the time spent at 37°C, from the start of the experiment. The grey rectangular boxes represent the time spent at 42°C with MG132 and BafA1 or without. The dotted box demonstrates the duration of MG132 and BafA1 treatments.

3.6 Proteasome Inhibition Modulates KY Aggregation and Degradation During Heat Shock

To evaluate the contribution of the proteasome to the clearance or stability of hKY-GFP-positive structures, C2C12 myoblasts were treated with the proteasome inhibitor MG132 for 2 hours at 37 °C before fixation and harvest. Fluorescence microscopy revealed a marked increase in hKY-GFP-positive foci following MG132 treatment, compared to untreated controls, suggesting that inhibition of proteasomal activity promotes the accumulation of KY-associated structures. While these foci may represent misfolded protein aggregates, it is essential to note that they have not been confirmed as classical protein aggregates, such as those labelled with ubiquitin, and are referred to here as putative hKY-positive aggregates.

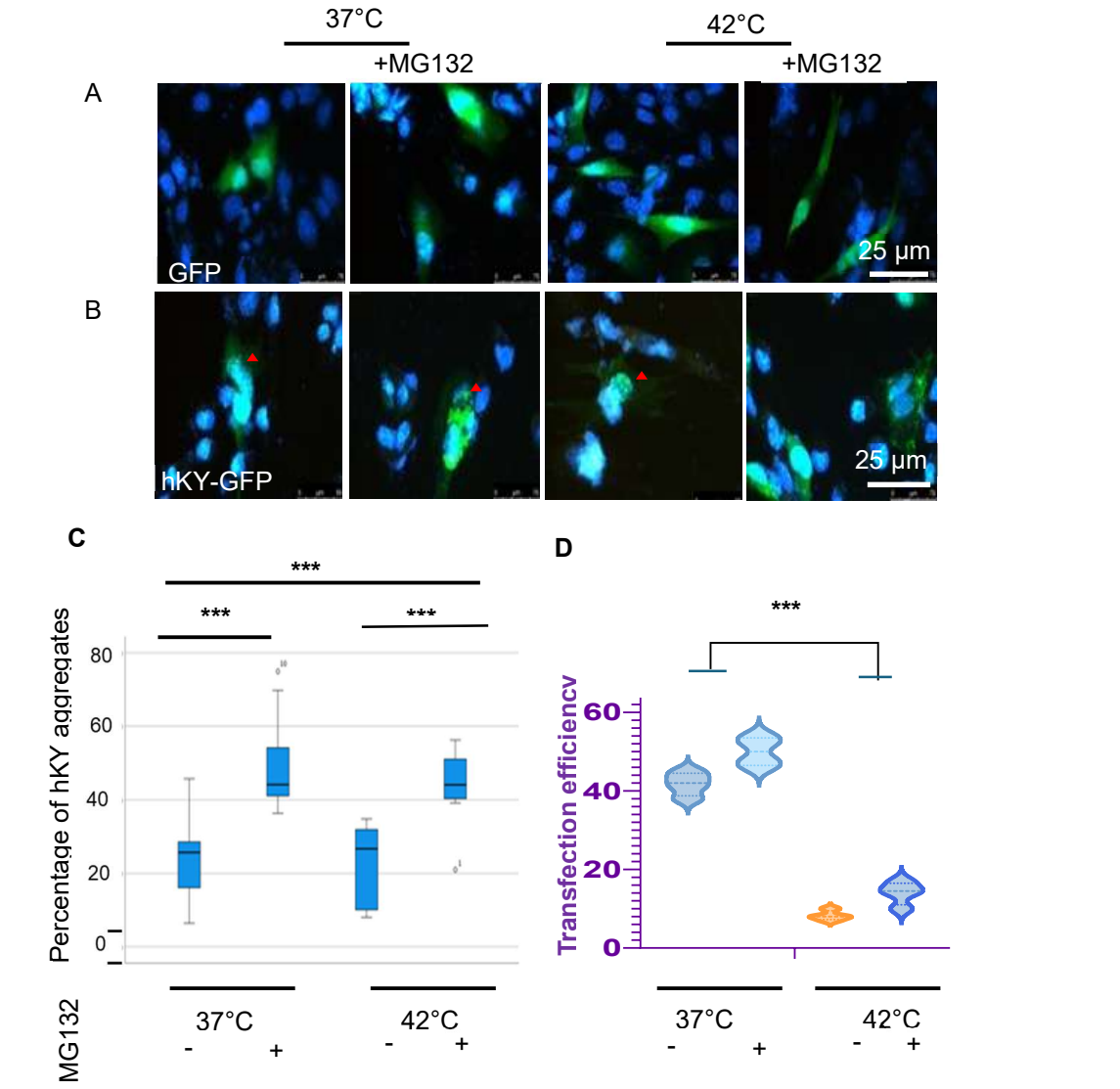
37°C
+MG132
42°C
+MG132
A
GFP
25 µm
B
hKY-GFP
25 µm
C
***
***
***
Percentage of hKY aggregates
80
60
40
20
0
MG132
37°C
42°C
-
+
-
+
D
***
Transfection efficiency
60
40
20
0
37°C
42°C
-
+
-
+

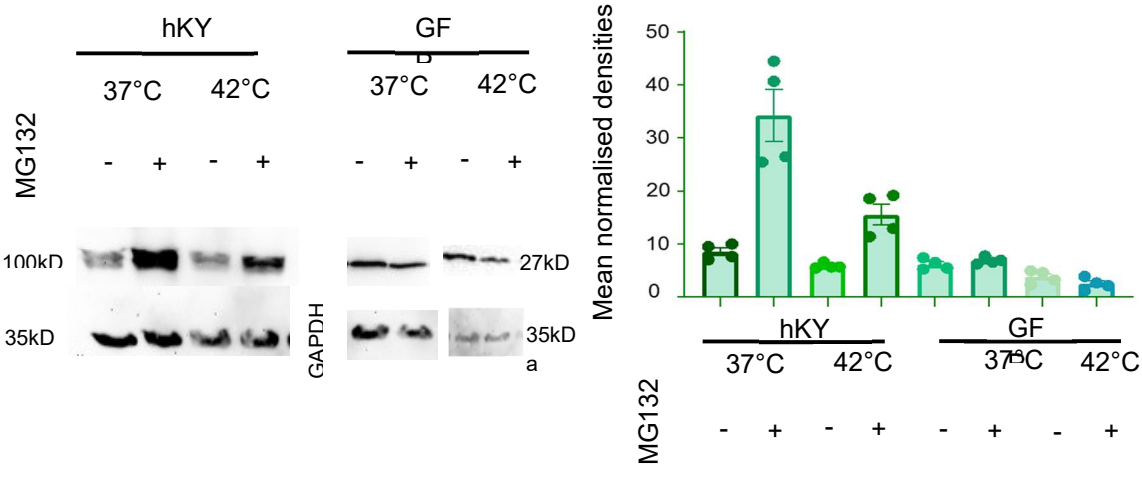
E
hKY
GF
37°C
42°C
37°C
42°C
MG132
-
+
-
+
-
+
-
+
100kD
35kD
GAPDH
27kD
35kD
a
F
Average measurements of hKY and GFP bands densities
**
**
*
Mean normalised densities
50
40
30
20
10
0
hKY
GF
37°C
42°C
37°C
42°C
MG132
-
+
-
+
-
+
-
+

Figure 3.6 hKY protein accumulates when proteasome inhibited by mg132 during heat stress, indicating proteasome-independent turnover of KY protein.

A) GFP-only control cells display diffuse cytoplasmic localisation under all conditions with no formation of structured foci, confirming that stress-induced foci formation is specific to hKY and not due to GFP instability. B) hKY-GFP–expressing cells show nuclear and cytoplasmic redistribution during heat stress (42 °C), with altered foci number in response to MG132, consistent with stress-dependent relocalisation of KY rather than irreversible aggregation. C) Quantification of the number of hKY-positive foci per cell. Data represent mean ± SEM from 4 biological replicates, each measured in technical triplicate. Two-way ANOVA revealed a significant main effect of treatment ($F(1.383, 4.150) = 27.57$, $p = 0.0048$). ***$p < 0.001$. D) Quantification of transfection efficiency from the same experiments. Data represent mean ± SEM from 4 biological replicates, with technical triplicates. E) Western blot analysis of hKY-GFP levels using anti-GFP antibody under the indicated conditions. GAPDH was used as loading control to confirm equal protein loading. F) Densitometric quantification of normalised band intensities from Western blots (panel E). Data represent mean ± SEM from 4 biological replicates, each measured in three technical repeats. Two-way ANOVA confirmed a significant effect of heat treatment on KY stability. These findings demonstrate that KY is a stress-responsive protein that undergoes dynamic relocalisation and partial degradation during heat shock. Inhibition of the proteasome by MG132 reduces, but does not prevent, KY loss, suggesting the involvement of proteasome-independent mechanisms such as autophagy in KY turnover.

This effect was more pronounced under heat shock conditions (42 °C), where MG132 treatment led to further accumulation of hKY-GFP-positive foci (Figure 3.6-B), suggesting that the ubiquitin-proteasome system is required for maintaining KY homeostasis during thermal stress. In contrast, cells transfected with GFP-only constructs did not show similar accumulation patterns under the same treatment, indicating that the observed structures are specific to hKY and not a general consequence of GFP instability.

Transfection efficiency was estimated by counting GFP-positive cells in randomly selected fields and was approximately 20–30%, although some variation was observed between experiments. All quantifications of hKY-positive structures were normalised to transfected cell numbers to account for this variability (figure 3.6).

3.7 Autophagy Inhibition Modulates KY Aggregation and Degradation During Heat Shock

To assess the role of autophagy in regulating hKY-GFP accumulation, C2C12 myoblasts were treated with the autophagy inhibitor BafA1 for 3 hours prior to fixation and imaging. Fluorescence microscopy revealed a significant increase in hKY-GFP-positive structures in BafA1-treated cells compared to untreated controls, suggesting that inhibition of autophagic flux leads to the accumulation of KY-associated material. These structures were quantified using fluorescence image analysis, normalised to the number of transfected cells.

This effect was further evaluated under heat shock conditions (42 °C), where BafA1 treatment again resulted in elevated KY-positive accumulations relative to heat-

shocked cells without BafA1. While the identity of these structures remains unconfirmed, their increased abundance upon autophagy inhibition is consistent with a role for autophagic pathways in regulating KY stability or turnover under stress conditions (Figure 3.7).

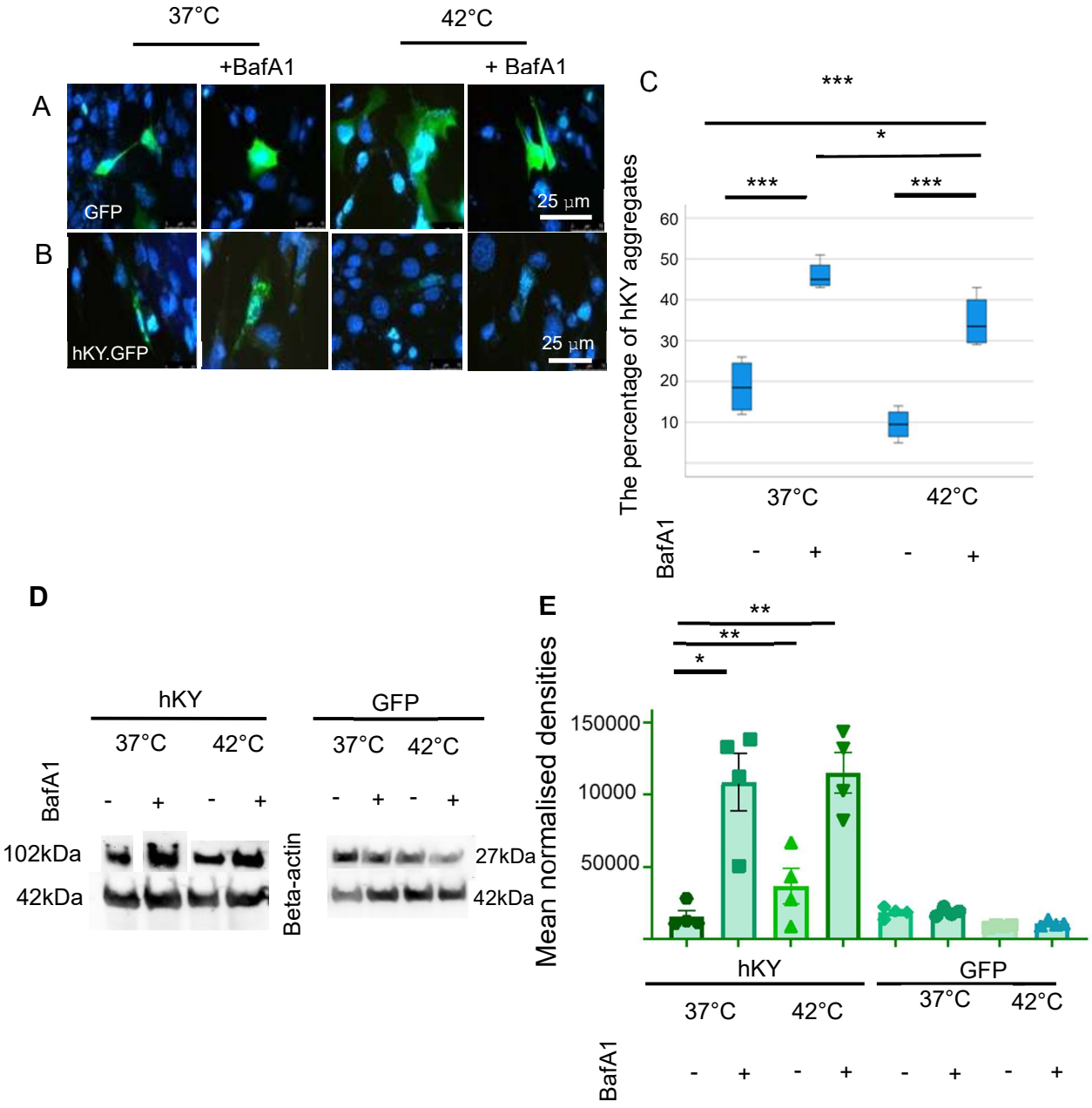

Figure 3.7 hKY protein accumulates when Autophagy inhibited by BafA1 during heat stress

A) Expression of GFP-only under the indicated conditions, showing no evidence of aggregate formation. Transfection efficiency ranged between 38.5–41.6%. B, C) Expression of hKY-GFP under the indicated conditions, showing nuclear and cytoplasmic hKY-positive foci. All images show GFP/DAPI overlay, were acquired at 40× magnification, and include a scale bar in the lower right corner. Exposure time was 1750 ms with a digital gain of 2.5. D) Quantification of hKY-GFP–positive foci under each condition. Box plots represent individual measurements; error bars indicate SEM. $P < 0.05$. Two-way ANOVA: $F = 36.297$, $df = 12$, $p = 3.0 \times 10^{-6}$. E) Western blot analysis using anti-GFP (top panels) and anti-β-actin (bottom panels) antibodies, using protein extracts from transfected C2C12 cells exposed to the indicated conditions. F) Quantification of normalised band intensities from Western blots (panel E), based on ImageJ densitometry analysis. Error bars represent SEM. Treatment with BafA1 led to a significant increase in hKY-GFP levels compared to untreated controls. n = 3 independent biological replicates. Two-way ANOVA: $F = 6.487$, $df = 8$, $p = 0.0155$.

3.8 Expression analysis of mKY in C2C12 myoblasts

3.8.1 mKY Exhibits No Detectable Response to Heat Shock in C2C12 Myoblasts

To determine whether the heat shock–induced response observed in hKY is conserved in its mouse homologue, we examined the effect of thermal stress on mKY-td in transfected C2C12 myoblasts. Fluorescence microscopy revealed that mKY consistently exhibited a diffuse cytoplasmic distribution under both control (37 °C) and heat shock (42 °C) conditions, with no notable changes in localisation or signal intensity. Unlike hKY, mKY did not form visible foci or display altered expression patterns in response to heat, suggesting that mKY is more stable or less responsive to thermal perturbation under these conditions (Figure 3.8).

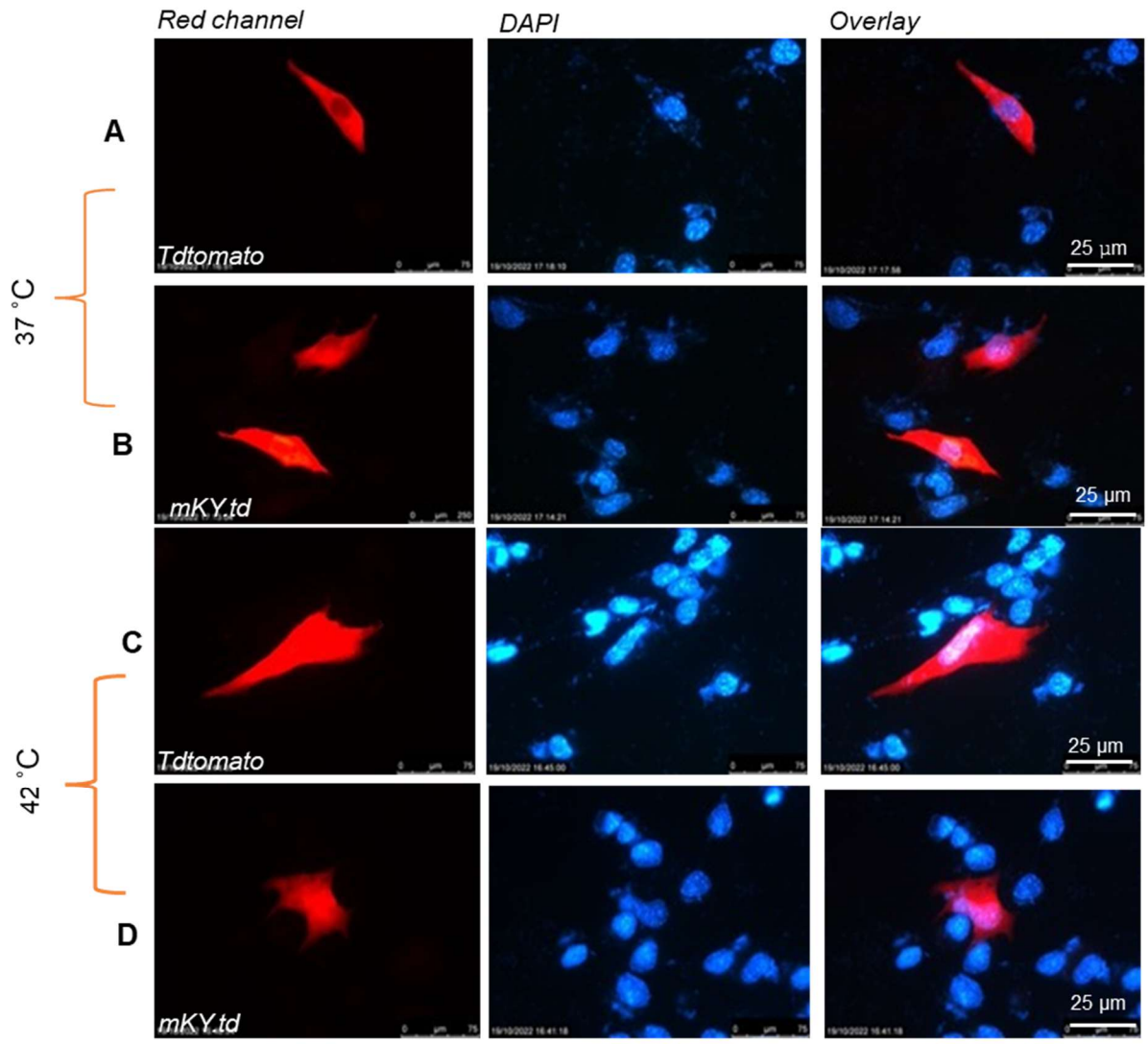

Figure 3.8 Expressed mKY protein with no response to heat shock in C2C12 myoblast.

Examples of transfected cells maintained at 37°C or exposed at 42°C for 2 hours, as indicated in the figure. Images show an overlay of the red channel and DAPI channels. A) An example of expressed tdtomato as a control at 37℃ that shows strong red signals. B) An example of mKY at 37℃ for 2 hours, indicating the strong intensity of red signals. C) An example of expressed tdtomato as a control at 42℃ that shows strong red signals. D) An example of mKY at 42℃ for 2 hours, indicating the strong intensity of red signals. Scale bar in the bottom right corner of each group of images. All images were snapped at a magnification of 40x.

Tdtom controls' results proved the transfections were excellent; all samples showed the bright and robust red, as presented in Figure 3.9, without any indication of fluorescence intensity diminishing, suggesting that the observations above regarding the weak expression at 42 °C were *hKY.gfp* specific.

3.9 Discussion

This chapter investigated the subcellular behaviour of hKY and mKY proteins in C2C12 cells under heat stress, with a focus on their localisation dynamics, degradation pathways, and association with proteostasis systems. The findings reveal clear isoform- and species-specific differences, supporting a role for KY as a stress-responsive protein linked to, but dissimilar from, recognised Z-disc–associated proteostasis regulators such as FLNC and BAG3.

Under basal conditions (37 °C), hKY displayed diffuse distribution throughout both the cytoplasm and nucleus, while mKY remained strictly cytoplasmic. This difference likely arises from intrinsic structural divergence, particularly the presence of a functional NLS in hKY, which is absent in the murine isoform. Upon acute heat shock (42 °C), hKY rapidly redistributed into punctate structures and was depleted from its diffuse background, an effect not observed in mKY or GFP-only controls. These data confirm that hKY's redistribution reflects an isoform-specific stress response rather than an artefact of fluorophore tagging.

The formation of cytoplasmic and nuclear hKY-positive puncta suggests a stress-induced relocalisation process, potentially involving sequestration into aggresomes or stress granules. Although the identity of these structures remains to be confirmed using classical aggregation markers such as p62, ubiquitin, their morphology is consistent with proteotoxic stress-induced compartments described in other systems (Kopito, 2000; Mateju et al., 2017). Nuclear accumulation of hKY under heat shock implies a possible regulatory role in transcriptional stress responses, perhaps analogous to BAG3, which translocates to the nucleus to modulate gene expression under proteotoxic stress (Ganassi et al., 2016). Whether KY engages with nuclear transcriptional machinery or chaperones in a similar fashion remains to be determined, but its dynamic behaviour underscores a broader stress-adaptive potential.

The degradation pathways regulating KY turnover were examined using MG132 and Bafilomycin A1. Treatment with either compound resulted in elevated hKY signal intensity and increased puncta formation, suggesting that KY undergoes degradation via both the ubiquitin–proteasome and autophagy–lysosome pathways. However, neither treatment prevented heat-induced signal loss, suggesting that KY turnover involves partially redundant or parallel degradation routes. This supports a model where misfolded or stress-damaged proteins are sequentially processed by overlapping quality control systems depending on solubility, chaperone engagement, and localisation (Ciechanover & Kwon, 2015; Koga et al., 2011). KY may also undergo turnover via alternative routes such as chaperone-mediated autophagy or endosomal sorting, which are not inhibited by MG132 or Bafilomycin A1. Similar dual-pathway degradation mechanisms have been reported for sarcomeric proteins, including FLNC and Desmin, especially under conditions of mechanical strain (Kley et al., 2013; Ulbricht et al., 2013).

Importantly, these findings align with previous studies describing heat-induced aggregation of Z-disc–associated proteins such as FLNC and BAG3. Both undergo relocalisation to stress granules or insoluble compartments in response to proteotoxic stimuli (Arndt et al., 2010; Ulbricht et al., 2013). FLNC is cleared via the CASA pathway, which relies on BAG3 for cargo recognition and delivery. KY's redistribution under heat stress mirrors that of FLNC and BAG3, suggesting it may act within a comparable proteostasis framework, potentially as a scaffold or adaptor rather than a cargo protein. Although this study did not directly quantify FLNC turnover or CASA pathway markers, previous work in KY-deficient models demonstrated disrupted FLNC clearance, strengthening the hypothesis that KY contributes to proteostasis regulation at the Z-disc (Jokl et al., 2018).

It has been observed clear species-specific differences in how KY responds to stress. Compared to mKY, the hKY showed a much greater tendency to redistribute within the cell and undergo degradation, even though both were expressed under the same conditions. These differences could point to evolutionary changes in hKY, such as the presence of an NLS or modifications in its C-terminal region, that may affect how the protein is regulated. This kind of divergence could help explain why KY-related disease looks different across species: *ky/ky* mice tend to develop a severe and early-onset muscle disorder, while in humans, KY mutations more often result in a milder, slowly progressive condition (Hedberg-Oldfors et al., 2016). The capacity of hKY to undergo dynamic relocalisation may represent a human-specific adaptation enabling enhanced stress responsiveness in muscle.

While the findings provide key insights, several limitations should be acknowledged. First, a single acute heat stress protocol (42 °C for 2 hours) was used, based on prior studies (Kampinga et al., 1994), but future work should explore a broader range of durations and temperatures. Second, although morphological evidence suggested protein aggregation, we did not confirm this using biochemical assays such as detergent solubility or co-labelling with ubiquitin/p62. Moreover, although we used pharmacological inhibitors to suggest which degradation pathways might be involved, direct measurements of protein turnover, such as cycloheximide chase experiments, would be needed to accurately determine KY's half-life. It's also worth noting that our experiments were carried out in undifferentiated C2C12 myoblasts. While these cells are convenient and widely used, they don't fully reflect the environment of mature muscle fibres, where KY normally functions. Mature fibres are post-mitotic and rich in organised sarcomeres, which may influence KY's localisation, stability, or function in ways that myoblasts cannot fully replicate.

A general limitation of this study is the use of undifferentiated C2C12 myoblasts, which lack mature sarcomeric organisation and do not contain Z-disc structures—the primary localisation site of KY in skeletal muscle. This is particularly relevant given that KY's role is tightly associated with Z-disc–mediated mechanosensing and proteostasis. The absence of sarcomeres in myoblasts may affect KY localisation, turnover, and interaction with its native binding partners such as FLNC and BAG3. Therefore, the

observed redistribution and degradation dynamics in this system may not fully represent KY behaviour in differentiated myotubes or mature muscle fibres. Future studies using differentiated C2C12 myotubes or *in vivo* muscle fibres will be essential to validate these findings under physiologically relevant conditions, where Z-disc–dependent stress signalling and autophagy regulation are fully established.

In conclusion, these findings position KY as a stress-responsive, Z-disc–associated protein whose subcellular localisation and stability are modulated by both autophagic and proteasomal degradation mechanisms. The parallels observed with FLNC and BAG3 under stress support a model in which KY contributes to muscle protein quality control, particularly during proteotoxic challenge. Its heat-induced nuclear redistribution and selective turnover suggest functional roles that extend beyond static sarcomeric anchorage, potentially involving transcriptional regulation, stress-responsive signalling, or chaperone-mediated surveillance. Together, these results broaden the current understanding of KY's contribution to muscle proteostasis and provide a foundation for future studies aimed at defining its mechanistic involvement in stress adaptation and myopathic pathology.

CHAPTER FOUR: RESULTS

In Vivo Overexpression of KY Constructs Rescues Muscle Size in the KY-Deficient Mouse Model

CHAPTER 4. *In Vivo* Overexpression of KY Constructs Rescues Muscle Size in the KY-Deficient Mouse Model

4.1 Introduction

This chapter examines the impact of KY overexpression on muscle phenotype within an *in vivo* mouse model of KY deficiency. Given the progressive myopathic features characteristic of *ky/ky* mice, the study aimed to assess whether reintroduction of KY via genetically engineered constructs could restore normal muscle fibre size or structural integrity. The central objective of this rescue experiment was to determine the functional requirement of KY in maintaining muscle mass and to evaluate whether its absence leads to persistent structural abnormalities in skeletal muscle.

Although KY contains a conserved transglutaminase/protease (TGN/PROT) domain featuring residues analogous to a cysteine–histidine–aspartate catalytic triad, biochemical investigations have shown that KY lacks detectable enzymatic activity. Harrad (2020) systematically tested the catalytic potential of KY using both recombinant protein assays and in silico structural predictions. *In vitro* transglutaminase assays were performed with purified full-length KY and its isolated TGN/PROT domain using the SIGMA-ALDRICH transglutaminase assay kit. This assay detects enzyme-mediated covalent linkage between biotin-labelled glutamine donor peptides (biotin-TVQQEL-OH) and poly-L-lysine acceptors, measured via streptavidin–peroxidase detection. Both full-length KY and its domain construct demonstrated no detectable substrate crosslinking activity compared with the active transglutaminase control, indicating an absence of catalytic function (Harrad, 2021).

Similarly, protease activity was assessed using succinylated casein as a substrate, in which proteolytic cleavage releases primary amines subsequently detected by reaction with trinitrobenzenesulfonic acid (TNBSA). Both full-length and domain constructs of KY exhibited absorbance values indistinguishable from buffer and MBP controls, and markedly lower than the trypsin positive control, revealing no measurable proteolytic cleavage. These consistent findings confirmed that KY lacks measurable transglutaminase or protease activity *in vitro*.

Collectively, these results suggest that, despite sequence similarity to catalytically active transglutaminases, the KY TGN/PROT domain fulfils a non-catalytic role, potentially acting as a structural or scaffolding element at the Z-disc. On this basis, the experiments described in this chapter were designed to determine whether the integrity of the TGN/PROT domain, including its conserved catalytic residues, is nevertheless required for KY's biological role in sustaining normal muscle fibre size.

The *ky/ky* mouse model provides a powerful system to investigate this question. This model represents a well-characterised loss-of-function mutant in which a two-base-pair deletion in exon 2 of the Ky gene produces a frameshift and premature stop codon (Blanco et al., 2001). This mutation triggers nonsense-mediated decay of the transcript, leading to complete loss of KY protein expression.

One of the most conserved regions of the KY protein is the transglutaminase-like/protease (TGN/PROT) domain, located centrally within the protein. Although this domain shows sequence similarity to enzymatically active transglutaminases, including conservation of a putative catalytic triad (histidine, cysteine, and aspartate), no biochemical evidence currently supports enzymatic activity in KY.

This raises the possibility that the TGN/PROT domain contributes to KY function via non-catalytic roles, such as maintaining structural integrity or mediating protein–protein interactions relevant to muscle fibre organisation.

In this chapter, we focus on evaluating the functional significance of the TGN/PROT domain and its conserved residues by using a panel of engineered KY constructs. These include:

- A construct in which the three conserved residues of the predicted catalytic triad are substituted with alanine, and
- A construct lacking the entire TGN/PROT domain.

These variants were tested in *ky/ky* mice to assess their ability to restore muscle fibre size, enabling a direct evaluation of the requirement for this domain in KY's biological function in skeletal muscle.

Additionally, the experiment employed a human KY construct that differs from the mouse KY sequence by an additional 49 amino acids at the N-terminus, encompassing a predicted nuclear localization signal (Harrad, 2021). This interspecies difference provided an opportunity to assess whether the human form of KY can functionally compensate for KY deficiency in the mouse model, thereby evaluating functional conservation between species.

Previous studies have shown that KY is required for muscle hypertrophy in response to overload (Blanco et al., 2001), and that *ky/ky* mice fail to exhibit such hypertrophic responses. However, whether KY expression alone is sufficient to restore fibre size in the absence of physiological challenge remains unresolved.

In this context, the experiments described here aim to determine whether reintroducing functional or modified KY constructs can reverse the muscle fibre atrophy and structural disorganisation characteristic of the *ky/ky* phenotype. A successful rescue would indicate that KY plays an active, non-enzymatic role in maintaining muscle integrity, whereas failure to rescue with domain-deleted or mutant constructs would pinpoint regions of KY that are essential for its structural function.

Working Hypothesis

Our working hypothesis is that mKY-tdTomato retains the full functional capacity of endogenous KY, including correct localisation and activity within skeletal muscle. Therefore, mKY-td is expected to rescue fibre size in *ky/ky* mice. If confirmed, this system provides a robust platform for testing KY variants with domain-specific modifications, enabling direct investigation of the contribution of the TGN/PROT domain and its conserved residues to KY's biological function *in vivo*.

4.2 Experimental design

This chapter investigates whether the TGN/PROT domain of the KY protein is essential for its biological function in muscle fibre size maintenance. Specifically, we tested whether deletion or targeted mutation within this domain affects KY's ability to rescue muscle fibre size in *ky/ky* mice.

To systematically evaluate the structural and functional domains of KY *in vivo*, six expression constructs were generated and electroporated into the tibialis anterior muscles of *ky/ky* mice. Each construct was tagged with either GFP or tdTomato to enable detection and comparison under identical experimental conditions (Figure 4.1).

The constructs used were:

Control Constructs (Fluorescent-only):

- **GFP-only**: Negative control to assess effects of GFP expression alone.
- **tdTomato-only**: Negative control to assess effects of tdTomato expression alone.

Mouse KY Constructs (tdTomato-tagged):

- **mKY-td**: Wild-type mouse KY fused to tdTomato (functional positive control).
- **KY-TM (Catalytic Triad Mutant)**: Mouse KY with alanine substitutions at Cys-His-Asp active site residues, fused to tdTomato — designed to assess the requirement of catalytic activity.
- **KY-ΔTGN**: Mouse KY lacking the entire TGN/PROT domain, fused to tdTomato, used to evaluate the functional significance of this structural region.

Human KY Construct (GFP-tagged):

- **hKY-GFP**: Full-length human KY with N-terminal NLS fused to GFP, included to assess cross-species rescue ability and the role of the N-terminal extension.

These constructs allowed domain-specific functional interrogation of KY, distinguishing between catalytic versus structural contributions to muscle fibre maintenance, and enabling comparison between human and mouse KY isoforms.

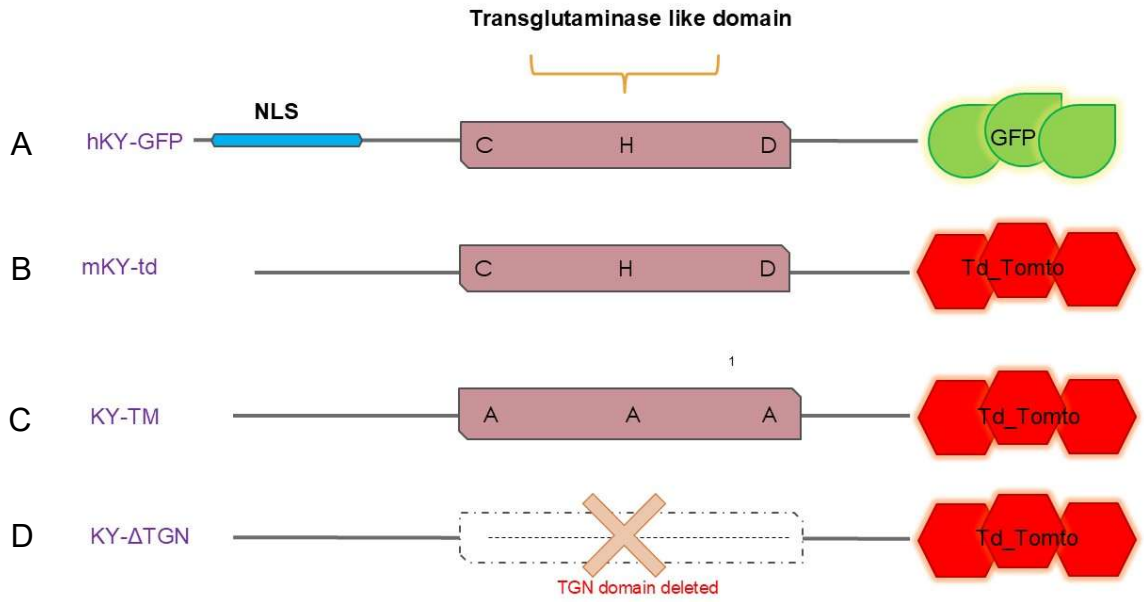

Figure 4.1 Schematic representation of KY protein constructs used for in vivo electroporation.

Each construct contains a fluorescent tag for identification (GFP or tdTomato).A) hKY-GFP: Full-length human KY protein fused to GFP. This construct includes the transglutaminase-like (TGN/PROT) domain (orange box) with the conserved catalytic triad residues — cysteine (C), histidine (H), and aspartate (D) — and an N-terminal extension containing a predicted nuclear localization signal (NLS) (indicated in blue). B) mKY-td: Full-length wild-type mouse KY protein fused to tdTomato, containing the same conserved catalytic triad (C, H, D) within the TGN domain.C) KY-TM: A catalytically inactive KY mutant in which the triad residues (C, H, D) are replaced with alanine (A), fused to tdTomato. D) KY-ΔTGN: A deletion construct lacking the entire TGN domain, including the catalytic residues, fused to tdTomato.

After an 8-day expression period, allowing for protein expression and phenotype development, the muscles were collected, embedded, and cryosectioned for histological analysis. Fibre CSA was used as the primary quantitative outcome measure.

Due to intrinsic variability in fibre size in the *ky/ky* background, data were normalised by calculating the ratio of CSA in transfected fibres to adjacent non-transfected fibres within the same muscle section. A ratio >1.0 was interpreted as a rescue of fibre size, while a ratio <1.0 or equal suggested either no effect or continued atrophy.

This experimental strategy served two main objectives:

1. To determine the structural importance of the TGN/PROT domain for KY's function in maintaining normal muscle fibre size.
2. To evaluate the functional impact of mutating the conserved residues within this domain using a domain-targeted construct comparison approach (Figure 2).

The experimental workflow involved: (1) preparation and verification of constructs; (2) electroporation into the TA muscle; (3) post-electroporation recovery for 8 days; (4) dissection and tissue processing, including both cross and longitudinal cryosectioning; (5) mounting of tissue samples for imaging; and (6) CSA measurement and data analysis. This systematic design ensured consistent evaluation of construct effects on muscle morphology (Figure 4.2).

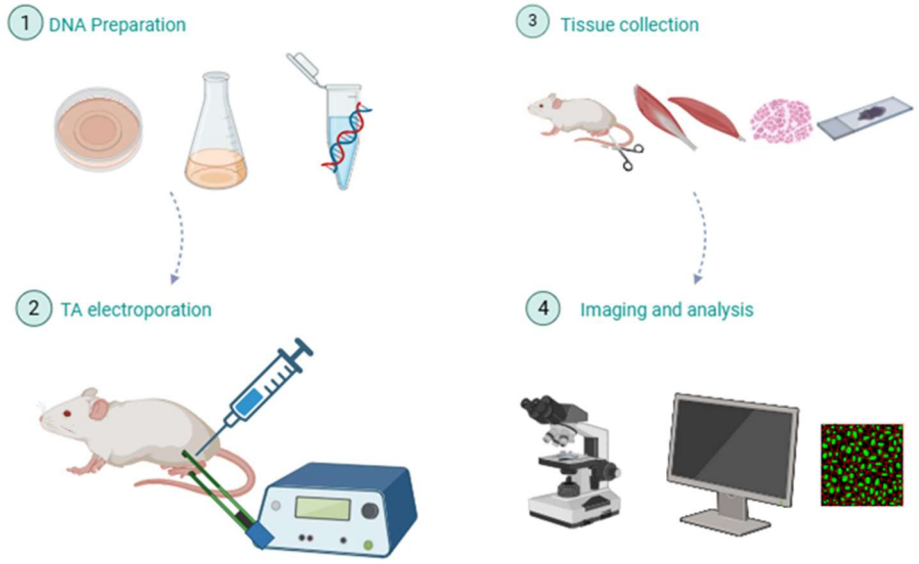

Figure 4.2 The major processes and experimental flow:

1) preparing the indicated constructs. 2) Electroporation of TA muscle for 7 days. 3) Collecting tissue and conducting cross and longitudinal sectioning and mounting on slides. 4) Finally, visualising the products, imaging and performing proper analysis.

4.2.1 Genotyping

Genotype verification was performed routinely to ensure accurate selection of *ky/ky* and wild-type animals for *in vivo* experiments. Figure 4 shows representative genotyping data confirming the presence of a 2-bp deletion in the Ky gene in mutant mice. A combination of Sanger sequencing and gel-based heteroduplex analysis was used to distinguish between wild-type, heterozygous, and homozygous mutant genotypes. This screening strategy ensured consistency across experimental cohorts and maintained colony integrity. See (Figure 4.3).

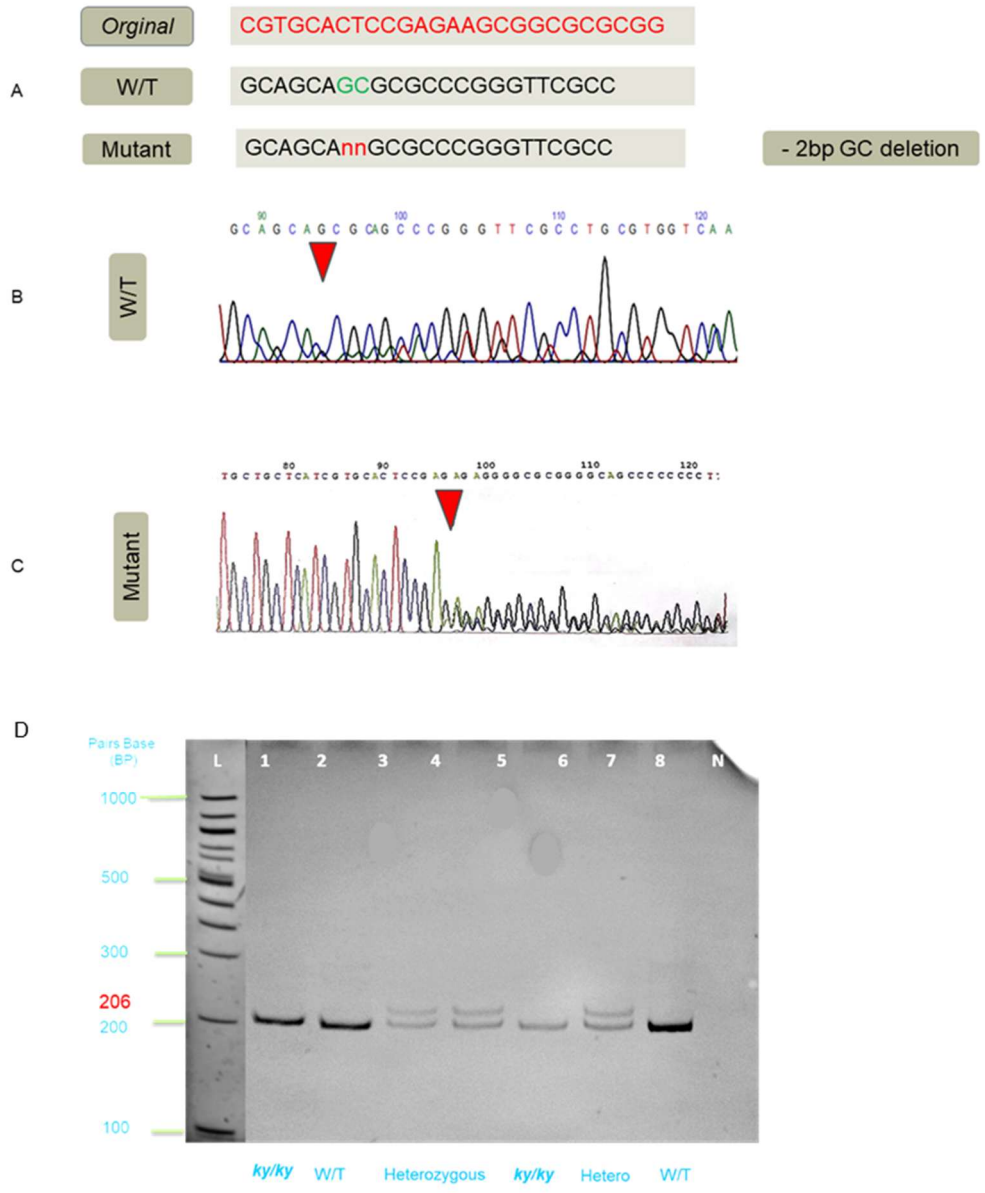

Figure 4.3 Shows genotyping and confirmation of ky/ky mutant mice.

A) Alignment of wild-type (WT) and mutant sequences showing a 2-bp GC deletion (red bases) in the Ky gene. B) Representative Sanger sequencing chromatogram from a wild-type mouse, showing the expected sequence.C) Representative chromatogram from a ky/ky homozygous mutant showing a frameshift pattern following the 2-bp deletion (red arrowhead). D) Gel electrophoresis of PCR products from representative mice. Lanes correspond to different genotypes as labelled. ky/ky homozygotes show a distinct lower band, wild-type samples show a single upper band, and heterozygous samples display both bands due to heteroduplex formation.

4.3 Fluorescent Reporters (tdTomato and GFP) alone have no effect on fibre size

To verify that fluorescent reporters alone do not influence muscle phenotype, control electroporation were performed using plasmids expressing tdTomato or GFP without KY. Both constructs showed robust and localised expression in transfected fibres of the TA muscle, as shown by fluorescence microscopy (Figure 4.4) and (Figure 4. 5).

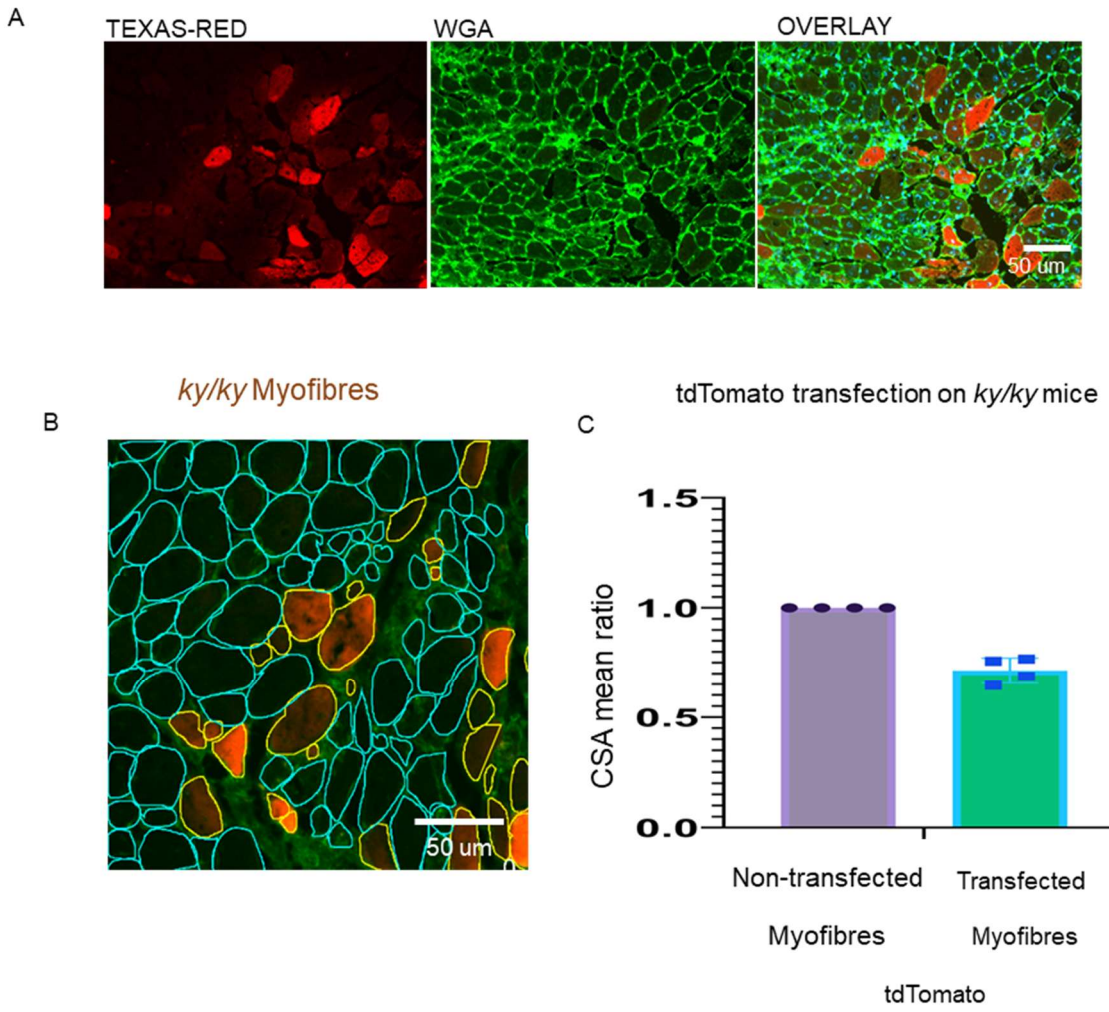

Figure 4.4 tdTomato control construct does not affect muscle fibre size in ky/ky mice.

(A) Representative fluorescence images of TA muscle sections electroporated with the tdTomato-only control construct. The first column shows tdTomato fluorescence (Texas Red filter) indicating transfected fibres. The second column shows laminin immunostaining (FITC filter) outlining muscle fibre boundaries. The third column presents a merged image with DAPI nuclear staining. Scale bar: 50 µm. (B) CSA) measurements of tdTomato-positive versus non-transfected fibres. Data represent mean ± SEM from n = 4 mice, with >150 fibres analysed per condition. (C) Quantification of mean fibre size shows no significant difference between tdTomato-expressing fibres and adjacent non-transfected fibres (p = 0.0654, unpaired t-test), confirming that tdTomato expression alone does not influence muscle fibre morphology and therefore serves as an appropriate fluorescent control.

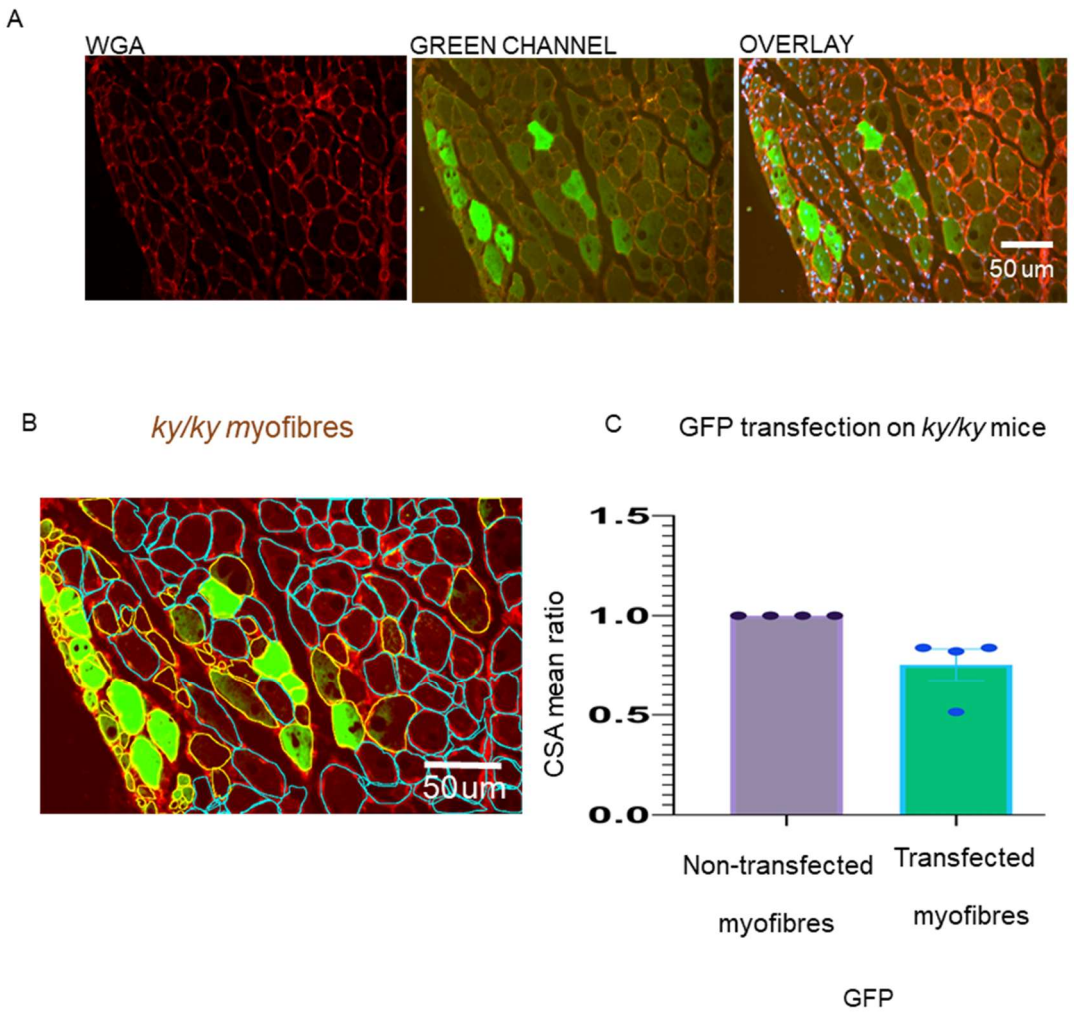

Figure 4.5 GFP-positive myofibres exhibited no significant differences in size compared to adjacent non-transfected neighbouring myofibres.

Fluorescence imaging of GFP-expressing muscles revealed robust reporter signal without inducing any discernible changes in muscle morphology. (A) The panels display GFP that were electroporated into ky/ky mice. The left column highlights the green channel to identify the overexpressed construct in the mice. The next column highlights cellular membranes using WGS. The rightmost column shows an overlay of the two filters along with DAPI. The scale bar on bottom right. (C) Quantitative analysis of fibre cross-sectional area and quantification of mean ratio confirmed that GFP-positive myofibres exhibited no significant differences in size compared to non-transfected controls (p = 0.0570, unpaired t-test), indicating that GFP expression alone does not promote hypertrophy. Data represent mean ± SEM from n = 4 mice, with >150 fibres analysed per condition.

Quantitative analysis of fibre CSA revealed no statistically significant difference between tdTomato or GFP-expressing fibres and adjacent non-transfected fibres. This indicates that expression of either reporter alone does not induce hypertrophy or atrophy.

Together, these data confirm that tdTomato and GFP act as neutral reporters, enabling accurate interpretation of KY construct effects without confounding changes in muscle size.

4.4 Full-Length KY-tdTomato Rescues Fibre Size in *ky/ky* Muscle but Has No Effect in Wild-Type

To evaluate the functional capacity of full-length KY in skeletal muscle, the mKY-td construct was electroporated into the TA muscles of wild-type mice. This allowed us to assess whether KY overexpression is sufficient to induce hypertrophy in normal muscle, and whether it can rescue fibre size in the KY-deficient background.

In wild-type muscle, fluorescence imaging confirmed successful expression of mKY-td, but quantitative analysis of fibre revealed no significant difference between transfected and adjacent non-transfected fibres (Figure 4.6). This indicates that KY overexpression does not induce hypertrophy under baseline conditions in healthy muscle.

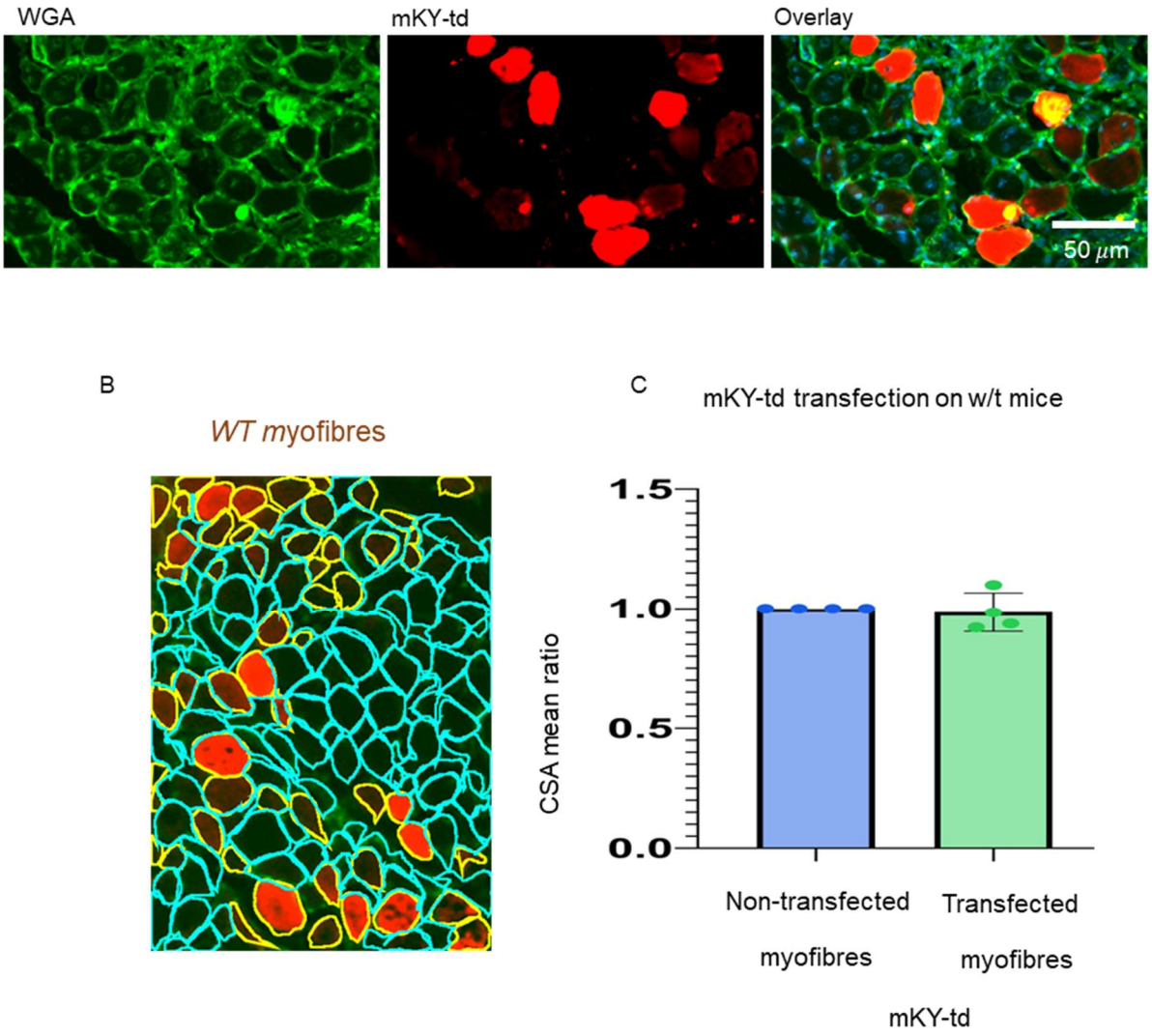

Figure 4.6 Expression of mKY-td does not induce hypertrophy in wild-type (WT) muscle.

(A) Representative images of cross-sections from the TA muscle electroporated with mKY-td. The first column highlights cellular membranes using WGA, the next column shows tdTomato (red) marking transfected fibres, and the merged images illustrate overall fibre morphology. (B) Immunohistochemical segmentation using CellProfiler, highlighting transfected (yellow) and untransfected (cyan) fibres for fibre size analysis. (C) Quantitative analysis of mean CSA ratios between transfected (tdTomato-positive) and adjacent untransfected fibres. No significant difference in fibre size was observed (p = 0.3905, unpaired t-test), indicating that mKY-td expression alone does not elicit a hypertrophic response in WT muscle after 8 days. Data represent mean ± SEM from n = 4 mice, with >150 fibres analysed per condition. Scale bar = 50 µm.

In contrast, when mKY-td was electroporated into *ky/ky* muscle, a significant increase in CSA was observed in transfected fibres compared to contralateral tdTomato controls ($p < 0.01$). These results show that full-length KY is sufficient to restore fibre size in the absence of endogenous KY (figure 4.7).

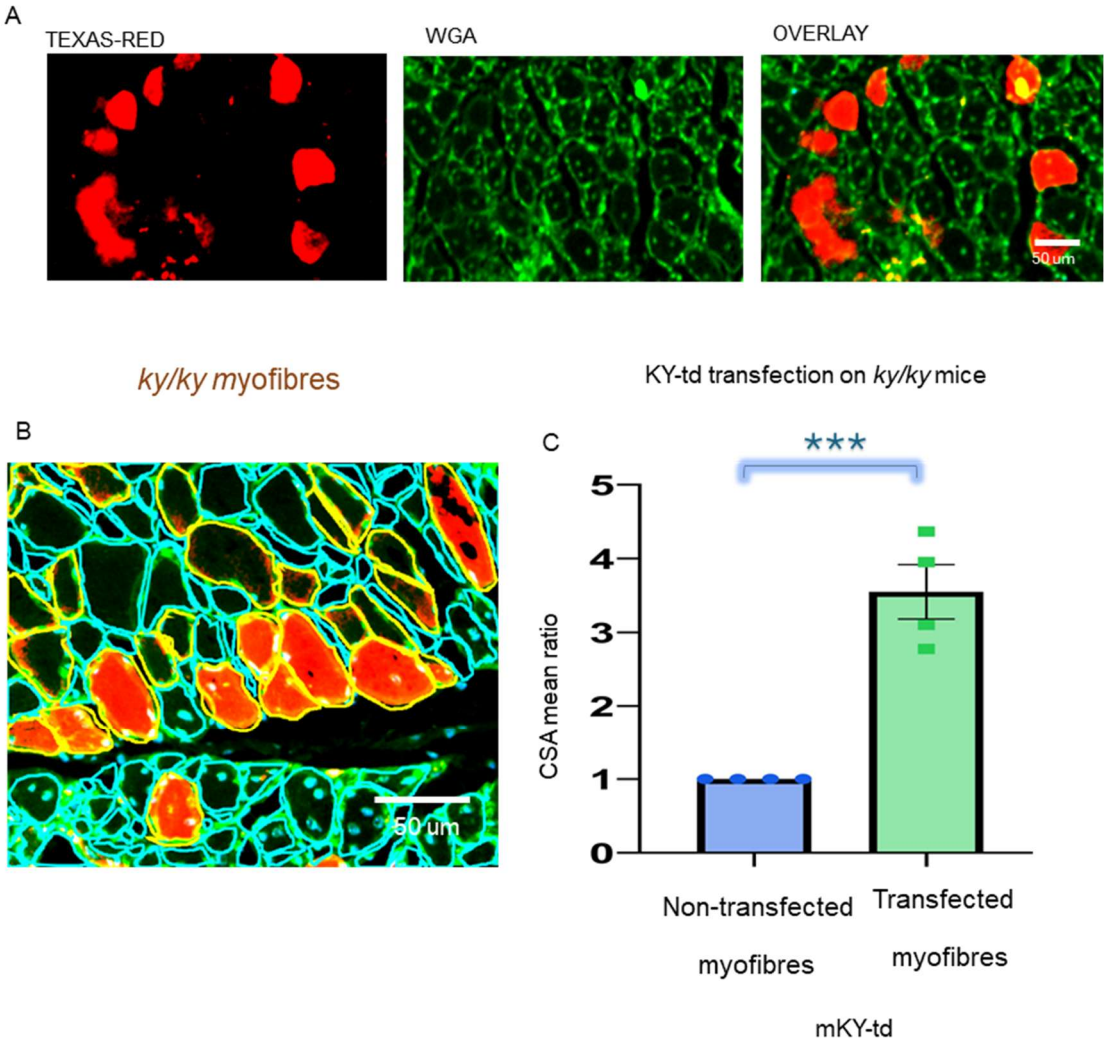

Figure 4.7 KY-deficient muscle fibres exhibit a hypertrophic response when provided with a functional form of KY, compared to adjacent non-transfected myofibres.

(A) The panels display mKY-td expression in ky/ky mice 8 days after electroporation. The left column shows tdTomato fluorescence (Texas Red), the middle column highlights cellular membranes using the green, fluorescent filter, and the right column presents the merged image with DAPI. Scale bar shown at bottom right.(B) Quantitative analysis of fibre CSA. (C) Quantification of the mean CSA ratio demonstrated a significant increase in the size of mKY-td–positive fibres compared to adjacent non-transfected fibres, indicating that mKY-td expression promotes hypertrophy in KY-deficient muscle. p = 0.00045172. Data represent mean ± SEM from n = 4 mice, with >150 fibres analysed per condition.

These findings suggest that KY is essential for muscle fibre maintenance in the *ky/ky* context but is not sufficient to drive fibre growth in wild-type muscle, where the endogenous hypertrophic pathways are intact.

4.5 Mutation of the Catalytic Triad Does Not Impair KY-Dependent Rescue of Fibre Size in *ky/ky* Muscle

To assess the functional relevance of the conserved catalytic triad residues in KY, KY-TM was used in which histidine, cysteine, and aspartate within the TGN/PROT domain were each substituted with alanine. This construct was designed to test whether these residues are essential for KY's role in maintaining muscle fibre size.

KY-TM was electroporated into the TA muscles of *ky/ky* mice, and the response was evaluated eight days post-transfection. The tdTomato-only construct served as the control.

Quantitative CSA analysis showed a significant increase in fibre size in muscles expressing KY-TM compared to tdTomato controls ($p < 0.01$; Figure 4.8). These results indicate that mutation of the catalytic triad does not impair KY's ability to rescue fibre size in *ky/ky* muscle, suggesting that these residues are not essential for KY's function in this context.

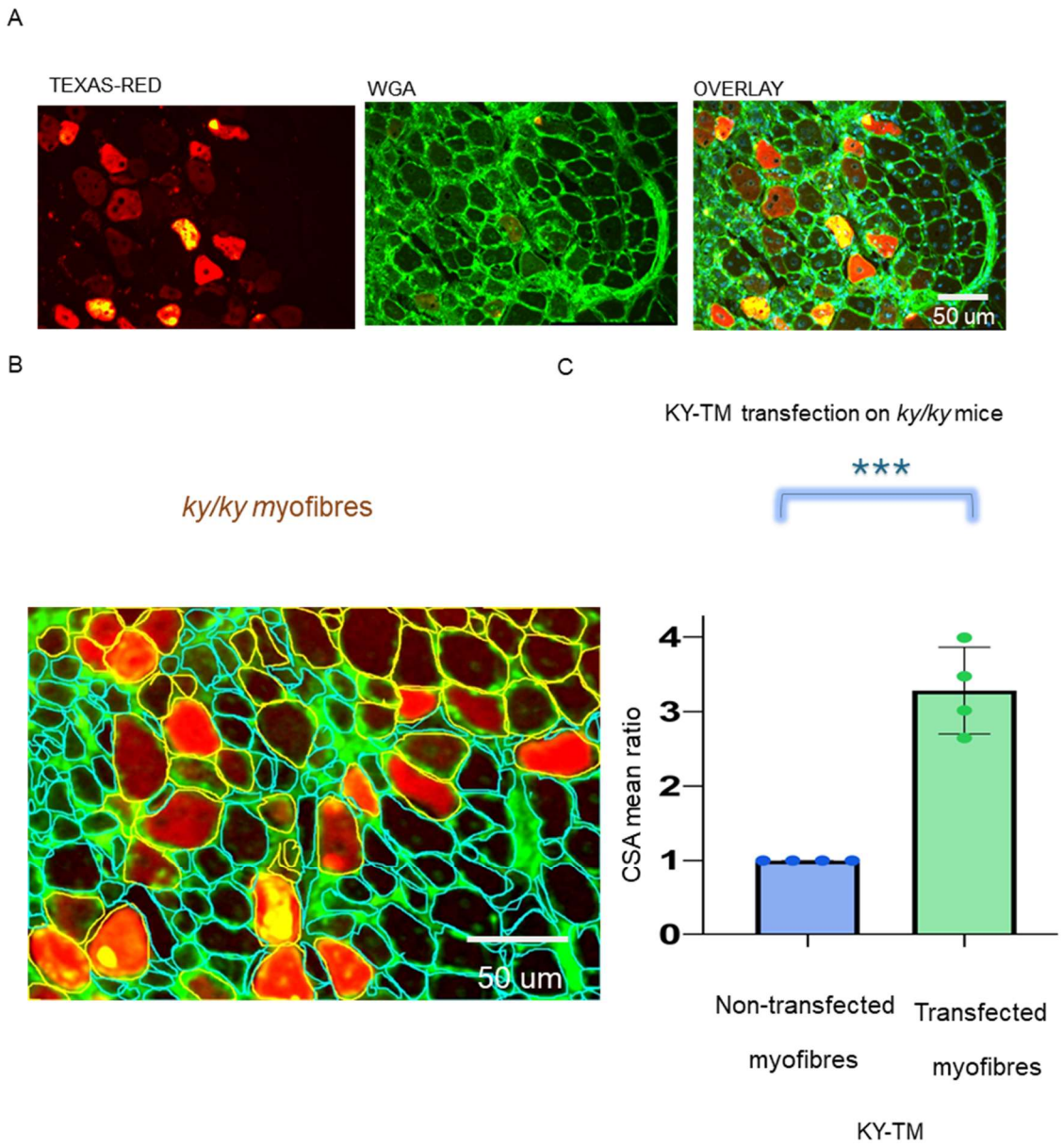

Figure 4.8 Expression of catalytically inactive KY-TM promotes fibre size in KY-deficient ky/ky muscle.

(A) Representative images of TA muscle sections electroporated with the KY-TM construct (tdTomato-tagged) and harvested after 8 days. The left panel shows tdTomato fluorescence marking transfected fibres; the middle panel displays membrane staining; and the right panel presents the merged image with DAPI. Scale bar in the final panel.(B) Quantitative analysis of fibre CSA comparing transfected and neighbouring non-transfected fibres. (C) Mean CSA ratio analysis demonstrates a significant increase in fibre size in KY-TM–expressing fibres relative to non-transfected controls, indicating that the catalytically inactive KY variant retains the capacity to enhance fibre size in ky/ky muscle (p = 0.000114). Data represent mean ± SEM from n = 4 mice, with >150 fibres analysed per condition.

4.6 Impact of TGN/PROT Domain Loss on Fibre Size Rescue

KY-ΔTGN construct was electroporated into the TA muscles of *ky/ky* mice, and fibre size was evaluated eight days post-transfection.

Quantitative analysis revealed no significant increase in fibre CSA compared to tdTomato controls, indicating that the TGN/PROT domain is required for KY-mediated rescue of fibre size in the *ky/ky* background (Figure 4.9).

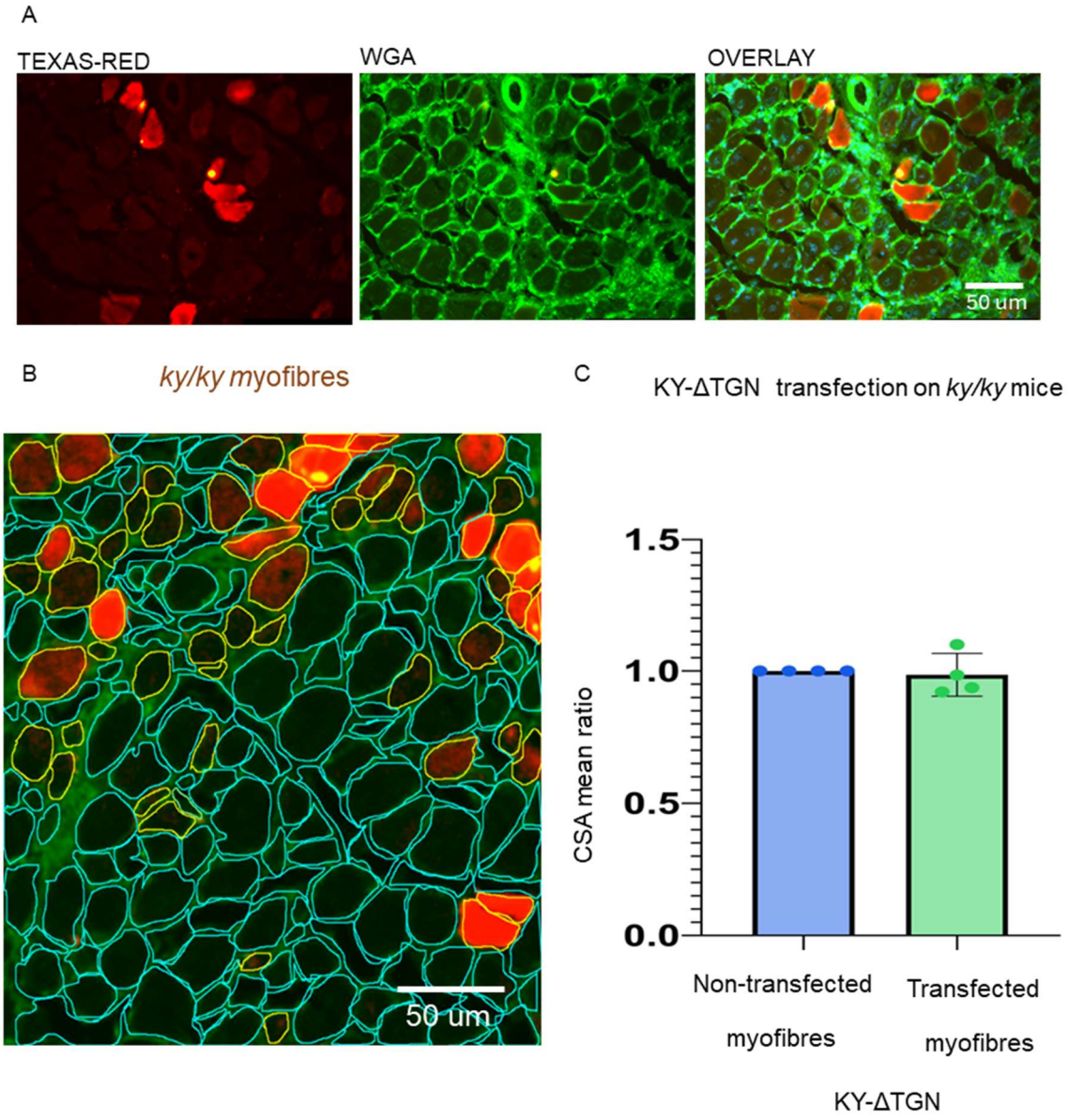

Figure 4.9 Deletion of the TGN/PROT domain abolishes KY-dependent fibre size rescue in ky/ky muscle.

(A) Representative images of TA muscle sections electroporated with the KY-ΔTGN construct and collected after 8 days. The left panel shows tdTomato fluorescence identifying transfected fibres; the middle panel displays membrane staining; and the right panel presents the merged image with DAPI. Scale bar shown in the final panel.(B) Quantitative analysis of CSA comparing KY-ΔTGN–expressing fibres with adjacent non-transfected fibres.(C) Mean CSA ratio analysis shows no significant difference between transfected and non-transfected fibres (p = 0.286685), indicating that deletion of the entire TGN/PROT domain abolishes KY's ability to increase fibre size in ky/ky muscle. Data represent mean ± SEM from n = 4 mice, with >150 fibres analysed per condition.

These results suggest that the TGN/PROT domain is essential for KY function in maintaining normal muscle fibre size.

4.7 Human KY Rescues Fibre Size in *ky/ky* Muscle, Indicating Functional Conservation

To assess the functional conservation between human and mouse KY proteins, the potential of hKY to rescue muscle fibre size was assessed in the TA muscles of *ky/ky* mice. Notably, the human KY protein possesses an N-terminal extension incorporating a predicted NLS, which is not present in the murine orthologue. Eight days after electroporation, muscles were collected and analysed for fibre CSA.

Fibre size was significantly increased in hKY-transfected regions compared to adjacent non-transfected fibres ($p < 0.01$; Figure 4.10). These results demonstrate that human KY is functionally conserved and capable of rescuing the fibre size deficit in *ky/ky* muscle.

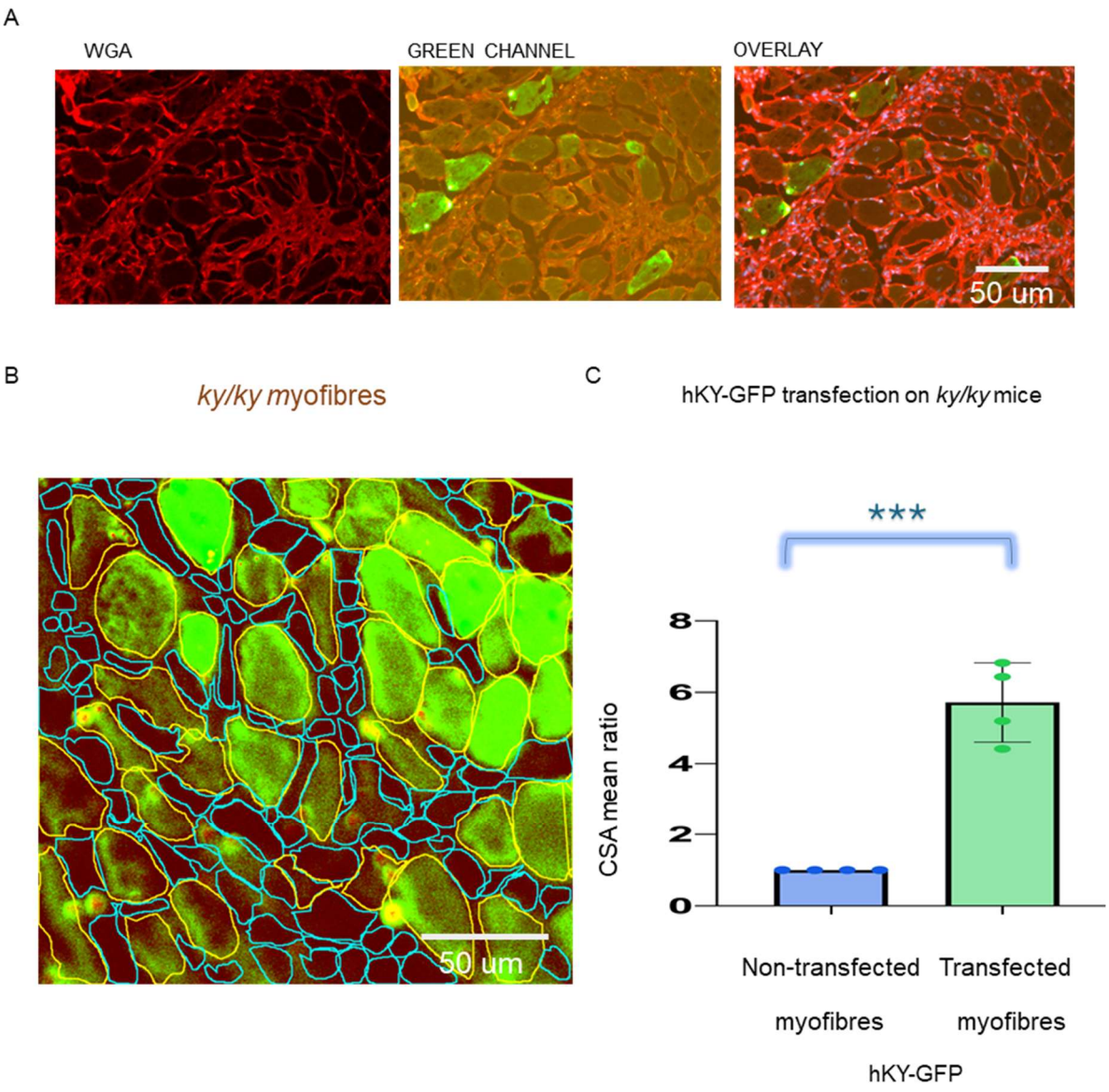

Figure 4.10 Expression of hKY-GFP containing the NLS increases muscle fibre size in ky/ky mice.

A) Representative images of TA muscle sections electroporated with hKY-GFP for 8 days. The first column shows membrane staining using WGA, the second column shows GFP fluorescence identifying transfected fibres, and the third column presents the merged image with DAPI. Scale bar = 50 µm. B) Quantitative analysis of fibre CSA comparing transfected and adjacent non-transfected fibres. C) Mean CSA ratio analysis demonstrates that hKY-GFP–expressing fibres are significantly larger than non-transfected neighbouring fibres, indicating that the NLS-containing hKY construct restores fibre size in ky/ky muscle (p = 0.00014678). Data represent mean ± SEM from n = 4 mice, with >150 fibres analysed per condition.

4.8 Summary of Functional Effects of KY Variants on Fibre Size Rescue

A one-way ANOVA comparing CSA ratios across all constructs showed that mKY-td, KY-TM, and hKY-GFP significantly increased fibre size relative to non-transfected, tdTomato, GFP, and KY-ΔTGN controls ($p < 0.01$). In contrast, KY-ΔTGN, tdTomato, and GFP constructs produced no detectable hypertrophic effect (Figure 4.11).

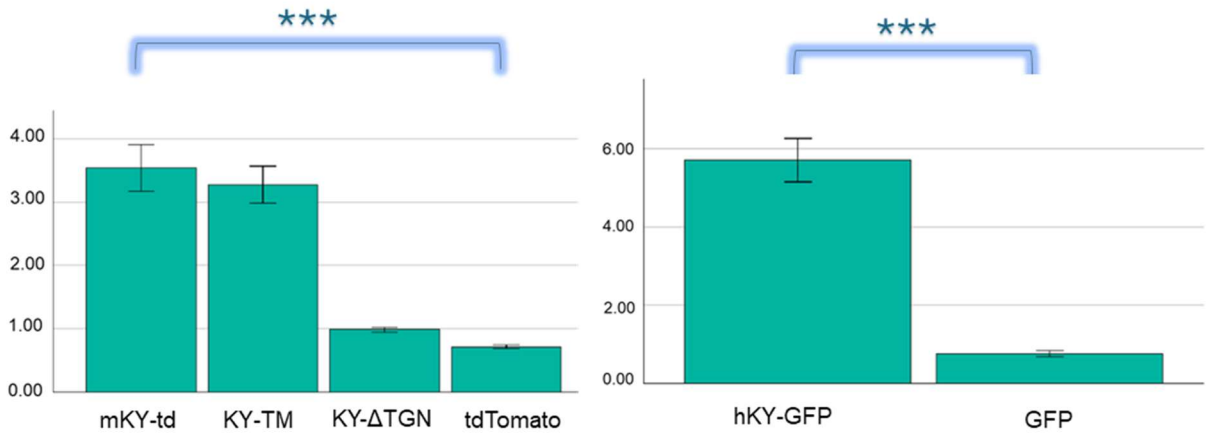

Figure 4.11 Functional rescue of muscle fibre size by KY constructs in ky/ky mice.

Left: Representative quantification of CSA ratios from TA muscles electroporated with different constructs. Constructs include: untransfected control, tdTomato (fluorescent control), GFP (fluorescent control), mKY-td (wild-type mouse KY), KY-TM (catalytic triad mutant), KY-ΔTGN (TGN/PROT domain deletion), and hKY-GFP (full-length human KY containing an NLS). Bars represent mean ± SEM of CSA ratios, normalised to the contralateral untransfected TA. Each point corresponds to a biological replicate (n = 4 mice per condition; >150 fibres analysed per mouse). Right: Summary comparison highlighting the hypertrophic effect of hKY-GFP relative to GFP control, demonstrating that full-length hKY is sufficient to rescue fibre size in ky/ky muscle.

These results indicate that:

- Full-length KY, from either species, is sufficient to rescue fibre size in *ky/ky* muscle.
- Mutation of the conserved catalytic triad residues (C, H, D) does not impair KY's ability to rescue fibre size, indicating that these residues are not essential for KY function in this context.
- Deletion of the entire TGN/PROT domain, however, eliminates the fibre size rescue effect, highlighting the structural necessity of this domain.

These results support a model in which KY's TGN/PROT domain is functionally required, even if individual catalytic residues are not, and that KY's function is conserved across species.

4.9 Discussion

This chapter investigated the functional significance of the TGN/PROT domain in the KY protein by evaluating its requirement for muscle fibre size maintenance *in vivo*. Using a *ky/ky* mouse model of KY deficiency, we tested whether KY variants bearing catalytic triad mutations or domain deletions could rescue the characteristic muscle fibre atrophy. The findings demonstrate that although KY harbours conserved catalytic residues, its biological function does not require enzymatic activity. However, the structural integrity of the TGN/PROT domain itself is essential for KY's ability to restore fibre size.

Transglutaminases TGs catalyse post-translational protein modification, the formation of ε-(γ-glutamyl) lysine isopeptide bonds, and play essential roles in diverse physiological processes, including extracellular matrix assembly, cell adhesion, and signal transduction (Griffin et al., 2002). A conserved catalytic triad of cysteine, histidine, and aspartate underpins the enzymatic activity of classical TGs such as TG2 (Prasanna Murthy et al., 2002). Although KY shares sequence and structural similarity with TGs and contains this canonical triad, previous studies have failed to detect enzymatic activity in KY, raising the possibility that KY represents a functional divergence within this protein family (Harrad, 2021; Makarova et al., 1999).

In vivo experiments in the TA muscles of KY-deficient *ky/ky* mice support this hypothesis. Mutation of the catalytic triad residues KY-TM did not impair the protein's ability to restore muscle fibre CSA, clearly indicating that the triad—and, by extension, catalytic activity is dispensable for KY function in this context. This finding distinguishes KY from enzymatically active TGs and supports the interpretation that KY operates through non-catalytic mechanisms. It is plausible that KY's function depends on its structural role as a scaffold or as a mediator of protein–protein interactions rather than enzymatic processing (Eyers & Murphy, 2016; Murphy et al., 2017).

This pseudoenzymatic behaviour places KY within an expanding class of catalytically inactive yet functionally indispensable proteins known as pseudoenzymes. These proteins retain structural domains resembling active enzymes but act primarily through scaffolding, mechanosensing, or allosteric regulation rather than catalysis. Reviews of pseudoenzymes highlight that many such proteins preserve enzyme-like folds that mediate signalling or complex assembly without catalytic turnover (Eyers & Murphy, 2016; Murphy et al., 2017).

Well-characterised examples include the HER3 pseudokinase, which lacks catalytic activity but functions as an allosteric scaffold in receptor tyrosine kinase signalling (Littlefield et al., 2014), and the kinase-like domain of titin, which acts as a mechanosensory module regulating sarcomeric tension rather than performing phosphorylation (Puchner et al., 2008). Similarly, ALPK3, a muscle-enriched pseudokinase mutated in familial cardiomyopathy, exemplifies how catalytically

deficient enzymes can still perform essential structural or signalling roles within muscle (Agarwal et al., 2022).

Within the transglutaminase family, catalytically inactive homologues have also been reported to serve regulatory or scaffolding functions instead of enzymatic crosslinking (Lorand & Graham, 2003). Collectively, these parallels support the interpretation that KY, despite possessing a transglutaminase-like fold, functions as a pseudoenzyme, a structural or regulatory scaffold at the Z-disc that contributes to sarcomeric integrity and proteostasis without requiring catalytic activity.

Crucially, while the catalytic triad is non-essential, deletion of the entire TGN/PROT domain KY^ΔTGN completely abolished KY's ability to rescue fibre size. This highlights the functional vitalness of the domain itself. The loss of function in KY^ΔTGN despite expression indicates that the domain likely contributes critical interaction motifs or structural features necessary for KY's role in muscle maintenance. Such a difference between enzymatic and structural necessity is also documented in TG2, where selective mutations abolish enzymatic function while preserving scaffolding capacity (Gaudry et al., 1999; Van Den Akker et al., 2012; Verderio et al., 2003). Though interaction partners were not assessed in this chapter, the results suggest that the TGN/PROT domain supports molecular functions beyond catalysis, likely through facilitating physical interactions with cytoskeletal or chaperone systems.

The results also revealed that full-length hKY, which possesses an extended N-terminal region including a predicted NLS, was able to restore fibre size in *ky/ky* mice. This provides *in vivo* evidence of functional conservation between human and murine KY, despite sequence divergence. Although we did not investigate nuclear import or gene regulatory roles of the NLS-containing hKY variant, its ability to compensate for endogenous mouse KY indicates that added sequence elements in the human isoform do not interfere with core muscle-stabilising function. It is possible that the N-terminal extension enhances subcellular trafficking or responsiveness to stress, features which may be further explored in later chapters.

Overexpression of KY in wild-type muscle did not increase fibre size, strengthening the conclusion that KY is not a hypertrophy-inducing protein. Rather, KY appears essential for maintaining baseline fibre integrity. In *ky/ky* muscle, the absence of KY results in marked atrophy, which can be reversed by reintroducing full-length or functionally competent KY variants. However, in wild-type muscle, where KY function is intact, additional expression has no additive effect. These findings underline KY's role as a homeostatic—not anabolic—regulator of muscle size, consistent with prior studies showing that KY mutations in humans cause slowly progressive myopathies rather than overt muscle hypertrophy (Hedberg-Oldfors et al., 2016).

While these findings offer valuable mechanistic insights, there are important caveats to consider. The rescue experiments were conducted via electroporation into the TA muscle, which provides strong evidence for local KY function, but may not fully capture the systemic or long-term consequences of KY deficiency. Additionally, although both

KY-TM and KY-ΔTGN constructs were tested for functional effects, their expression levels and protein stability were not thoroughly quantified. Differences in how these constructs are expressed or degraded could have influenced the observed changes in fibre size. Another unresolved issue is the precise role of the TGN/PROT domain in KY function. It remains unclear whether this domain is involved in recruiting chaperones, anchoring KY at the Z-disc, or facilitating interactions with other structural proteins. Finally, this chapter did not explore how domain integrity affects KY's ability to interact with binding partners. Further experiments, such as biochemical pulldown assays or high-resolution imaging, will be essential to clarify how deletion of the TGN/PROT domain alters KY's functional network.

These findings position KY as a structurally distinct, functionally essential pseudoenzyme within the transglutaminase-like protein family. While it retains a TG-like domain, its function does not depend on catalytic activity but rather on the structural integrity of the domain itself. The essential role of the TGN/PROT domain highlights its likely function in scaffolding or signalling, possibly through mediating interactions with other sarcomeric or proteostatic components. The successful rescue by hKY further underlines the evolutionary conservation of KY's structural role in muscle. These results add to the growing body of evidence that enzymatic domains can evolve to fulfil architectural or regulatory functions. Exploring the differential interactomes of KY-TM and KY-ΔTGN, as well as evaluating KY's dynamics under muscle stress conditions, may further illuminate its role in sarcomere maintenance. Ultimately, these findings provide a mechanistic framework for understanding how KY deficiency contributes to muscle fibre degeneration and progressive myopathy.

CHAPTER FIVE: RESULTS

Z-Disc Targeting of KY Protein Variants — A Colocalization Study

CHAPTER 5. Z-Disc Targeting of KY Protein Variants — A Colocalization Study

5.1 Introduction

KY is a skeletal muscle protein associated with the Z-disc, a key structural component of the sarcomere responsible for force transmission and mechanical stability in striated muscle. Mutations in the KY gene have been linked to neuromuscular conditions including MFM-7 and hereditary spastic paraplegia (HSP) (Baker et al., 2010; Ehsani et al., 2022; Yogev et al., 2017), highlighting the clinical importance of understanding its molecular function.

KY has been shown to localise specifically to the Z-disc, where it forms part of a structural complex with FLNC and IGFN1 (Baker et al., 2010; Beatham et al., 2004). Through these interactions, KY is thought to contribute to sarcomere organisation, possibly acting as a scaffold that supports structural and mechanical stability. However, despite these established associations, the specific domains within KY that mediate Z-disc targeting remain incompletely defined. The central TGN/PROT domain is structurally conserved, but its contribution to subcellular localisation has not been fully resolved. Prior studies suggest that interactions with Z-disc–associated proteins such as FLNC and IGFN1 may underlie KY's targeting, yet direct experimental validation of these mechanisms is limited.

The functional importance of correct localisation is evident in ky/ky mutant mice, which lack functional KY and develop hallmark features of myofibrillar disruption. These include Z-disc streaming, thickening, loss of structural integrity, increased central nucleation, fibre atrophy, and signs of ongoing regeneration—changes that occur despite the absence of central nervous system abnormalities (Beatham et al., 2004; Blanco et al., 2001). This phenotype underscores KY's crucial role in maintaining sarcomeric organisation.

Although KY reliably localises to the Z-disc, the precise motifs responsible remain uncharacterised. Emerging evidence, including observations from previous construct-based studies, suggests that the TGN/PROT domain may not be essential for Z-disc targeting (Harrad, 2021). This raises the possibility that other sequence elements or interaction interfaces within KY govern its recruitment to the Z-disc, but these remain to be systematically defined.

In this chapter, we investigate the subcellular localisation of the panel of KY constructs previously employed in Chapter 4, aiming to determine whether Z-disc targeting depends on specific functional domains namely, the catalytic triad and the full TGN/PROT region. Building on the fibre rescue experiments, we apply high-resolution confocal microscopy and immunofluorescence imaging to examine how each

construct behaves within the sarcomere. Co-localisation analyses were performed with α-actinin, an established Z-disc marker, and with a titin epitope located at the Z-disc, to assess the ability of each variant to localise correctly. This approach also allows comparison of mouse and human KY, providing insight into whether their targeting mechanisms are conserved.

These experiments aim to identify the structural determinants of KY localisation, clarify how specific domains contribute to sarcomere organisation, and illuminate how domain-specific mutations may contribute to KY-associated neuromuscular disease.

5.2 Experimental design

To examine the *in vivo* subcellular localisation of KY and evaluate the role of the conserved catalytic residues and the TGN/PROT domain in Z-disc targeting, a panel of fluorescently tagged KY constructs was introduced into mouse skeletal muscle via *in vivo* electroporation. The constructs included full-length KY, a variant with alanine substitutions in the conserved catalytic triad KY-TM, and a deletion variant lacking the entire TGN/PROT domain KY-ΔTGN. Each construct was tagged with either tdTomato or GFP to enable visual detection within muscle fibres.

Following an 8-day expression period to allow for protein synthesis and localisation, TA muscles were harvested and longitudinally sectioned. Sections were immunostained using antibodies against the Z-disc marker α-actinin to assess KY localisation relative to sarcomeric structures. In some experiments, an additional antibody targeting the N2A epitope of titin located adjacent to the Z-disc was used to further delineate sarcomere boundaries. While titin is not a core Z-disc protein, this region-specific antibody provides sufficient spatial resolution for assessing Z-disc–proximal localisation.

Subcellular localisation patterns were analysed using high-resolution confocal microscopy, allowing detailed visualisation of the co-localisation between KY variants and established Z-disc markers. This approach enabled a direct comparison of the targeting behaviour of each KY construct and provided insight into the domain requirements for proper Z-disc association under physiological conditions.

5.3 GFP and tdTomato Controls Do Not Localise to the Z-Disc

To confirm that the fluorescent reporters did not non-specifically localise to sarcomeric structures, control TA muscles were electroporated with GFP or tdTomato alone. Longitudinal sections of these muscles were imaged following immunostaining with α-actinin, a well-characterised Z-disc marker.

Both GFP and tdTomato exhibited diffuse cytoplasmic distribution, with no detectable enrichment at the Z-disc. No aggregation or aberrant subcellular localisation was observed, and fluorescence signal was uniformly distributed along muscle fibres, consistent with non-targeted protein expression.

These controls confirmed that: the fluorescent tags themselves do not localise to the Z-disc, no artefactual co-localisation occurs in the absence of KY fusion proteins, and imaging conditions and antibody staining protocols were specific and reliable.

These results provide a critical baseline for the interpretation of Z-disc co-localisation in KY-transfected samples and validate the specificity of the localisation patterns observed in subsequent experiments (Figure 5.1, Figure 5.2).

While the GFP and tdTomato controls showed diffuse cytoplasmic distribution and no apparent enrichment at the Z-disc, it is important to acknowledge that fixation and processing can sometimes influence the apparent localisation of soluble fluorescent proteins. Formaldehyde fixation has been reported to alter GFP and RFP fluorescence patterns by changing protein solubility or promoting weak interactions with cytoskeletal elements (Snapp et al., 2003). Such effects may, in some cases, produce low-level or artifactual signals at structured regions such as the Z-disc.

Although no such artefactual enrichment was evident in our control samples, live-cell imaging or detergent-extraction controls could further confirm that the Z-disc

localisation observed in KY fusion constructs represents genuine targeting rather than fixation-related redistribution.

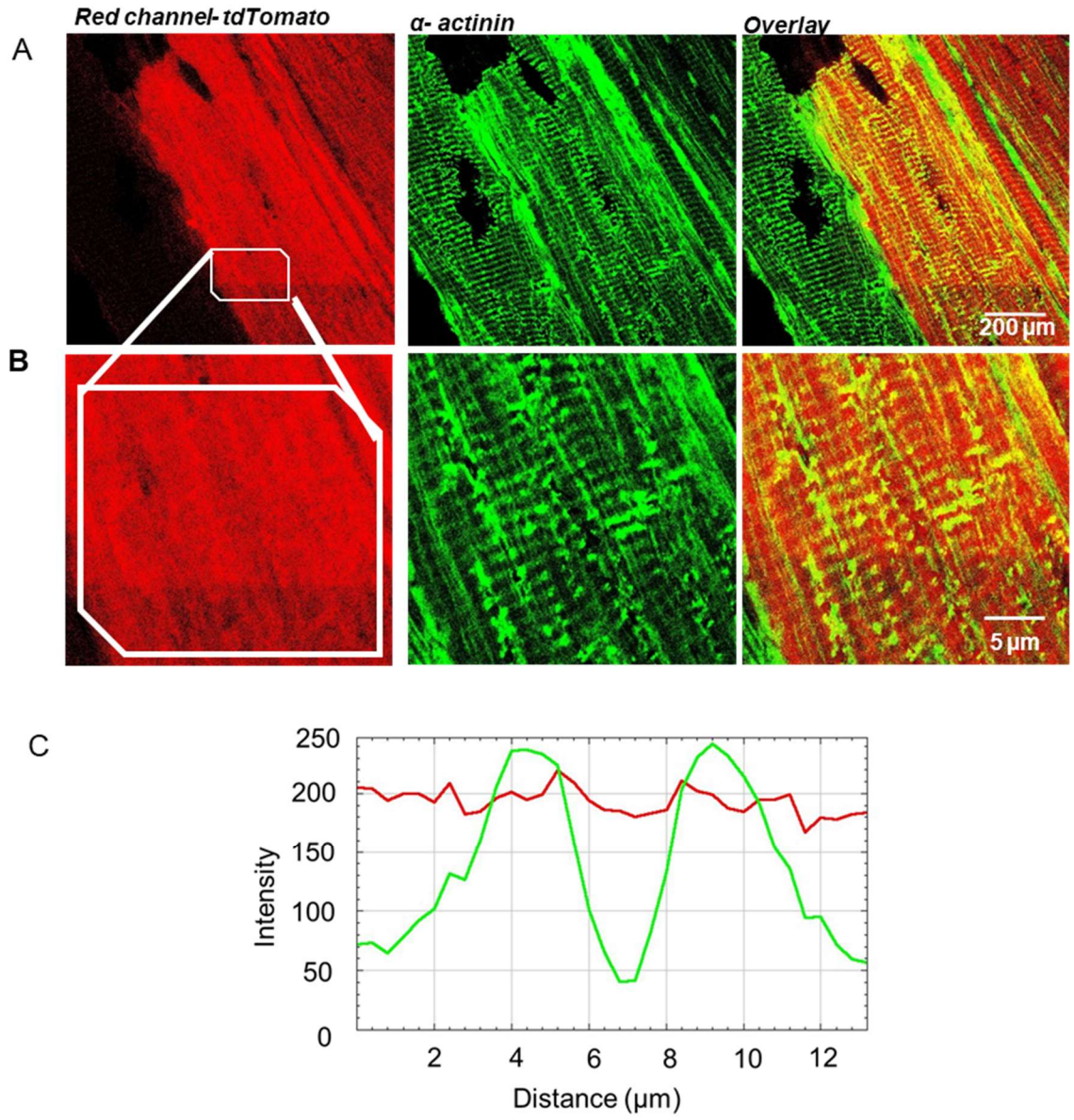

Figure 5.1 tdTomato does not localise to the Z-disc in skeletal muscle fibres.

A) Longitudinal section of TA muscle electroporated with tdTomato and immunostained with actinin to label the Z-disc. Titin columns (green) are clearly visible and indicated in the images. tdTomato expression (red) appears diffusely distributed throughout the cytoplasm, without enrichment at the Z-disc. The final column displays merged images of α-actinin, tdTomato, and DAPI staining, with a scale bar shown in the bottom right. B) A magnified view of the highlighted region. C) An RGB intensity profile plot, displaying fluorescence intensity along a selected line across the fibre. The x-axis denotes distance in pixels, and the y-axis indicates fluorescence intensity. Red and green curves represent the tdTomato and α-actinin signals, respectively, confirming the absence of co-localisation between the two channels.

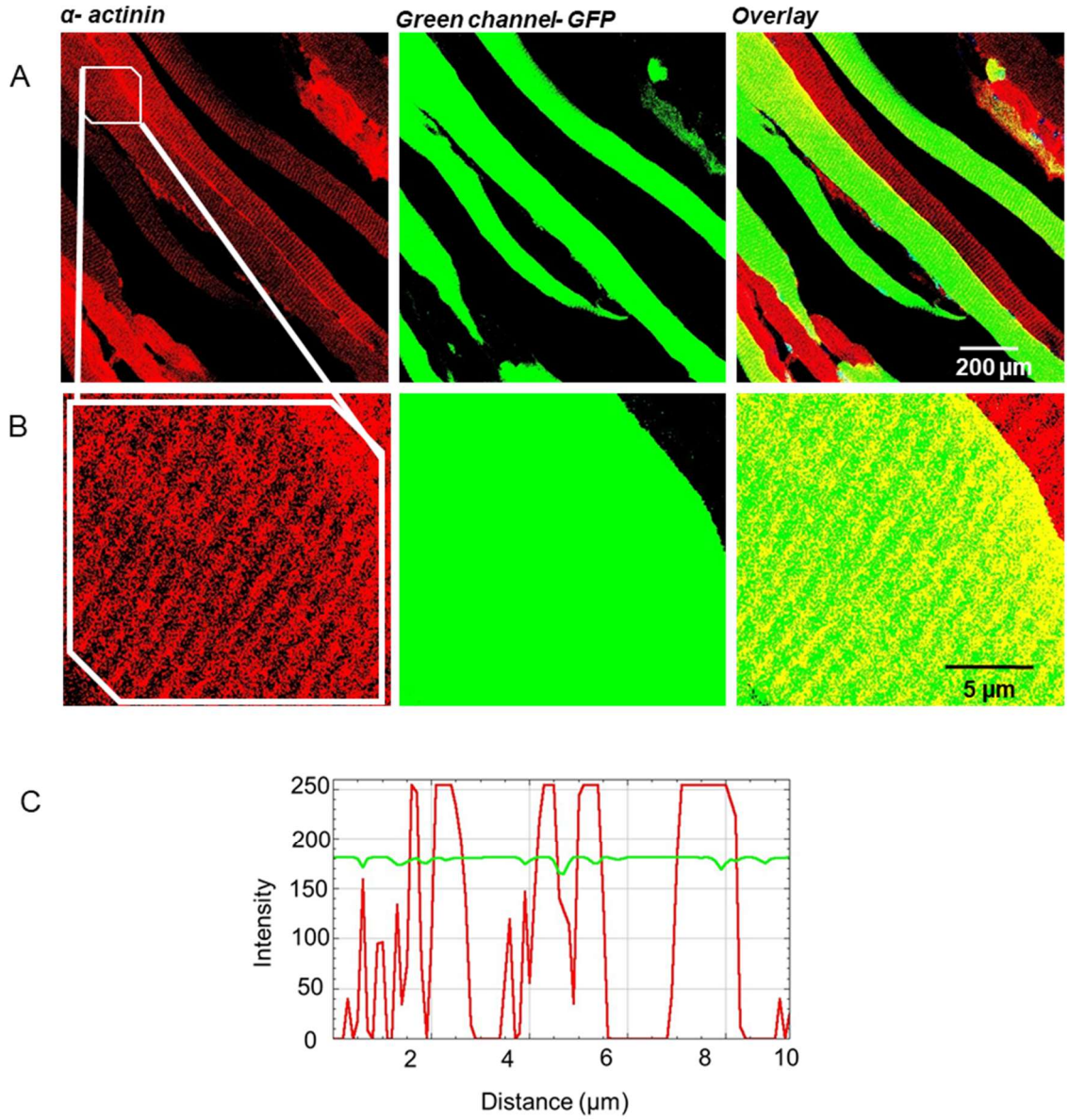

Figure 5.2 GFP does not localise to the Z-disc in skeletal muscle fibres.

A) Longitudinal section of TA muscle electroporated with GFP and immunostained with α-actinin to label the Z-disc. α-Actinin columns (green) are clearly visible and indicated in the images. GFP signal (green) displays a diffuse cytoplasmic distribution, with no enrichment at the Z-disc. The final column shows merged images of α-actinin, GFP, and DAPI staining, with a scale bar displayed in the bottom right. B) Magnified view of the region indicated in panel A. C) RGB intensity profile plot showing fluorescence distribution along a selected line across the fibre. The x-axis indicates distance in pixels, and the y-axis represents fluorescence intensity. Green and red curves correspond to GFP and α-actinin signals, respectively, confirming the absence of co-localisation between the two channels.

5.4 Human KY Localises to the Z-Disc in Mouse Muscle

To assess whether human KY retains Z-disc targeting capability *in vivo*, full-length hKY-GFP was electroporated into mouse TA muscles. This construct includes the conserved TGN/PROT domain as well as an N-terminal extension containing NLS unique to the human isoform. Following an 8-day expression period, immunostaining against titin combined with high-resolution confocal microscopy revealed that hKY-GFP consistently localised to the Z-disc. The observed fluorescence displayed a

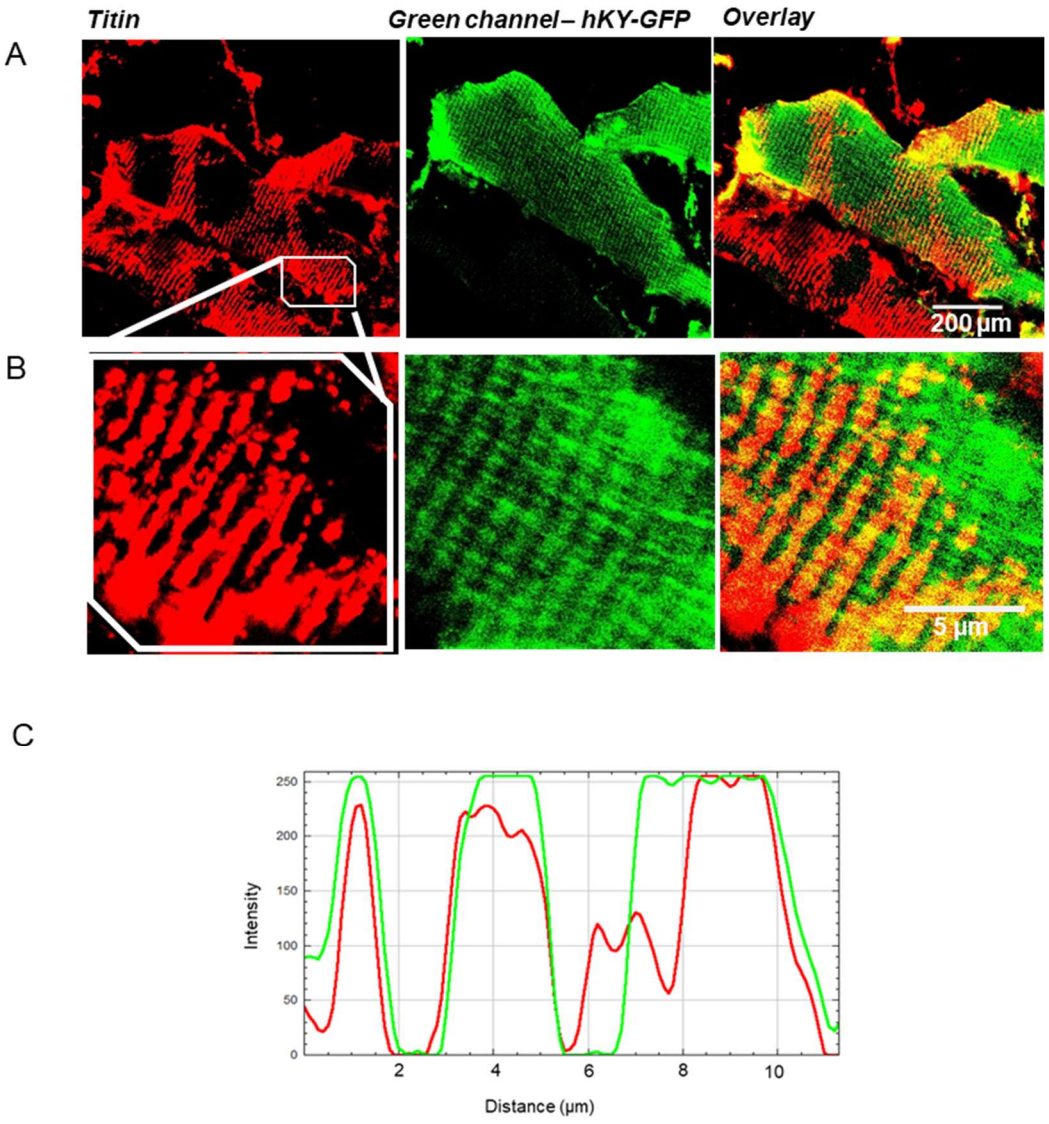

Figure 5.3 Human KY localises to z-disk.

A) The figure illustrates a longitudinal section for electroporated samples after being stained by Titin antibodies to label the Z-disc. Titin columns are indicated in the images. Red or green channels detecting the Huky construct are indicated in the images. The last column displays the overlays of the Titin, green channel and DAPI. A scale bar on the bottom right last column. hKY-GFP shows colocalization with Titin. Magnification of the inset indicated in B. C) RGB intensity profile plot showing the fluorescence intensity distribution along a selected line across the image. The x-axis represents the distance in pixels, while the y-axis indicates the intensity values. The red and green curves correspond to the intensity profiles of the red and green channels, respectively, highlighting differences in spatial distribution and signal overlap between the two channels.

punctate pattern that aligned precisely with Z-disc markers, indicating effective and specific recruitment of the human KY construct to sarcomeric structures(Figure 5.3).

These results demonstrate that human KY retains its Z-disc targeting signals when expressed in the mouse background, confirming functional conservation across species. Moreover, the data suggest that the presence of the TGN/PROT domain is not strictly necessary for Z-disc localisation, supporting the notion that other domains or motifs within the KY protein mediate this spatial targeting.

5.5 Mutation of Conserved Catalytic Residues Does Not Disrupt Z-Disc Targeting

To assess whether the conserved catalytic residues (histidine, cysteine, and aspartate) are required for KY localisation to the Z-disc, we evaluated the subcellular distribution of the KY-TM construct, in which these residues were replaced by alanines. The construct KY-TM was electroporated into mouse TA muscle, and longitudinal sections were analysed by confocal microscopy following α-actinin immunostaining.

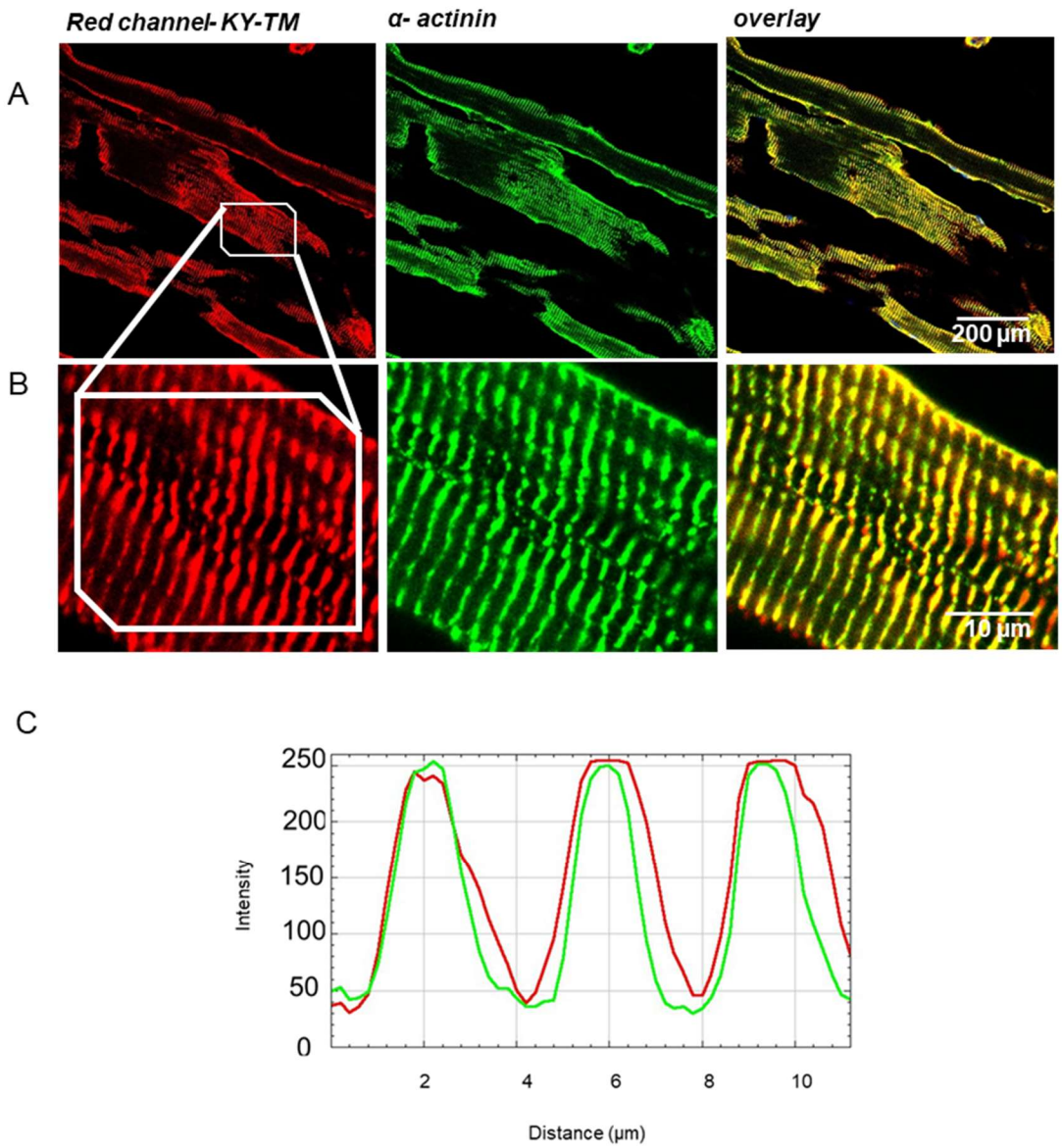

Figure 5.4 The three catalytic resdues in the mKY protein does not alter Z-disc localization.

A) The figure illustrates a longitudinal section for electroporated samples after being stained by α-Actinin antibodies to label the Z-disc. Alfa-actinin columns are indicated in the images. Red or green channels detect KY construct are indicated in the images. The last column displays the overlays of the α-actinin, red channel and DAPI. A scale bar on the bottom right last column. KY-TM shows colocalization with α-actin. Magnification of the inset indicated in B. C) RGB intensity profile plot showing the fluorescence intensity distribution along a selected line across the image. The x-axis represents the distance in pixels, while the y-axis indicates the intensity values. The red and green curves correspond to the intensity profiles of the red and green channels, respectively, highlighting differences in spatial distribution and signal overlap between the two channels.

The results showed that KY-TM remained consistently localised to the Z-disc (Figure 5.4), with a fluorescence pattern indistinguishable from that of the full-length KY construct. This indicates that mutation of the conserved catalytic residues does not impair KY's ability to target the Z-disc, suggesting that this triad is not required for subcellular localisation in skeletal muscle.

5.6 The Deletion of the TGN/PROT Domain Does Not Prevent Z-Disc Targeting

To investigate whether the TGN/PROT domain is required for KY localisation, we examined the subcellular distribution of a KY construct lacking the entire TGN/PROT region KY-ΔTGN. Following electroporation into mouse TA muscle and staining for titin, KY-ΔTGN showed a punctate pattern aligned with the Z-disc, similar to that observed for full-length KY (Figure 5.5).

These results indicate that removal of the TGN/PROT domain does not affect KY's ability to localise to the Z-disc, suggesting that this domain is not essential for subcellular targeting *in vivo*.

These results reinforce that Z-disc localisation is mediated by regions outside the TGN/PROT domain, which may instead serve other non-localisation-related functions.

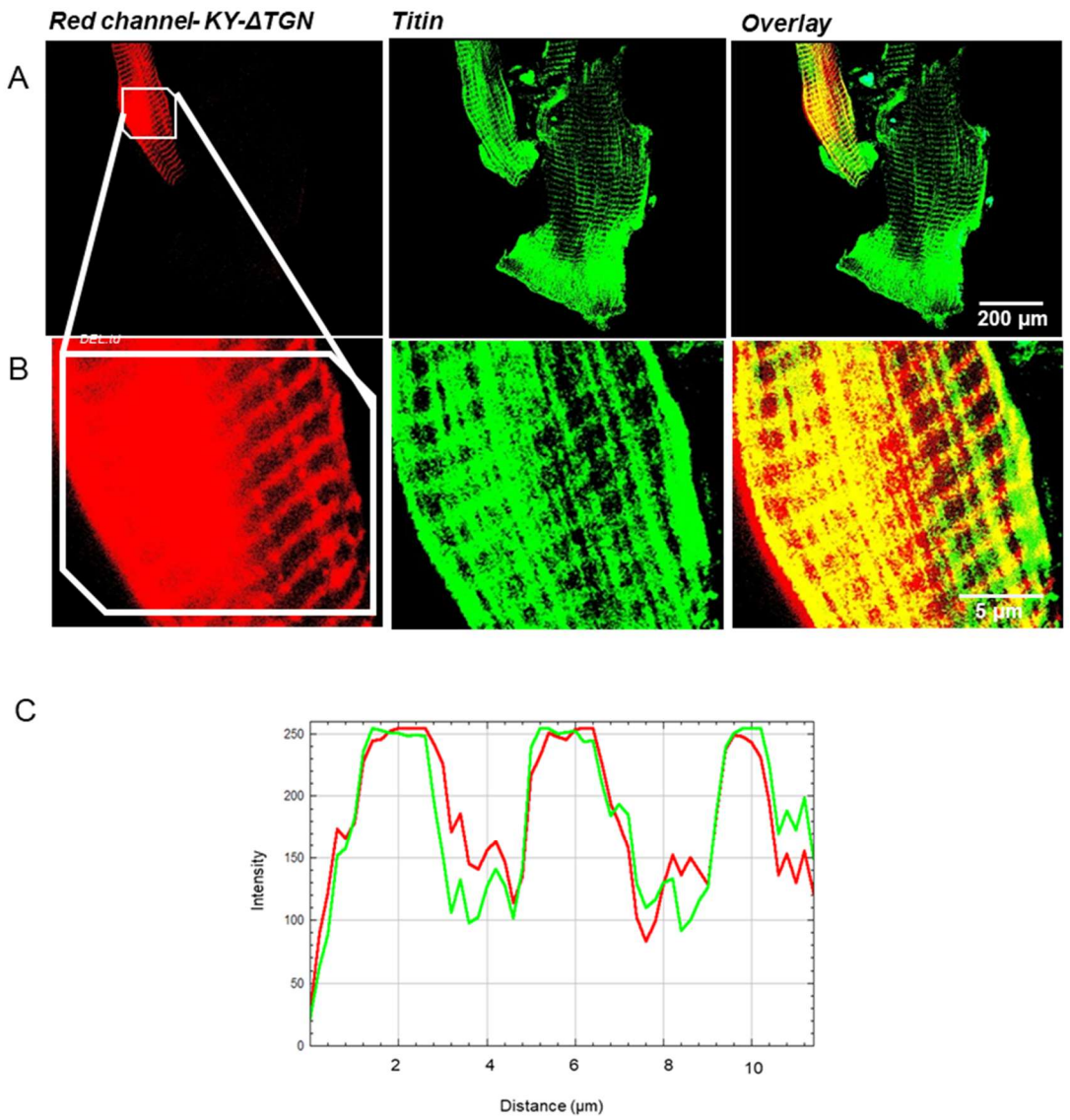

Figure 5.5 The Transglutaminase domain in the mKY protein does not alter Z-disc localization.

The figure illustrates a longitudinal section for electroporated samples after being stained by Titin antibodies to label the Z-disc. Titin columns are indicated in the images. Red or green channels detect KY construct are indicated in the images. The last column displays the overlays of the titin, red channel and DAPI. A scale bar on the bottom right last column. mky_KY-ΔTGN shows colocalisation with Titin. Magnification of the inset indicated in B. C) RGB intensity profile plot showing the fluorescence intensity distribution along a selected line across the image. The x-axis represents the distance in pixels, while the y-axis indicates the intensity values. The red and green curves correspond to the intensity profiles of the red and green channels, respectively, highlighting differences in spatial distribution and signal overlap between the two channels.

5.7 Discussion

This study investigated the subcellular localisation of KY protein constructs in skeletal muscle, with a particular focus on their targeting to the Z-disc. Using *in vivo* electroporation and confocal microscopy, we evaluated the distribution of various KY variants, including full-length mouse and human KY, catalytic triad mutants, and a construct lacking the TGN/PROT domain. These experiments allowed us to define which regions of KY are necessary for Z-disc localisation and provided new insights into KY's subcellular targeting mechanisms.

The results demonstrate that full-length hKY efficiently localises to the Z-disc in mouse TA muscle, highlighting a conserved targeting mechanism across species. This supports the hypothesis that the loss of KY function in ky/ky mice arises from the absence of protein rather than mislocalisation. This observation is consistent with the high sequence identity between mouse and human KY (identity: 90.5%; similarity: 94.7%) (Altschul et al., 1997; Blanco et al., 2001).

In vivo co-localisation experiments confirmed that KY constructs reliably target the Z-disc, as demonstrated by their overlap with established sarcomeric markers. Co-labelling with α-actinin and with a Z-disc–associated titin epitope provided complementary reference points for defining Z-disc localisation. As expected, control constructs expressing GFP or tdTomato alone showed no enrichment at the Z-disc, confirming that the observed localisation is specific to KY and validating the imaging approach.

Significantly, the deletion of the entire TGN/PROT domain KY-ΔTGN did not impair KY's ability to localise to the Z-disc. This result indicates that the TGN/PROT domain is not required for subcellular targeting and instead may serve other functions such as mediating protein–protein interactions or participating in stress responses (Lee et al., 2016). This observation builds on prior insights by Jokl et al. (2018), who highlighted the importance of KY's structural configuration in cytoskeletal dynamics but did not directly assign Z-disc targeting signals to the TGN/PROT domain. Our findings clarify that Z-disc anchoring is mediated elsewhere within the KY sequence. Equally, mutating the conserved catalytic triad residues (histidine, cysteine, and aspartate) did not disrupt Z-disc localisation, further supporting the notion that these residues are dispensable for targeting.

The findings suggest that alternative domains, particularly in the C-terminal region are responsible for mediating KY's Z-disc localisation. AlphaFold structural predictions support this, indicating ordered regions in the C-terminus that may facilitate subcellular targeting. The schematic in Figure 5.6 highlights the modular structure of KY, including a ubiquitin-like UBL domain and, in human KY, an additional N-terminal extension containing an NLS.

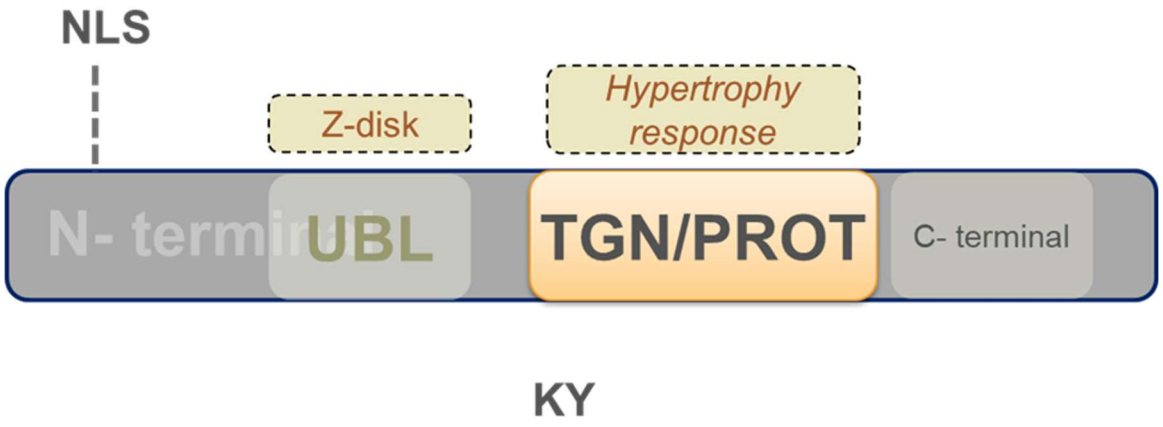

Figure 5.6 Illustrates a schematic representation of the KY protein domain structure.

The KY protein is composed of multiple conserved regions, including an N-terminal segment, a ubiquitin-like UBL domain, a central transglutaminase-like/protease (TGN/PROT) domain, and a C-terminal region. The human KY isoform additionally includes an N-terminal nuclear localisation signal (NLS), shown as a dashed line. The UBL domain is implicated in Z-disc targeting and protein–protein interactions. The TGN/PROT domain, although not required for Z-disc localisation, has been linked to hypertrophic response based on in vivo rescue experiments. The schematic highlights the functional associations of each region with Z-disc localisation and muscle fibre size regulation.

Mutations affecting these regions have been linked to neuromuscular phenotypes in both humans and mice, underscoring their functional relevance. For example, a mutation (p.R139X) in the KY gene has been reported in patients with MFM-7 (Hedberg-Oldfors et al., 2016). While this mutation was initially associated with loss of the UBL domain, it introduces a premature stop codon and is therefore predicted to abolish translation of the entire downstream region. Accordingly, its pathogenic effect likely stems from complete loss of KY function, rather than isolated disruption of the UBL domain alone.

These results complement prior hypotheses from (Jokl et al., 2018), which proposed that KY contributes to Z-disc–linked mechanosensory signalling. However, our study offers more direct visual evidence for domain-specific localisation and provides an experimental framework to dissect KY's structural determinants beyond computational or transcriptomic inference. Remarkably, Jokl et al. (2018) also employed colocalisation studies and observed partial overlap of KY with FLNC and BAG3, suggesting functional interplay at the Z-disc. While our study did not assess these interaction partners directly, the clear Z-disc targeting of full-length KY observed here provides a structural basis that could underlie those protein–protein interactions. These observations jointly support a model in which KY is embedded within a stress-responsive, proteostasis-regulating complex at the Z-disc.

While this study offers valuable insights into the subcellular localisation of KY protein constructs, several limitations remain. The experiments did not examine the endogenous protein–protein interactions or anchoring mechanisms that direct KY to

the Z-disc. As a result, it is still unclear whether KY binds directly to sarcomeric components or is instead recruited through intermediary adaptor proteins. Although deletion of the entire TGN/PROT domain showed that this region is not essential for localisation, we did not perform more detailed mapping such as finer truncations or domain-swapping experiments to identify the specific residues or motifs responsible for targeting. This leaves the precise structural determinants of Z-disc anchoring unresolved. Furthermore, while both mouse and human KY isoforms were tested, all constructs were expressed in a murine muscle environment. Whether human KY behaves similarly in native human muscle tissue or in human-derived muscle cell lines remains an open question and may uncover species-specific regulatory differences or localisation cues.

These findings highlight the view that the TGN/PROT domain, while evolutionarily conserved, is not essential for KY's Z-disc localisation. Instead, the critical determinants of KY targeting reside elsewhere in the protein, likely within the N-terminal UBL-containing region. This conclusion refines our understanding of KY's functional architecture and provides a framework for future studies aimed at identifying the specific motifs responsible for its anchoring within the sarcomere.

CHAPTER SIX: RESULTS

In Silico Analysis – KY Protein Structure Prediction

CHAPTER 6. In Silico Analysis – KY Protein Structure Prediction

6.1 Introduction and Rationale

KY is a muscle-enriched protein that localises to the Z-disc, a structural hub essential for sarcomere organisation and force transmission. Previous studies have shown that KY is critical for maintaining muscle fibre size, particularly in KY-deficient mice, where re-expression of KY constructs has been shown to rescue fibre cross-sectional area. However, the structural determinants underlying KY's function and localisation remain unclear.

A conserved feature of KY is a central TGN/PROT domain predicted to contain three putative catalytic residues: histidine, cysteine, and aspartate. Although mutating these residues does not prevent KY from rescuing muscle fibre size *in vivo*, the broader structural role of this domain in stabilising KY's conformation or mediating subcellular targeting has not been fully resolved.

To investigate this, full-length mouse KY and its variant constructs were subjected to in silico structural prediction using AlphaFold2. These included a predicted catalytically inactive KY mutant (KY-TM) in which the three conserved residues were substituted with alanine, and a predicted deletion variant lacking the entire TGN/PROT domain (KY-ΔTGN). Predicted structural comparisons were then performed using UCSF ChimeraX to assess the potential impact of these modifications on overall tertiary structure and domain folding. These analyses were intended to provide insight into how the TGN/PROT domain may contribute to KY's predicted structural stability and its localisation at the Z-disc.

6.2 Experimental Design

Predictive structural models of KY wild-type, KY-ΔTGN, and KY-TM were generated using AlphaFold2 via the ColabFold platform (Mirdita et al., 2022). These models represent computationally derived predictions of protein conformation rather than experimentally resolved structures. Comparative structural analyses were carried out using UCSF ChimeraX (Pettersen et al., 2021), focusing on predicted backbone alignment and interatomic distances. Root-mean-square deviation (RMSD) values were calculated to estimate the degree of predicted structural divergence between constructs, providing a quantitative measure of the average displacement between equivalent atoms in aligned models. These analyses were used to infer how deletion or mutation within the TGN/PROT domain may affect overall predicted protein architecture.

6.3 Structural Comparison Between KY and TG2 Catalytic Triads

To assess whether KY might possess a transglutaminase-like catalytic arrangement, we performed in silico structural comparisons between a predicted model of KY (UniProt Q8C8H8) and the experimentally solved structure of human transglutaminase 2 (TG2, PDB ID: 2Q3Z) using UCSF ChimeraX. Superimposition of the predicted KY model and TG2 suggested a spatial correspondence between the positions of three residues in KY (Cys225, His267, Asp282) and the canonical TG2 catalytic triad (Cys277, His335, Asp358) (Figure 6.1).

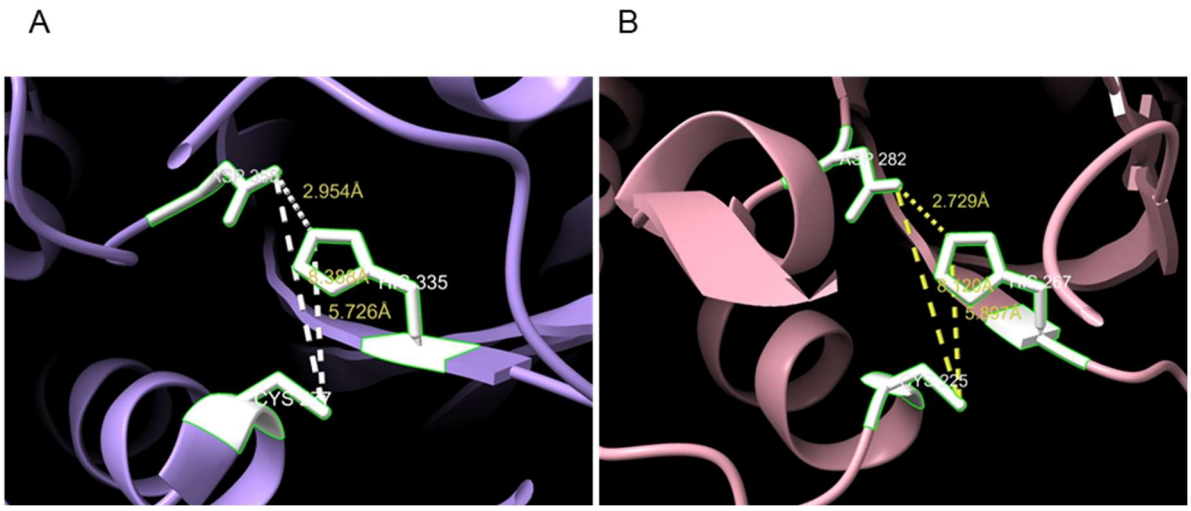

Figure 6.1 Structural comparison of the putative catalytic triads in human TG2) and KY protein.

Left: Active site configuration of human TG2 (PDB: 2Q3Z), highlighting the canonical catalytic triad composed of Cys277, His335, and Asp358. Right: Homology model of KY (UniProt ID: Q8C8H8) reveals a spatially aligned triad formed by Cys225, His267, and Asp282. Interatomic distances (Å) are indicated between the sulfur of cysteine, the imidazole nitrogen of histidine, and the carboxyl group of aspartate. Despite close geometric similarity (e.g., Cys–His and His–Asp distances ~5.9 Å and ~2.7 Å, respectively), functional assays suggest that KY lacks transglutaminase activity. Structures were visualized using UCSF ChimeraX.

Table 6-1 Predicted interatomic distances and structural alignment metrics for TG2 and KY models

Parameter	TG2	KY Model
Cys–His distance (Å)	5.73	5.90
His–Asp distance (Å)	2.95	2.73
Cys–Asp distance (Å)	8.39	8.12

Predicted interatomic distances measured on the models were similar between the two proteins (TG2: Cys277–His335 = 5.73 Å, His335–Asp358 = 2.95 Å, Cys277–Asp358 = 8.39 Å; KY model: Cys225–His267 = 5.90 Å, His267–Asp282 = 2.73 Å, Cys225–Asp282 = 8.12 Å).

Structural alignment using ChimeraX MatchMaker (Needleman–Wunsch algorithm, BLOSUM-62) produced a local alignment with a pruned RMSD of ~0.98 Å across 51 atom pairs, whereas the full-model alignment (498 atom pairs) gave a much larger RMSD (≈44.08 Å), consistent with local rather than global structural similarity owing to different overall domain architectures.

Taken together, these model-based observations predict that KY can adopt a triad-like geometry reminiscent of active transglutaminases. However, such predictions do not demonstrate catalytic competence: static structural similarity alone cannot report on substrate accessibility, dynamic conformational changes, post-translational modifications, or cofactor binding that are required for enzymatic activity. Indeed, the functional data (*in vivo* rescue assays) and prior biochemical evidence do not detect transglutaminase activity for KY. Therefore, while the predicted models are useful for generating mechanistic hypotheses, experimental biochemical assays (e.g. activity assays with defined substrates, cofactor dependence and accessibility mapping, or targeted mutagenesis combined with kinetic measurements) are required to establish whether KY is catalytically active or functions as a pseudoenzyme.

6.4 Protein Structure Modelling for Catalytic Residue Mutations KY-TM

To explore the predicted structural consequences of mutating the conserved residues within the TGN domain, AlphaFold2 was used to generate models of the wild-type TGN2 region and a triple-mutant variant (KY-TM) in which Cys225, His267, and Asp282 were substituted with alanine. The resulting models were aligned using UCSF ChimeraX, and the root-mean-square deviation (RMSD) was calculated to assess predicted structural divergence between the wild-type and mutant forms(figure 6.2). These *in silico* analyses were performed to evaluate whether substitution of the putative catalytic residues is predicted to induce local conformational alterations that could influence overall protein folding or stability.

A

WT VEAAQEKDRQAFKPTDILRTQKTNCDGYAGLFERMCRVAGVQCVTVPGYS 250

TM VEAAQEKDRQAFKPTDILRTQKTNADGYAGLFERMCRVAGVQCVTVPGYS 250

WT KGFGYQTGQSFSGEFDHAWNAVYLEGRWHLVDSTWGSGLVDTTTSKFTFL 300

TM KGFGYQTGQSFSGEFDAAWNAVYLEGRWHLVASTWGSGLVDTTTSKFTFL 300

B

C

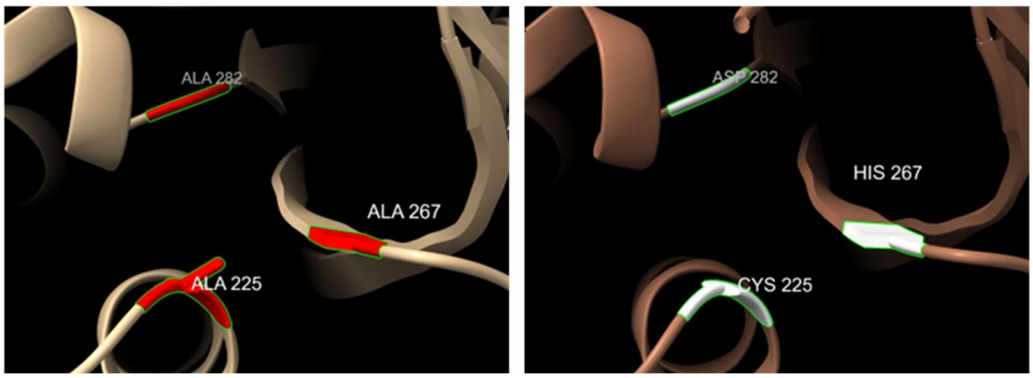

Figure 6.2 . Structural comparison of the wild-type TGN2 domain and its catalytically inactive triple mutant TGN2-TM.

A) Sequence alignment highlighting the three conserved catalytic residues—Cys225, His267, and Asp282—in the wild-type TGN2 domain. In the TGN2^TM mutant, these residues were substituted with alanine (Ala225, Ala267, and Ala282), as shown in blue. B) Superimposed 3D structures of the wild-type (beige) and TGN2-TM mutant (salmon) domains generated using AlphaFold2 and visualised in ChimeraX. The high structural similarity between the two is maintained despite the catalytic site substitutions. C) Close-up views of the catalytic site in both variants. In the wild type (right panel), the conserved catalytic triad is highlighted (Cys225, His267, and Asp282), whereas in the TGN2^TM mutant (left panel), these residues are replaced by alanine, leading to disruption of the active site geometry and potential loss of enzymatic function.

The RMSD values (0.512 Å for pruned atom pairs; 0.574 Å for full atom comparison) indicate that the overall structure of KY-TM is *predicted to remain globally conserved* relative to the wild-type model. Local conformational differences were predicted within the TGN domain, where alanine substitutions (figure 6.3) are expected to abolish the nucleophilic thiol of Cys225 and disrupt specific hydrogen-bonding interactions.

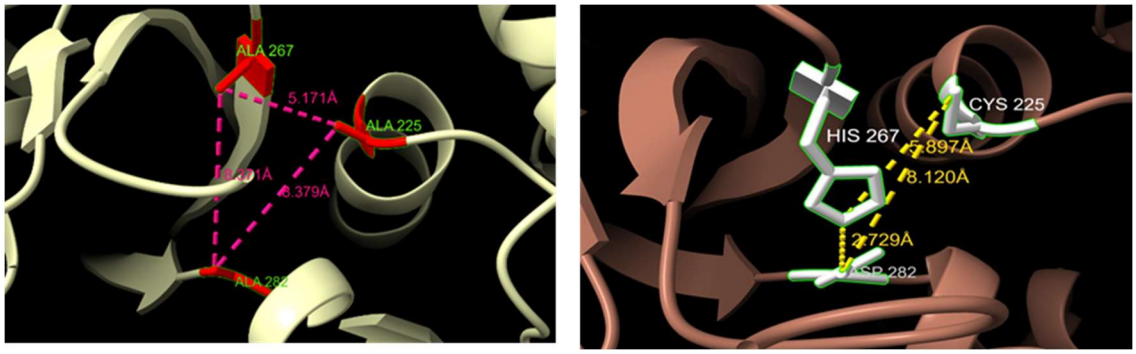

Figure 6.3 Structural comparison of the catalytic triad in wild-type and triple-mutant TGM2.

Structural overlay of the active site region from wild-type TGM2 (brown) and its catalytically inactive triple-mutant form (TM; beige), where the key catalytic residues Cys225, His267, and Asp282 are substituted with alanine (Ala225, Ala267, Ala282). (Left) In the TM structure, loss of side chain functionality alters spatial configuration and disrupts key inter-residue distances, shown by dashed magenta lines. These increased distances (all >5 Å) exceed the spatial threshold for effective catalysis, supporting functional inactivation. (Right) Wild-type TGM2 active site shows proper triad geometry and proximity (all <4 Å) necessary for catalytic function. Loss of the nucleophilic thiol from Cys225 and realignment of the triad in TM highlights the structural basis for catalytic disruption. All measurements reflect the distance between backbone or side chain functional atoms (e.g., SG of Cys225, NE2 of His267, OD2 of Asp282). Visualizations were generated in UCSF ChimeraX v1.5 using PDB: 3S3P as the wild-type reference.

However, these alterations did not appear to propagate across the protein, suggesting that the catalytic triad residues may be structurally conserved without being essential for maintaining the global fold.

These predicted structural features are consistent with experimental observations showing that KY-TM retains Z-disc localisation and is able to rescue muscle fibre size in ky/ky mice, supporting a model in which the catalytic triad is structurally present but not required for KY's core functional role in muscle maintenance.

6.5 Protein Structure Modelling of KY-ΔTGN Variant

To assess the predicted structural role of the TGN domain, full-length KY and the KY-ΔTGN variant (lacking residues 171–282) were modelled using AlphaFold2 and compared using ChimeraX.

Structural superimposition yielded a sequence alignment score of 2565.5, with a pruned RMSD of 0.690 Å across 353 aligned atom pairs and a full-length RMSD of 27.946 Å across 548 atom pairs. These values indicate that the overall fold is *predicted to remain largely conserved*, with structural divergence predominantly localised to

Figure 6.4 Protein sequence of the mice KY protein.

The region highlighted in red corresponds to the deleted segment introduced in this study, spanning amino acids 171-282. This deletion encompasses part of the central region of the KY protein, which affect hypertrophy response.

Table 6-2 show measurements of WT compared to mutant TGN deletion

Parameter	Value
Sequence Alignment Score	2565.5
Pruned RMSD (353 atoms)	0.690 Å
Full-length RMSD (548 atoms)	27.946 Å

regions surrounding the deleted TGN domain. This suggests that the TGN/PROT

domain may contribute to local stability or domain–domain interactions rather than determining the global protein architecture.

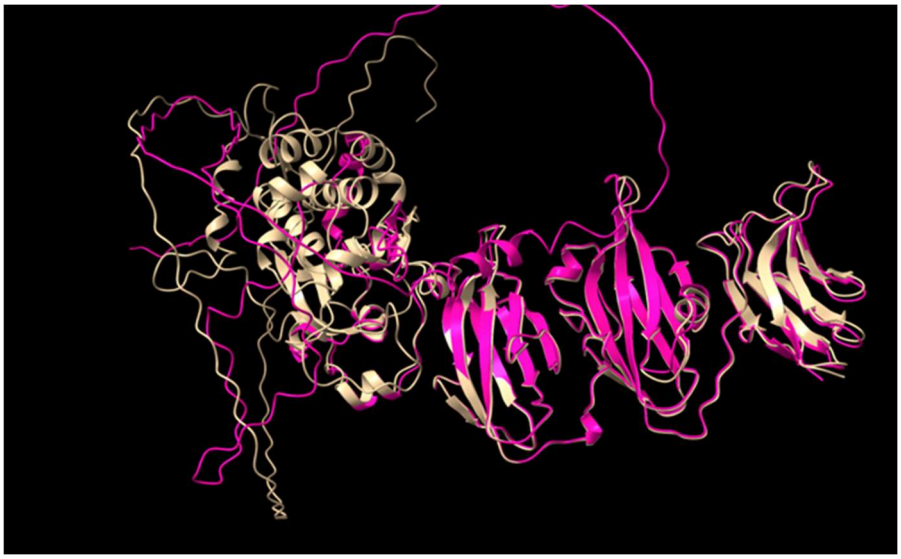

Figure 6.5 Structural alignment of KY wild-type and TGN-deletion mutant proteins.

The ribbon diagram shows the structural superposition of KY wild-type full-length (white) and KY mutant with the TGN domain deleted (red/magenta). The alignment highlights the overall structural differences, particularly the absence of the TGN domain in the mutant, while preserving other structural elements. This comparison provides insights into the potential role of the TGN domain in maintaining the protein's conformation and its functional interactions.

6.6 Structural Comparison Summary and Interpretation

Structural modelling predicts that neither deletion of the TGN/PROT domain nor mutation of its conserved catalytic residues leads to substantial disruption of the overall KY protein fold. Both KY-TM and KY-ΔTGN models showed high structural similarity to the predicted wild-type KY structure, with pruned RMSD values below 1 Å for core domains, indicating strong global stability. Importantly, these predictive models suggest that the TGN domain contributes to local conformational features rather than determining the global architecture of KY.

In vivo experiments demonstrated that both KY-TM and KY-ΔTGN retain the ability to localise to the Z-disc, indicating that Z-disc targeting is likely mediated by regions outside of the TGN domain—most probably within the C-terminal portion of the protein. Despite this conserved localisation, only KY-TM was able to rescue myofibre size in the ky/ky background, whereas KY-ΔTGN failed to do so. These findings indicate that, while the TGN domain is not required for KY's structural integrity or subcellular localisation, it is predicted to be essential for functional rescue of fibre size.

The alanine substitutions within the catalytic triad in KY-TM are predicted to alter local geometry and disrupt catalytic potential; however, these changes do not abolish the rescue function, suggesting that the catalytic residues themselves are not strictly

required for KY's physiological role in muscle maintenance. The evolutionary conservation of this triad across vertebrate KY homologues remains intriguing and may indicate a latent or condition-specific enzymatic function that was not activated under the experimental conditions tested in this study.

In contrast, the inability of KY-ΔTGN to restore fibre size, despite maintaining the overall structural fold and correct localisation, strongly supports a model in which the TGN domain serves a non-enzymatic but functionally indispensable role, potentially acting as a scaffold for protein–protein interactions or signalling events necessary for muscle fibre homeostasis.

6.7 Discussion

This chapter investigated the structural features of the KY protein using predictive in silico modelling, with a specific focus on assessing whether the conserved TGN/PROT domain adopts a catalytically competent transglutaminase-like fold. The central objective was not to assign enzymatic activity but to determine whether KY is predicted to structurally resemble members of the transglutaminase family, and how alterations within this domain affect predicted conformation and experimentally determined function.

AlphaFold2 structural modelling and ChimeraX superposition against human TG2 predicted that KY adopts a similar local fold around the putative catalytic triad. The corresponding residues in KY (Cys225, His267, Asp282) were predicted to align spatially with the canonical active site of TG2, with low RMSD values indicating local geometric conservation. These findings indicate that KY retains the architectural features of a transglutaminase-like domain. However, structural similarity alone does not imply catalytic function. Many proteins are now recognised as pseudoenzymes, where conserved catalytic motifs are retained for structural or scaffolding roles rather than catalysis.

This interpretation is strongly supported by functional data from Chapter 4, where mutation of the catalytic triad (KY-TM) did not impair the ability of KY to rescue muscle fibre size in *ky/ky* mice. These findings indicate that the conserved triad, although structurally present, is not required for KY's biological function under the tested conditions. This suggests that either KY lacks catalytic activity altogether or that its enzymatic activity may only be relevant under specific physiological or stress conditions not captured in this study.

Comparative predictive modelling of KY deletion mutants further supported this model. KY-TM and KY-ΔTGN were both predicted to maintain the overall fold of the protein, with RMSD values below 1 Å across core domains, indicating strong global structural conservation. Consistent with this, experimental observations from Chapter 5 demonstrated that both variants correctly localised to the Z-disc, confirming that the TGN/PROT domain is not required for structural stability or localisation.

However, despite maintaining predicted structure and localisation, only KY-TM (mutated triad) was able to rescue muscle fibre size, whereas KY-ΔTGN (domain deletion) failed to do so. This suggests that while the catalytic residues themselves are not essential for function, the presence of the TGN/PROT domain as a structural module is required. The domain is therefore predicted to mediate critical interactions or conformational dynamics necessary for KY's physiological role, consistent with non-enzymatic scaffold functions described for pseudoenzymatic domains in other regulatory proteins.

Importantly, this chapter highlights that predictive structural models must be interpreted in conjunction with functional assays. While modelling predicted a catalytically competent active-site geometry, experimental evidence clearly indicated that enzymatic catalysis is not required for KY function *in vivo* (Harrad, 2021). These findings advance KY as a predicted pseudoenzymatic scaffold protein rather than an active transglutaminase.

This chapter supports a model in which KY retains a transglutaminase-like fold that is structurally conserved but functionally repurposed. The catalytic triad residues are predicted to contribute to local structural stability rather than enzymatic function. Conversely, the TGN/PROT domain itself is predicted to fulfil an essential non-catalytic role likely as an interaction interface required for KY's role in maintaining muscle fibre integrity. These structural insights highlight the likelihood that KY functions as a pseudoenzymatic scaffold rather than a catalytic enzyme, raising the critical question of which protein partners interact with its TGN/PROT domain to mediate its biological role. The next chapter addresses this by experimentally identifying KY-interacting proteins using immunoprecipitation and proteomic analysis.

CHAPTER SEVEN: RESULTS

Proteomic resolution of KY-associated proteins

CHAPTER 7. Proteomic resolution of KY-associated proteins

7.1 Introduction

Following the rescue muscle fibres studies and co-localisation experiments, we observed that all KY constructs, including those with point mutations, were able to localise to the Z-disk, suggesting that Z-disk targeting is preserved across these variants. However, the molecular mechanisms by which KY interacts with other proteins remain unclear. To explore this, we performed immunoprecipitation (IP) experiments to identify proteins that interact with KY. Protein–protein interaction analysis offers a powerful approach to uncover potential binding partners that may either co-localise with KY at the Z-disk or participate in KY-mediated signalling pathways. We aim to capture and characterise the repertoire of proteins that associate with KY. Mapping these interactions will help elucidate KY's role as a scaffold or regulatory molecule in maintaining muscle structure and function. Furthermore, identifying novel KY-binding partners could provide mechanistic insights into its involvement in muscle-specific pathways and disease processes. This chapter presents the methodology and findings of KY IP experiments, with the overarching goal of defining the KY interactome.

7.2 Experimental design

To identify proteins interacting with KY, we performed IP experiments using both skeletal muscle tissue and transfected cells expressing full-length KY constructs. KY was tagged with tdTomato, a red fluorescent protein variant, to enable selective pulldown and visualisation (Figure 7.1).

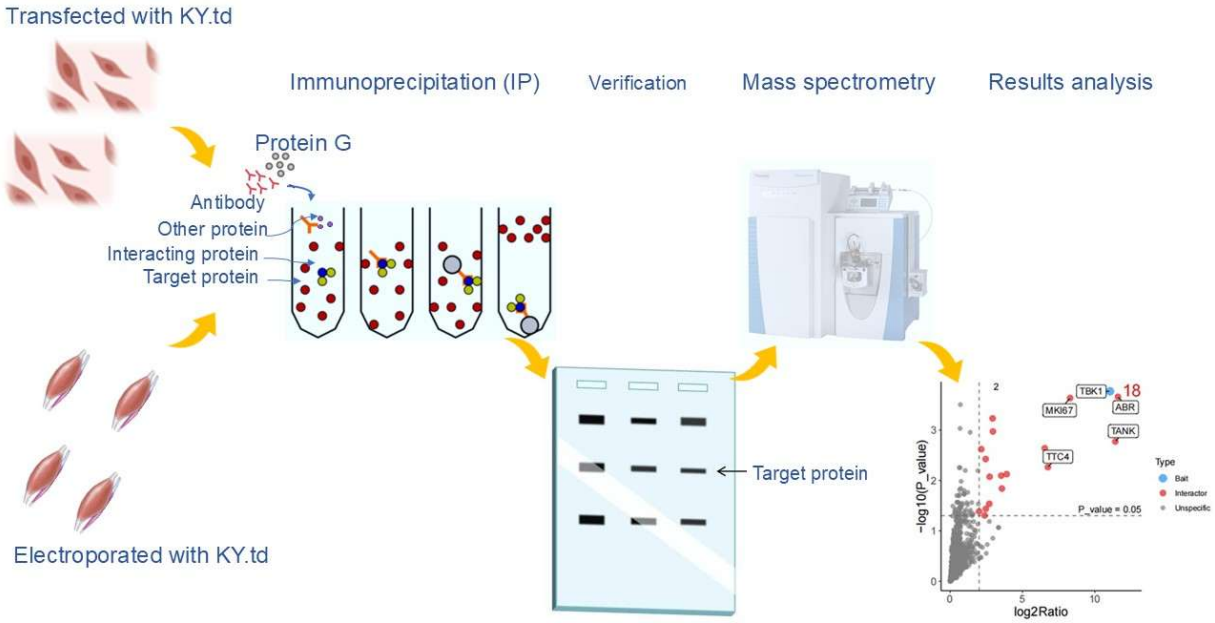

Figure 7.1 The workflow for KY Protein–Protein Interaction Analysis by Immunoprecipitation and Mass Spectrometry.

Cells transfected with KY.td or muscle tissue electroporated with KY.td constructs were lysed and subjected to immunoprecipitation (IP) using Protein G magnetic beads and anti-RFP antibody to isolate KY-containing protein complexes. Following IP, samples were verified by SDS-PAGE and Western blot to confirm successful pulldown of the target protein. Verified samples were then processed for mass spectrometry to identify KY-interacting proteins. Data obtained from mass spectrometry were further analysed to determine specific interaction partners and assess their potential functional relevance.

IP was carried out using the Invitrogen™ Dynabeads™ Protein G IP Kit, following the manufacturer's protocol. Lysates were incubated with anti-RFP antibody (Rockland Immunochemical, Cat. #600-401-379-RTU), which recognises tdTomato, to specifically capture tdTomato-tagged KY and its associated protein partners. The immune complexes were then bound to Protein G-conjugated magnetic beads, allowing magnetic separation and stringent washing to minimise non-specific interactions.

Bound proteins were subsequently eluted, denatured, and separated by SDS-PAGE. The eluted protein complexes were then analysed by mass spectrometry (MS) to identify candidate KY interactors. This approach enabled the characterisation of the KY interactome under near-physiological conditions and provided a robust foundation for downstream validation and functional annotation of potential binding partners.

7.3 Verification by Western Blot

To validate successful enrichment of tdTomato-tagged KY (KY-td) prior to proteomic analysis, IP was performed from both transfected C2C12 cell lysates and electroporated mouse muscle tissue, followed by Western blotting using an anti-RFP antibody. As shown in (Figure 7.2), the IP eluates revealed a prominent band at the expected molecular weight for full-length KY.td (~125 kDa) in both cell and muscle samples, confirming effective pulldown of the target construct (Figure 7.2).

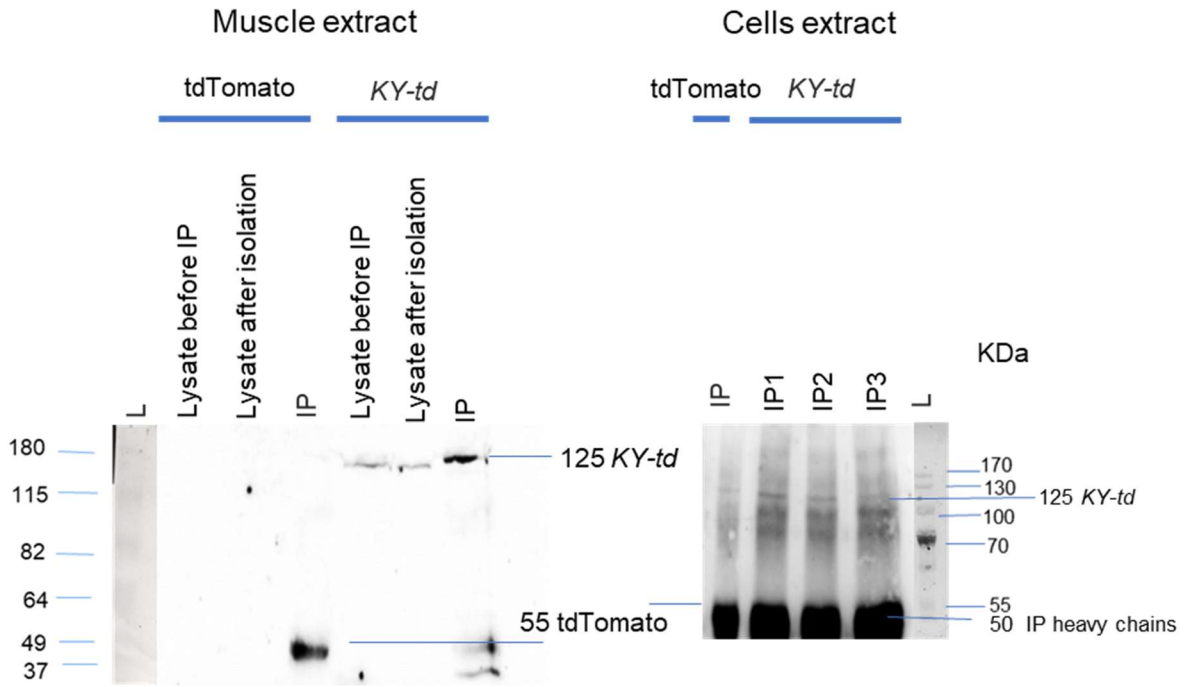

Figure 7.2 The verification of KY.td IP by Western blot.

Muscle lysates from electroporated tissue and lysates from transfected C2C12 cells expressing tdTomato-tagged KY were subjected to immunoprecipitation using anti-RFP antibody and Protein G magnetic beads. Western blotting was performed with anti-RFP antibody to verify enrichment of the KY-td fusion protein. Left panel: Muscle tissue samples. Lanes (left to right); Molecular weight ladder, tdTomato samples (negative control), total muscle lysate before IP, Post-IP lysate, and tdTomato IP (negative control). KY-td samples, total muscle lysate before IP, Post-IP lysate, and KY-td IP. The upper band (~125 kDa) corresponds to KY-td, and the lower band (~55 kDa) corresponds to tdTomato. KY-td is specifically enriched in the IP lane, confirming successful pulldown. The ~50–55 kDa band may include IgG heavy chains eluted from the beads. Right panel: Transfected C2C12 cell samples. Lanes (left to right): tdTomato IP (negative control), 2–4. Independent KY.td IP replicates (IP1–IP3) and Molecular weight ladder. KY-td appears as a strong upper band in IP lanes, while nonspecific or antibody-derived signals are observed below. The absence of a tdTomato band in KY IP samples and its potential masking by antibody heavy chains in the control lane support the specificity of KY pulldown. These data confirm that the IP protocol effectively and specifically enriches KY-td complexes for downstream interactome analysis by mass spectrometry.

In contrast, the tdTomato-only control lanes lacked a clear band at 55 kDa. A faint signal near ~55 kDa was present, likely corresponding to antibody heavy chains eluted from the beads, which may have obscured any potential tdTomato-specific band in these controls. Importantly, the observed KY-td band pattern in IP samples aligns with previous expression data, reinforcing the specificity and efficiency of the IP protocol.

This Western blot analysis confirmed the suitability of the samples for downstream mass spectrometry. It is important to note that the purpose of this experiment was not to validate specific protein–protein interactions via Western blot, but rather to ensure the successful enrichment of KY-containing complexes as a preparatory step for defining the KY-associated interactome through proteomics.

7.4 Mass Spectrometry Analysis for muscle extract

Immunoprecipitated complexes from muscle lysates were prepared from four independent biological replicates per condition, digested on-bead with trypsin, and analysed using PASEF-DIA mass spectrometry on a Bruker timsTOF platform coupled to an EvoSep One UPLC. Data were processed in Spectronaut v19 using the UniProt *Mus musculus* database supplemented with the tdTomato sequence and common contaminants. A q-value < 0.01 and at least two unique peptides were required for confident protein identification (Figure 7.3).

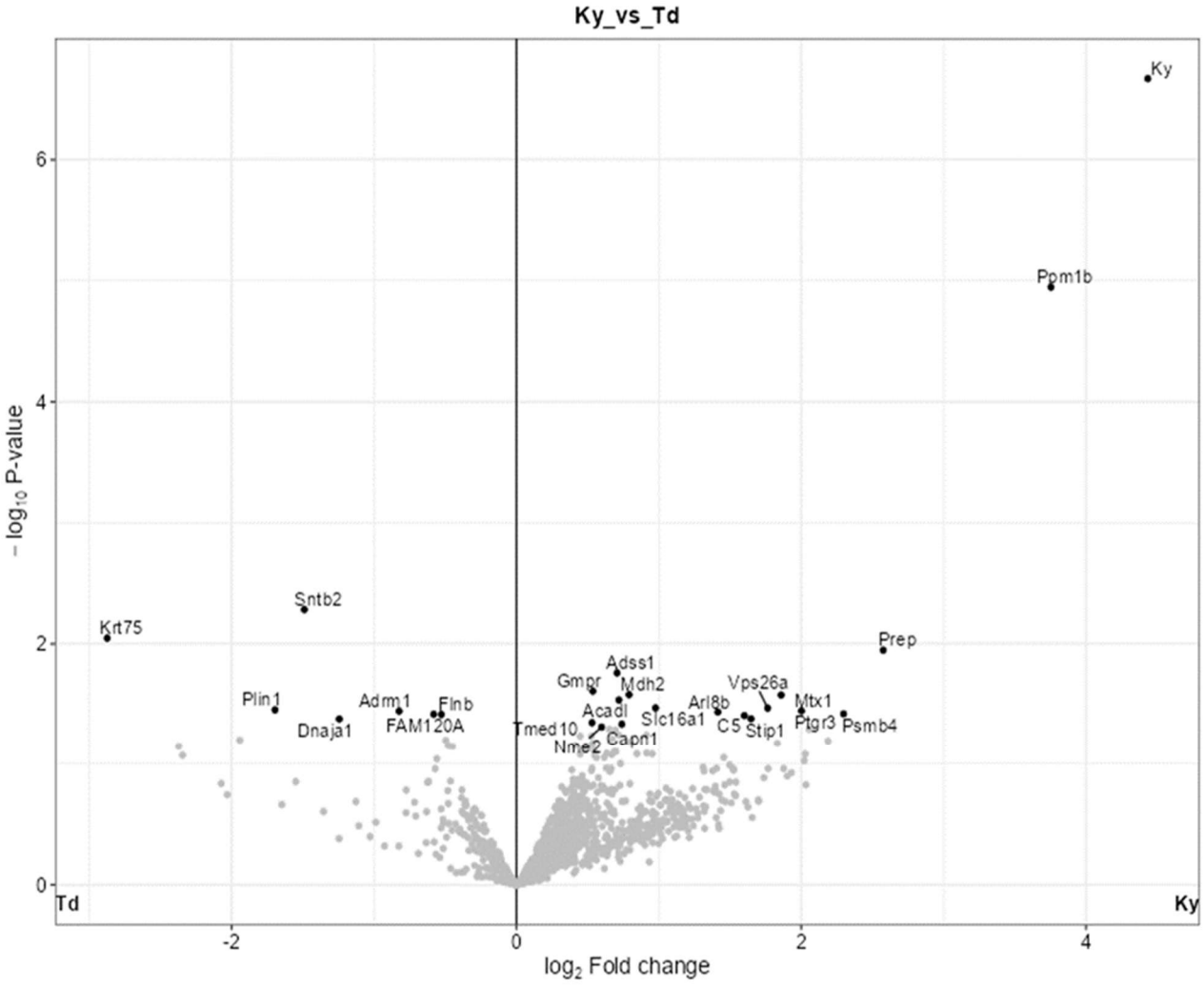

Figure 7.3 Volcano plot showing differentially enriched proteins in KY immunoprecipitates versus tdTomato control (Ky_vs_Td) in muscle extract.

Protein identification was filtered using a false discovery rate (FDR) threshold of q < 0.01, requiring at least two unique peptides per protein. Quantitative intensity values from four biological replicates were extracted from Spectronaut, and statistical comparisons were performed in FragPipe-Analyst using the limma package with Hochberg and Benjamini correction. The x-axis represents the log_2 fold change in protein abundance between KY and tdTomato groups, and the y-axis shows the $–log_{10}$ adjusted p-value. Only KY and PPM1B met the adjusted significance threshold (padj < 0.05), validating specific enrichment. Proteins enriched in the KY condition (KY, PPM1B, PREP) appear in the upper-right quadrant, while those enriched in the control (KRT75, SNTB2) are positioned to the left. Non-significant proteins are shown in grey. Labeled points represent candidates for further validation. This analysis highlights potential KY-associated proteins implicated in autophagy and proteostasis..

Statistical analysis was conducted in FragPipe-Analyst using the limma package. KY emerged as the most significantly enriched protein in KY IP samples, validating the IP approach. Protein Phosphatase 1B PPM1B was the only statistically significant interactor after correction (adjusted $p < 0.05$), suggesting a potential association. Volcano plots showing both corrected and uncorrected significance thresholds are provided to highlight potential additional candidates for future study.

7.4.1 Functional Interpretation of PPM1B

PPM1B is a Ser/Thr phosphatase involved in multiple cellular stress-response pathways, including autophagy regulation. Notably, PPM1B directly dephosphorylates ULK1, a master regulator of autophagosome initiation within the AMPK–mTOR signalling network (Chang et al., 2016) The association between KY and PPM1B therefore suggests a mechanistic link between KY and upstream autophagy-induction mechanisms.

Under nutrient-rich conditions, mTORC1 phosphorylates and inhibits ULK1, thereby suppressing autophagosome formation. Conversely, during metabolic or proteotoxic stress, AMPK phosphorylates and activates ULK1 while concurrently inhibiting mTORC1 (Egan et al., 2011; Kim et al., 2011; Laplante & Sabatini, 2012). This reciprocal regulation ensures that autophagy is selectively activated in response to cellular energy status or stress. Within this framework, PPM1B acts as a counter-regulator that can dephosphorylate ULK1 to reset or fine-tune autophagy initiation once stress is resolved.

Given this role, the interaction between KY and PPM1B may enable spatially restricted modulation of ULK1 activity. KY could act as a scaffold that recruits or positions PPM1B at specific subcellular regions—such as the Z-disc—where local turnover of damaged sarcomeric components is required. This would allow targeted activation of autophagy in defined microdomains of muscle fibres, avoiding widespread degradation and preserving sarcomeric integrity. The KY–PPM1B association highlights a potential mechanism through which KY contributes to proteostasis maintenance by linking cytoskeletal organisation with stress-responsive autophagy signalling.

7.4.2 Orthogonal Validation of KY–PPM1B Interaction

To validate the interaction between KY and PPM1B, confocal microscopy was used to assess their spatial relationship in muscle fibres expressing KY-td. While tdTomato-only controls exhibited diffuse cytoplasmic fluorescence, KY-td–expressing fibres displayed a clear striated pattern overlapping with PPM1B staining. Fluorescence intensity line plots demonstrated aligned peaks between KY-td and PPM1B signals, suggesting co-localisation at or near the Z-disc (Figure 7.4). Although there was a small spatial gap in PPM1B banding, the distribution pattern was consistent with Z-disc–flanking proteins such as titin N2A, supporting gross co-localisation within sarcomeric compartments.

A-1

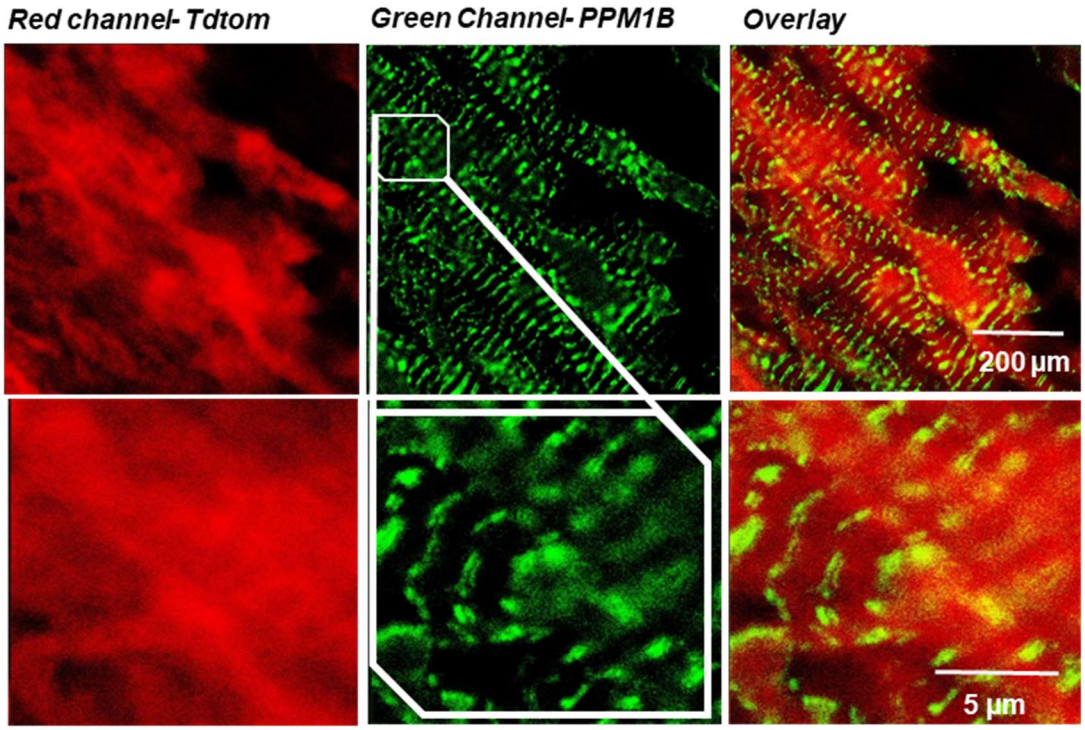
Red channel- Tdtom
Green Channel- PPM1B
Overlay
200 µm
5 µm

A-2

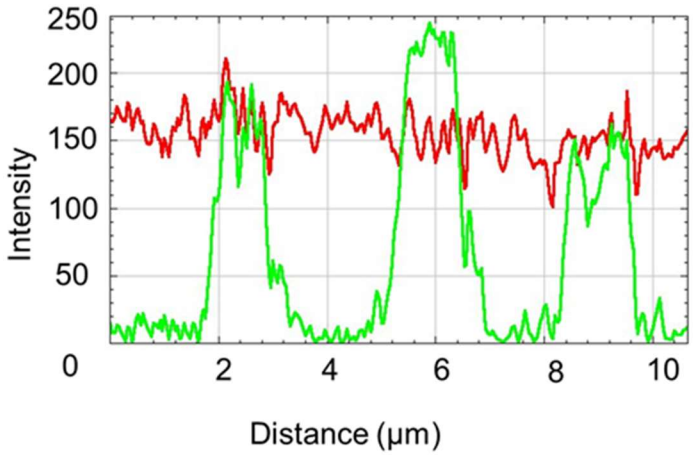
250
200
150
100
50
0
Intensity
2
4
6
8
10
Distance (µm)

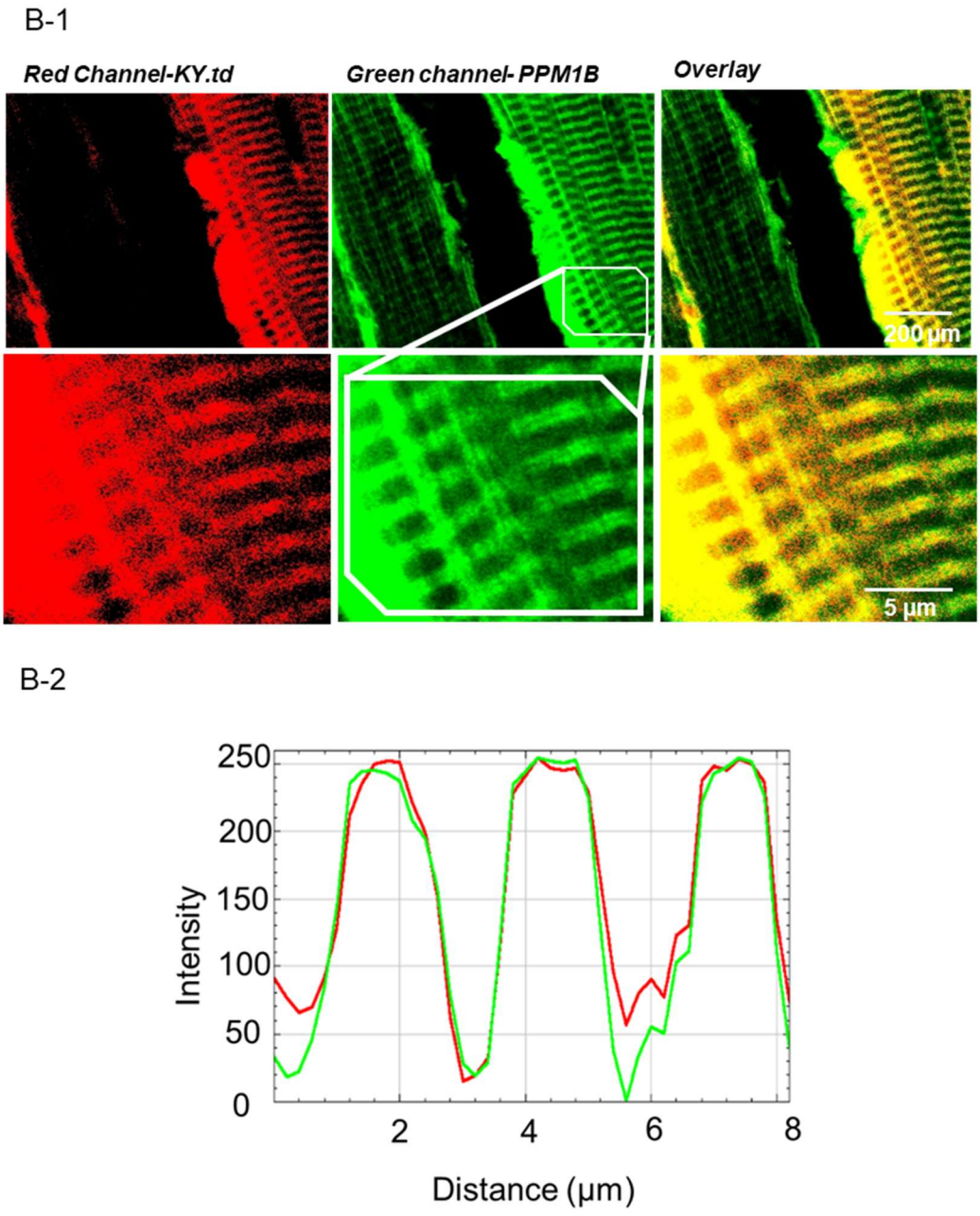

Figure 7.4 The confocal microscopy analysis showing co-localization of KY and PPM1B in skeletal muscle fibres.

A-1 Control muscle electroporated with tdtomato alone shows diffuse distribution without Z-disc localisation. Confocal images of tibialis anterior muscle electroporated with tdtomato alone (red) and stained for ppm1b (green). Top row: low-magnification views showing tdtomato, ppm1b (middle), and merged channels (right). Scale bar: 200 µm. Bottom row: higher magnification of the same area (scale bar: 10 µm) confirms that tdtomato remains diffusely distributed, with no enrichment at Z-discs. Inset shows magnified region of tdtonato signal lacking sarcomeric periodicity. A-2 Bottom panel: fluorescence intensity profiles across sarcomeres demonstrate strong periodic tdtomat signal (red), while ppm1b signal (green) remains unpatterned and non-overlapping. B-1) Representative images of muscle fibres stained for KY (red) and PPM1B (green). Top panels show wide-field views (scale bar: 200 µm), and bottom panels display high-magnification images of selected areas (scale bar: 10 µm). In KY-expressing fibres, PPM1B displays a distinct striated pattern that aligns precisely with KY signal, indicating perfect co-localization. An enlarged inset highlights the structured overlap. The bottom graph shows fluorescence intensity profiles along a selected linear region, with matching peak distributions in red (KY) and green (PPM1B) channels, supporting their spatial co-localization at the sarcomeric level.

However, it is important to acknowledge that co-localisation does not prove direct molecular interaction. Fluorescent overlap indicates proximity within the optical resolution of the microscope but cannot distinguish between direct binding and association within a shared structural region. Therefore, while these imaging data provide valuable spatial context, they should be interpreted as supportive rather than definitive evidence of protein–protein interaction.

Complementary biochemical validation was therefore performed using immunoprecipitation (IP) assays. Western blot analysis of IP complexes confirmed the presence of PPM1B specifically in KY-tdTomato pull-downs, but not in tdTomato controls, supporting a specific physical association between the two proteins (Figure 7.5). Because only a subset of muscle fibres were transfected by *in vivo* electroporation, KY-tdTomato was present at low abundance in total muscle lysates and was therefore often below the detection limit in the input lanes. Immunoprecipitation enriched KY-containing complexes, allowing reliable detection of the associated protein PPM1B in the IP lanes. After the initial probing, the membrane was stripped and reprobed for PPM1B, confirming that KY-tdTomato was visible only in the IP lanes of KY-expressing samples and absent from tdTomato control IPs. The absence of a KY-tdTomato band in total lysate thus reflects low transfection efficiency and limited expression rather than lack of protein production. Together with the

Figure 7.5 Western blot validation of the interaction between KY and PPM1B using anti-PPM1B IB compared to Tdtomato control sample in muscle fibre.

Protein complexes were immunoprecipitated from skeletal muscle lysates using an anti-PPM1B antibody in KY.td-expressing and TdTomato control samples. Lanes from left to right show: KY.td lysate before IP, KY.td lysate after IP, KY.td IP (two biological replicates), TdTomato control lysates before IP (two samples), and TdTomato immunoprecipitate. A clear band at ~37 kDa, corresponding to PPM1B, was observed only in the KY.td immunoprecipitated samples, indicating specific enrichment of PPM1B in complexes associated with KY. No PPM1B bands were detected in TdTomato control samples or in the lysate lanes, supporting the specificity of the interaction. The absence of a visible KY-tdTomato band in total lysate reflects low transfection efficiency and dilution of the transgene signal in whole-muscle extracts, as immunoprecipitation enriches KY-containing complexes for detection. These results independently confirm the KY–PPM1B interaction observed in the mass spectrometry and co-localisation experiments.

microscopy data, these results indicate that KY and PPM1B occupy overlapping sarcomeric regions and are part of the same molecular complex, although additional biophysical assays (e.g. proximity ligation, FRET, or cross-linking mass spectrometry) would be needed to confirm direct binding.

7.5 MS of KY Complexes from Cell Extracts

Parallel IP-MS analysis performed on undifferentiated transfected C2C12 cell lysates revealed additional KY-associated proteins. Among the significantly enriched proteins were three members of the HSP70 family: Hspa8 (cytosolic HSC70), Hspa5 (ER-resident BiP), and Hspa9 (mitochondrial GRP75). These chaperones are core components of cellular protein quality-control pathways and were robustly enriched in KY-tdTomato samples (adjusted $p = 0.00$), indicating that KY interacts with molecular chaperones even in the absence of myogenic differentiation.

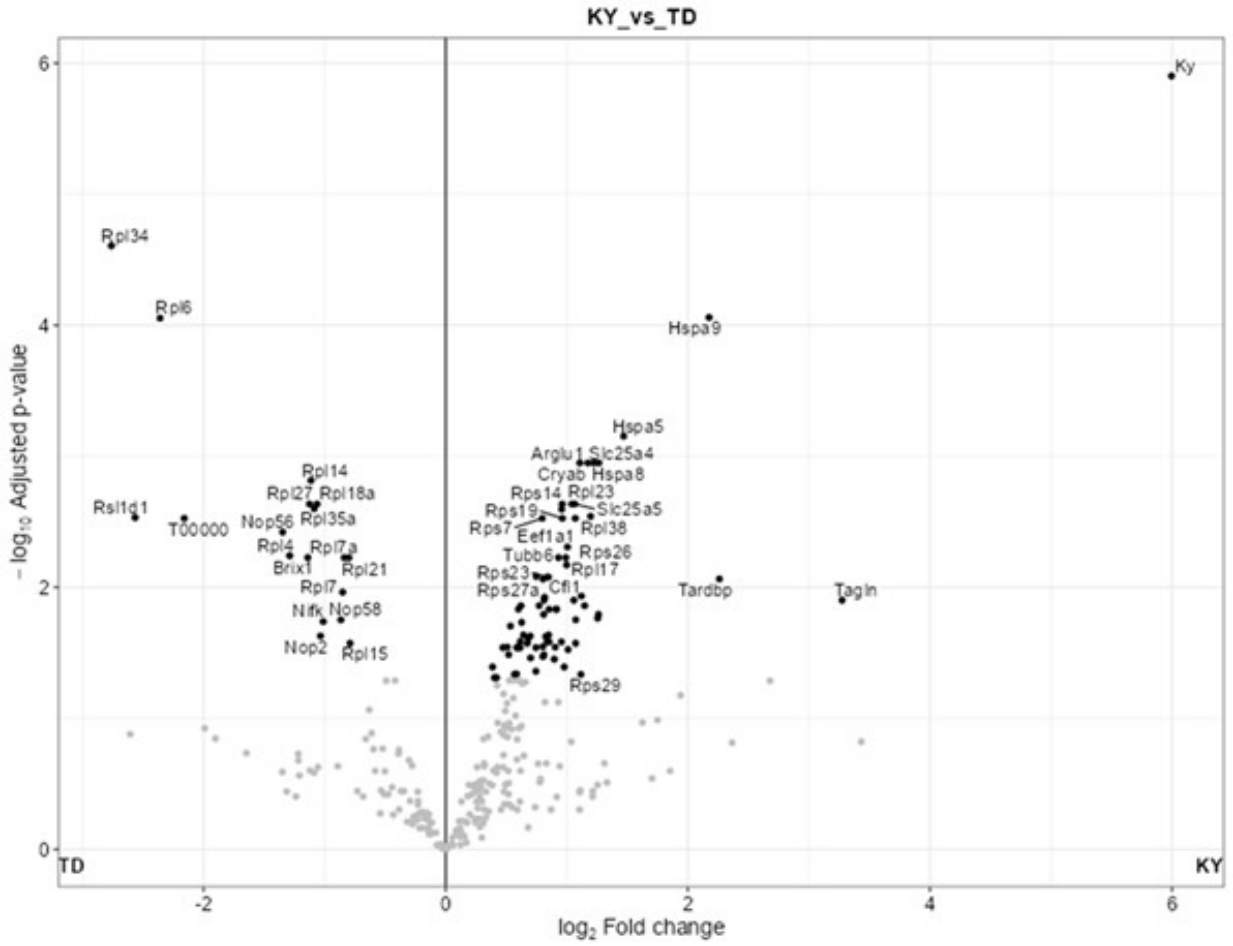

Figure 7.6 Volcano plot representing the mass spectrometry results of KY pulldown versus TD control (Ky_vs_Td) in cells extract.

The x-axis shows the log_2 fold change in protein abundance between KY and TD conditions, while the y-axis indicates the $–log_{10}$ of the p-value, reflecting statistical significance. Proteins significantly enriched in the KY pulldown (Hspa9, Hspa5, and Hspa8) appear in the upper right quadrant, while proteins potentially enriched in the TD control (Rp134, Rp16) are shown on the left. Grey dots represent proteins not significantly differentially abundant, while labelled points highlight significantly enriched candidate interactors. These results suggest specific protein partners that preferentially bind to KY compared to the control.

Table 7-1 Summary of Selected Proteins precipitated with KY from Cell Lysates

Gene	Protein Name	Protein q-value	log2 Fold Change (KY vs. Ctrl)	p-value	Adjusted p-value
Ky	Kyphoscoliosis peptidase	0.00E+00	5.99	0.00	0.00
Hspa9	Stress-70 protein, mitochondrial (GRP75)	0.00E+00	2.18	0.00	0.00
Hspa5	BiP, Endoplasmic reticulum chaperone	0.00E+00	1.47	0.00	0.00
Hspa8	Heat shock cognate 71 kDa protein (HSC70)	0.00E+00	1.27	0.00	0.00

These findings are notable because Hspa8 is a central regulator of chaperone-mediated autophagy CMA, while Hspa5 and Hspa9 play roles in ER and mitochondrial stress responses, respectively. All three proteins are functionally linked to autophagy induction under stress conditions, suggesting that KY may participate in coordinating proteostasis across multiple subcellular compartments.

7.5.1 Functional Interpretation of HSP70 Interactors

The identification of Hspa8, Hspa5, and Hspa9 in KY immunoprecipitates points to a broader role for KY in regulating proteostasis. HSPA8 plays a central role in chaperone-mediated autophagy, helping to selectively deliver cytosolic proteins to the lysosome for degradation. HSPA5 is involved in protein folding within the endoplasmic reticulum and is a key player in activating the unfolded protein response during ER stress. Hspa9, which localises to mitochondria, supports mitochondrial protein import and is involved in stress-related signalling. The fact that these chaperones were consistently enriched with KY suggests that KY may help coordinate quality control mechanisms across multiple organelles, particularly under stress conditions that are highly relevant in muscle tissue (Bernales et al., 2006; Hassan et al., 2019; Kaushik & Cuervo, 2018).

However, a limitation of the present study is that these interactions were identified from immunoprecipitation–mass spectrometry data and were not independently validated using reciprocal IP, co-localisation, or proximity-based assays such as PLA or BioID. As such, the association between KY and HSP70 family members should be regarded as *putative* until confirmed experimentally. Future validation will be essential to distinguish between direct physical binding and indirect co-complex association within shared proteostasis networks.

7.6 Discussion

This chapter identified key KY-interacting proteins using IP and proteomic analysis from both cultured C2C12 cells and *in vivo* muscle tissue. Among the most confidently enriched interactors were PPM1B and members of the HSP70 family, including Hspa8, Hspa5, and Hspa9. These findings expand KY's functional profile beyond its established role at the sarcomere, suggesting additional involvement in stress-responsive signalling and proteostasis regulation.

The robust identification of PPM1B (protein phosphatase Mg^{2+}/Mn^{2+}-dependent 1B) as a KY-associated protein raises important mechanistic possibilities. PPM1B is a negative regulator of autophagy initiation, known to dephosphorylate ULK1 (Zheng et al., 2022). Its co-isolation with KY suggests that KY may act as a scaffold or adaptor that spatially recruits phosphatases to sarcomeric or stress-sensitive compartments. Rather than being a passive structural component, KY may coordinate the subcellular targeting or activation state of PPM1B, thereby influencing the initiation or feedback regulation of autophagic signalling in response to cytoskeletal damage or mechanical overload.

This model aligns with established paradigms in muscle biology in which Z-disc–associated proteins integrate mechanical input with proteolytic pathways. Notably, FLNC and BAG3 function within CASA pathway, linking cytoskeletal strain to protein degradation (Arndt et al., 2010; Ulbricht et al., 2015). The parallel of KY's interactions to these proteins supports a shared mechanistic role in proteostasis and stress adaptation, particularly under conditions that challenge sarcomeric integrity.

The enrichment of Hspa8, Hspa5, and Hspa9 further suggests that KY participates in diverse proteostasis networks. Hspa8 is the core chaperone in CMA, a selective degradation pathway for cytosolic proteins. Its association with KY raises the possibility that KY modulates substrate recognition or trafficking during CMA, especially under stress conditions where CMA is upregulated. Correspondingly, the identification of Hspa5 and Hspa9 key regulators of ER and mitochondrial unfolded protein responses points to a broader cross-organelle role for KY in buffering proteotoxic stress. These findings extend KY's functional scope, positioning it at the interface of cytoskeletal architecture and cellular quality control systems.

This broader interpretation is particularly relevant in physiological contexts requiring high protein turnover, such as myogenesis, muscle repair, or adaptation to load. In

these settings, tight coordination between structural resilience and degradation capacity is essential. By associating with both phosphatases and stress chaperones, KY may function as a nodal integrator of mechanical sensing and proteostatic response.

Critically, these findings align with and extend those of (Jokl et al., 2018), whose transcriptomic and proteomic profiling of *ky/ky* muscle indicated disruptions in protein folding and degradation pathways. The enrichment of HSPs and PPM1B observed in the present study is consistent with those earlier dataset-level changes and may help explain why proteostasis-related processes are altered in the absence of KY. Rather than providing a direct molecular basis, these associations suggest that KY contributes to the organisation of stress-responsive or chaperone-linked complexes. Overall, the results support a more nuanced view of KY as a dynamic scaffold within a stress-sensing network, comparable to other multifunctional Z-disc–associated proteins such as FLNC and BAG3.

Moreover, the absence of these interactions in tdTomato control samples strengthens their specificity, ruling out artefactual association due to overexpression or nonspecific pulldown. This experimental control strengthens the interpretation that KY's interaction with stress chaperones and phosphatases reflects genuine biological relationships.

Nevertheless, some important caveats should be considered. It remains unclear whether the observed interactions between KY and associated proteins are direct or occur within larger multiprotein complexes. For instance, in the CASA pathway, BAG3 links FLNC to HSPA8 without necessarily forming stable binary interactions (Ulbricht et al., 2013). A similar model may apply to KY, suggesting it functions as part of broader stress-adaptive assemblies rather than acting in isolation. Furthermore, this study did not examine how these interactions are regulated under different physiological conditions. It is still unknown whether the composition or abundance of KY-associated complexes shifts in response to mechanical stress, nutrient deprivation, or proteotoxic stress, factors highly relevant to muscle biology. Although tdTomato controls were included to confirm the specificity of pulldown assays, further validation using complementary approaches such as co-immunoprecipitation, proximity-based biotinylation, or live-cell imaging would help strengthen confidence in both the interaction dynamics and the subcellular context in which they occur.

These findings propose that KY functions as more than a structural component of the sarcomere; instead, it may serve as a regulatory hub linking Z-disc integrity with autophagy and broader stress-responsive proteostasis pathways. Rather than acting in isolation, KY could coordinate the degradation systems that maintain muscle homeostasis under physiological stress. Future studies mapping the complete spectrum of KY-associated protein complexes and their regulatory mechanisms will be crucial to determine whether disruptions in these interactions contribute to the onset or progression of myofibrillar myopathies and other muscle-wasting disorders.

CHAPTER EIGHT: RESULTS Autophagy Assessment in KY-Deficient Models

CHAPTER 8. Autophagy Assessment in KY-Deficient Models

8.1 Introduction

Autophagy is a critical cellular process involved in the degradation and recycling of cytoplasmic components, essential for maintaining cellular homeostasis, particularly under stress conditions or during metabolic shifts. In skeletal muscle, proper regulation of autophagic flux is vital for the preservation of muscle mass, protein quality control, and overall muscle integrity. Dysregulation of this pathway has been implicated in a variety of muscular disorders, including myopathies characterised by protein aggregation and structural degeneration.

The KY protein, previously characterised primarily by its localisation to the Z-disc and its contribution to sarcomeric structure in striated muscle, has more recently been considered a potential modulator of intracellular quality-control pathways. Although KY has long been viewed as a structural protein, observations from KY-deficient models have suggested broader consequences for muscle homeostasis, including phenotypes that resemble impaired protein clearance. However, its specific involvement in autophagy remains poorly defined.

Proteomic analyses presented in Chapter 7 identified possible associations between KY and several proteins that participate in cellular stress-response or proteostasis pathways. While some of these candidates have roles in autophagy, the data at this stage provide indicative, rather than definitive, evidence of interaction; the identities of these proteins require further biochemical validation before firm conclusions can be drawn. As such, these findings raise the possibility that KY may intersect with autophagic processes, but they do not establish direct mechanistic involvement.

Additional experimental observations described in Chapter 3 showed that KY-deficient myoblasts exhibit altered protein-clearance behaviour under conditions of heat shock, proteasome inhibition, and autophagy blockade. These stress-based assays suggested that loss of KY impacts cellular proteostasis, but because multiple degradation pathways are simultaneously engaged during stress, these experiments could not resolve whether autophagy itself was specifically affected.

To investigate this question more directly, the current chapter employs a targeted dual-reporter system (GFP-LC3/RFP-LC3ΔG), a well-established tool for measuring autophagic flux. Validation of this probe follows previously published protocols (Kaizuka et al., 2016). When combined with complementary biochemical approaches—namely LC3-I/LC3-II Western blotting and immunofluorescence-based quantification—this system permits assessment of autophagosome formation, maturation, and degradation under defined basal and stress conditions.

Using this approach in both wild-type and KY-deficient models allowed direct examination of whether KY influences autophagic activity or flux efficiency. Together, these experiments were designed to determine whether disruption of KY affects the

autophagy–lysosome pathway specifically, or whether previously observed proteostasis defects arise from broader, upstream disturbances in cellular stress handling and muscle homeostasis.

8.2 Experiential Design

8.2.1 GFP-LC3 -RFP-LC3∆G Assay

In this experiment, we used a dual-colour autophagy reporter system consisting of GFP-LC3 and RFP-LC3ΔG (Kaizuka et al., 2016), to monitor autophagic flux in both cultured cells and skeletal muscle tissue under KY-deficient conditions. Once expressed, endogenous ATG4 proteases cleave the reporter at a specific site, producing two proteins in equal amounts. GFP-LC3 retains a key glycine residue, allowing it to be lipidated and incorporated into autophagosomal membranes, making it a marker for active autophagy. In contrast, RFP-LC3ΔG lacks this glycine, so it cannot be lipidated and remains freely distributed in the cytosol. This makes it a stable internal reference for assessing relative changes in autophagosome formation and turnover.

During autophagosome maturation, GFP-LC3 is incorporated into the autophagosomal inner membrane and subsequently degraded upon fusion with lysosomes (autolysosomes). Simultaneously, the outer membrane-associated GFP-LC3 is delipidated and recycled by ATG4. In contrast, RFP-LC3ΔG remains stable in the cytoplasm and is not targeted by autophagic degradation, enabling ratiometric

quantification of flux through the autophagy pathway, see the (Figure 8.1) the experimental workflow.

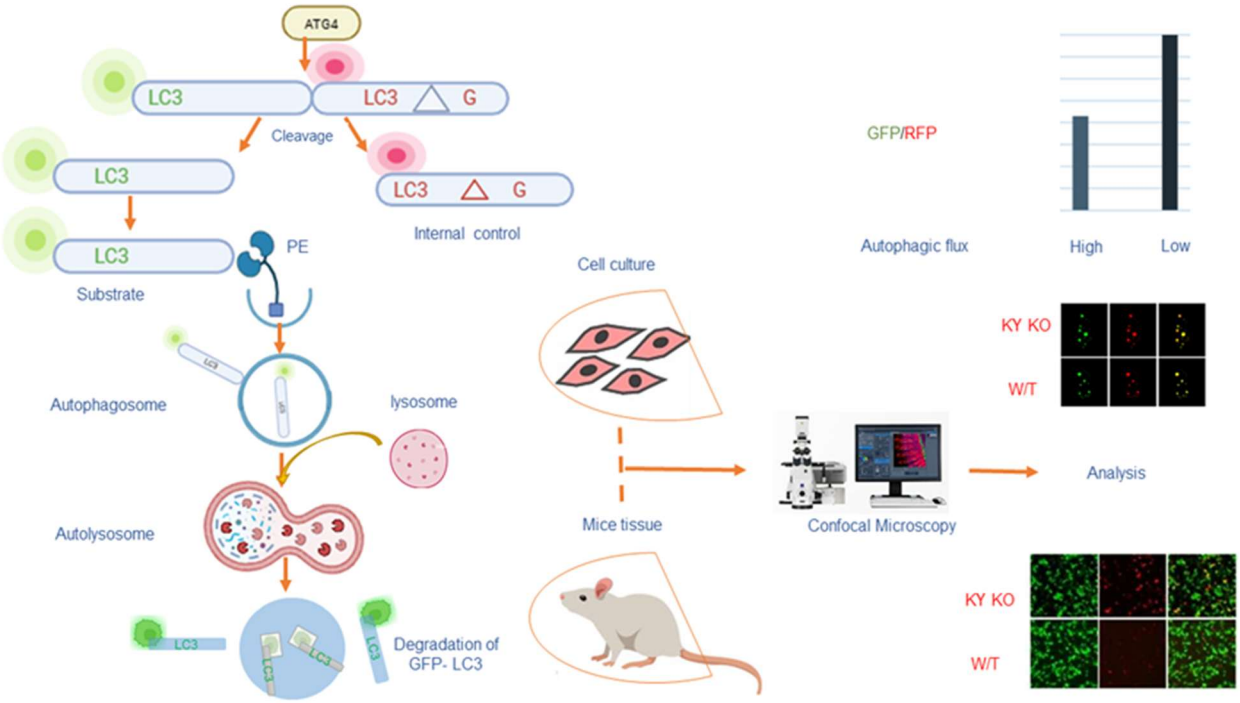

Figure 8.1 The experimental workflow for assessing autophagic flux using the GFP-LC3–RFP-LC3ΔG reporter system.

Upon expression in cultured cells or mouse skeletal muscle, the probe is cleaved by ATG4 into two components: GFP-LC3, which becomes lipidated and integrates into autophagosomes, and RFP-LC3ΔG, which remains cytosolic and undegraded. Upon autophagosome–lysosome fusion, GFP-LC3 on the inner membrane is degraded, while RFP-LC3ΔG remains stable and serves as an internal control. Confocal microscopy quantifies GFP and RFP fluorescence, and the GFP/RFP ratio inversely reflects autophagic activity. Comparative analysis between wild-type and KY-deficient samples allows evaluation of KY's role in autophagic flux. Adapted from Kaizuka et al. (2016), Molecular Cell, 64(4), 835–849.

8.2.2 Autophagic Flux Measurements

To assess autophagic activity, we used the GFP–LC3/RFP–LC3ΔG reporter system, in which the ratio of GFP to RFP fluorescence provides a quantitative readout of autophagic flux (Kaizuka et al., 2016). When autophagy is active, GFP–LC3 is delivered to autolysosomes and degraded, resulting in a low GFP/RFP ratio; conversely, a high GFP/RFP ratio indicates impaired autophagic degradation, typically due to disrupted autophagosome–lysosome fusion or reduced lysosomal function.

This system was applied in both *in vitro*, using undifferentiated myoblast derived from wild-type and KY-knockout C2C12 cells, and *in vivo*, by expressing the reporter in skeletal muscle under the same genetic conditions. Confocal microscopy images were acquired using identical exposure settings across all conditions. For quantification,

regions of interest (ROIs) were manually drawn around individual myofibres (*in vivo*) or myoblast (*in vitro*), and the mean fluorescence intensity for GFP and RFP channels was measured using ImageJ. Background fluorescence was subtracted from each measurement, and the GFP/RFP ratio was calculated for each fibre. At least 50 fibres per sample and four biological replicates per condition were analysed to ensure statistical robustness. This approach enabled direct comparison of autophagic flux between wild-type and KY-deficient muscle at both the cellular and tissue levels.

8.3 *In Vitro* Assessment of Autophagic Flux

GFP-LC3–RFP-LC3ΔG probe was transiently expressed in C2C12 myoblasts, wild-type, and KY-knockout (KY_Del) cell lines. Three independent KY-knockout clones (designated D, I, and K) were used to confirm reproducibility. The KY_Del C2C12 lines were generated in our laboratory (Gonzalo group) by Eliot Jokl using CRISPR/Cas9-mediated gene editing, targeting exon 2 of the Ky gene. Guide RNAs were designed using the CRISPR Design Tool to introduce frameshift-inducing indels. Clonal populations were isolated by limiting dilution and screened by PCR amplification of the target region followed by Sanger sequencing to confirm the presence of biallelic deletions. Complete loss of KY protein expression was validated by Western blotting using an anti-KY antibody, with GAPDH as a loading control (Jokl et al., 2018).

Cells were transfected with the reporter construct and incubated for 24–48 hours. After incubation, cells were fixed, mounted, and imaged using confocal microscopy. The GFP and RFP fluorescence intensities were quantified to calculate the GFP/RFP ratio, serving as a readout for autophagic flux.

8.3.1 KY Deficiency Impairs Autophagic Flux in C2C12 Cells

In wild-type C2C12 cells, the GFP/RFP fluorescence ratio was consistently low, indicating efficient autophagic flux, as GFP-LC3 was selectively degraded in autolysosomes while RFP-LC3ΔG remained cytosolic and stable. In contrast, KY-deficient C2C12 clones (D, I, and K) displayed significantly elevated GFP/RFP ratios, suggesting impaired autophagic degradation and accumulation of autophagosomes.

Representative confocal images further supported this observation. Wild-type cells exhibited strong RFP fluorescence and faint GFP signals, whereas KY KO cells showed immediate accumulation of both fluorophores, consistent with stalled autophagy. Quantitative analysis of normalised fluorescence intensities confirmed a statistically significant increase in the GFP/RFP ratio in KY KO cells (***$P < 0.05$, unpaired t-test, $p = 0.0051$), highlighting a disruption in autophagic progression due to KY deficiency (Figure 8.2).

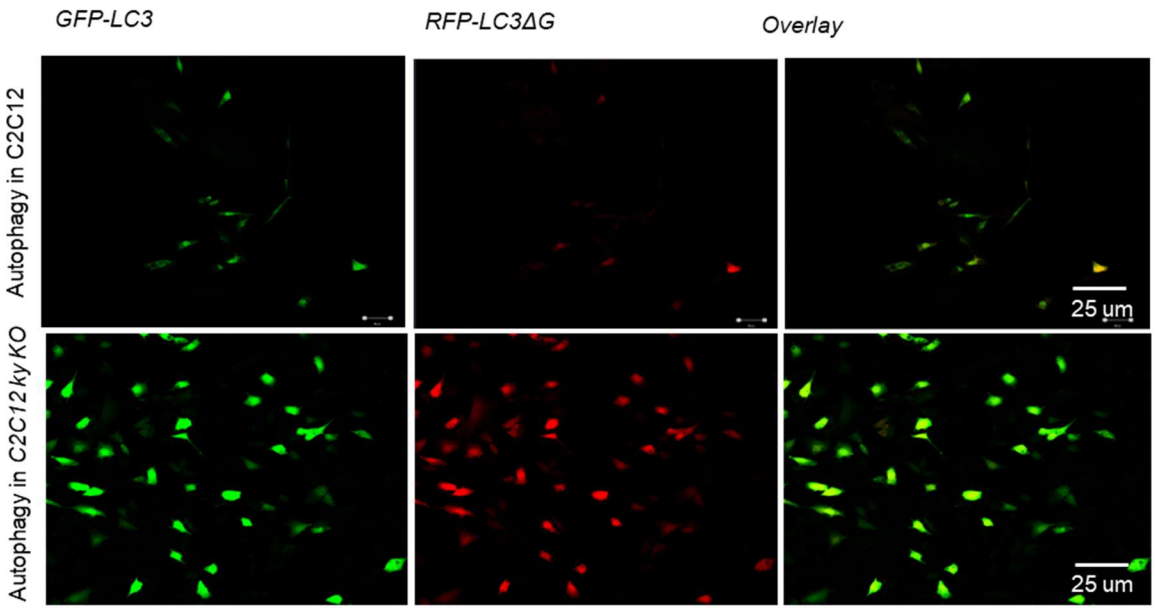

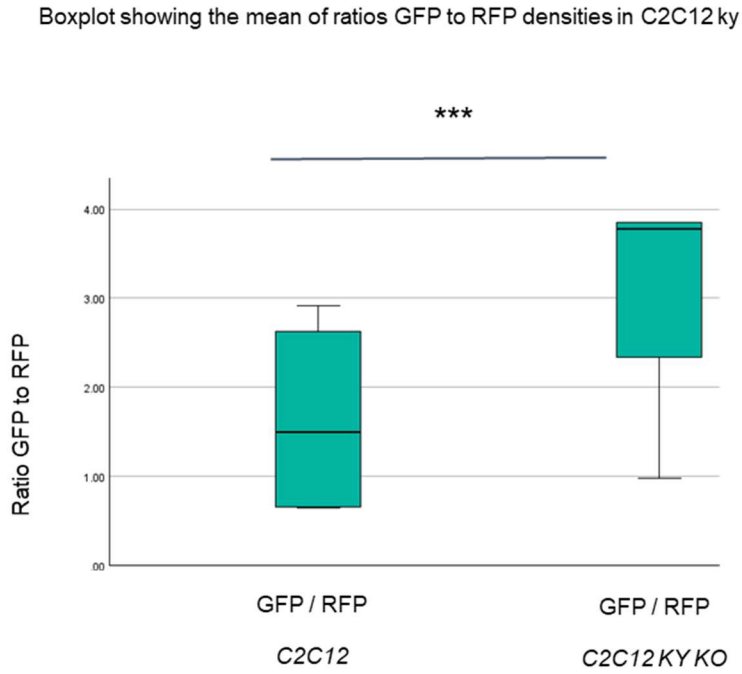

Figure 8.2 KY Deficiency Disrupts Autophagic Activity in C2C12 Myoblasts Assessed via GFP-LC3–RFP-LC3ΔG Probe.

Autophagic flux is reduced in KY-deficient C2C12 myoblasts, as indicated by altered GFP/RFP signal ratios. In normal C2C12 cells, efficient autophagy results in degradation of GFP-LC3 in the lysosome, leading to low GFP/RFP ratios. In contrast, KY-deficient cells exhibit significantly higher GFP/RFP ratios, consistent with impaired autophagic degradation. (Upper panel) Representative images of wild-type C2C12 cells transfected with the GFP-LC3–RFP-LC3ΔG probe. Cells show strong GFP and faint RFP fluorescence, reflecting active autophagy. (Lower panel) Representative images of KY-deficient cells transfected with the same probe. These cells display both strong GFP and RFP signals, indicating accumulation of autophagosomes and reduced autophagic degradation. (Box plot) Quantitative analysis of normalized GFP and RFP signal intensities per cell under each condition, based on ZEN software densitometry. Data are expressed as mean ± SEM. Statistical analysis was performed using an unpaired t-test: ***P < 0.05; F = 77; df = 164; p = 0.0051. Images were acquired at 20× magnification with identical exposure settings for all conditions (750 ms exposure, digital gain = 0.5). Scale bars are shown in the bottom right of each panel.

These findings demonstrate that KY is required for normal autophagic flux *in vitro* and suggest that its absence may impair autophagosome maturation or lysosomal fusion, thereby compromising cellular protein homeostasis in muscle cells.

8.4 *In Vivo* Assessment of Autophagic Flux

GFP-LC3–RFP-LC3ΔG were electroporated into the TA, in both wild-type and *ky/ky* mice. This reporter allows for a ratiometric measurement of autophagic flux by distinguishing between GFP-LC3, which is incorporated into autophagosomes and degraded, and RFP-LC3ΔG, which remains stable in the cytosol as a reference signal. After eight days of expression, the mice were sacrificed, and the TA muscles were collected, cryo-sectioned, and prepared for imaging. Confocal microscopy was then used to visualise and quantify GFP and RFP signals, with all samples imaged under identical acquisition settings. By analysing the GFP/RFP fluorescence ratio, we were able to directly compare autophagic degradation efficiency in muscle fibres with and without functional KY protein.

8.4.1 KY Deficiency Impairs Autophagic Flux *In Vivo*

Confocal image analysis revealed clear differences in autophagy dynamics between wild-type and KY-deficient muscle. In wild-type fibres, GFP-LC3 levels were relatively low, steady with normal lysosomal degradation, while RFP-LC3ΔG remained evenly distributed in the cytosol, resulting in a low GFP/RFP ratio indicative of healthy autophagic flux. In contrast, *ky/ky* muscle fibres showed noticeably higher GFP-LC3 fluorescence and elevated GFP/RFP ratios, suggesting that degradation of GFP-LC3 was reduced and that autophagic progression was impaired. Quantitative analysis confirmed a statistically significant increase in GFP/RFP ratios in KY-deficient tissue compared to wild-type controls (Figure 8.3). These *in vivo* results closely reflect *in vitro* findings and reinforce the conclusion that KY plays a critical role in maintaining efficient autophagic flux in skeletal muscle under normal physiological conditions.

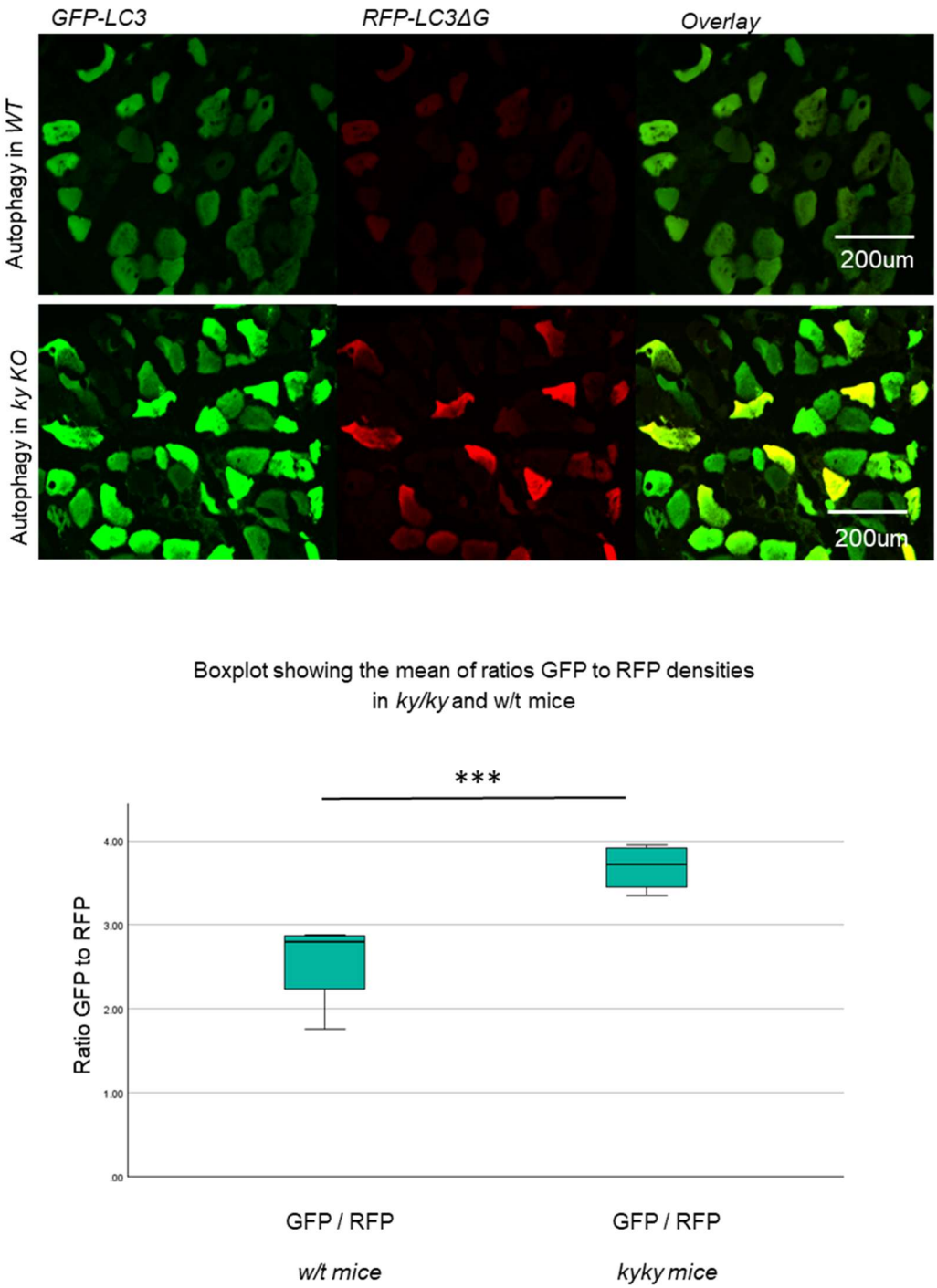

Figure 8.3 KY Deficiency Impairs Autophagic Activity in Skeletal Muscle of ky/ky Mice.

Autophagic flux is reduced in ky/ky mice compared to WT controls, as indicated by altered GFP/RFP ratios using the GFP-LC3–RFP-LC3ΔG reporter. In WT muscle fibres, active autophagy leads to efficient lysosomal degradation of GFP-LC3, resulting in low GFP/RFP ratios. In contrast, ky/ky mice display significantly elevated GFP/RFP ratios, suggesting impaired autophagic degradation and accumulation of autophagosomes. (Upper panel) Representative images of TA muscle fibres from WT mice electroporated with GFP-LC3–RFP-LC3ΔG, showing strong GFP and faint RFP signals, consistent with normal autophagic activity. (Lower panel) Representative images of TA fibres from ky/ky mice, showing both strong GFP and RFP fluorescence, indicative of autophagic impairment. (Box plot) Quantification of normalized GFP and RFP signal intensities per fibre across conditions, performed using ZEN software densitometry analysis. Data represent mean ± SEM. Statistical analysis was performed using an unpaired t-test: ***P < 0.05; F = 6.257; df = 152; p = 0.0083. All images were captured at 20× magnification. Exposure settings were kept constant across samples: 750 ms exposure time, digital gain = 0.5 for the GFP (green) channel and 4.0 for the RFP (red) channel. Scale bars are shown in the bottom right of each image panel.

To better understand the underlying cause, further investigation is reasonable. Therefore, we plan to conduct additional analyses focusing on the individual behaviour and regulation of GFP and RFP signals under both experimental conditions. This will help clarify whether the altered RFP levels reflect biological relevance or technical variability, and ultimately, provide deeper insight into KY's role in autophagy and protein turnover.

8.5 KY Deficiency Leads to Accumulation of GFP-LC3 and Impaired Autophagosome Turnover *In Vivo*

To better characterise autophagic dynamics and address limitations identified in earlier analyses, a dedicated assessment of GFP-LC3 and RFP-LC3 accumulations were performed *in vivo*. In the previous experiment, autophagic flux was evaluated using the GFP-LC3/RFP-LC3ΔG ratio, which provides a sensitive readout of flux changes but does not allow the behaviour of each fluorophore to be examined independently. As a result, it was not possible to determine whether the observed alterations arose from changes in autophagosome formation (GFP-LC3), altered processing of the RFP-LC3ΔG internal control, or a combined effect.

To resolve this ambiguity, the present analysis focused specifically on GFP-LC3 and RFP-LC3ΔG individual intensities within individual muscle fibres of *ky/ky* and WT mice. This approach allows direct comparison of accumulations. All samples were processed together, cryo-sectioned under identical conditions, and imaged on the same confocal system using fixed laser power, gain, and exposure parameters to ensure reliable signal comparability between genotypes.

By analysing GFP-LC3 and RFP-LC3ΔG separately in this complementary experiment, it becomes possible to determine whether the autophagy impairment in ky/ky muscle reflects enhanced autophagosome formation, reduced cargo turnover, disruption of the LC3 signal, or a combination of these mechanisms. This dissection of the individual fluorophore signals provides a clearer basis for interpreting flux defects and offers deeper insight into how loss of KY influences autophagosome dynamics and protein turnover *in vivo*.

In wild-type muscle, GFP-LC3 fluorescence was relatively low, consistent with efficient fusion of autophagosomes with lysosomes and subsequent degradation of the GFP-tagged protein. In contrast, *ky/ky* muscle fibres showed a marked increase in GFP signal under the same conditions. Although absolute GFP intensity should be interpreted with caution, the relative increase in KY-deficient tissue suggests a slowdown in GFP-LC3 degradation, likely reflecting an accumulation of autophagosomes. This pattern is consistent with impaired autophagic flux in the absence of KY. The difference in GFP signal between wild-type and KY-deficient muscles was both visually apparent and statistically significant (Figure 8.4), supporting the conclusion that KY plays an active role in promoting autophagosome turnover *in vivo*, and that its loss disrupts normal autophagic processing.

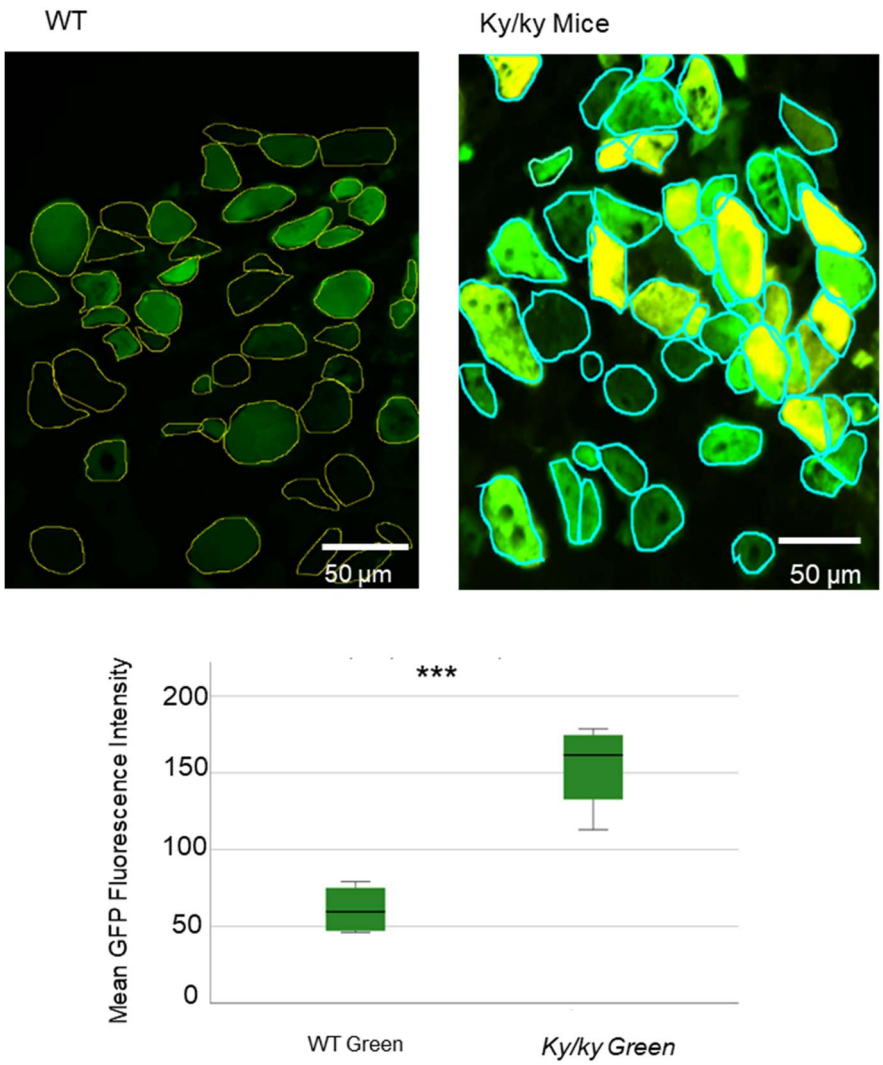

Figure 8.4 GFP fluorescence intensity is elevated in KY-deficient muscle fibres compared to controls.

Confocal images of TA muscle from WT and ky/ky mice expressing the GFP-LC3–RFP-LC3ΔG reporter. GFP-LC3 fluorescence (green) reflects autophagosome accumulation, and fibres were manually segmented for per-fibre quantification. WT fibres show low GFP signal, consistent with normal autophagosome turnover, whereas ky/ky fibres display markedly brighter GFP fluorescence, indicating impaired GFP-LC3 degradation. Quantitative analysis of GFP intensity per fibre revealed a significant increase in ky/ky muscle compared with WT (unpaired t-test, p = 0.0016; n = 37 fibres per genotype, 4 biological replicates). All samples were processed in parallel and imaged using identical confocal settings (exposure 750 ms; digital gain 0.5). Scale bar = 50 µm.

8.6 KY Deficiency Increases RFP-LC3ΔG Signal, Suggesting Altered Cytosolic Protein Handling

RFP-LC3ΔG signals were examined here on its own. Again, this construct is designed to remain in the cytosol and resist degradation, as it lacks the C-terminal glycine required for lipidation and autophagosome incorporation. For this reason, RFP-LC3ΔG serves as a stable internal reference, allowing comparison and normalisation of GFP-LC3 levels.

in vivo studies, RFP fluorescence was consistently higher in *ky/ky* muscle fibres than in controls, even though all samples were imaged using the same confocal settings and exposure parameters (Figure 8.5). While RFP-LC3ΔG is not expected to accumulate under normal conditions, its increased signal in KY-deficient tissue suggests a possible disruption in cytosolic protein handling. This may reflect broader impairments in proteostasis pathways, hinting that the absence of KY affects not only autophagy but also the stability or clearance of cytosolic proteins more normally.

Although RFP-LC3ΔG is not subject to autophagic degradation, the observed increase in KY-deficient tissue indicates that KY deficiency alters the intracellular environment in a manner that indirectly affects LC3-based constructs. This highlights the importance of interpreting both GFP and RFP signals in context when using dual-reporter systems to assess autophagic flux. (Figure 8.5).

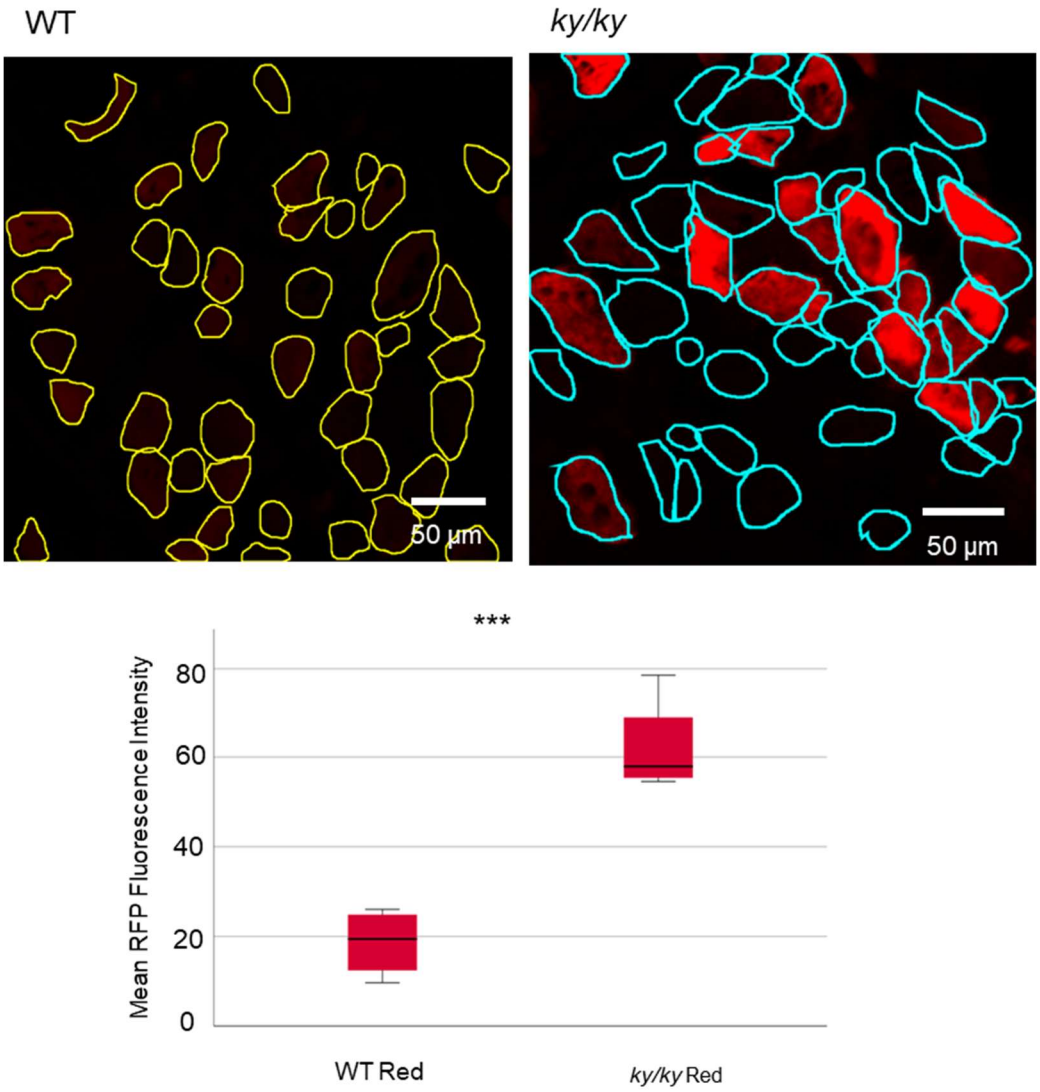

Figure 8.5 RFP-LC3ΔG fluorescence is elevated in KY-deficient muscle fibres compared to controls.

Confocal images of TA muscle from WT and ky/ky mice expressing the GFP-LC3–RFP-LC3ΔG autophagy reporter. RFP-LC3ΔG (red), a non-lipidated and degradation-resistant probe, serves as an internal readout of cytosolic reporter handling. WT fibres showed relatively low RFP signal, whereas ky/ky fibres exhibited markedly higher fluorescence, indicating altered accumulation of the cytosolic reporter in the absence of KY. Quantitative analysis of RFP intensity per fibre demonstrated a significant increase in ky/ky muscle compared with WT (unpaired t-test, p = 0.0005; n = 38 fibres per genotype, 4 biological replicates per group). All samples were processed in parallel and imaged using identical confocal settings (exposure 750 ms; digital gain 0.5). Scale bar = 50 µm.

The observed increase in RFP-LC3ΔG signal intensity in KY-deficient muscle fibres. despite the probe's design to remain unaffected by autophagic degradation, suggests that KY may influence LC3 protein turnover through mechanisms independent of canonical autophagy. Since both GFP-LC3 and RFP-LC3ΔG are expressed under the control of the same promoter, differential transcriptional regulation is unlikely to explain the discrepancy.

Instead, these results raise the possibility that KY contributes to LC3 regulation via effects on protein stability, trafficking, or cytosolic processing. While RFP-LC3ΔG is not degraded through autophagy, its increased abundance in KY-deficient tissue implies broader dysregulation of LC3-handling mechanisms. This finding underscores the need for further investigation into KY-dependent regulation of LC3 proteins and suggests that KY may have a previously unrecognised role in maintaining proteostatic balance beyond its established link to autophagic flux.

8.7 Altered LC3 Processing and Reporter Accumulation in KY-Deficient Cells (Quantitative Immunoblot analysis)

To complement the fluorescence imaging and more precisely evaluate protein levels, we performed Western blotting on lysates from wild-type and KY-deficient cell cultures expressing the GFP-LC3–RFP-LC3ΔG probe. This technique allows us to distinguish between the non-lipidated GFP-LC3-I and the lipidated GFP-LC3-II forms based on their distinct migration patterns during SDS-PAGE. By separating and detecting these two forms, Western blotting provides an additional layer of insight into autophagic dynamics that goes beyond what can be captured through imaging alone.

Furthermore, RFP levels were assessed to confirm whether the increased fluorescence observed in KY-deficient samples reflected genuine protein accumulation. Since confocal imaging can be influenced by cell morphology, transfection variability, or local concentration gradients, Western blotting served as an orthogonal technique to validate these findings.

Blotting results revealed that RFP protein levels were consistently elevated in KY-deficient samples, supporting the imaging data and indicating that RFP-LC3ΔG is indeed more abundant in the absence of KY, rather than this being a result of imaging artefacts or differences in probe expression.

In equivalent, Western blot analysis of GFP-LC3 showed an altered distribution between the LC3-I and LC3-II isoforms. Specifically, the GFP-LC3-I/LC3-II ratio was significantly higher in KY-deficient cells compared to wild-type controls. This shift could indicate a disruption in autophagosome formation or maturation; however, since this analysis was performed in the absence of autophagy inhibitors, the interpretation remains ambiguous. The reduced levels of GFP-LC3-II in KY-deficient cells may result

either from increased degradation or reduced lipidation and incorporation into autophagosomes (Figure 8.6).

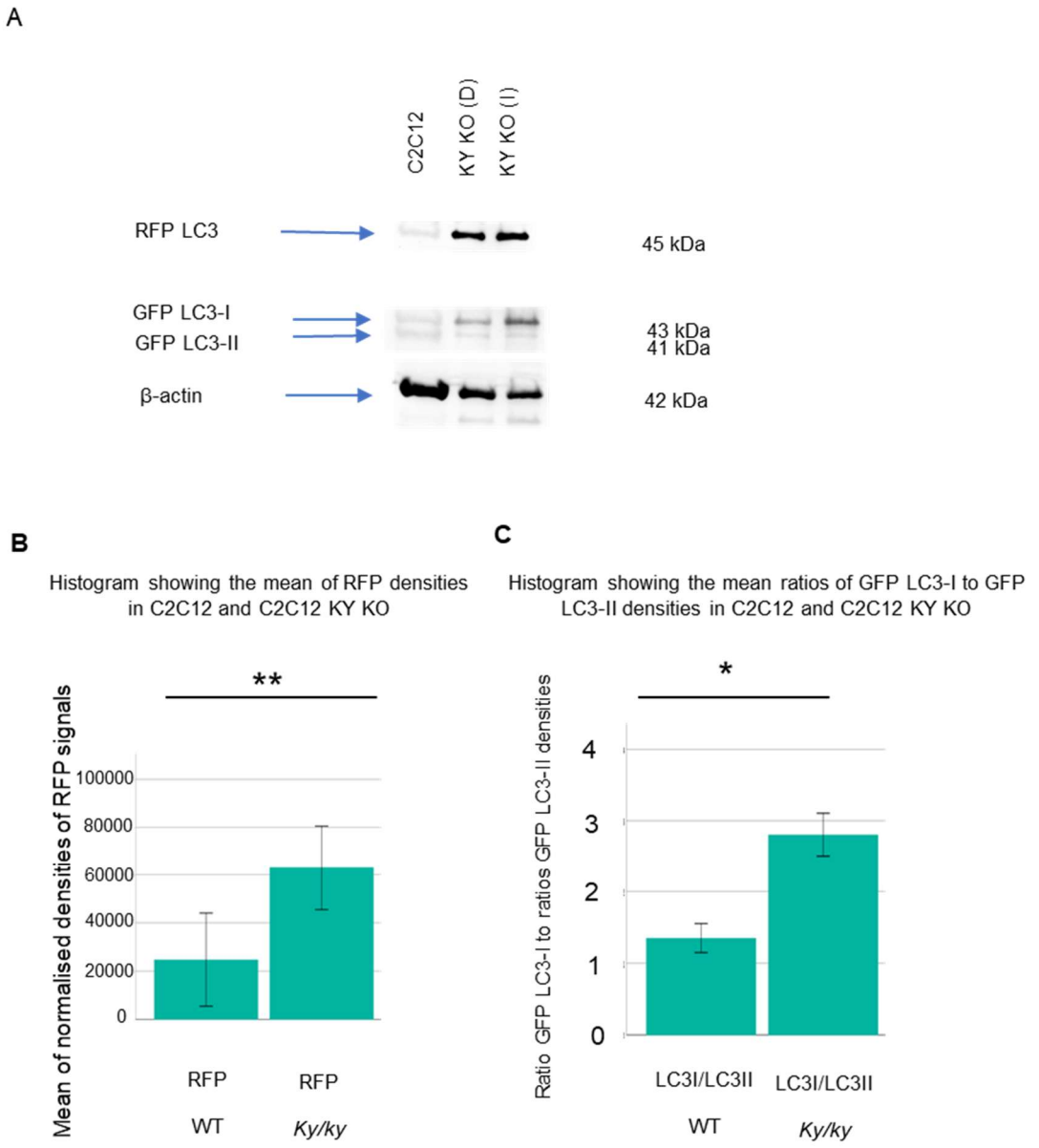

Figure 8.6 Western blot analysis of GFP-LC3 and RFP-LC3ΔG in wild-type and KY-deficient C2C12 cells.

Cell lysates from WT and KY-knockout (KY_Del_D and KY_Del_K) myoblasts expressing the GFP-LC3–RFP-LC3ΔG reporter were analysed by Western blot to examine the levels of GFP-LC3-I, GFP-LC3-II, and RFP-LC3ΔG. Representative blots show distinct bands corresponding to GFP-LC3-I, GFP-LC3-II, and RFP-LC3ΔG. Total protein staining was used as a loading control. Densitometric quantification of RFP-LC3ΔG levels (left graph) and the GFP-LC3-I/LC3-II ratio (right graph) revealed a significant increase in RFP levels and a higher LC3-I/LC3-II ratio in KY-deficient lines compared to WT. This pattern suggests altered LC3 processing and reporter protein accumulation in the absence of KY. Data represent mean ± SEM from 4 independent experiments.

Western blot analysis confirmed increased accumulation of RFP-LC3ΔG in KY-deficient cells and revealed changes in the distribution of GFP-LC3 isoforms. Specifically, KY-deficient cells showed a higher GFP-LC3-I to LC3-II ratio, suggesting a disruption in normal autophagic processing. However, since lysosomal inhibitors were not used to block autophagosome degradation, we cannot definitively conclude whether autophagic flux is enhanced or impaired. Despite this limitation, the results support the idea that KY plays a role in regulating the turnover or processing of LC3-tagged proteins, reinforcing its broader involvement in muscle proteostasis.

8.7.1 Basal Autophagy Activity in KY-Deficient Cells

To assess basal autophagic flux, we examined LC3 processing in wild-type and KY-knockout cells as previously described (Jokl et al., 2018).

Cells were treated with (BafA1; 100 nM, 3 hours) (Pettersen et al., 2017; Summers & Valentine, 2020) to block autophagosome–lysosome fusion and prevent LC3-II degradation. Under these conditions, accumulation of LC3-II serves as an indicator of ongoing autophagic flux. Lysates were then analysed by Western blot using an anti-GFP antibody to detect GFP-tagged LC3. Two bands were resolved, corresponding to non-lipidated GFP-LC3-I and lipidated GFP-LC3-II.

In wild-type C2C12 cells, LC3-II levels were detectable but relatively low under basal conditions and did not show marked accumulation following BafA1 treatment, suggesting either a low autophagy turnover rate at baseline or an unusually efficient flux, in which LC3-II is rapidly turned over even under blocked degradation conditions. In contrast, KY-deficient cells exhibited elevated levels of both LC3-I and LC3-II, with LC3-II persisting regardless of BafA1 treatment. This pattern indicates that autophagosomes are being formed in the absence of KY, but degradation may be impaired, leading to LC3-II accumulation (Figure 8.7).

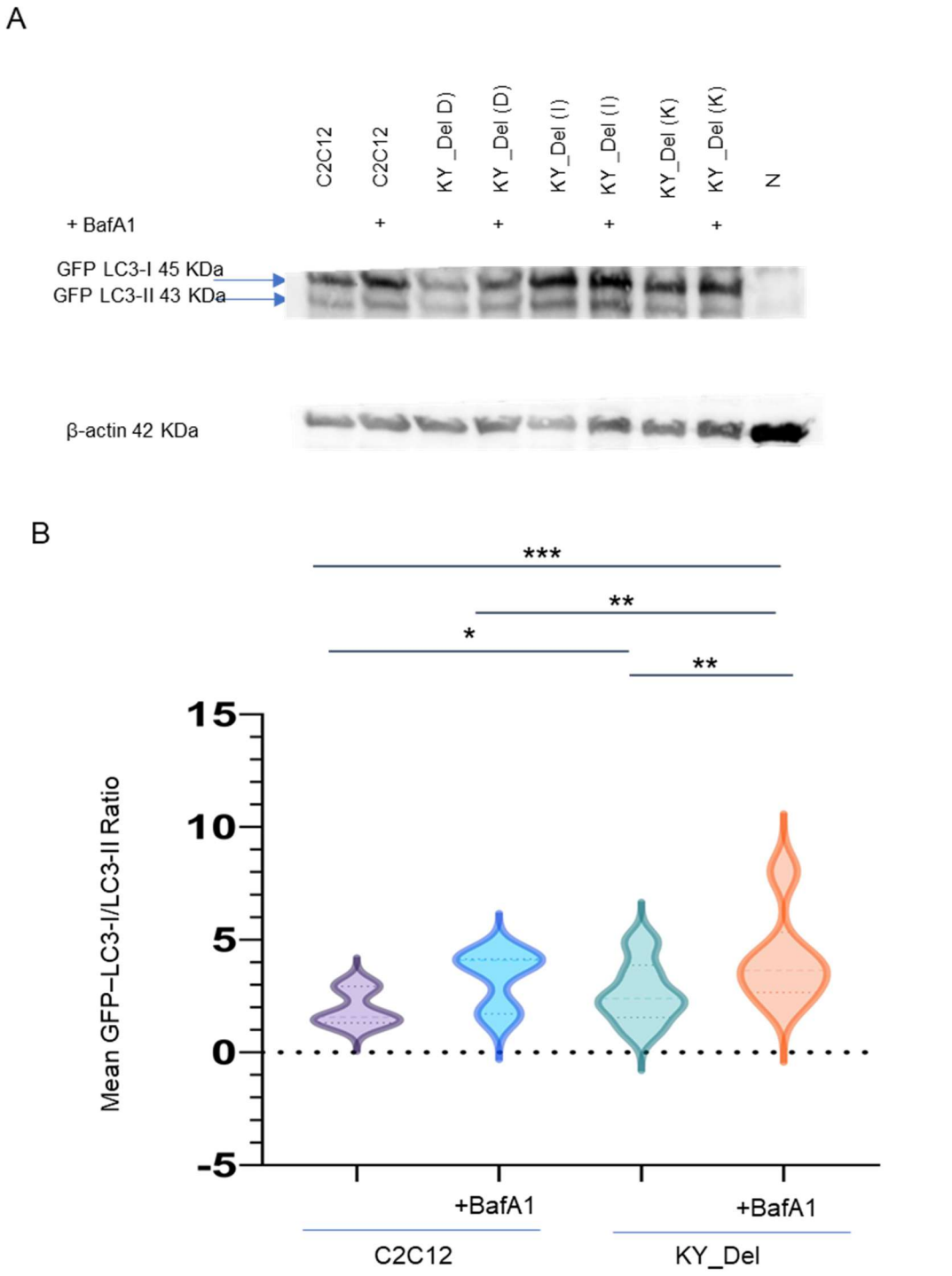

Figure 8.7 The evaluation of basal autophagic activity in wild-type and KY-deficient in C2C12 cells under lysosomal inhibition.

Western blot analysis of GFP–LC3 was performed in wild-type and KY-deficient clones (KY_Del_D, KY_Del_K, KY_Del_I) following treatment with Bafilomycin A1 (BafA1, 100 nM, 3 h) or under untreated basal conditions. Representative blot (top) shows LC3-I and isoforms. β-Actin (42 kDa) served as a loading control (middle panel). Quantification of the LC3-I/LC3-II ratio (bottom) revealed a significant increase in KY-deficient cells upon BafA1 treatment compared to their untreated counterparts, indicating impaired autophagosome clearance. In contrast, wild-type cells showed no significant difference in LC3-I/II ratio with or without BafA1, suggesting efficient autophagic flux. Data represent mean ± SEM from n = 6 independent experiments. Statistical analysis was performed using one-way ANOVA; *p < 0.05.

Quantitative analysis across independent replicates (Figure 8.7) revealed that in wild-type, LC3-II levels increased upon BafA1 treatment, leading to a drop in the LC3-I/LC3-II ratio from approximately 11.5 to 6.5, consistent with effective autophagic flux and BafA1-induced blockade of degradation. In contrast, KY-deficient cells (KY_Del_D and KY_Del_K) showed elevated basal levels of both LC3-I and LC3-II but only limited additional LC3-II accumulation after BafA1 treatment. Unexpectedly, the LC3-I/LC3-II ratio increased from ~5.43 to ~9.10 after BafA1 exposure, the opposite of what is expected under functional autophagic flux. This reversal suggests that KY-deficient cells may have impaired autophagosome-lysosome fusion or LC3 processing, and that the flux is likely already disrupted under basal conditions.

These results indicate that KY is not only required for autophagosome formation but also effective clearance, likely at the stage of autophagosome–lysosome fusion or lysosomal degradation. The accumulation of LC3-II in KY-deficient cells under basal conditions, combined with the lack of expected LC3-II increase upon BafA1 treatment, suggests that autophagic flux is compromised. Importantly, the elevated altered LC3-I/LC3-II ratio after BafA1 exposure in KY-deficient cells supports a model where KY loss disrupts normal LC3 processing and turnover, supporting KY's role in maintaining functional autophagy.

8.7.2 Autophagy Induction Under Starvation in KY-Deficient Cells

To further examine autophagic activity in KY-deficient myoblasts, we assessed LC3 processing under nutrient deprivation, with and without BafA. treatment. Thereby prevents the degradation of LC3-II and allows accumulation to be used as a marker of ongoing autophagic flux. Wild-type and KY-deficient cells were subjected to serum starvation for 3 hours, with or without co-treatment with 100 nM BafA1.

Western blotting using anti-GFP antibodies revealed baseline levels of both GFP-LC3-I and GFP-LC3-II in all cell lines. Under starvation conditions, LC3-II levels generally increased and were further modulated by BafA1 treatment. However, the observed changes were not fully consistent across all conditions or clones, and interpretation was limited by the availability of a single blot per treatment group (Figure 8.8).

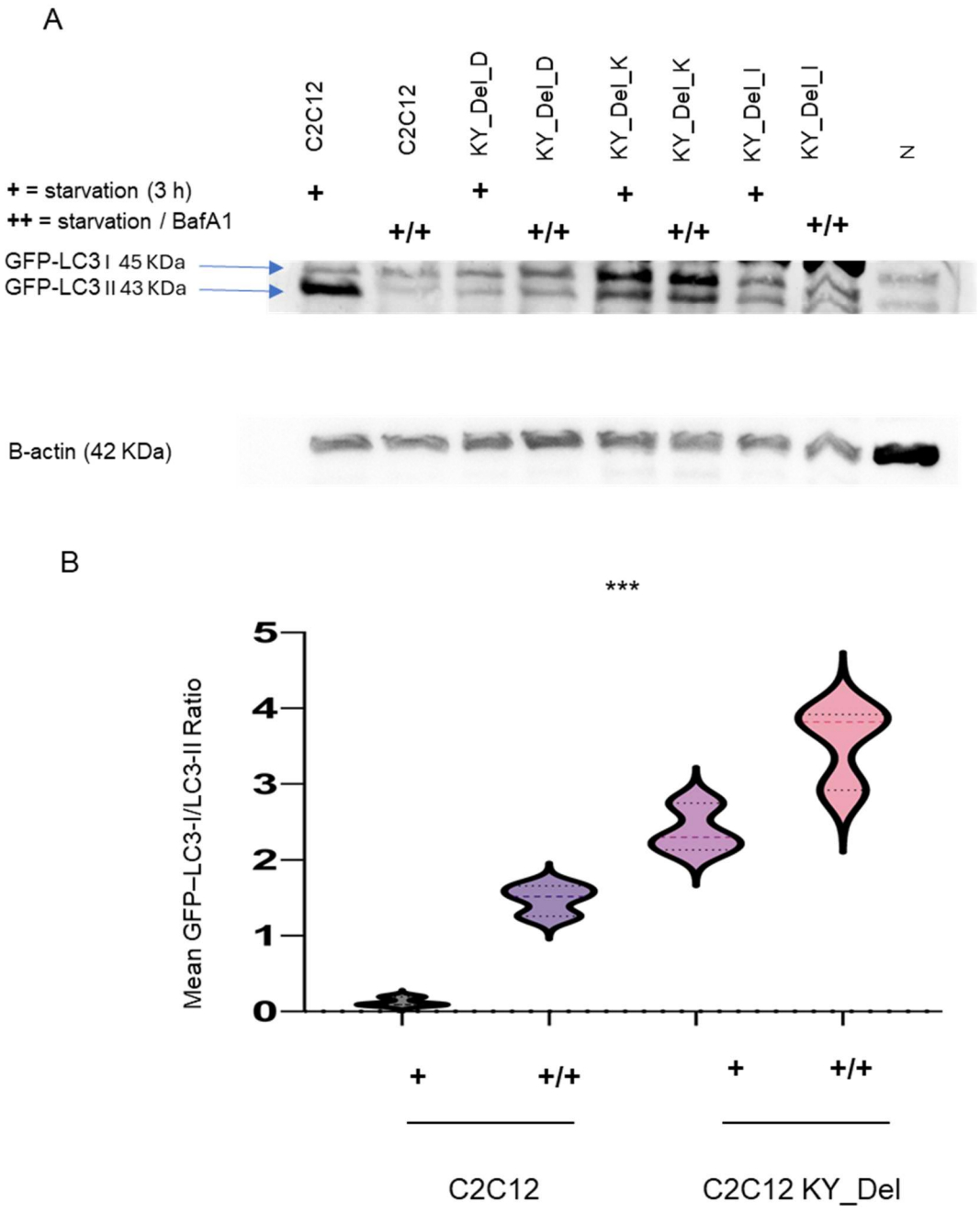

***Figure 8.8* The assessment of autophagy activity in wild-type and KY-deficient C2C12 cells under starvation and BafA1 treatment.**

A) Representative Western blot showing levels of GFP-tagged LC3b-I and LC3b-II in C2C12 wild-type and KY-knockout clones (KY_Del_D, KY_Del_I, KY_Del_K) following treatment with 100 nM BafA1 for 3 hours. B-Actin (42 kDa) served as a loading control. B) Quantification of LC3-I/LC3-II ratio based on densitometric analysis from three independent replicates. KY-deficient cells exhibited significantly higher LC3-I/LC3-II ratios compared to wild-type cells, indicating impaired autophagic flux. Data are presented as mean ± SEM n = 3. *p < 0.05; p = 9.33 × 10^{-6}.

In wild-type cells, LC3-II showed a modest increase upon starvation but did not consistently increase further with BafA1 treatment. In KY-deficient cells, LC3-II was elevated under basal conditions, and although LC3-II accumulation was observed

under starvation and BafA1 co-treatment in some clones, the response varied between replicates. These results suggest that autophagosomes are formed in both wild-type and KY-deficient cells under nutrient stress, but the dynamics of LC3-II accumulation differ, potentially indicating altered processing or clearance in the KY-deficient background.

While the two blots analysis limits the strength of conclusions, the observed elevation of LC3-II in KY-deficient myoblast, both at baseline and following starvation aligns with prior imaging data and supports a possible disruption in late-stage autophagy. These findings are consistent with the hypothesis that KY may be required for efficient autophagosome maturation or lysosomal fusion, though further replicates and quantitative analyses are needed to confirm this role.

8.8 Discussion

This chapter investigated autophagic flux in KY-deficient skeletal muscle cells and tissue using tandem fluorescent LC3 reporters and biochemical markers. The combined imaging and Western blot data revealed consistent evidence of impaired autophagy in the absence of KY, particularly at the stages of LC3 lipidation and autophagosome clearance. These findings build on previous chapters by extending KY's functional role beyond Z-disc organisation and into the domain of proteostasis regulation.

In both basal and starvation conditions, KY-deficient myoblasts displayed enhanced accumulation of RFP-LC3ΔG signal relative to wild-type controls. Given that this probe is resistant to lysosomal degradation and marks autophagosomes independently of fusion events, its increased abundance indicates impaired downstream processing. Crucially, this observation was substantiated by Western blot analyses showing an increased altered recombinant LC3-I/LC3-II ratio in KY-deficient cells, suggesting that the conversion of LC3-I to its lipidated, autophagosome-associated form is disrupted. Such defects are commonly associated with impaired autophagosome maturation or fusion with lysosomes (Klionsky et al., 2021), and parallel findings have been reported in BAG3, or FLNC-deficient muscle models, Z-disc proteins that, like KY, are implicated in cytoskeletal quality control (Arndt et al., 2010; Ulbricht et al., 2013).

Treatment with Bafilomycin A1, a well-established inhibitor of autophagosome–lysosome fusion, further increased LC3-II levels in both genotypes, as expected. However, the disproportionately elevated LC3-II accumulation in KY-deficient cells suggests a heightened reliance on efficient lysosomal degradation to maintain autophagic flux. These findings are consistent with reports that disruptions in autophagosome processing, whether arising from impaired macroautophagy or defects in associated quality-control pathways such as CASA, can lead to the buildup of undegraded autophagic intermediates (Arndt et al., 2010). Based on the current

data, it is not yet possible to conclude whether the defect observed in KY-deficient cells reflects a direct impairment of canonical autophagy, a disturbance in CASA-linked turnover of specific cytoskeletal clients, or a combination of both. Nonetheless, the results indicate that KY function contributes to efficient autophagosome resolution, a step at which vesicle trafficking or fusion may become rate-limiting in its absence.

Notably, starvation-induced autophagy remained detectable in KY-deficient cells, indicating that the core autophagy machinery retains its ability to respond to stress. However, this response was clearly attenuated compared to controls, as evidenced by the reduced accumulation of LC3-II and the weaker activation of the autophagy reporter. These observations suggest that, while KY is not strictly required for the initiation of autophagy, it appears to influence the efficiency and robustness of the process under stress conditions. A similar regulatory role has been attributed to FLNC, which modulates BAG3 recruitment and autophagic flux during mechanical stretch in muscle cells (Ulbricht et al., 2013). It is therefore plausible that KY fulfils a comparable, context-dependent function—possibly by coordinating the recruitment of fusion machinery or by stabilising contact sites between autophagosomes and lysosomes.

These findings support a model in which KY influences autophagic flux, although the precise stage at which KY acts remain unresolved. The data suggest that KY deficiency disrupts steps involved in LC3 processing and autophagosome maturation; however, this should not be interpreted as evidence that KY directly participates at the lysosome itself. Instead, any regulatory role is likely to occur upstream, at the level of autophagosome formation, cargo handling, or the coordination of stress-responsive signalling pathways. Although KY localises to the Z-disc,this region is increasingly recognised as a site enriched in mechanosensitive and proteostasis-related regulators, including components associated with CASA and chaperone-assisted quality control. Interactions identified in Chapter 7, such as PPM1B and HSPA8, further raise the possibility that KY may function as a scaffold or adaptor that links sarcomeric mechanotransduction to broader cellular proteolytic pathways, rather than acting directly at the lysosome. These observations point towards an indirect but potentially important role for KY in the regulation of autophagic efficiency. Definitive mechanistic clarification will require targeted assays that specifically dissect autophagosome formation, trafficking, and degradation in KY-deficient models.

These findings further reveal dysregulation of autophagy-related and stress-response pathways in *ky/ky* muscle, including transcriptional upregulation of BAG3, HSPB8, and FLNC, consistent with activation of the CASA pathway (Jokl et al., 2018). While Blanco et al. (2001) first identified the KY gene and documented sarcomeric disorganisation and fibre degeneration, earlier ultrastructural studies of the classical *ky* mouse line, also reported Z-disc thickening and the presence of autophagic vacuole–like structures in postural muscles (Bridges et al., 1992). These historical observations align with later molecular findings and support the interpretation that proteostasis disturbances are a consistent feature of the ky phenotype. The present study builds upon this groundwork by directly demonstrating that KY deficiency impairs autophagic

flux, thereby providing functional evidence that defective protein turnover is a central pathological mechanism in KY-associated myopathy.

To gain a more complete understanding of the underlying mechanism, it is important to distinguish whether the accumulation of LC3-II reflects increased autophagosome formation or impaired degradation, it would be valuable to use dynamic autophagy sensors such as the tandem fluorescent LC3 reporter (mCherry-GFP-LC3). This system discriminates autophagosomes from autolysosomes by exploiting the differential pH sensitivity of GFP (quenched in acidic lysosomes) and RFP stable, allowing direct evaluation of fusion efficiency (Kimura et al., 2007; Tanida et al., 2014). Complementary assays using LysoTracker or LysoSensor dyes could then assess lysosomal pH and functionality—parameters that may be altered under KY deficiency but are not captured by static LC3 measurements (Lu et al., 2017).

Although the use of RFP-LC3ΔG reporters provides insight into cargo accumulation, it does not fully capture substrate specificity or the efficacy of cargo degradation, particularly under selective autophagy conditions. For instance, CMA relies on different machinery and selective substrate recognition by HSPA8 and LAMP2A. Reporter systems targeting CMA or ubiquitinated protein aggregates, like (p62/SQSTM1-tagged probes), could help identify whether KY influences selective cargo degradation or interacts with parallel proteostasis pathways.

The downstream consequences of impaired autophagy—such as defects in mitochondrial quality control, sarcomere maintenance, or cellular stress tolerance were not assessed in this study. These aspects are highly relevant, as many myopathies show that disruption of mitophagy can drive muscle dysfunction independently of, or in parallel with, general autophagy defects. For example, in zebrafish lacking BAG3, failure to remove damaged mitochondria leads to mitochondrial swelling and subsequent myofibrillar disintegration (Ruparelia et al., 2014). More broadly, impaired mitophagy has been linked to oxidative stress and progressive loss of muscle fibre integrity (Gkikas et al., 2018), phenomena that frequently accompany proteostasis disturbances in skeletal muscle (Bonaldo & Sandri, 2013). Investigating whether KY deficiency produces similar mitochondrial vulnerabilities would therefore be a valuable extension of the present findings. Approaches such as assessing mitochondrial membrane potential using tetramethylrhodamine ethyl ester (TMRE) staining, or quantifying markers of oxidative stress, could help determine whether perturbations in autophagic flux in KY-deficient muscle are accompanied by secondary defects in mitochondrial quality control.

Additionally, there are some technical limitations should be considered when interpreting autophagic flux measurements. Although we assessed basal and starvation-induced autophagy *in vitro*, we were unable to perform equivalent *in vivo* assays due to constraints on mouse numbers and the variability between animals in autophagy induction timing. Factors such as age, sex, and genetic background can further influence basal autophagy and stress sensitivity in mouse models, adding

complexity to cross-condition comparisons. From a methodological standpoint, Western blot data were derived from two independent experimental replicates, each including three KY_DEL clonal lines (K, D, and I), which provides statistical power but falls short of ideal biological replication. Moreover, while Bafilomycin A1 was used consistently to block autophagosome-lysosome fusion, we did not incorporate other agents such as quinacrine, which can offer complementary insight into lysosomal acidification and cargo degradation (Fourrier et al., 2021). These technical caveats do not diminish the main findings but should inform interpretation and guide the design of future studies.

These findings demonstrate that KY deficiency disrupts autophagic flux in skeletal muscle, affecting both LC3 processing and the clearance of autophagosomes. Such defects likely contribute to the broader imbalance in proteostasis observed in *ky/ky* models and reinforce KY's role in helping muscle adapt to stress. By linking impaired autophagy to structural features of myopathy, this chapter positions KY as a novel regulator of degradation pathways that are critical for maintaining sarcomeric integrity and overall muscle health.

CHAPTER NINE- RESULTS Functional Interplay Between *ZAKβ* and *KY* in Skeletal Muscle

CHAPTER 9. Functional Interplay Between ZAKβ and KY in Skeletal Muscle

9.1 Introduction

ZAKβ is a serine/threonine MAPKKK kinase implicated in mechanosensitive signalling within skeletal muscle, particularly at the Z-disc, where mechanical forces are transduced into biochemical responses. Activated ZAKβ phosphorylates downstream MAPK pathways, including JNK and p38, which are key regulators of stress adaptation and hypertrophic growth (Gotoh et al., 2001; Martineau & Gardiner, 2001). Recent evidence suggests that constitutively active ZAKβ can drive myotube hypertrophy *in vitro*, underscoring its role as a positive regulator of muscle fibre size (Nordgaard et al., 2022).

In parallel, KY plays a key role in maintaining the structural integrity of the sarcomere. KY deficiency leads to Z-disc disorganisation, myofibrillar collapse, and impaired stress adaptation in both mice and humans (Blanco et al., 2001; Jokl et al., 2018). Transcriptomic profiling of ky/ky muscle revealed dysregulation of MAPK-related genes (A. Stonadge et al., 2023), suggesting that KY may functionally intersect with kinase-mediated signalling cascades such as those controlled by ZAKβ. Notably, both proteins share interaction networks involving IGFN1 and other Z-disc scaffolds, raising the possibility that KY facilitates ZAKβ-dependent mechanotransduction.

Unpublished data from the laboratory indicate that overexpression of constitutively active ZAKβ (ZAKβ^CA) promotes muscle fibre hypertrophy in wild-type mice, but this effect is markedly reduced in ky/ky muscle. This suggests that KY may be required for efficient ZAKβ signalling at the sarcomere, potentially acting as a scaffold or stabilising element that links kinase activation to downstream structural remodelling (A. J. Stonadge, 2023).

Building on these findings, we hypothesised that ZAKβ relies on KY to trigger a Z-disc–based hypertrophic signalling cascade, and that in the absence of KY, ZAKβ's ability to promote muscle growth is impaired. To test this, we re-examined the effects of constitutively active and kinase-dead ZAKβ constructs in both wild-type and ky/ky muscle using *in vivo* electroporation combined with morphometric analysis. This approach aimed to clarify the signalling relationship between KY and ZAKβ and to determine whether KY acts as a necessary co-factor or scaffold for stress-responsive hypertrophic pathways.

.

9.2 Experimental flow

To investigate whether ZAKβ-induced hypertrophy depends on KY, *in vivo* expression studies in wild-type and KY-deficient mice were performed. Plasmids encoding the constitutively active (ZAKβ^CA) and kinase-dead (ZAKβ^KD) forms of ZAKβ were generated as described by (Liu et al., 2000a, 2000b) and subsequently adapted for skeletal muscle expression following the approaches of Nordgaard et al. (2022) and Stonadge (2023).

In the constitutively active ZAKβ^CA mutant, removal of the C-terminal inhibitory S domain eliminates a built-in “off switch” that normally keeps the kinase inactive. Without this regulatory region, ZAKβ can activate itself through autophosphorylation, continuously stimulating downstream MAPK pathways such as JNK and p38. This makes the kinase active even in the absence of mechanical or stress signals, promoting persistent growth-related signalling.

In contrast, the kinase-dead ZAKβ^KD mutant contains a single amino acid substitution (K45M) in the ATP-binding site, which prevents it from transferring phosphate groups needed for catalytic activity. Although structurally intact and still able to bind other proteins, this mutant cannot phosphorylate its targets. ZAKβ^KD therefore acts as a dominant-negative form, providing a useful control to distinguish effects that rely directly on ZAKβ’s enzymatic function.

Both constructs were expressed as C-terminal tdTomato fusion proteins under a (CMV) promoter, allowing direct visual confirmation of transfection efficiency and enabling identification of transfected fibres during histological analysis.

Plasmids were introduced into the TA muscle via intramuscular injection followed by electroporation to enhance uptake efficiency. A tdTomato-only control was included to assess electroporation efficiency and to confirm that the delivery procedure itself did not induce hypertrophy.

After an eight-day expression period, muscles were harvested, cryo-sectioned, and analysed histologically. Robust tdTomato fluorescence confirmed efficient expression in both wild-type and ky/ky fibres. CSA measurements were then performed on transfected fibres to quantify hypertrophic responses.

This experimental design enabled direct comparison of ZAKβ^CA-induced hypertrophy in the presence or absence of KY, allowing us to assess whether KY is required for the transmission of ZAKβ-mediated growth signals at the Z-disc.

9.3 Expression of Constitutively Active ZAKβ Induces Hypertrophy Independent of KY Status

Expression of constitutively active ZAKβ^CA in TA muscle resulted in a significant increase in muscle fibre CSA in both wild-type and KY-deficient mice, compared to tdTomato controls (Figure 9.1). This hypertrophic effect was consistently observed across multiple regions of the muscle. Quantitative analysis confirmed a statistically significant increase in CSA ($p < 0.05$) in both genotypes, with no notable difference in hypertrophy magnitude between them, see (Figure 9.2) and (Figure 9.3).

These findings contrast with previous reports using earlier construct designs, where hypertrophy was observed only in wild-type muscle, implying that KY was required for ZAKβ-mediated growth. In contrast, the current results show that ZAKβ^CA induces hypertrophy even in KY-deficient muscle, demonstrating that ZAKβ's growth effect does not depend on KY. These data establish that ZAKβ activation is sufficient to drive muscle hypertrophy independently of KY status.

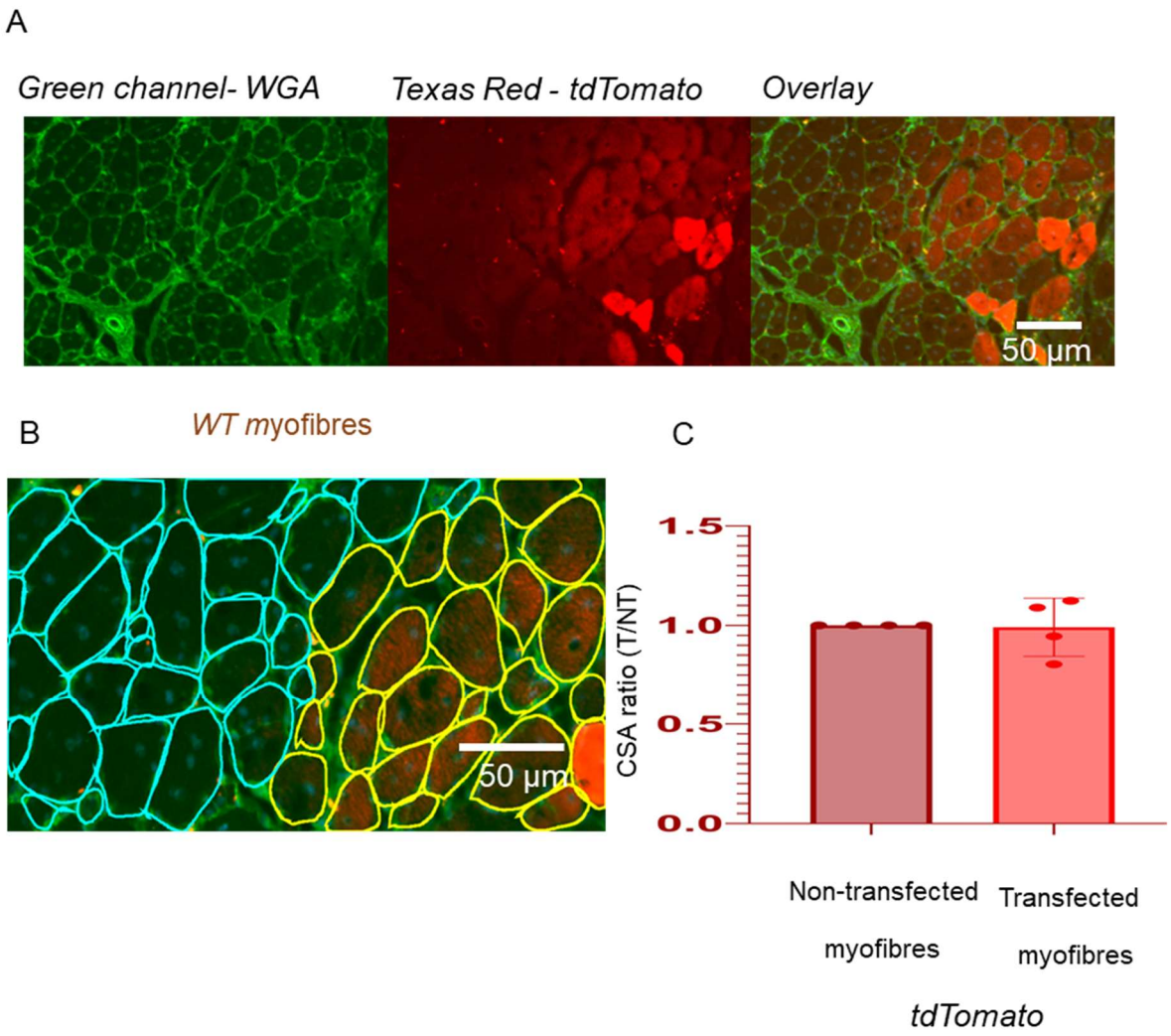

Figure 9.1 TdTomato electroporation does not alter TA muscle fibre size.

A) Representative fluorescence images of TA muscle sections electroporated with the TdTomato-only control construct. Panels (left to right) show WGA membrane staining (green), TdTomato signal identifying transfected fibres (Texas Red), and the merged image with DAPI. Scale bar: 50 µm. B) Quantitative analysis of fibre CSA from transfected and adjacent non-transfected fibres. C) CSA ratio comparison demonstrates no significant difference between TdTomato-positive and neighbouring non-transfected fibres, indicating that TdTomato expression alone does not influence muscle fibre morphology (p = 0.9845). Data represent mean ± SEM from n = 4 mice, with >150 fibres analysed per condition.

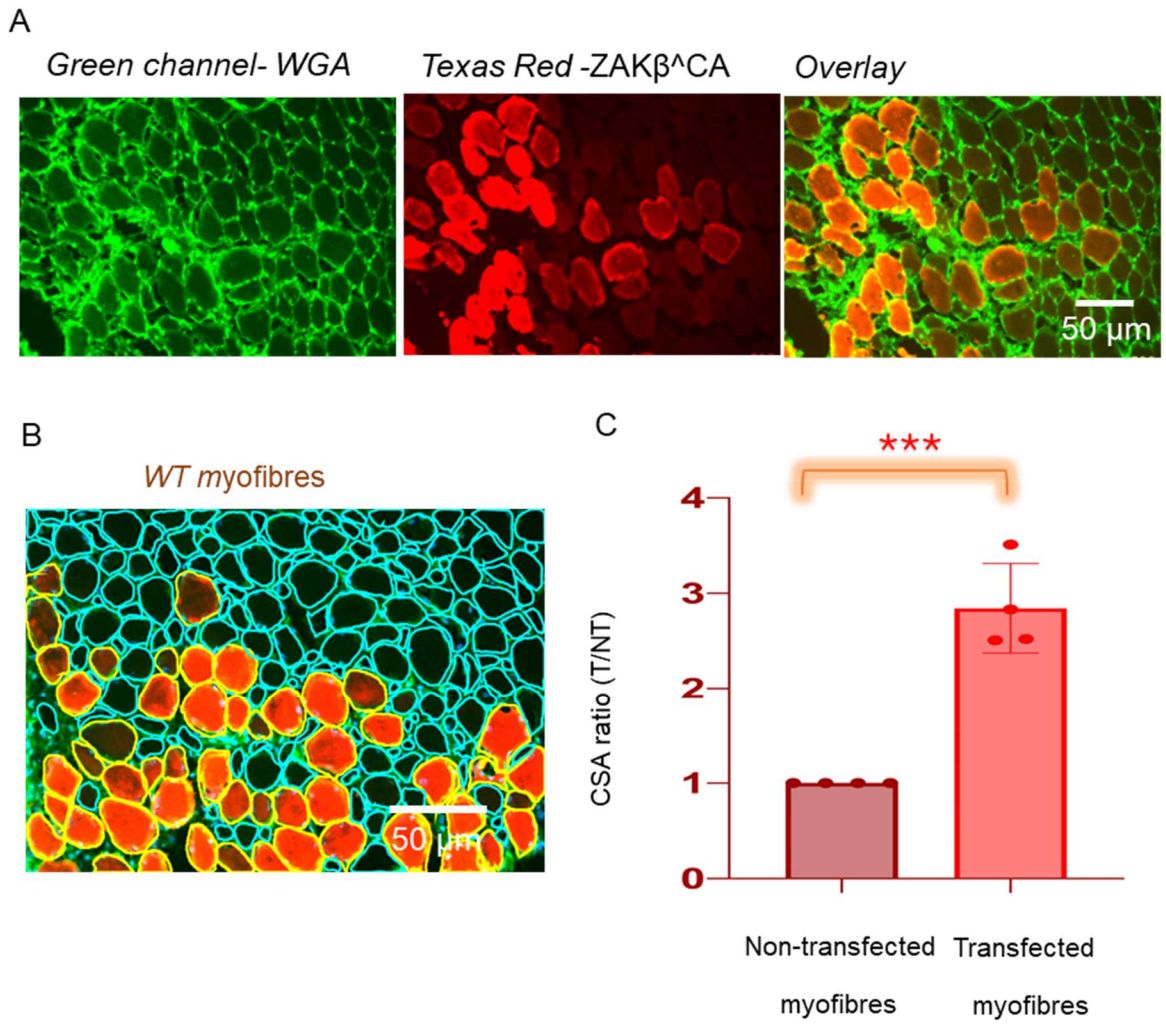

Figure 9.2 ZAKβ^CA expression induces muscle hypertrophy in wild-type mice.

A) Representative immunofluorescence images of transverse TA muscle sections electroporated with ZAKβ^CA–tdTomato. WGA staining (green) outlines muscle fibre membranes, while tdTomato (red) identifies ZAKβ^CA-expressing fibres. The merged image shows the distribution of the construct within the muscle. Scale bar: 50 µm. B) Quantitative analysis of fibre CSA from transfected and adjacent non-transfected fibres. C) CSA ratio analysis demonstrates a significant increase in muscle fibre size in ZAKβ^CA-expressing fibres compared with neighbouring non-transfected fibres (*p < 0.05, unpaired two-tailed t-test). Data represent mean ± SEM from n = 4 mice, with >150 fibres analysed per condition. These findings indicate that constitutively active ZAKβ promotes hypertrophy in wild-type muscle.

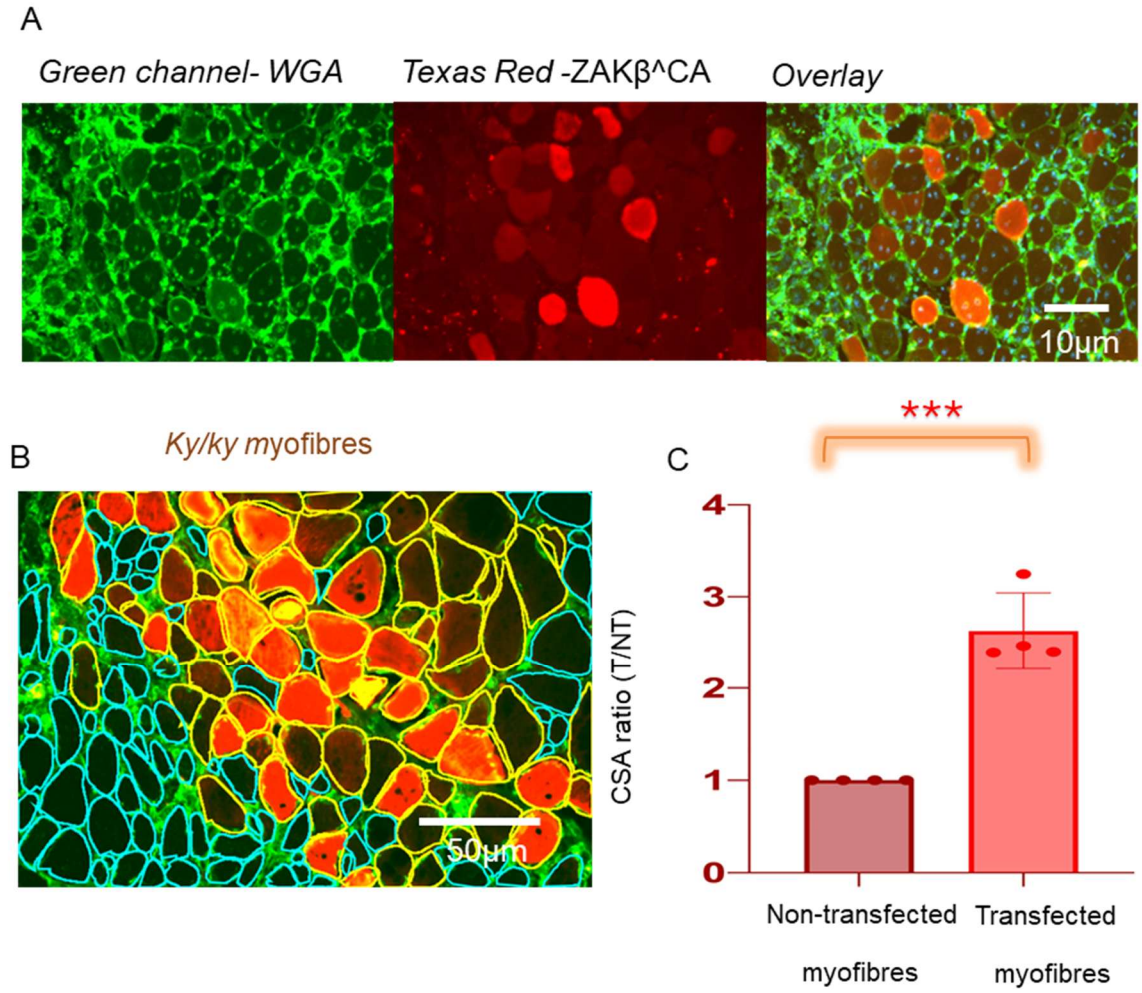

Figure 9.3 ZAKβ^CA expression induces muscle hypertrophy in ky/ky mice.

A) Representative immunofluorescence images of transverse TA muscle sections from ky/ky mice electroporated with ZAKβ^CA–tdTomato. WGA staining (green) outlines muscle fibre membranes, while tdTomato (red) identifies ZAKβ^CA-expressing fibres. The merged panel shows the distribution of the construct within the muscle. Scale bar: 50 µm. B) Quantitative analysis of fibre CSA from transfected and adjacent non-transfected fibres. C) CSA ratio analysis demonstrates a significant increase in muscle fibre size in ZAKβ^CA-expressing fibres compared with neighbouring non-transfected fibres (*p < 0.05, unpaired two-tailed t-test). Data represent mean ± SEM from n = 4 mice, with >150 fibres analysed per condition. These findings indicate that ZAKβ activation can drive muscle hypertrophy even in the absence of functional KY.

9.4 ZAKβ-Induced Hypertrophy Requires Kinase Activity and Is Independent of KY Status

Expression of ZAKβ^CA in the TA muscle led to a significant hypertrophic response in both wild-type and KY-deficient mice, with increased CSA observed consistently across muscle regions compared to tdTomato controls. In contrast, muscles

expressing the ZAKβ^KD exhibited no CSA increase and remained indistinguishable from tdTomato controls, despite confirmed expression of the construct.

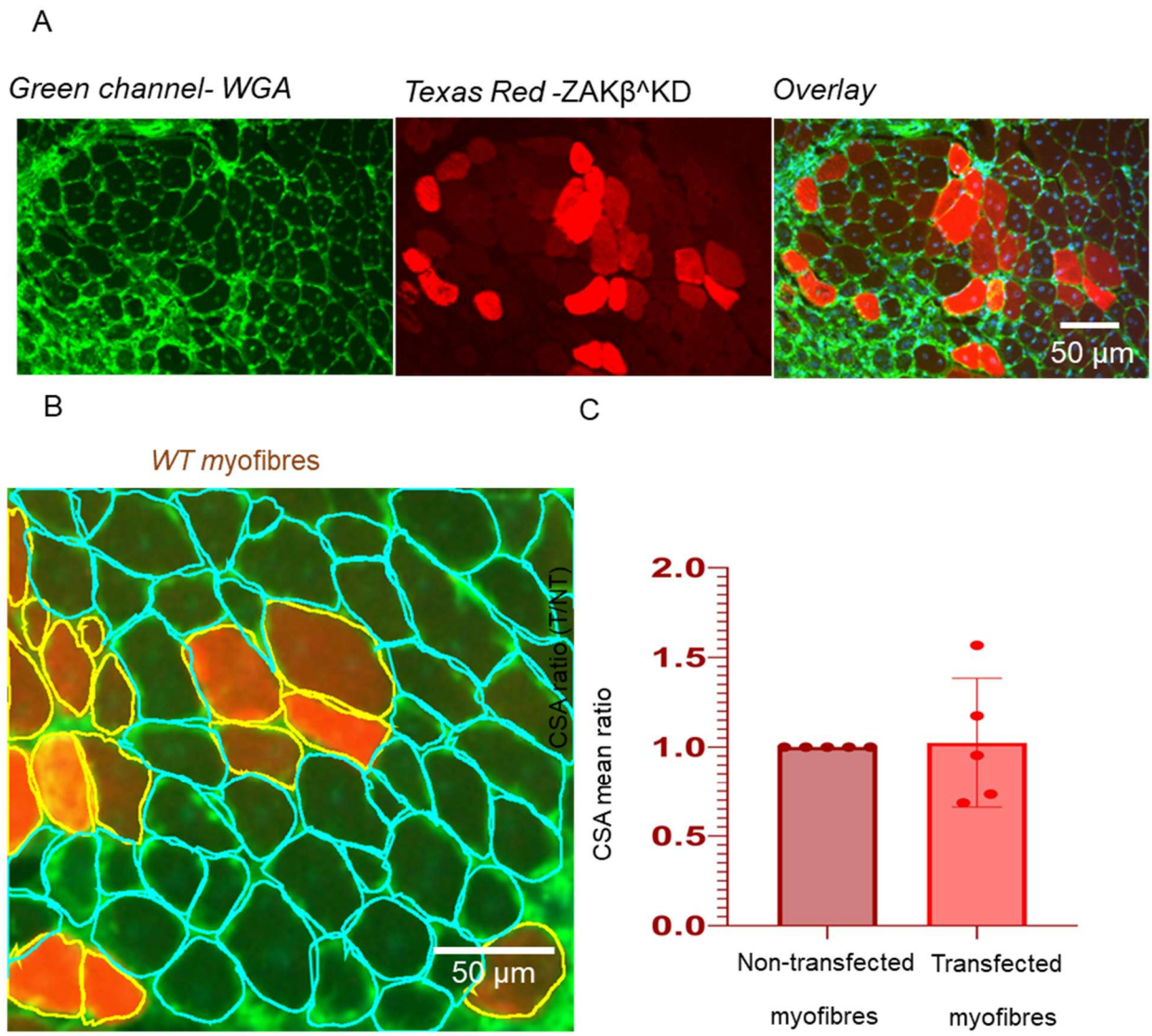

Quantitative analysis confirmed a significant CSA increase ($p < 0.05$) in ZAKβ^CA-

Figure 9.4 . Expression of ZAKβ^KD does not induce muscle hypertrophy in wild-type mice.

A) Representative immunofluorescence images of transverse TA muscle sections from wild-type mice electroporated with ZAKβ^KD–tdTomato. WGA staining (green) outlines muscle fibre membranes, while tdTomato (red) identifies ZAKβ^KD-expressing fibres. The merged panel shows the distribution of the construct within the muscle. Scale bar: 50 µm.B) Quantitative analysis of fibre CSA from transfected and adjacent non-transfected fibres.C) CSA ratio analysis shows no significant difference between ZAKβ^KD-expressing and non-expressing fibres (p = 0.7421, unpaired two-tailed t-test), indicating that inhibition of ZAKβ signalling does not induce hypertrophy in a wild-type background. Data represent mean ± SEM from n = 4 mice, with >150 fibres analysed per condition.

treated muscles in both genotypes, with no significant difference in hypertrophy magnitude between wild-type and KY-deficient mice. By comparison, ZAKβ^KD showed no significant effect in either genotype (Figure 9.4) (Figure 9.5).

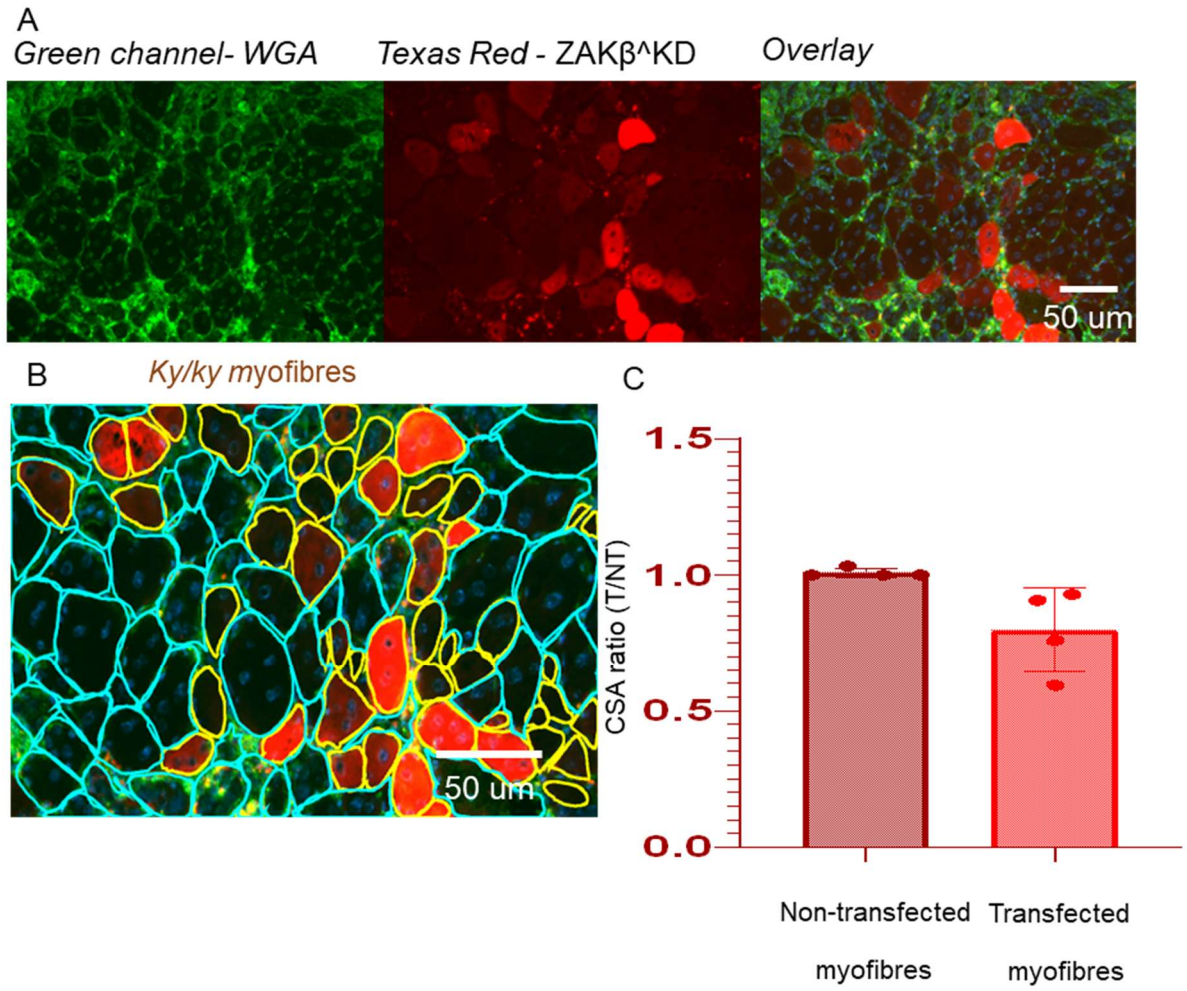

Figure 9.5 ZAKβ^KD expression does not induce muscle hypertrophy in ky/ky mice.

A) Representative immunofluorescence images of transverse skeletal muscle sections from ky/ky mice electroporated with ZAKβ^KD–tdTomato. WGA staining (green) outlines the basal lamina of individual fibres, while tdTomato (red) marks ZAKβ^KD-expressing fibres. The merged image confirms successful expression within the tissue. Scale bar: 50 µm. B) Quantitative analysis of fibre CSA. C) CSA ratio analysis shows no significant difference between ZAKβ^KD-expressing fibres and adjacent non-transfected fibres (p = 0.3124, unpaired two-tailed t-test). Transfected fibres displayed a slightly smaller mean CSA, indicating that ky/ky muscles do not exhibit increased sensitivity to ZAKβ inhibition. Data represent mean ± SEM from n = 4 mice, with >150 fibres analysed per condition.

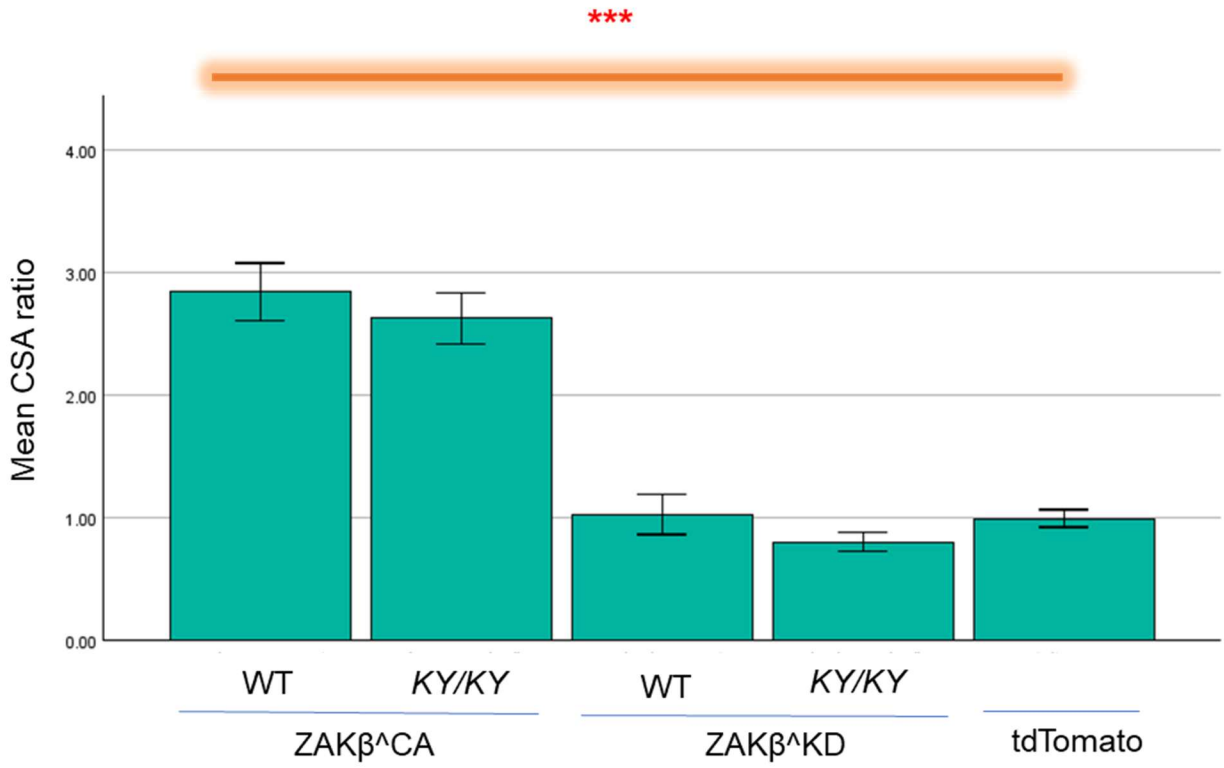

Figure 9.6 Figure 9.3. Constitutively active ZAKβ promotes muscle hypertrophy independently of KY

.
Quantification of fibre cross-sectional area (CSA) ratios in wild-type (WT) and KY-deficient (ky/ky) tibialis anterior muscles expressing ZAKβ^CA (constitutively active), ZAKβ^KD (kinase-dead), or tdTomato control. ZAKβ^CA significantly increased fibre size in both WT and ky/ky muscles, whereas ZAKβ^KD and control constructs had no effect, confirming that ZAKβ promotes hypertrophy in a kinase-dependent manner. Data represent mean ± SEM from n = 4 biological replicates per condition. Statistical significance determined by one-way ANOVA with Tukey's post hoc test; P < 0.01.

These findings demonstrate that ZAKβ promotes muscle hypertrophy in a kinase-dependent manner, and that its pro-growth effect is independent of KY. The absence of hypertrophic response with ZAKβ^KD underscores the requirement for enzymatic activity, while the preserved responsiveness in KY-deficient muscle suggests that downstream ZAKβ signalling remains intact in the absence of KY.

9.5 Discussion

These findings identify ZAKβ as a kinase-dependent regulator of muscle hypertrophy. Expression of constitutively active ZAKβ in the tibialis anterior muscle led to a

significant increase in muscle fibre CSA in both wild-type and KY-deficient mice. This demonstrates that ZAKβ^CA can trigger hypertrophic responses independently of KY, suggesting that ZAKβ signalling does not rely solely on KY as a co-factor or scaffold. Instead, ZAKβ may act through alternative or parallel downstream effectors that remain active in the absence of KY.

This observation contrasts with earlier findings suggesting that KY was necessary for hypertrophy induction and raises the possibility that the ZAKβ^CA construct used here exhibits enhanced kinase activity, improved expression, or altered subcellular localisation *in vivo*. Notably, this result challenges previous models based on FLNC and BAG3 studies, which proposed that KY might be essential for anchoring or organising Z-disc–associated stress sensors such as ZAKβ (Arndt et al., 2010; Ulbricht et al., 2013; Tedesco et al., 2023). While such anchoring may remain important under physiological strain, the data suggest that forced activation of ZAKβ^CA can bypass this dependency, potentially by altering its localisation or interaction dynamics (Egerman & Glass, 2014).

Further supporting this interpretation, Stonadge (2023) reported that overexpression of ZAKβ in C2C12 cells promotes nuclear accumulation of p38 and ERK1/2, consistent with its upstream role in stress-activated MAPK pathways (A. Stonadge et al., 2023). The present findings extend this model by demonstrating that constitutively active ZAKβ can drive functional hypertrophic remodelling *in vivo*, even in the absence of KY. One plausible conclusion is that KY and ZAKβ act in partially independent but converging pathways that share common downstream effectors such as MAPKs or mTOR complexes, rather than forming a strict linear cascade (Egerman & Glass, 2014).

This revised framework also encourages reconsideration of earlier hypotheses suggesting a direct signalling relationship between KY and ZAKβ mediated by the shared interactor IGFN1. IGFN1 has been reported to bind both proteins and was thought to facilitate KY-dependent recruitment of ZAKβ to the Z-disc under mechanical strain. However, the finding that ZAKβ^CA induces hypertrophy in KY-deficient muscle suggests that such interactions are not obligatory for ZAKβ's function under these experimental conditions. Instead, IGFN1 may act as a modular adaptor whose association with ZAKβ is dynamically regulated, rather than constant. This interpretation aligns with broader models of Z-disc–associated stress-sensing complexes that undergo compositional changes to modulate signalling during adaptation or repair (Baker et al., 2010; Egerman & Glass, 2014; A. Stonadge et al., 2023).

The absence of hypertrophy following expression of kinase-dead ZAKβ (ZAKβ^KD) in both wild-type and KY-deficient muscle reinforces the requirement for ZAKβ's catalytic activity in promoting anabolic remodelling. This finding supports a kinase-dependent mechanism and excludes artefacts such as plasmid delivery effects or inflammatory responses. These results are consistent with *in vitro* studies showing that ZAKβ

activation leads to phosphorylation of p38 and JNK in mechanically stimulated skeletal muscle cells (Nordgaard et al., 2022)) and with observations that ZAKβ depletion compromises muscle maintenance and regeneration under mechanical load (A. J. Stonadge, 2023).

Importantly, the current results expand on previous work by showing that constitutively active ZAKβ can promote hypertrophy even in the absence of external mechanical cues. This suggests that once activated, ZAKβ can autonomously engage anabolic pathways in mature muscle fibres. The persistence of this effect in KY-deficient tissue further indicates that KY is not strictly required for ZAKβ-driven hypertrophic signalling under these conditions. Given KY's established role in proteostasis and its localisation to stress-sensitive regions of the sarcomere (Jokl et al., 2018), it is plausible that KY and ZAKβ contribute to remodelling through complementary but distinct mechanisms: KY primarily supporting sarcomeric stability and protein quality control, and ZAKβ serving as a signal transducer linking stress perception to growth regulation (Kramer & Goodyear, 2007; Martineau & Gardiner, 2001).

Several limitations should be acknowledged. While CSA is a widely accepted marker of muscle hypertrophy, incorporating additional measurements, such as myonuclear number, fibre-type composition, and protein synthesis rates would yield a more comprehensive picture of the underlying remodelling process. These complementary assessments could distinguish between true anabolic growth and other adaptations such as fibre-type switching or cytoskeletal reorganisation. Moreover, phosphorylation analyses of recognised ZAKβ targets including p38, ERK1/2, and JNK would help verify MAPK pathway activation and delineate the molecular mechanisms underlying ZAKβ^CA function *in vivo* (Kramer & Goodyear, 2007; Martineau & Gardiner, 2001).

Future investigations should examine whether ZAKβ and KY physically interact or co-localise at the Z-disc under mechanical loading, and whether this relationship changes in muscle disease or ageing. It will also be important to determine whether KY influences the spatial activation, substrate specificity, or temporal regulation of ZAKβ signalling. Such studies could clarify whether KY acts as a regulatory checkpoint, adaptor, or permissive scaffold within the sarcomeric stress-response network. Overall, this chapter identifies ZAKβ as a potent kinase-dependent driver of muscle hypertrophy that can function independently of KY when constitutively active. Collectively, these findings refine earlier assumptions of a linear KY–ZAKβ–MAPK cascade and instead support a modular, context-dependent framework in which mechanical, proteostatic, and anabolic pathways are integrated through multiple, partially compensatory mechanisms. A deeper understanding of the ZAKβ–KY axis will be crucial for elucidating how skeletal muscle adapts during growth, regeneration, and disease.

CHAPTER TEN-Discussion and Future Direction

CHAPTER 10. General Discussion and Future Direction

10.1 General Discussion

10.1.1 Overview

This thesis examined the multifaceted role of the KY protein in skeletal muscle, focusing on its structural, regulatory, and stress-responsive functions. A combination of cell-based imaging, biochemical assays, *in vivo* electroporation, computational modelling, and proteomic analyses was employed to investigate how KY contributes to muscle maintenance and proteostasis. The findings collectively suggest that KY functions as more than a passive Z-disc component, acting instead as a context-dependent modulator of stress adaptation and cellular quality-control pathways.

Key insights gained from this work include:

• Heat stress reveals distinct, species-specific differences in KY localisation and stability.

• Catalytically inactive KY variants can restore fibre size in ky/ky muscle, whereas deletion of the TGN/PROT domain abolishes this rescue effect.

• Z-disc localisation is governed by specific structural determinants within KY.

• Computational models predict a conserved transglutaminase-like fold that may have scaffolding rather than enzymatic significance.

• Proteomic profiling identifies potential KY-interacting proteins, notably the phosphatase PPM1B and several HSP70 family chaperones.

• Autophagy assays in KY-deficient models show reduced LC3-II formation and delayed cargo degradation, indicating compromised autophagic flux.

• Constitutively active ZAKβ promotes hypertrophy in a KY-independent, kinase-dependent manner.

Together, these results refine the understanding of KY as a stress-responsive regulator within skeletal muscle and highlight its possible role at the intersection of sarcomeric structure, proteostasis, and adaptive signalling. This framework provides a foundation for future studies examining how KY dysregulation contributes to muscle degeneration and myofibrillar myopathies (Blanco et al., 2001; Arndt et al., 2010; Jokl et al., 2018).

10.1.2 KY and Proteostasis: Insights into Structure and Function

The findings presented in this thesis suggest that KY contributes to the regulation of proteostasis in skeletal muscle, extending its functional identity beyond that of a structural Z-disc component. Multiple lines of evidence support this expanded role, particularly KY's association with molecular chaperones, phosphatases, and autophagy-related markers.

The identification of HSPA8 as a KY-associated protein provides a key link between KY and selective protein quality control mechanisms. HSPA8 serves as the core chaperone in CMA, a selective lysosomal pathway that recognises and transports cytosolic proteins containing KFERQ-like motifs to the lysosome for degradation (Kaushik & Cuervo, 2018). Its co-isolation with KY suggests that KY may contribute to the spatial organisation or recruitment of CMA machinery within muscle fibres, particularly under conditions of proteotoxic or mechanical stress. This interpretation is consistent with findings from Chapter 8, where KY-deficient myoblast and muscle tissue exhibited accumulation of RFP-LC3ΔG, indicating impaired autophagic degradation and disrupted proteostatic balance.

The enrichment of HSPA9, a mitochondrial HSP70 chaperone, further broadens KY's potential role. HSPA9 supports mitochondrial protein import and helps preserve mitochondrial integrity during cellular stress (Wadhwa et al., 2002). Its association with KY raises the possibility that KY participates in cross-organelle coordination of proteostasis, integrating mitochondrial and cytoskeletal quality-control responses. Such cross-compartmental coordination is increasingly recognised as essential for muscle maintenance, where mechanical strain, metabolic demand, and protein turnover are tightly coupled (Cohen et al., 2012; Sandri, 2013). These findings point to KY as a possible scaffold or regulatory adaptor that links chaperone networks and autophagic pathways at the Z-disc, thereby supporting cellular homeostasis during stress and muscle remodelling.

Importantly, the predicted structural models described in the *In Silico Analysis* chapter provide valuable insight into how KY may function. Although KY's central region is predicted to adopt a three-dimensional fold resembling that of TG2, closer examination suggests several crucial differences. Specifically, the three amino acids that normally form the catalytic triad in active transglutaminases (histidine, cysteine, and aspartate) are predicted to be spatially misaligned, likely preventing the formation of a functional catalytic centre. In addition, the putative substrate-binding pocket is modelled as partially occluded, suggesting that KY may not accommodate or process substrates in the same way as enzymatically active TG family members (Griffin et al., 2002; Iismaa et al., 2009).

These structural predictions are consistent with the experimental findings from the *Muscle Rescue* chapter, in which KY variants containing mutations in the catalytic triad or a complete deletion of the TGN/PROT domain were still able to restore muscle fibre size in *ky/ky* mice. Together, these data indicate that KY's physiological function does not require enzymatic catalysis. Instead, KY is proposed to act as a structural or regulatory scaffold, facilitating protein–protein interactions that support muscle fibre integrity and proteostasis. In this context, the TGN/PROT domain may serve as a non-catalytic interaction module, comparable to pseudoenzymatic domains described in other signalling and structural proteins (Murphy et al., 2014, 2017; Ribeiro et al., 2019).

These findings support a model in which KY functions as an atypical scaffold protein at the Z-disc, bridging mechanotransduction and proteostasis by assembling or stabilising chaperone–phosphatase complexes. This is conceptually similar to BAG3, a Z-disc protein that anchors CASA complexes via interactions with FLNC and HSP70s (Arndt et al., 2010; Ulbricht et al., 2013). KY appears to mediate its interactions via structurally conserved but enzymatically silent domains, possibly enabling more versatile complex assembly.

Further supported by the data presented in the autophagy focused chapter, where KY-deficient cells showed an abnormal buildup of non-lipidated LC3-I and a reduced conversion to the lipidated LC3-II form under both normal and starvation conditions. This pattern suggests a blockage in autophagosome formation or progression. Moreover, when cells were treated with Bafilomycin A1, a drug that blocks autophagosome–lysosome fusion the expected accumulation of LC3-II was markedly reduced in KY-deficient cells. This points to a breakdown in the later stages of autophagy, possibly at the point of autophagosome maturation or lysosomal fusion. Such disruptions are not unique to KY deficiency and have been reported in other models where key components of the proteostasis network are impaired. For example, blocking chaperone-mediated autophagy, as in LAMP2 or HSC70-deficient models, leads to similar defects in LC3 processing and turnover (Massey et al., 2006). This parallel supports the idea that KY may play a coordinating role in maintaining proper communication between chaperones and the lysosomal machinery during autophagy.

Overall, the combined evidence from proteomic analyses, structural modelling, and functional experiments strongly supports the idea that KY plays a central role in maintaining muscle health not by acting as an enzyme, but by serving as a scaffold that helps organise protein quality control machinery. By anchoring key components of the autophagy and proteostasis networks at the Z-disc and near organelles, KY ensures efficient degradation of damaged or misfolded proteins, especially under stress. When KY is absent, as seen in KY-deficient muscle, this system breaks down, leading to impaired autophagic flux and a buildup of cellular damage. These disruptions likely contribute to the progressive muscle degeneration seen in *ky/ky* models, a pattern previously reported by Jokl et al. (2018) and resonated in autophagy experiments.

10.1.3 Rethinking KY's Role in Muscle Growth and Fibre Size Regulation

The role of KY in regulating muscle fibre size was explored through *in vivo* rescue experiments in KY-deficient mice. Electroporation of full-length human KY-GFP into the tibialis anterior muscle significantly increased muscle fibre CSA, restoring size relative to adjacent non-transfected fibres. This finding highlights a functional requirement for KY in maintaining muscle mass under basal physiological conditions.

To assess the contribution of specific regions to KY's function, two variants were tested in parallel: one containing a triple mutation in the predicted catalytic triad, and another lacking the entire TGN/PROT domain. Both constructs correctly localised to the Z-disc, indicating that spatial targeting alone is insufficient for functional rescue. Notably, KY-TM was still able to restore fibre size, whereas KY-ΔTGN failed to do so. These results suggest that enzymatic activity is not required for KY's growth supporting role. Instead, the structural integrity of the TGN/PROT domain is essential, likely due to its involvement in protein–protein interactions or mechanical signal transduction.

Structural modelling further supports this conclusion. Predictions show that KY adopts a fold similar to TG2, retaining a conserved catalytic triad and surface features associated with substrate interaction. However, the triad residues in KY are not geometrically aligned for catalysis, and the putative substrate-binding cleft appears occluded. These features, together with the *in vivo* results, argue that KY's function does not rely on enzymatic activity. Rather, the TGN/PROT domain likely serves as a structural scaffold or interaction hub.

The observation that modest alterations in the central domain as in KY-TM do not abolish rescue, while complete domain deletion KY-ΔTGN does, highlights the importance of domain presence rather than catalytic configuration. This supports the idea that KY's ability to promote fibre growth depends on structural properties that enable it to engage with regulatory or structural partners at the Z-disc.

These findings refine earlier models of KY function. While previous studies established KY as essential for preserving sarcomeric integrity (Jokl et al., 2018), the data extend its role to fibre size regulation even in the absence of overt structural collapse. The restoration of fibre CSA by wild-type KY suggests that KY contributes to anabolic or maintenance pathways at the Z-disc. This function may involve cooperation with mechanosensitive or chaperone complexes such as FLNC and BAG3, both of which are critical for sarcomeric adaptation under mechanical strain (Arndt et al., 2010; Ulbricht et al., 2013).

Unlike classical hypertrophy regulators such as the IGF1–Akt–mTOR pathway, KY's contribution appears more tightly linked to cytoskeletal organisation and proteostasis. It likely supports muscle fibre integrity through domain-mediated recruitment of effectors, rather than through activation of transcriptional or translational programmes.

Importantly, the Z-disc localisation of all tested KY variants wild-type, KY-TM, and KYΔTGN rules out mislocalisation as a confounding variable in their differential rescue outcomes. The inability of KY^ΔTGN to restore fibre size underscores the functional importance of the TGN/PROT domain. This supports an emerging model in Z-disc biology: that precise domain architecture, not just localisation, dictates functional specificity. Comparable roles have been reported for other Z-disc proteins, such as FLNC, BAG3, Desmin, and ZASP, where domain mutations disrupt critical interactions and lead to impaired sarcomeric stability or stress adaptation (Bär et al., 2005; Konersman et al., 2015; Ramaswami et al., 2013).

These findings suggest that KY's TGN/PROT domain serves as a key interface for engaging proteostatic or mechanosensory partners. It plays an vital role in maintaining muscle fibre size under physiological demand, even in the absence of catalytic activity.

10.1.4 Structural Modelling of KY: Interpreting Domain Function Through in Silico and Mutational Insights

To investigate the structural basis of KY's function, we employed in silico predictions alongside domain-targeted mutagenesis and *in vivo* rescue assays. AlphaFold2 modelling revealed that the central TGN/PROT domain adopts a transglutaminase-like fold, including a conserved catalytic triad (His-Cys-Asp) and surface features consistent with substrate interaction, such as polar grooves and electrostatic patches. Despite these enzymatic hallmarks, KY has not demonstrated transamidation activity, suggesting a possible divergence between structural conservation and functional output.

This hypothesis was tested through site-directed mutagenesis. A catalytically inactivated KY variant, carrying alanine substitutions in the triad residues, retained full ability to restore muscle fibre size in *ky/ky* mice. In contrast, a deletion mutant lacking the entire TGN/PROT domain failed to rescue fibre size, despite proper Z-disc localisation. These results indicate that enzymatic activity is nonessential for KY's physiological role, whereas the presence of the domain itself is essential, supporting a non-catalytic function, likely related to structural scaffolding or protein–protein interaction.

Further structural comparisons with TG2 highlighted key deviations in the geometry of KY's catalytic core. Specifically, misalignment of the triad residues and partial occlusion of the substrate-binding cleft argue against enzymatic functionality. These distinctions point to an evolutionary adaptation in which KY's TGN/PROT domain has been repurposed to serve as an interaction platform, potentially facilitating spatial coordination of proteostatic or mechanical effectors at the Z-disc.

This structural interpretation is consistent with proteomic analyses identifying KY interactors such as HSPA8 and PPM1B, both of which are involved in autophagy and stress signalling pathways. It also aligns with broader trends in Z-disc biology, where non-enzymatic proteins such as myopalladin and ZASP orchestrate sarcomeric architecture and mechanosensing via modular binding domains (Faulkner et al., 1999).

A broader implication of this work is that we may need to rethink how we define functional proteins within the transglutaminase family. Although proteins like TG2 are typically known for their enzymatic activity, KY appears to belong to a growing group of pseudoenzymes, proteins that still look like enzymes in structure but no longer carry out chemical reactions. Instead, these proteins often take on other important cellular roles, such as acting as scaffolds that help organise molecular complexes. This

concept is similar to what has been observed in catalytically inactive kinases or E3 ligase-like adaptors, which are now known to regulate signalling pathways not by modifying other proteins, but by physically bringing them together (Kung & Jura, 2019; Murphy et al., 2017).

In this light, KY's TGN/PROT domain, although structurally similar to active enzymes, may serve a different purpose. Given that TGN domains are often involved in organising the cytoskeleton and responding to cellular stress (Eckert et al., 2015; Lorand & Graham, 2003), KY may play a similar role at the sarcomere, acting as a non-enzymatic regulator that helps maintain muscle structure and respond to stress.

10.1.5 KY as a Stress Sensor: Heat Shock Responses and Degradation Pathways

A key emerging theme from this thesis is KY's potential role as a stress-responsive regulator, particularly under proteotoxic conditions. The data presented here demonstrate that acute heat stress modulates both KY protein abundance and subcellular localisation in undifferentiated C2C12 myoblasts. Notably, the human KY-GFP construct exhibited pronounced cytoplasmic redistribution and formation of aggregation-like foci, in contrast to the more stable localisation pattern of mouse KY-td. These species-specific differences may reflect underlying sequence or structural variations, such as the extended N-terminal nuclear localisation signal present in human KY, which could influence its trafficking or sensitivity to thermal stress (Kaushik & Cuervo, 2018).

Upon heat shock, human KY accumulated alongside markers of proteostasis disruption, including elevated LC3-II levels and partial colocalization with autophagy receptors. Blocking autophagy with Bafilomycin A1 or inhibiting the proteasome with MG132 further intensified KY aggregation, suggesting that KY is normally cleared via both the autophagy and proteasome pathways. These observations align with broader models of Z-disc protein turnover, where components like filamin C and α-actinin are degraded through chaperone-assisted selective autophagy (Arndt et al., 2010; Ulbricht et al., 2013). KY's responsiveness to both thermal and pharmacological stress supports its integration into a stress-sensing proteostasis network at the Z-disc.

Importantly, the stress-induced KY foci did not colocalise with classical aggresomal or ER stress markers (Johnston et al., 1998), suggesting that KY is handled by a distinct degradation mechanism, likely linked to sarcomeric quality control. This is further supported by KY's partial colocalization with LC3 and altered degradation kinetics in autophagy-deficient contexts. These findings suggest that KY may act not merely as a substrate but potentially as an upstream coordinator of proteostasis responses during cytoskeletal damage.

This proposed role echoes the function of CASA pathway proteins such as BAG3, which mediate the clearance of damaged Z-disc proteins under mechanical or

oxidative stress. Consistent with this, Chapter 7 identified KY interactions with several key heat shock proteins (HSPA8, HSPA5, and HSPA9) all central regulators of cellular proteostasis. Their association with KY suggests that KY may serve as a scaffold and sensor, helping to translate mechanical strain into targeted degradation responses.

While early studies primarily described KY as a structural Z-disc component (Blanco et al., 2001), the results expand this understanding. We now propose that KY also functions as a sensor and modulator of muscle proteostasis (Doyle et al., 2013; Kampinga & Bergink, 2016), especially under conditions of heightened protein turnover such as development, regeneration, or stress. This is in line with transcriptomic data from Jokl et al. (2018), which revealed upregulation of autophagy-related and stress-responsive genes in KY-deficient muscle. The data provide a mechanistic explanation: KY's stress-dependent localisation, accumulation, and degradation are integral to maintaining protein quality control in muscle.

Nevertheless, several questions remain. It is unclear whether KY actively recruits autophagic components or is passively degraded when damaged. Moreover, the molecular signals that govern KY aggregation or turnover, such as ubiquitination, phosphorylation, or chaperone binding, remain to be defined. These could be investigated in future studies using KY variants lacking specific post-translational modification sites, or proximity-based labelling techniques to map stress-induced interactomes.

10.1.6 KY and Autophagy: Coordinating Quality Control Under Stress

Autophagy is a central process for maintaining cellular homeostasis in skeletal muscle, particularly during mechanical strain and proteotoxic stress. To investigate KY’s involvement in this pathway, we assessed autophagic flux in KY-deficient undifferentiated C2C12 cells and tibialis anterior muscle using dual fluorescent reporters (GFP-LC3 and RFP-LC3ΔG) alongside LC3 isoform analysis by Western blotting. These complementary approaches consistently revealed impaired autophagy in KY-deficient contexts, including elevated RFP-LC3ΔG signal and increased recombinant altered LC3-I/LC3-II ratios, hallmarks of defective autophagosome maturation and turnover.

Importantly, these disruptions were evident under basal, starvation-induced, and Bafilomycin A1-treated conditions, indicating that KY modulates both constitutive and stress-induced autophagic pathways. While autophagy could still be triggered in KY-deficient cells, the attenuated response relative to wild-type suggests a modulatory, rather than crucial role. This phenotype repeats defects seen in models lacking key Z-disc autophagy regulators such as BAG3 and FLNC, both central to the chaperone-assisted selective autophagy pathway (Arndt et al., 2010; Ulbricht et al., 2013). In this context, KY may play a parallel role facilitating the spatial coordination or efficiency of autophagic machinery at mechanically sensitive sites.

Supporting this interpretation, the proteomic data identified several KY-interacting proteins linked to proteostasis, including HSPA8, a core chaperone in chaperone-mediated autophagy, and PPM1B, a phosphatase that negatively regulates the autophagy-initiating kinase ULK1(Torii et al., 2016). These associations suggest that KY may serve as a scaffold that spatially recruits or regulates autophagy effectors, thereby modulating thresholds for autophagosome initiation or cargo degradation efficiency.

The findings are consistent with prior transcriptomic and proteomic studies in KY-deficient muscle, which reported upregulation of stress-responsive genes, chaperones, and components of the ubiquitin–proteasome system (Jokl et al., 2018). However, the work adds mechanistic resolution by demonstrating that KY loss directly impairs LC3 lipidation and autophagosome progression, offering a molecular basis for the broader stress phenotypes observed.

A particular strength of this analysis lies in the triangulation of multiple orthogonal assays, fluorescent imaging, biochemical markers, and stress models, enabling us to probe distinct phases of autophagy. Nonetheless, limitations remain we did not evaluate lysosomal pH or protease activity and were unable to dynamically track autophagosome–lysosome fusion using tandem probes such as mCherry-GFP-LC3 (Kimura et al., 2007). Ethical constraints precluded starvation experiments *in vivo*, and variability due to strain, age, or sex may have introduced additional noise into autophagy readouts.

Interestingly, KY-deficient cells retained some autophagic capacity, implying partial redundancy or compensation. Whether KY directly binds recognised autophagy adaptors such as p62, NBR1, or LC3-interacting region LIR motifs remains unresolved. It is also unclear whether KY influences autophagy via direct interaction with ULK1 or ATG proteins, or indirectly via upstream regulators like mTORC1 or AMPK. These hypotheses could be explored through proximity biotinylation BioID or stress-responsive co-immunoprecipitation experiments.

Consistent with these mechanistic interpretations, the autophagy reporter analyses further demonstrated that loss of KY function leads to impaired autophagic flux in both *in vitro* and *in vivo* systems. Using the GFP-LC3–RFP-LC3ΔG reporter, KY-deficient C2C12 cells and *ky/ky* muscle fibres showed elevated GFP/RFP ratios relative to wild-type controls, reflecting inefficient degradation of autophagosomal GFP-LC3 in lysosomes. The increase in RFP intensity under KY-deficient conditions suggests reporter accumulation or impaired turnover, consistent with autophagy blockade. Together, these data support the hypothesis that KY contributes to the regulation of autophagic efficiency and proteostasis maintenance in muscle cells.

The findings identify KY as a modulator of autophagic flux in skeletal muscle, likely operating at the interface between chaperone signalling and cargo degradation. KY's interaction with key proteostasis regulators, together with its relocalisation and altered degradation under stress, support its emerging role as a dynamic coordinator of quality

control pathways. These results contribute to a growing recognition that sarcomeric proteins serve not only structural functions but also regulatory roles in cellular homeostasis.

10.1.7 The KY Interactome: Linking Sarcomeric Structure to Cellular Stress Pathways

Among the most robust interactors identified was PPM1B, the central regulator of autophagy initiation (Torii et al., 2016).This interaction supports the hypothesis that KY may act as a spatial scaffold, positioning regulatory enzymes like PPM1B near the Z-disc to fine-tune autophagy thresholds in response to mechanical or proteotoxic strain. Such a function echoes the role of BAG3, a well-characterized Z-disc protein that links cytoskeletal tension to autophagic degradation by coordinating complexes of HSP70, p62, and ubiquitin ligases (Arndt et al., 2010; Ulbricht et al., 2013).

Notably, the KY interaction also included organellar stress regulators such as HSPA5 and HSPA9, suggesting that KY may participate in cross-compartmental quality control under strain. While HSPA8 was also recovered a chaperone involved in chaperone-mediated autophagy its association with KY in the proteomic dataset complements rather than duplicates findings from functional autophagy assays. These interactors suggest KY’s reach may extend beyond sarcomeric organisation to include ER and mitochondrial proteostasis, which are critical during high protein turnover phases such as differentiation, hypertrophy, or repair.

Interestingly, the composition of the KY interaction varied by context. In C2C12 cell extracts, enrichment for chaperones and autophagy regulators was more prominent, whereas in muscle tissue, PPM1B was the dominant interactor. This divergence may reflect cell state-dependent recruitment, with stress levels, developmental stage, or post-translational modifications influencing complex formation. Such dynamic rewiring is characteristic of stress-adaptive protein complexes and is consistent with broader paradigms of context-sensitive Z-disc signalling (Kedersha et al., 2013; Ramaswami et al., 2013).

Although these findings support KY's role as a scaffold, some limitations remain. The exact nature of these interactions whether direct or mediated via adaptors is not fully resolved. For instance, KY lacks known phosphatase-binding motifs, suggesting that its association with PPM1B may involve intermediate proteins. Similarly, recruitment of HSP70s typically requires cochaperones or engagement with unfolded substrates. Analogous to the CASA complex, which depends on multi-protein coordination involving BAG3, FLNC, and HSPB8, KY may act within a larger protein assembly rather than functioning independently.

Nevertheless, this proteomic evidence provides a mechanistic bridge between KY's structural localisation at the Z-disc and its involvement in cellular stress responses. Unlike earlier transcriptomic studies in *ky/ky* muscle that broadly reported changes in stress-related gene expression (Jokl et al., 2018), these experiments approach identifies specific protein-level interactions, thereby narrowing down actionable regulatory nodes most notably PPM1B and HSPA8 for future functional testing.

10.1.8 ZAKβ, KY, and Context-Dependent Pathways in Muscle Growth

The final chapter of this thesis explored the relationship between ZAKβ and KY in the context of muscle fibre growth, revealing that ZAKβ is a potent inducer of hypertrophy when constitutively activated. The finding that ZAKβ^CA increased muscle fibre CSA in both wild-type and KY-deficient muscle indicates that ZAKβ operates independently of KY when its kinase domain is forcibly activated. This challenges earlier assumptions of a linear KY–ZAKβ–MAPK cascade and compels a revaluation of the hierarchical relationship between these proteins.

The kinase-dependence of ZAKβ's hypertrophic activity was confirmed by the lack of effect observed with the kinase-dead construct ZAKβ^KD, ruling out nonspecific overexpression effects. This observation is consistent with prior findings that ZAKβ activates p38 and JNK signalling upon mechanical stimulation (Huang et al., 2009; Mathea et al., 2016). Notably, Stonadge (2023) reported that ZAKβ knockdown impairs muscle regeneration and structural integrity under mechanical load, placing ZAKβ as a critical upstream regulator in mechanosensitive signalling.

However, the study expands upon these findings by demonstrating that ZAKβ^CA can bypass physiological stimuli and induce hypertrophy *in vivo* even in the absence of KY. This suggests that KY is not required as a co-factor for ZAKβ activation, at least under constitutive expression conditions. Importantly, this does not negate KY's functional role but rather positions it as a context-dependent modulator rather than a necessary scaffold. For instance, KY may influence the localisation, temporal activation, or substrate specificity of ZAKβ under mechanical stress—roles not captured by constitutive activation constructs.

This distinction is significant in light of prior work on FLNC and BAG3, which suggested that Z-disc proteins anchor or organise upstream kinases during mechanical challenge (Arndt et al., 2010). The data suggest that while such anchoring may occur under native conditions, the overexpression of ZAKβ^CA may saturate or bypass normal localisation requirements. This concept is supported by Stonadge's observation that ZAKβ overexpression increases nuclear translocation of phosphorylated MAPKs, even in the absence of mechanical stress, consistent with an upstream role in the stress response pathway.

Nonetheless, several critical gaps remain. We did not assess phosphorylation of canonical ZAKβ targets such as p38, JNK, or ERK1/2 *in vivo*, limiting the ability to confirm engagement of these pathways. Moreover, the reliance on CSA as the sole hypertrophic endpoint, without data on myonuclear domain size, protein synthesis rates, or fibre-type transitions, prevents full characterisation of the remodelling response. These limitations are particularly relevant given the possibility of pseudohypertrophy fibre swelling or cytoskeletal accumulation in the absence of increased contractile content, which cannot be excluded without further analysis.

From a mechanistic standpoint, one unresolved question is whether KY and ZAKβ physically interact or merely converge on common downstream targets. Chapter 7 identified no ZAKβ in KY immunoprecipitates, arguing against a stable or constitutive interaction. This is particularly noteworthy given that IGFN1 has been reported as a shared interactor of both proteins and was initially proposed to mediate a KY-dependent hypertrophic response. However, the ability of ZAKβ^CA to induce hypertrophy in KY-deficient muscle suggests that IGFN1 may facilitate modular or context-dependent interactions rather than serving as an obligate signalling bridge.

Nonetheless, transient or mechanically induced associations between KY and ZAKβ remain possible. To clarify these possibilities, future experiments should prioritise co-localisation analyses under mechanical stimulation or injury and assess whether KY deletion alters the spatial or temporal activation dynamics of ZAKβ and its downstream effectors.

These findings advance a more nuanced view of ZAKβ and KY in muscle growth regulation. Rather than forming a rigid, linear axis, these proteins may participate in overlapping yet distinct modules of the mechano-transduction network. ZAKβ acts as a kinase switch that can independently trigger hypertrophic pathways, while KY appears to function as a stress-responsive scaffold coordinating proteostasis and possibly modulating signal transduction under specific physiological conditions.

10.2 Future Directions

This thesis has uncovered new insights into the role of KY in muscle proteostasis, structural organisation, and stress adaptation, as well as its potential interface with hypertrophic signalling through ZAKβ. While these findings provide a substantial foundation, several key questions remain unanswered, and future research should address these in order to refine the mechanistic understanding and therapeutic targeting of KY-related pathways.

10.2.1 Domain-Specific Interactome Mapping

One of the most pressing next steps involves defining the domain-specific interaction landscape of KY. While Chapter 7 identified several candidate interactors including PPM1B, HSPA8, HSPA5, and HSPA9 these were based on immunoprecipitation of full-length KY constructs. Future studies should perform comparative immunoprecipitation-mass spectrometry using KY variants such as KY-ΔTGN and KY-TM. This would help delineate which interactions are dependent on the conserved TGN/PROT domain, and which are mediated via other regions. Identifying domain-dependent partners may clarify KY's non-enzymatic functions and uncover therapeutic targets for proteostasis modulation. Although these findings demonstrate that this domain is structurally conserved and essential for fibre size rescue, its precise biochemical role remains undefined. The absence of detectable enzymatic activity suggests a non-catalytic function, possibly as a scaffold for protein–protein interactions or a mediator of dynamic regulatory complexes. Domain-specific interactome profiling, structure-guided mutagenesis, and *in vitro* binding assays may help identify specific interfaces or partners that are functionally dependent on this domain's preserved architecture. High-resolution structural studies using cryo-EM or co-crystallisation could also reveal interaction motifs that escape homology-based modelling (Alvarez-Castelao et al., 2019; Fan et al., 2023).

10.2.2 Live-Cell Imaging of Autophagy Dynamics

The findings implicate KY in autophagosome maturation and LC3 lipidation, yet the current data are based on endpoint imaging and western blotting. Future experiments should incorporate live-cell imaging of autophagic flux using dynamic reporters such as tandem mCherry-GFP-LC3 (Kimura et al., 2007), LysoTracker-based assays for lysosomal acidity, or time-resolved measurements of LC3 turnover. These techniques would resolve whether the autophagic block in KY-deficient cells arises from defects in cargo trafficking, vesicle fusion, or degradation kinetics. While this thesis established that KY deficiency impairs autophagic flux, it remains unclear whether KY directly modulates autophagosome formation, lysosome fusion, or cargo recognition. Clarifying whether KY acts as a structural platform, signalling adaptor, or indirect modulator will be key to understanding its influence on proteostasis.

10.2.3 *In Vivo* Autophagy under Stress Conditions

A key limitation of Chapter 8 was the reliance on *in vitro* assays and the absence of basal autophagy measurements in muscle tissue due to practical constraints. *In vivo* studies using autophagy reporter mice (GFP-LC3 or RFP-GFP-LC3 transgenics) crossed with ky/ky backgrounds could provide critical insight into KY's role under physiological and pathological stress. Particular attention should be paid to conditions of mechanical overload, fasting, or denervation, which are known to modulate autophagy (Masiero & Sandri, 2010; Mizushima et al., 2004). Conditional knockout models will help determine KY's position within the autophagy cascade and assess its role under stress

10.2.4 Mapping the KY–PPM1B Interface

The identified interaction between KY and PPM1B also opens an important line of inquiry. Given PPM1B's role in autophagy initiation via ULK1 dephosphorylation (Zheng et al., 2022), understanding whether KY spatially organises this phosphatase during stress responses could reveal a novel regulatory axis. Structure-guided mutagenesis combined with phospho-specific ULK1 assays may determine whether KY recruits, stabilises, or regulates PPM1B within autophagy signalling hubs. This line of investigation may uncover whether KY contributes to tuning autophagic initiation thresholds in response to proteotoxic stimuli.

10.2.5 Chaperone-Mediated Interactions and Organelle Stress

Moreover, the interaction of KY with members of the HSP70 chaperone family including Hspa8, Hspa5, and Hspa9 suggests a potential role in organelle-specific stress responses. Whether KY facilitates client handoff between chaperones and degradation machinery or coordinates multi-compartmental stress adaptation remains unknown. HSP70s are known to participate in stress granule formation and organellar quality control (Fernández-Fernández et al., 2017; Vos et al., 2008), which may parallel KY's role. Functional dissection using chaperone overexpression or inhibition, coupled with KY mutants, may uncover whether these interactions are structurally mediated or conditionally regulated.

10.2.6 Species-Specific Nuclear Relocalisation

Another critical direction involves species-specific aspects of KY nuclear relocalisation. The observed stress-induced nuclear accumulation of human KY, but not its murine counterpart, suggests a divergent function potentially mediated by the human-specific N-terminal NLS. Whether nuclear KY plays a transcriptional or nuclear proteostasis role can be tested using chromatin association assays, nuclear fraction proteomics, and transcriptomic profiling under stress conditions.

10.2.7 KY in Muscle Regeneration and Repair

Beyond the protein level, examining KY function during muscle regeneration and differentiation remains a priority. Most experiments in this thesis focused on

undifferentiated myoblasts or stable fibre states. KY may have heightened significance during dynamic processes such as myotube formation or muscle repair. Injury-regeneration models, such as cardiotoxin injection in *ky/ky* mice, could illuminate whether KY modulates satellite cell activity, myofiber turnover, or structural repair during regeneration (Kuang et al., 2008).

10.2.8 Disease Models and Translational Potential

Translational questions also remain regarding KY's role in human neuromuscular disease. While its disruption causes myofibrillar myopathy (Selcen, 2011), it is unclear whether KY loss is a primary driver of pathology or a secondary consequence of broader proteostasis failure. Generating patient-derived iPSC myotubes with KY mutations, and applying multi-omics and rescue strategies, could help uncover disease-relevant functions and therapeutic targets. Translational questions also remain regarding KY's role in human neuromuscular disease. While its disruption causes myofibrillar myopathy (Selcen et al., 2011), it is unclear whether KY loss is a primary driver of pathology or a secondary consequence of broader proteostasis failure. Generating patient-derived iPSC myotubes with KY mutations, and applying multi-omics and rescue strategies, could help uncover disease-relevant functions and therapeutic targets.

10.2.9 Integration with ZAKβ and Mechanotransduction Pathways

Finally, the finding that ZAKβ-induced hypertrophy occurs independently of KY raises the possibility that KY functions in a distinct pathway dedicated to maintenance rather than growth. Future work should test whether KY intersects with mechanical signalling networks such as MAPK, mTOR, or YAP/TAZ, especially in response to mechanical loading, injury, or fatigue (L. et al., 2015). Conditional knockouts combined with mechanical stress paradigms could determine whether KY contributes to adaptive remodelling, not just maintenance. Co-localisation studies under stretch or injury models, proximity ligation assays, or crosslinking-IP techniques could clarify the spatial and temporal relationship between these two proteins.

These directions highlight the complexity of KY biology and its integration into muscle maintenance systems. Pursuing these questions will not only clarify KY's multifaceted role but may also uncover new avenues for therapeutic intervention in muscle degeneration and stress-related pathologies. Future research should aim to characterise KY as a non-enzymatic, modular adaptor within the muscle proteostasis network functionally bridging autophagy, chaperone systems, and mechanosensitive structures. By elucidating its interactome, regulatory contexts, and disease implications, such work may reveal KY as both a therapeutic target and a molecular marker of muscle health and stress resilience.

10.3 Conclusion

This study presents an integrated analysis of KY as a non-enzymatic, multifunctional regulator of muscle homeostasis and stress adaptation

- **Human KY, but not mouse KY, relocalises to nuclear and cytoplasmic foci after heat shock**, suggesting a human-specific role in stress adaptation. This redistribution was not fully blocked by proteasome MG132 or autophagy BafA1 inhibition, indicating the involvement of additional degradation mechanisms.
- **Re-expression of hKY in *ky/ky* muscle rescued the fibre size**, confirming KY's essential role in maintaining muscle size. However, KY overexpression in wild-type muscle did not induce hypertrophy, showing that KY is not a hypertrophic driver.
- **Mutation of the conserved catalytic triad in KY did not impair its ability to rescue muscle fibre size**, whereas full deletion of the TGN/PROT domain abolished this rescue. These results suggest a structural or scaffolding function for the domain, rather than enzymatic activity.
- **KY localisation to the Z-disc was preserved in constructs lacking the TGN/PROT domain**, indicating that other regions likely the C-terminal UBL domain mediate Z-disc anchoring.
- **AlphaFold modelling revealed structural conservation of the KY TGN/PROT domain with catalytically active transglutaminases,** but no catalytic activity has been demonstrated to date.
- **KY was shown to interact with key proteostasis regulators**, including the phosphatase PPM1B and the chaperones Hspa8, Hspa5 and Hspa9 , consist with a role in coordinating stress responses across cellular compartments.
- **Loss of KY impaired autophagic flux, evidenced by altered LC3-II accumulation in both C2C12 cells and muscle tissue**, without affecting autophagy initiation. This suggests KY acts at later stages of the autophagy process, possibly in vesicle maturation or cargo processing.
- **Constitutively active ZAKβ induced hypertrophy in both wild-type and *ky/ky* muscle**, while kinase-dead ZAKβ did not. These findings show that ZAKβ promotes hypertrophy through a KY-independent, kinase-dependent mechanism.
- **Overall, KY is a non-enzymatic structural regulator that contributes to muscle proteostasis, stress response coordination, and fibre maintenance**

These findings refine the current understanding of KY’s role in muscle biology and establish a foundation for future studies into its mechanistic function and therapeutic potential.

Glossary of abbreviations

ABBREVIATION	FULL TERM
ADP	Adenosine diphosphate
AKT	Protein Kinase B
ATP	Adenosine triphosphate
BAFA1	Bafilomycin A1
BAG3	Bcl2 Associated Athanogen 3
BSA	Bovine serum albumin
C2C12	Skeletal muscle-derived myoblast cell line
CASA	Chaperone Assisted Selective Autophagy
COS7	CV-1 in Origin, carrying the SV40 genetic material
CRISPR	Clustered regularly interspaced short palindromic repeats
CRYO-EM	Cryogenic Electron Microscopy
CSA	Cross-Sectional Area
DAPI	4â€²,6-Diamidino-2-Phenylindole (nuclear stain)
DM	Differentiation Media
DMD	Duchenne muscular dystrophy
ECM	Extracellular matrix
EM	Electron Microscopy
ER	Endoplasmic Reticulum
FBS	Foetal bovine serum
FLNC	Filamin C
FOXO	Forkhead Box Transcription Factors
FSBA	5â€²-4-fluorosulphonylbenzoyladenosine
GAPDH	Glyceraldehyde 3-phosphate dehydrogenase
GFP	Green Fluorescent Protein
GM	Growth Media
HKY	Human KY
HSPA5	Heat Shock Protein Family A (Hsp70) Member 5 (BiP/GRP78)
HSPA8	Heat Shock Protein Family A (Hsp70) Member 8 (HSC70)
HSPA9	Heat Shock Protein Family A (Hsp70) Member 9 (GRP75/mortalin)
I.P.	Intraperitoneal
IG	Immunoglobulin domain
IGF-1R	Insulin-like growth factor 1 Receptor
IGF1	Insulin-like growth factor 1
IGFN1	Immunoglobulin-Like and Fibronectin Type III Domain-Containing Protein 1
IP	Immunoprecipitation
IRS-1	Insulin Receptor Substrate 1
KO	Knockout

KY	Kyphoscoliosis Peptidase
LC-MS/MS	Liquid Chromatography with tandem mass spectrometry
LC3	Microtubule-Associated Proteins 1A/1B Light Chain 3
LZ	Leucine zipper domain
MAPK	Mitogen-Activated Protein Kinase
MFM	Myofibrillar myopathy
MG132	Proteasome Inhibitor
MKY	Mouse KY
MTOR	Mechanistic Target of Rapamycin
MUSC	Muscle stem cell
NCBI	National Center for Biotechnology Information
NLS	Nuclear Localisation Signal
ON	Overnight
PAGE	Polyacrylamide gel electrophoresis
PBS	Phosphate Buffered Saline
PCR	Polymerase Chain Reaction
PI3K	Phosphatidylinositol 3 kinase
PPM1B	Protein Phosphatase, Mg2+/Mn2+ Dependent 1B
QPCR	Quantitative Polymerase Chain Reaction
RFP	Red Fluorescent Protein
RIPA	Radioimmunoprecipitation assay
RMSD	Root-Mean-Square Deviation
RT	Room temperature
SDS	Sodium dodecyl sulphate
SFBD	Stress fibre binding domain
SMAD2/3	SMAD Family Member 2/3
SR	Sarcoplasmic Reticulum
TA	Tibialis Anterior
TG2	Transglutaminase 2
TGN/PROT	Transglutaminase-like/Protease Domain
UBL	Ubiquitin-Like Domain
ULK1	Unc-51 Like Autophagy Activating Kinase 1
WB	Western Blot
WGA	Wheat germ agglutinin
WT	Wild Type
Y2H	Yeast 2 Hybrid
YAP/TAZ	Yes-Associated Protein / Transcriptional Coactivator with PDZ-Binding Motif
Z-DISC	Z-line or Z-band (sarcomeric boundary structure)
ZAK	Leucine Zipper-and Sterile Alpha Motif-Containing Kinase
ZAKÃŽâ€™	Leucine Zipper and Sterile Alpha Motif Kinase Beta Isoform
ZAKÃŽâ€™^CA	Constitutively Active ZAKÎ²
ZAKÃŽâ€™^KD	Kinase-Dead ZAKÎ²

Bibliography

Agarwal, R., Wakimoto, H., Paulo, J. A., Zhang, Q., Reichart, D., Toepfer, C., Sharma, A., Tai, A. C., Lun, M., Gorham, J., Depalma, S. R., Gygi, S. P., Seidman, J. G., & Seidman, C. E. (2022). Pathogenesis of Cardiomyopathy Caused by Variants in ALPK3, an Essential Pseudokinase in the Cardiomyocyte Nucleus and Sarcomere. *Circulation*, *146*(22). https://doi.org/10.1161/CIRCULATIONAHA.122.059688

Altschul, S. F., Madden, T. L., Schäffer, A. A., Zhang, J., Zhang, Z., Miller, W., & Lipman, D. J. (1997). Gapped BLAST and PSI-BLAST: A new generation of protein database search programs. In *Nucleic Acids Research* (Vol. 25, Issue 17). https://doi.org/10.1093/nar/25.17.3389

Alvarez-Castelao, B., Schanzenbächer, C. T., Langer, J. D., & Schuman, E. M. (2019). Cell-type-specific metabolic labeling, detection and identification of nascent proteomes in vivo. *Nature Protocols*, *14*(2). https://doi.org/10.1038/s41596-018-0106-6

Alway, S. E., Siu, P. M., Murlasits, Z., & Butler, D. C. (2005). Muscle hypertrophy models: Applications for research on aging. *Canadian Journal of Applied Physiology*, *30*(5). https://doi.org/10.1139/h05-143

Arif, B., Rasheed, A., Kumar, K. R., Fatima, A., Abbas, G., Wohler, E., Sobriera, N., Lohmann, K., & Naz, S. (2020). A novel homozygous KY variant causing a complex neurological disorder. *European Journal of Medical Genetics*, *63*(11). https://doi.org/10.1016/j.ejmg.2020.104031

Arndt, V., Dick, N., Tawo, R., Dreiseidler, M., Wenzel, D., Hesse, M., Fürst, D. O., Saftig, P., Saint, R., Fleischmann, B. K., Hoch, M., & Höhfeld, J. (2010). Chaperone-Assisted Selective Autophagy Is Essential for Muscle Maintenance. *Current Biology*, *20*(2). https://doi.org/10.1016/j.cub.2009.11.022

Attaix, D., Combaret, L., Kee, A. J., & Taillandier, D. (2003). Mechanisms of ubiquitination and proteasome-dependent proteolysis in skeletal muscle. In *Molecular nutrition*. https://doi.org/10.1079/9780851996790.0219

Baker, J., Riley, G., Romero, M. R., Haynes, A. R., Hilton, H., Simon, M., Hancock, J., Tateossian, H., Ripoll, V. M., & Blanco, G. (2010). Identification of a Z-band associated protein complex involving KY, FLNC and IGFN1. *Experimental Cell Research*, *316*(11). https://doi.org/10.1016/j.yexcr.2010.02.027

Bär, H., Fischer, D., Goudeau, B., Kley, R. A., Clemen, C. S., Vicart, P., Herrmann, H., Vorgerd, M., & Schröder, R. (2005). Pathogenic effects of a novel heterozygous R350P desmin mutation on the assembly of desmin intermediate

filaments in vivo and in vitro. *Human Molecular Genetics*, *14*(10). https://doi.org/10.1093/hmg/ddi136

Bareja, A., Holt, J. A., Luo, G., Chang, C., Lin, J., Hinken, A. C., Freudenberg, J. M., Kraus, W. E., Evans, W. J., & Billin, A. N. (2014). Human and mouse skeletal muscle stem cells: Convergent and divergent mechanisms of myogenesis. *PLoS ONE*, *9*(2). https://doi.org/10.1371/journal.pone.0090398

BARER, R. (1948). THE STRUCTURE OF THE STRIATED MUSCLE FIBRE. *Biological Reviews*, *23*(2). https://doi.org/10.1111/j.1469-185X.1948.tb00461.x

Beatham, J., Romero, R., Townsend, S. K. M., Hacker, T., van der Ven, P. F. M., & Blanco, G. (2004). Filamin C interacts with the muscular dystrophy KY protein and is abnormally distributed in mouse KY deficient muscle fibres. *Human Molecular Genetics*, *13*(22). https://doi.org/10.1093/hmg/ddh308

Bernales, S., McDonald, K. L., & Walter, P. (2006). Autophagy counterbalances endoplasmic reticulum expansion during the unfolded protein response. *PLoS Biology*, *4*(12). https://doi.org/10.1371/journal.pbio.0040423

Blanco, G., Coulton, G. R., Biggin, A., Grainge, C., Moss, J., Barrett, M., Berquin, A., Maréchal, G., Skynner, M., Van Mier, P., Nikitopoulou, A., Kraus, M., Ponting, C. P., Mason, R. M., & Brown, S. D. M. (2001). The kyphoscoliosis (ky) mouse is deficient in hypertrophic responses and is caused by a mutation in a novel-specific protein. *Human Molecular Genetics*, *10*(1). https://doi.org/10.1093/hmg/10.1.9

Bloemberg, D., & Quadrilatero, J. (2012). Rapid determination of myosin heavy chain expression in rat, mouse, and human skeletal muscle using multicolor immunofluorescence analysis. *PLoS ONE*, *7*(4). https://doi.org/10.1371/journal.pone.0035273

Bohnert, K. R., McMillan, J. D., & Kumar, A. (2018). Emerging roles of ER stress and unfolded protein response pathways in skeletal muscle health and disease. In *Journal of Cellular Physiology* (Vol. 233, Issue 1). https://doi.org/10.1002/jcp.25852

Bonaldo, P., & Sandri, M. (2013). Cellular and molecular mechanisms of muscle atrophy. In *DMM Disease Models and Mechanisms* (Vol. 6, Issue 1). https://doi.org/10.1242/dmm.010389

Bridges, L. R., Coulton, G. R., Howard, G., Moss, J., & Mason, R. M. (1992). The neuromuscular basis of hereditary kyphoscoliosis in the mouse. *Muscle & Nerve*, *15*(2). https://doi.org/10.1002/mus.880150208

Burattini, S., Ferri, R., Battistelli, M., Curci, R., Luchetti, F., & Falcieri, E. (2004). C2C12 murine myoblasts as a model of skeletal muscle development: Morpho-functional characterization. *European Journal of Histochemistry*, *48*(3).

Chal, J., & Pourquié, O. (2017). Making muscle: Skeletal myogenesis in vivo and in vitro. In *Development (Cambridge)* (Vol. 144, Issue 12). https://doi.org/10.1242/dev.151035

Chang, Y., Zhang, Q., Li, Z., Ding, K., & Lu, X. (2016). Leucine-zipper and Sterile-α Motif Kinase (ZAK): A Potential Target for Drug Discovery. *Current Medicinal Chemistry*, *23*(33). https://doi.org/10.2174/0929867323666160920104121

Ciechanover, A., & Kwon, Y. T. (2015). Degradation of misfolded proteins in neurodegenerative diseases: therapeutic targets and strategies. In *Experimental and Molecular Medicine* (Vol. 47, Issue 3). https://doi.org/10.1038/EMM.2014.117

Cohen, S., Zhai, B., Gygi, S. P., & Goldberg, A. L. (2012). Ubiquitylation by Trim32 causes coupled loss of desmin, Z-bands, and thin filaments in muscle atrophy. *Journal of Cell Biology*, *198*(4). https://doi.org/10.1083/jcb.201110067

Davids, C. J., Roberts, L. A., Bjørnsen, T., Peake, J. M., Coombes, J. S., & Raastad, T. (2023). Where Does Blood Flow Restriction Fit in the Toolbox of Athletic Development? A Narrative Review of the Proposed Mechanisms and Potential Applications. In *Sports Medicine* (Vol. 53, Issue 11). https://doi.org/10.1007/s40279-023-01900-6

Dickinson, A. G., & Meikle, V. M. H. (1973). GENETIC KYPHOSCOLIOSIS IN MICE. In *The Lancet* (Vol. 301, Issue 7813, p. 1186). Elsevier. https://doi.org/10.1016/S0140-6736(73)91186-0

Doyle, S. M., Genest, O., & Wickner, S. (2013). Protein rescue from aggregates by powerful molecular chaperone machines. In *Nature Reviews Molecular Cell Biology* (Vol. 14, Issue 10). https://doi.org/10.1038/nrm3660

Eckert, R. L., Fisher, M. L., Grun, D., Adhikary, G., Xu, W., & Kerr, C. (2015). Transglutaminase is a tumor cell and cancer stem cell survival factor. *Molecular Carcinogenesis*, *54*(10). https://doi.org/10.1002/mc.22375

Egan, D. F., Shackelford, D. B., Mihaylova, M. M., Gelino, S., Kohnz, R. A., Mair, W., Vasquez, D. S., Joshi, A., Gwinn, D. M., Taylor, R., Asara, J. M., Fitzpatrick, J., Dillin, A., Viollet, B., Kundu, M., Hansen, M., & Shaw, R. J. (2011). Phosphorylation of ULK1 (hATG1) by AMP-activated protein kinase connects energy sensing to mitophagy. *Science*, *331*(6016). https://doi.org/10.1126/science.1196371

Egerman, M. A., & Glass, D. J. (2014). Signaling pathways controlling skeletal muscle mass. In *Critical Reviews in Biochemistry and Molecular Biology* (Vol. 49, Issue 1). https://doi.org/10.3109/10409238.2013.857291

Ehsani, E., Khamirani, H. J., Abbasi, Z., Gohari, M., Zoghi, S., Mohammadi, S., Dianatpour, M., Tabei, S. M. B., Mohamadjani, O., & Dastgheib, S. A. (2022).

Genotypic and phenotypic spectrum of Myofibrillar Myopathy 7 as a result of Kyphoscoliosis Peptidase deficiency: The first description of a missense mutation in KY and literature review. *European Journal of Medical Genetics*, *65*(8). https://doi.org/10.1016/j.ejmg.2022.104552

Eyers, P. A., & Murphy, J. M. (2016). The evolving world of pseudoenzymes: Proteins, prejudice and zombies. *BMC Biology*, *14*(1). https://doi.org/10.1186/s12915-016-0322-x

Fan, X., Huang, J., Jin, X., & Yan, N. (2023). Cryo-EM structure of human voltage-gated sodium channel Nav1.6. *Proceedings of the National Academy of Sciences of the United States of America*, *120*(5). https://doi.org/10.1073/pnas.2220578120

Fanzani, A., Conraads, V. M., Penna, F., & Martinet, W. (2012). Molecular and cellular mechanisms of skeletal muscle atrophy: An update. In *Journal of Cachexia, Sarcopenia and Muscle* (Vol. 3, Issue 3). https://doi.org/10.1007/s13539-012-0074-6

Faulkner, G., Pallavicini, A., Formentin, E., Comelli, A., Ievolella, C., Trevisan, S., Bortoletto, G., Scannapieco, P., Salamon, M., Mouly, V., Valle, G., & Lanfranchi, G. (1999). ZASP: A new Z-band alternatively spliced PDZ-motif protein. *Journal of Cell Biology*, *146*(2). https://doi.org/10.1083/jcb.146.2.465

Fernández-Fernández, M. R., Gragera, M., Ochoa-Ibarrola, L., Quintana-Gallardo, L., & Valpuesta, J. M. (2017). Hsp70 – a master regulator in protein degradation. In *FEBS Letters* (Vol. 591, Issue 17). https://doi.org/10.1002/1873-3468.12751

Ferreira, R. P., & Duarte, J. A. (2022). Protein turnover in skeletal muscle: looking at molecular regulation towards active lifestyle. In *International Journal of Sports Medicine*. https://doi.org/10.1055/a-2044-8277

Fichna, J. P., Maruszak, A., & Żekanowski, C. (2018). Myofibrillar myopathy in the genomic context. In *Journal of Applied Genetics* (Vol. 59, Issue 4). https://doi.org/10.1007/s13353-018-0463-4

Fourrier, C., Bryksin, V., Hattersley, K., Hein, L. K., Bensalem, J., & Sargeant, T. J. (2021). Comparison of chloroquine-like molecules for lysosomal inhibition and measurement of autophagic flux in the brain. *Biochemical and Biophysical Research Communications*, *534*. https://doi.org/10.1016/j.bbrc.2020.12.008

Franco-Romero, A., & Sandri, M. (2021). Role of autophagy in muscle disease. *Molecular Aspects of Medicine*, *82*. https://doi.org/10.1016/j.mam.2021.101041

Frank, D., Kuhn, C., Katus, H. A., & Frey, N. (2007). Role of the sarcomeric Z-disc in the pathogenesis of cardiomyopathy. In *Future Cardiology* (Vol. 3, Issue 6). https://doi.org/10.2217/14796678.3.6.611

Frontera, W. R., & Ochala, J. (2015). Skeletal Muscle: A Brief Review of Structure and Function. In *Behavior Genetics* (Vol. 45, Issue 2). https://doi.org/10.1007/s00223-014-9915-y

Gamerdinger, M., Kaya, A. M., Wolfrum, U., Clement, A. M., & Behl, C. (2011). BAG3 mediates chaperone-based aggresome-targeting and selective autophagy of misfolded proteins. *EMBO Reports*, *12*(2). https://doi.org/10.1038/embor.2010.203

Ganassi, M., Mateju, D., Bigi, I., Mediani, L., Poser, I., Lee, H. O., Seguin, S. J., Morelli, F. F., Vinet, J., Leo, G., Pansarasa, O., Cereda, C., Poletti, A., Alberti, S., & Carra, S. (2016). A Surveillance Function of the HSPB8-BAG3-HSP70 Chaperone Complex Ensures Stress Granule Integrity and Dynamism. *Molecular Cell*, *63*(5). https://doi.org/10.1016/j.molcel.2016.07.021

Gaudry, C. A., Verderio, E., Aeschlimann, D., Cox, A., Smith, C., & Griffin, M. (1999). Cell surface localization of tissue transglutaminase is dependent on a fibronectin-binding site in its N-terminal β-sandwich domain. *Journal of Biological Chemistry*, *274*(43). https://doi.org/10.1074/jbc.274.43.30707

Gkikas, I., Palikaras, K., & Tavernarakis, N. (2018). The role of mitophagy in innate immunity. In *Frontiers in Immunology* (Vol. 9, Issue JUN). https://doi.org/10.3389/fimmu.2018.01283

Gotoh, I., Adachi, M., & Nishida, E. (2001). Identification and Characterization of a Novel MAP Kinase Kinase Kinase, MLTK. *Journal of Biological Chemistry*, *276*(6). https://doi.org/10.1074/jbc.M008595200

Griffin, M., Casadio, R., & Bergamini, C. M. (2002). Transglutaminases: Nature's biological glues. In *Biochemical Journal* (Vol. 368, Issue 2). https://doi.org/10.1042/BJ20021234

Harrad, O. (2021). *Novel functional domains in the muscle disease-associated protein KY* [MRes thesis]. University of York.

Hassan, F. ul, Nawaz, A., Rehman, M. S., Ali, M. A., Dilshad, S. M. R., & Yang, C. (2019). Prospects of HSP70 as a genetic marker for thermo-tolerance and immuno-modulation in animals under climate change scenario. In *Animal Nutrition* (Vol. 5, Issue 4). https://doi.org/10.1016/j.aninu.2019.06.005

Haun, C. T., Vann, C. G., Roberts, B. M., Vigotsky, A. D., Schoenfeld, B. J., & Roberts, M. D. (2019). A critical evaluation of the biological construct skeletal muscle hypertrophy: Size matters but so does the measurement. *Frontiers in Physiology*, *10*(MAR). https://doi.org/10.3389/fphys.2019.00247

Hedberg-Oldfors, C., Darin, N., Olsson Engman, M., Orfanos, Z., Thomsen, C., Van Der Ven, P. F. M., & Oldfors, A. (2016). A new early-onset neuromuscular

disorder associated with kyphoscoliosis peptidase (KY) deficiency. *European Journal of Human Genetics*, *24*(12). https://doi.org/10.1038/ejhg.2016.98

Hicks, M. R., Hiserodt, J., Paras, K., Fujiwara, W., Eskin, A., Jan, M., Xi, H., Young, C. S., Evseenko, D., Nelson, S. F., Spencer, M. J., Handel, B. Van, & Pyle, A. D. (2018). ERBB3 and NGFR mark a distinct skeletal muscle progenitor cell in human development and hPSCs. *Nature Cell Biology*, *20*(1). https://doi.org/10.1038/s41556-017-0010-2

Hindi, S. M., Tajrishi, M. M., & Kumar, A. (2013). Signaling mechanisms in mammalian myoblast fusion. In *Science Signaling* (Vol. 6, Issue 272). https://doi.org/10.1126/scisignal.2003832

Huang, C. Y., Yang, L. C., Liu, K. Y., Liao, P. H., Chou, J. I. Y., Chou, M. Y., Lin, W. W., & Yang, J. J. (2009). RhoGDI-induced hypertrophic growth in H9c2 cells is negatively regulated by ZAK. *Journal of Biomedical Science*, *16*(1). https://doi.org/10.1186/1423-0127-16-11

Iismaa, S. E., Mearns, B. M., Lorand, L., & Graham, R. M. (2009). Transglutaminases and disease: Lessons from genetically engineered mouse models and inherited disorders. In *Physiological Reviews* (Vol. 89, Issue 3). https://doi.org/10.1152/physrev.00044.2008

Isayeva, M. O., Gadzhiyeva, F. T., Abalenikhina, Y. V., Shchul'kin, A. V., & Yakusheva, E. N. (2023). Culture Method and Regulation Mechanisms of Stages of C2C12 Cell Line Myogenesis. *I.P. Pavlov Russian Medical Biological Herald*, *31*(4). https://doi.org/10.17816/PAVLOVJ375362

Jiao, J., & Demontis, F. (2017). Skeletal muscle autophagy and its role in sarcopenia and organismal aging. In *Current Opinion in Pharmacology* (Vol. 34). https://doi.org/10.1016/j.coph.2017.03.009

Johnston, J. A., Ward, C. L., & Kopito, R. R. (1998). Aggresomes: A cellular response to misfolded proteins. *Journal of Cell Biology*, *143*(7). https://doi.org/10.1083/jcb.143.7.1883

Jokl, E. J., Hughes, G. L., Cracknell, T., Pownall, M. E., & Blanco, G. (2018). Transcriptional upregulation of Bag3, a chaperone-assisted selective autophagy factor, in animal models of KY-deficient hereditary myopathy. *DMM Disease Models and Mechanisms*, *11*(7). https://doi.org/10.1242/dmm.033225

Kaizuka, T., Morishita, H., Hama, Y., Tsukamoto, S., Matsui, T., Toyota, Y., Kodama, A., Ishihara, T., Mizushima, T., & Mizushima, N. (2016). An Autophagic Flux Probe that Releases an Internal Control. *Molecular Cell*, *64*(4). https://doi.org/10.1016/j.molcel.2016.09.037

Kampinga, H. H., & Bergink, S. (2016). Heat shock proteins as potential targets for protective strategies in neurodegeneration. In *The Lancet Neurology* (Vol. 15, Issue 7). https://doi.org/10.1016/S1474-4422(16)00099-5

Kampinga, H. H., Brunsting, J. F., Stege, G. J. J., Konings, A. W. T., & Landry, J. (1994). Cells overexpressing Hsp27 show accelerated recovery from heat-induced nuclear protein aggregation. *Biochemical and Biophysical Research Communications*, *204*(3). https://doi.org/10.1006/bbrc.1994.2586

Kaushik, S., & Cuervo, A. M. (2018). The coming of age of chaperone-mediated autophagy. In *Nature Reviews Molecular Cell Biology* (Vol. 19, Issue 6). https://doi.org/10.1038/s41580-018-0001-6

Kedersha, N., Ivanov, P., & Anderson, P. (2013). Stress granules and cell signaling: More than just a passing phase? In *Trends in Biochemical Sciences* (Vol. 38, Issue 10). https://doi.org/10.1016/j.tibs.2013.07.004

Kim, J., Kundu, M., Viollet, B., & Guan, K.-L. (2011). AMPK and mTOR regulate autophagy through direct phosphorylation of Ulk1 : Nature Cell Biology : Nature Publishing Group. *Nature Cell Biology*, *advance on*(2).

Kimura, S., Noda, T., & Yoshimori, T. (2007). Dissection of the autophagosome maturation process by a novel reporter protein, tandem fluorescent-tagged LC3. *Autophagy*, *3*(5). https://doi.org/10.4161/auto.4451

Kitajima, Y., Yoshioka, K., & Suzuki, N. (2020). The ubiquitin-proteasome system in regulation of the skeletal muscle homeostasis and atrophy: From basic science to disorders. In *Journal of Physiological Sciences* (Vol. 70, Issue 1). https://doi.org/10.1186/s12576-020-00768-9

Kley, R. A., Van Der Ven, P. F. M., Olivé, M., Höhfeld, J., Goldfarb, L. G., Fürst, D. O., & Vorgerd, M. (2013). Impairment of protein degradation in myofibrillar myopathy caused by FLNC/filamin C mutations. *Autophagy*, *9*(3). https://doi.org/10.4161/auto.22921

Klionsky, D. J., Abdel-Aziz, A. K., Abdelfatah, S., Abdellatif, M., Abdoli, A., Abel, S., Abeliovich, H., Abildgaard, M. H., Abudu, Y. P., Acevedo-Arozena, A., Adamopoulos, I. E., Adeli, K., Adolph, T. E., Adornetto, A., Aflaki, E., Agam, G., Agarwal, A., Aggarwal, B. B., Agnello, M., … Tong, C. K. (2021). Guidelines for the use and interpretation of assays for monitoring autophagy (4th edition)1. In *Autophagy* (Vol. 17, Issue 1). https://doi.org/10.1080/15548627.2020.1797280

Knöll, R., Buyandelger, B., & Lab, M. (2011). The sarcomeric Z-disc and Z-discopathies. In *Journal of Biomedicine and Biotechnology* (Vol. 2011). https://doi.org/10.1155/2011/569628

Koga, H., Kaushik, S., & Cuervo, A. M. (2011). Protein homeostasis and aging: The importance of exquisite quality control. In *Ageing Research Reviews* (Vol. 10, Issue 2). https://doi.org/10.1016/j.arr.2010.02.001

Konersman, C. G., Bordini, B. J., Scharer, G., Lawlor, M. W., Zangwill, S., Southern, J. F., Amos, L., Geddes, G. C., Kliegman, R., & Collins, M. P. (2015). BAG3 myofibrillar myopathy presenting with cardiomyopathy. *Neuromuscular Disorders*, *25*(5). https://doi.org/10.1016/j.nmd.2015.01.009

Konieczny, P., Fuchs, P., Reipert, S., Kunz, W. S., Zeöld, A., Fischer, I., Paulin, D., Schröder, R., & Wiche, G. (2008). Myofiber integrity depends on desmin network targeting to Z-disks and costameres via distinct plectin isoforms. *Journal of Cell Biology*, *181*(4). https://doi.org/10.1083/jcb.200711058

Kopito, R. R. (2000). Aggresomes, inclusion bodies and protein aggregation. In *Trends in Cell Biology* (Vol. 10, Issue 12). https://doi.org/10.1016/S0962-8924(00)01852-3

Kramer, H. F., & Goodyear, L. J. (2007). Exercise, MAPK, and NF-κB signaling in skeletal muscle. In *Journal of Applied Physiology* (Vol. 103, Issue 1). https://doi.org/10.1152/japplphysiol.00085.2007

Kuang, S., Gillespie, M. A., & Rudnicki, M. A. (2008). Niche Regulation of Muscle Satellite Cell Self-Renewal and Differentiation. In *Cell Stem Cell* (Vol. 2, Issue 1). https://doi.org/10.1016/j.stem.2007.12.012

Kung, J. E., & Jura, N. (2019). Prospects for pharmacological targeting of pseudokinases. In *Nature Reviews Drug Discovery* (Vol. 18, Issue 7). https://doi.org/10.1038/s41573-019-0018-3

L., B., P.S., Z., & J.E., M. (2015). Satellite cells from dystrophic muscle retain regenerative capacity. *Stem Cell Research*, *14*(1).

Laplante, M., & Sabatini, D. M. (2012). MTOR signaling in growth control and disease. In *Cell* (Vol. 149, Issue 2). https://doi.org/10.1016/j.cell.2012.03.017

Lee, F. X. Z., Houweling, P. J., North, K. N., & Quinlan, K. G. R. (2016). How does α-actinin-3 deficiency alter muscle function? Mechanistic insights into ACTN3, the "gene for speed." In *Biochimica et Biophysica Acta - Molecular Cell Research* (Vol. 1863, Issue 4). https://doi.org/10.1016/j.bbamcr.2016.01.013

LESMANA, R., GOENAWAN, H., TARAWAN, V. M., SETIAWAN, I., HIDAYAT, A., & SUPRATMAN, U. (2019). Short Communication: Optimazing culture and differentiation L6 cell, C2C12 cell and primary myoblast cells culture. *Cell Biology and Development*, *2*(2). https://doi.org/10.13057/cellbioldev/v020201

Liang, R., Dong, W., Shen, X., Peng, X., Aceves, A. G., & Liu, Y. (2016). Modeling myotonic dystrophy 1 in C2C12 myoblast cells. *Journal of Visualized Experiments*, *2016*(113). https://doi.org/10.3791/54078

Liewluck, T. (2021). A Window Into the Myofibrillar Myopathy Proteome. In *Neurology: Genetics* (Vol. 7, Issue 3). https://doi.org/10.1212/NXG.0000000000000587

Littlefield, P., Moasser, M. M., & Jura, N. (2014). An ATP-competitive inhibitor modulates the allosteric function of the HER3 pseudokinase. In *Chemistry and Biology* (Vol. 21, Issue 4). https://doi.org/10.1016/j.chembiol.2014.02.011

Liu, T. C., Huang, C. J., Chu, Y. C., Wei, C. C., Chou, C. C., Chou, M. Y., Chou, C. K., & Yang, J. J. (2000a). Cloning and expression of ZAK, a mixed lineage kinase-like protein containing a Leucine-Zipper and a sterile-alpha motif. *Biochemical and Biophysical Research Communications*, *274*(3). https://doi.org/10.1006/bbrc.2000.3236

Liu, T. C., Huang, C. J., Chu, Y. C., Wei, C. C., Chou, C. C., Chou, M. Y., Chou, C. K., & Yang, J. J. (2000b). Cloning and expression of ZAK, a mixed lineage kinase-like protein containing a Leucine-Zipper and a sterile-alpha motif. *Biochemical and Biophysical Research Communications*, *274*(3). https://doi.org/10.1006/bbrc.2000.3236

Locke, M., Noble, E. G., Tanguay, R. M., Feild, M. R., Ianuzzo, S. E., & Ianuzzo, C. D. (1995). Activation of heat-shock transcription factor in rat heart after heat shock and exercise. *American Journal of Physiology - Cell Physiology*, *268*(6 37-6). https://doi.org/10.1152/ajpcell.1995.268.6.c1387

Lorand, L., & Graham, R. M. (2003). Transglutaminases: Crosslinking enzymes with pleiotropic functions. In *Nature Reviews Molecular Cell Biology* (Vol. 4, Issue 2). https://doi.org/10.1038/nrm1014

Lu, S., Sung, T., Lin, N., Abraham, R. T., & Jessen, B. A. (2017). Lysosomal adaptation: How cells respond to lysosomotropic compounds. *PLoS ONE*, *12*(3). https://doi.org/10.1371/journal.pone.0173771

Luther, P. K. (2009). The vertebrate muscle Z-disc: Sarcomere anchor for structure and signalling. *Journal of Muscle Research and Cell Motility*, *30*(5–6). https://doi.org/10.1007/s10974-009-9189-6

Makarova, K. S., Aravind, L., & Koonin, E. V. (1999). A superfamily of archaeal, bacterial, and eukaryotic proteins homologous to animal transglutaminases. *Protein Science*, *8*(8). https://doi.org/10.1110/ps.8.8.1714

Martineau, L. C., & Gardiner, P. F. (2001). Insight into skeletal muscle mechanotransduction: MAPK activation is quantitatively related to tension. *Journal of Applied Physiology*, *91*(2). https://doi.org/10.1152/jappl.2001.91.2.693

Marzetti, E., Calvani, R., Cesari, M., Buford, T. W., Lorenzi, M., Behnke, B. J., & Leeuwenburgh, C. (2013). Mitochondrial dysfunction and sarcopenia of aging: From signaling pathways to clinical trials. In *International Journal of*

Biochemistry and Cell Biology (Vol. 45, Issue 10). https://doi.org/10.1016/j.biocel.2013.06.024

Masiero, E., & Sandri, M. (2010). Autophagy inhibition induces atrophy and myopathy in adult skeletal muscles. In *Autophagy* (Vol. 6, Issue 2). https://doi.org/10.4161/auto.6.2.11137

Mason, R. M., & Palfrey, A. J. (1984). Intervertebral disc degeneration in adult mice with hereditary kyphoscoliosis. *Journal of Orthopaedic Research*, *2*(4). https://doi.org/10.1002/jor.1100020405

Massey, A. C., Kaushik, S., Sovak, G., Kiffin, R., & Cuervo, A. M. (2006). Consequences of the selective blockage of chaperone-mediated autophagy. *Proceedings of the National Academy of Sciences of the United States of America*, *103*(15). https://doi.org/10.1073/pnas.0507436103

Mateju, D., Franzmann, T. M., Patel, A., Kopach, A., Boczek, E. E., Maharana, S., Lee, H. O., Carra, S., Hyman, A. A., & Alberti, S. (2017). An aberrant phase transition of stress granules triggered by misfolded protein and prevented by chaperone function. *The EMBO Journal*, *36*(12). https://doi.org/10.15252/embj.201695957

Mathea, S., Abdul Azeez, K. R., Salah, E., Tallant, C., Wolfreys, F., Konietzny, R., Fischer, R., Lou, H. J., Brennan, P. E., Schnapp, G., Pautsch, A., Kessler, B. M., Turk, B. E., & Knapp, S. (2016). Structure of the Human Protein Kinase ZAK in Complex with Vemurafenib. *ACS Chemical Biology*, *11*(6). https://doi.org/10.1021/acschembio.6b00043

McKendry, J., Stokes, T., McLeod, J. C., & Phillips, S. M. (2021). Resistance Exercise, Aging, Disuse, and Muscle Protein Metabolism. *Comprehensive Physiology*, *11*(3). https://doi.org/10.1002/cphy.c200029

Meister-Broekema, M., Freilich, R., Jagadeesan, C., Rauch, J. N., Bengoechea, R., Motley, W. W., Kuiper, E. F. E., Minoia, M., Furtado, G. V., van Waarde, M. A. W. H., Bird, S. J., Rebelo, A., Zuchner, S., Pytel, P., Scherer, S. S., Morelli, F. F., Carra, S., Weihl, C. C., Bergink, S., … Kampinga, H. H. (2018). Myopathy associated BAG3 mutations lead to protein aggregation by stalling Hsp70 networks. *Nature Communications*, *9*(1). https://doi.org/10.1038/s41467-018-07718-5

Mirdita, M., Schütze, K., Moriwaki, Y., Heo, L., Ovchinnikov, S., & Steinegger, M. (2022). ColabFold: making protein folding accessible to all. *Nature Methods*, *19*(6). https://doi.org/10.1038/s41592-022-01488-1

Mizushima, N., & Levine, B. (2020). Autophagy in Human Diseases. *New England Journal of Medicine*, *383*(16). https://doi.org/10.1056/nejmra2022774

Mizushima, N., Yamamoto, A., Matsui, M., Yoshimori, T., & Ohsumi, Y. (2004). In Vivo Analysis of Autophagy in Response to Nutrient Starvation Using Transgenic Mice Expressing a Fluorescent Autophagosome Marker. *Molecular Biology of the Cell*, *15*(3). https://doi.org/10.1091/mbc.E03-09-0704

Murphy, J. M., Mace, P. D., & Eyers, P. A. (2017). Live and let die: insights into pseudoenzyme mechanisms from structure. In *Current Opinion in Structural Biology* (Vol. 47). https://doi.org/10.1016/j.sbi.2017.07.004

Murphy, J. M., Zhang, Q., Young, S. N., Reese, M. L., Bailey, F. P., Eyers, P. A., Ungureanu, D., Hammaren, H., Silvennoinen, O., Varghese, L. N., Chen, K., Tripaydonis, A., Jura, N., Fukuda, K., Qin, J., Nimchuk, Z., Mudgett, M. B., Elowe, S., Gee, C. L., … Lucet, I. S. (2014). A robust methodology to subclassify pseudokinases based on their nucleotide-binding properties. *Biochemical Journal*, *457*(2). https://doi.org/10.1042/BJ20131174

Neel, B. A., Lin, Y., & Pessin, J. E. (2013). Skeletal muscle autophagy: A new metabolic regulator. In *Trends in Endocrinology and Metabolism* (Vol. 24, Issue 12). https://doi.org/10.1016/j.tem.2013.09.004

Nguyen Ba, A. N., Pogoutse, A., Provart, N., & Moses, A. M. (2009). NLStradamus: A simple Hidden Markov Model for nuclear localization signal prediction. *BMC Bioinformatics*, *10*. https://doi.org/10.1186/1471-2105-10-202

Nordgaard, C., Vind, A. C., Stonadge, A., Kjøbsted, R., Snieckute, G., Antas, P., Blasius, M., Reinert, M. S., Del Val, A. M., Bekker-Jensen, D. B., Haahr, P., Miroshnikova, Y. A., Mazouzi, A., Falk, S., Perrier-Groult, E., Tiedje, C., Li, X., Jakobsen, J. R., Jørgensen, N. O., … Bekker-Jensen, S. (2022). ZAKβ is activated by cellular compression and mediates contraction-induced MAP kinase signaling in skeletal muscle . *The EMBO Journal*, *41*(17). https://doi.org/10.15252/embj.2022111650

Noureddine, M., & Gehmlich, K. (2023). Structural and signaling proteins in the Z-disk and their role in cardiomyopathies. In *Frontiers in Physiology* (Vol. 14). https://doi.org/10.3389/fphys.2023.1143858

Oda, T., & Yanagisawa, H. (2020). Cryo-electron tomography of cardiac myofibrils reveals a 3D lattice spring within the Z-discs. *Communications Biology*, *3*(1). https://doi.org/10.1038/s42003-020-01321-5

Ordway, G. A., Neufer, P. D., Chin, E. R., & DeMartino, G. N. (2000). Chronic contractile activity upregulates the proteasome system in rabbit skeletal muscle. *Journal of Applied Physiology*, *88*(3). https://doi.org/10.1152/jappl.2000.88.3.1134

Ottenheijm, C. A. C., & Granzier, H. (2010). Lifting the nebula: Novel insights into skeletal muscle contractility. In *Physiology* (Vol. 25, Issue 5). https://doi.org/10.1152/physiol.00016.2010

Palmio, J., & Udd, B. (2016). Myofibrillar and distal myopathies. In *Revue Neurologique* (Vol. 172, Issue 10). https://doi.org/10.1016/j.neurol.2016.07.019

Park, S. S., Seo, Y. K., & Kwon, K. S. (2019). Sarcopenia targeting with autophagy mechanism by exercise. In *BMB Reports* (Vol. 52, Issue 1). https://doi.org/10.5483/BMBRep.2019.52.1.292

Peters, S. E. (1989). Structure and function in vertebrate skeletal muscle. *Integrative and Comparative Biology*, *29*(1). https://doi.org/10.1093/icb/29.1.221

Pettersen, K., Andersen, S., Degen, S., Tadini, V., Grosjean, J., Hatakeyama, S., Tesfahun, A. N., Moestue, S., Kim, J., Nonstad, U., Romundstad, P. R., Skorpen, F., Sørhaug, S., Amundsen, T., Grønberg, B. H., Strasser, F., Stephens, N., Hoem, D., Molven, A., … Bjørkøy, G. (2017). Cancer cachexia associates with a systemic autophagy-inducing activity mimicked by cancer cell-derived IL-6 trans-signaling. *Scientific Reports*, *7*(1). https://doi.org/10.1038/s41598-017-02088-2

Prasanna Murthy, S. N., Iismaa, S., Begg, G., Freymann, D. M., Graham, R. M., & Lorand, L. (2002). Conserved tryptophan in the core domain of transglutaminase is essential for catalytic activity. *Proceedings of the National Academy of Sciences of the United States of America*, *99*(5). https://doi.org/10.1073/pnas.052715799

Puchner, E. M., Alexandrovich, A., Ay, L. K., Hensen, U., Schäfer, L. V., Brandmeier, B., Gräter, F., Grubmüller, H., Gaub, H. E., & Gautel, M. (2008). Mechanoenzymatics of titin kinase. *Proceedings of the National Academy of Sciences of the United States of America*, *105*(36). https://doi.org/10.1073/pnas.0805034105

Purslow, P. P. (2002). The structure and functional significance of variations in the connective tissue within muscle. *Comparative Biochemistry and Physiology - A Molecular and Integrative Physiology*, *133*(4). https://doi.org/10.1016/S1095-6433(02)00141-1

Pyle, W. G., & Solaro, R. J. (2004). At the Crossroads of Myocardial Signaling: The Role of Z-Discs in Intracellular Signaling and Cardiac Function. In *Circulation Research* (Vol. 94, Issue 3). https://doi.org/10.1161/01.RES.0000116143.74830.A9

Ramaswami, M., Taylor, J. P., & Parker, R. (2013). Altered “Ribostasis”: RNA-protein granule formation or persistence in the development of degenerative disorders. *Cell*, *154*(4).

Reimann, L., Wiese, H., Leber, Y., Schwable, A. N., Fricke, A. L., Rohland, A., Knapp, B., Peikert, C. D., Drepper, F., Van Der Ven, P. F. M., Radziwill, G., Furst, D. O., & Warscheid, B. (2017). Myofibrillar Z-discs are a protein phosphorylation hot spot with protein kinase C (PKCα) modulating protein dynamics. *Molecular and Cellular Proteomics*, *16*(3). https://doi.org/10.1074/mcp.M116.065425

Ribeiro, A. J. M., Das, S., Dawson, N., Zaru, R., Orchard, S., Thornton, J. M., Orengo, C., Zeqiraj, E., Murphy, J. M., & Eyers, P. A. (2019). Emerging concepts in pseudoenzyme classification, evolution, and signaling. In *Science Signaling* (Vol. 12, Issue 594). https://doi.org/10.1126/scisignal.aat9797

Roth, D. M., Hutt, D. M., Tong, J., Bouchecareilh, M., Wang, N., Seeley, T., Dekkers, J. F., Beekman, J. M., Garza, D., Drew, L., Masliah, E., Morimoto, R. I., & Balch, W. E. (2014). Modulation of the Maladaptive Stress Response to Manage Diseases of Protein Folding. *PLoS Biology*, *12*(11). https://doi.org/10.1371/journal.pbio.1001998

Ruparelia, A. A., Oorschot, V., Vaz, R., Ramm, G., & Bryson-Richardson, R. J. (2014). Zebrafish models of BAG3 myofibrillar myopathy suggest a toxic gain of function leading to BAG3 insufficiency. *Acta Neuropathologica*, *128*(6). https://doi.org/10.1007/s00401-014-1344-5

S. Hikida, R. (2012). Aging Changes in Satellite Cells and Their Functions. *Current Aging Sciencee*, *4*(3). https://doi.org/10.2174/1874609811104030279

Sandri, M. (2008). Signaling in muscle atrophy and hypertrophy. In *Physiology* (Vol. 23, Issue 3). https://doi.org/10.1152/physiol.00041.2007

Sandri, M. (2013). Protein breakdown in muscle wasting: Role of autophagy-lysosome and ubiquitin-proteasome. In *International Journal of Biochemistry and Cell Biology* (Vol. 45, Issue 10). https://doi.org/10.1016/j.biocel.2013.04.023

Sarnat, H. B. (2020). CONGENITAL MYOPATHIES 2: P.95 Novel mutation in KY gene causes a novel congenital myopathy with early contractures. *Neuromuscular Disorders*, *30*(2), S75. https://doi.org/10.1016/J.NMD.2020.08.101

Schiaffino, S., Dyar, K. A., Ciciliot, S., Blaauw, B., & Sandri, M. (2013). Mechanisms regulating skeletal muscle growth and atrophy. In *FEBS Journal* (Vol. 280, Issue 17). https://doi.org/10.1111/febs.12253

Schiaffino, S., & Reggiani, C. (2011). Fiber types in Mammalian skeletal muscles. *Physiological Reviews*, *91*(4). https://doi.org/10.1152/physrev.00031.2010

Schiaffino, S., Reggiani, C., Akimoto, T., & Blaauw, B. (2021). Molecular Mechanisms of Skeletal Muscle Hypertrophy. In *Journal of Neuromuscular Diseases* (Vol. 8, Issue 2). https://doi.org/10.3233/JND-200568

Selcen, D. (2011). Myofibrillar myopathies. In *Neuromuscular Disorders* (Vol. 21, Issue 3). https://doi.org/10.1016/j.nmd.2010.12.007

Selcen, D., Bromberg, M. B., Chin, S. S., & Engel, A. G. (2011). Reducing bodies and myofibrillar myopathy features in FHL1 muscular dystrophy. *Neurology*, *77*(22). https://doi.org/10.1212/WNL.0b013e31823a0ebe

Snapp, E. L., Hegde, R. S., Francolini, M., Lombardo, F., Colombo, S., Pedrazzini, E., Borgese, N., & Lippincott-Schwartz, J. (2003). Formation of stacked ER cisternae by low affinity protein interactions. *Journal of Cell Biology*, *163*(2). https://doi.org/10.1083/jcb.200306020

Solaro, R. J., & De Tombe, P. P. (2008). Review focus series: Sarcomeric proteins as key elements in integrated control of cardiac function. In *Cardiovascular Research* (Vol. 77, Issue 4). https://doi.org/10.1093/cvr/cvn004

Squire, J. M. (1975). Muscle filament structure and muscle contraction. In *Annual review of biophysics and bioengineering* (Vol. 4). https://doi.org/10.1146/annurev.bb.04.060175.001033

Stonadge, A., Genzor, A. V., Russell, A., Hamed, M. F., Romero, N., Evans, G., Pownall, B., Bekker-Jensen, S., & Blanco, G. (2023). Myofibrillar myopathy hallmarks associated with ZAK deficiency. *Human Molecular Genetics*, *32*(17). https://doi.org/10.1093/hmg/ddad113

Stonadge, A. J. (2023). *Understanding the Role of ZAKβ in the Maintenance and Regulation of Skeletal Muscle Function*.

Straussberg, R., Schottmann, G., Sadeh, M., Gill, E., Seifert, F., Halevy, A., Qassem, K., Rendu, J., van der Ven, P. F. M., Stenzel, W., & Schuelke, M. (2016). Kyphoscoliosis peptidase (KY) mutation causes a novel congenital myopathy with core targetoid defects. In *Acta Neuropathologica* (Vol. 132, Issue 3). https://doi.org/10.1007/s00401-016-1602-9

Summers, C. M., & Valentine, R. J. (2020). Acute Heat Exposure Alters Autophagy Signaling in C2C12 Myotubes. *Frontiers in Physiology*, *10*. https://doi.org/10.3389/fphys.2019.01521

Taillandier, D., Combaret, L., Pouch, M.-N., Samuels, S. E., Béchet, D., & Attaix, D. (2004). The role of ubiquitin–proteasome-dependent proteolysis in the remodelling of skeletal muscle. *Proceedings of the Nutrition Society*, *63*(2). https://doi.org/10.1079/par2004358

Takahashi, K., & Yamanaka, S. (2006). Induction of Pluripotent Stem Cells from Mouse Embryonic and Adult Fibroblast Cultures by Defined Factors. *Cell*, *126*(4). https://doi.org/10.1016/j.cell.2006.07.024

Takeda, K., Yu, Z. X., Qian, S., Chin, T. K., Adelstein, R. S., & Ferrans, V. J. (2000). Nonmuscle myosin II localizes to the Z-lines and intercalated discs of cardiac muscle and to the Z-lines of skeletal muscle. *Cell Motility and the Cytoskeleton*, *46*(1). https://doi.org/10.1002/(SICI)1097-0169(200005)46:1<59::AID-CM6>3.0.CO;2-Q

Tanida, I., Ueno, T., & Uchiyama, Y. (2014). A super-ecliptic, phluorin-mkate2, tandem fluorescent protein-tagged human LC3 for the monitoring of mammalian autophagy. *PLoS ONE*, *9*(10). https://doi.org/10.1371/journal.pone.0110600

Tedesco, B., Vendredy, L., Timmerman, V., & Poletti, A. (2023). The chaperone-assisted selective autophagy complex dynamics and dysfunctions. In *Autophagy* (Vol. 19, Issue 6). https://doi.org/10.1080/15548627.2022.2160564

Thomas, G. D. (2013). Functional muscle ischemia in Duchenne and Becker muscular dystrophy. In *Frontiers in Physiology: Vol. 4 DEC*. https://doi.org/10.3389/fphys.2013.00381

Torii, S., Yoshida, T., Arakawa, S., Honda, S., Nakanishi, A., & Shimizu, S. (2016). Identification of PPM1D as an essential Ulk1 phosphatase for genotoxic stress-induced autophagy. *EMBO Reports*, *17*(11). https://doi.org/10.15252/embr.201642565

Ulbricht, A., Eppler, F. J., Tapia, V. E., Van Der Ven, P. F. M., Hampe, N., Hersch, N., Vakeel, P., Stadel, D., Haas, A., Saftig, P., Behrends, C., Fürst, D. O., Volkmer, R., Hoffmann, B., Kolanus, W., & Höhfeld, J. (2013). Cellular mechanotransduction relies on tension-induced and chaperone-assisted autophagy. *Current Biology*, *23*(5). https://doi.org/10.1016/j.cub.2013.01.064

Ulbricht, A., Gehlert, S., Leciejewski, B., Schiffer, T., Bloch, W., & Höhfeld, J. (2015). Induction and adaptation of chaperone-assisted selective autophagy CASA in response to resistance exercise in human skeletal muscle. *Autophagy*, *11*(3). https://doi.org/10.1080/15548627.2015.1017186

Van Den Akker, J., Van Weert, A., Afink, G., Bakker, E. N. T. P., Van Der Pol, E., Böing, A. N., Nieuwland, R., & VanBavel, E. (2012). Transglutaminase 2 is secreted from smooth muscle cells by transamidation-dependent microparticle formation. *Amino Acids*, *42*(2–3). https://doi.org/10.1007/s00726-011-1010-3

Venn, G., & Mason, R. M. (1986). Changes in mouse intervertebral-disc proteoglycan synthesis with age. Hereditary kyphoscoliosis is associated with elevated synthesis. *Biochemical Journal*, *234*(2). https://doi.org/10.1042/bj2340475

Verderio, E. A. M., Telci, D., Okoye, A., Melino, G., & Griffin, M. (2003). A Novel RGD-independent Cell Adhesion Pathway Mediated by Fibronectin-bound Tissue Transglutaminase Rescues Cells from Anoikis. *Journal of Biological Chemistry*, *278*(43). https://doi.org/10.1074/jbc.M303303200

Vos, M. J., Hageman, J., Carra, S., & Kampinga, H. H. (2008). Structural and functional diversities between members of the human HSPB, HSPH, HSPA, and DNAJ chaperone families. In *Biochemistry* (Vol. 47, Issue 27). https://doi.org/10.1021/bi800639z

Wadhwa, R., Taira, K., & Kaul, S. C. (2002). An Hsp70 family chaperone, mortalin/mthsp70/PBP74/Grp75: What, when, and where? In *Cell Stress and Chaperones* (Vol. 7, Issue 3). https://doi.org/10.1379/1466-1268(2002)007<0309:AHFCMM>2.0.CO;2

Wadmore, K., Azad, A. J., & Gehmlich, K. (2021). The role of z-disc proteins in myopathy and cardiomyopathy. In *International Journal of Molecular Sciences* (Vol. 22, Issue 6). https://doi.org/10.3390/ijms22063058

Wang, X., & Su, H. (2010). Unraveling enigma in the z-disk. In *Circulation Research* (Vol. 107, Issue 3). https://doi.org/10.1161/CIRCRESAHA.110.225615

Weins, A., Schwarz, K., Faul, C., Barisoni, L., Linke, W. A., & Mundel, P. (2001). Differentiation- and stress-dependent nuclear cytoplasmic redistribution of myopodin, a novel actin-bundling protein. *Journal of Cell Biology*, *155*(3). https://doi.org/10.1083/jcb.200012039

Wilkins, J. T., Krivickas, L. S., Goldstein, R., Suh, D., & Frontera, W. R. (2001). Contractile properties of adjacent segments of single human muscle fibers. *Muscle and Nerve*, *24*(10). https://doi.org/10.1002/mus.1150

Xia, Q., Huang, X., Huang, J., Zheng, Y., March, M. E., Li, J., & Wei, Y. (2021). The Role of Autophagy in Skeletal Muscle Diseases. In *Frontiers in Physiology* (Vol. 12). https://doi.org/10.3389/fphys.2021.638983

Yin, H., Price, F., & Rudnicki, M. A. (2013). Satellite cells and the muscle stem cell niche. *Physiological Reviews*, *93*(1). https://doi.org/10.1152/physrev.00043.2011

Yin, L., Li, N., Jia, W., Wang, N., Liang, M., Yang, X., & Du, G. (2021). Skeletal muscle atrophy: From mechanisms to treatments. In *Pharmacological Research* (Vol. 172). https://doi.org/10.1016/j.phrs.2021.105807

Yogev, Y., Perez, Y., Noyman, I., Madegem, A. A., Flusser, H., Shorer, Z., Cohen, E., Kachko, L., Michaelovsky, A., Birk, R., Koifman, A., Drabkin, M., Wormser, O., Halperin, D., Kadir, R., & Birk, O. S. (2017). Progressive hereditary spastic paraplegia caused by a homozygous KY mutation. *European Journal of Human Genetics*, *25*(8). https://doi.org/10.1038/ejhg.2017.85

Zammit, P. S. (2017). Function of the myogenic regulatory factors Myf5, MyoD, Myogenin and MRF4 in skeletal muscle, satellite cells and regenerative myogenesis. In *Seminars in Cell and Developmental Biology* (Vol. 72). https://doi.org/10.1016/j.semcdb.2017.11.011

Zamorani, M. P., & Valle, M. (2007). *Muscle and Tendon*. https://doi.org/10.1007/978-3-540-28163-4_3

Zheng, Z., Yan, G., Li, X., Fei, Y., Sun, L., Yu, H., Niu, Y., Gao, W., Zhong, Q., & Yan, X. (2022). Lysine crotonylation regulates leucine-deprivation-induced autophagy

by a 14-3-3ε-PPM1B axis. *Cell Reports*, *41*(12). https://doi.org/10.1016/j.celrep.2022.111850